

2005

## Morphology development of layered silicate epoxy based nanocomposites

Tia Benson Tolle  
*University of Dayton*

Follow this and additional works at: [https://ecommons.udayton.edu/graduate\\_theses](https://ecommons.udayton.edu/graduate_theses)

---

### Recommended Citation

Benson Tolle, Tia, "Morphology development of layered silicate epoxy based nanocomposites" (2005).  
*Graduate Theses and Dissertations*. 1505.  
[https://ecommons.udayton.edu/graduate\\_theses/1505](https://ecommons.udayton.edu/graduate_theses/1505)

This Dissertation is brought to you for free and open access by the Theses and Dissertations at eCommons. It has been accepted for inclusion in Graduate Theses and Dissertations by an authorized administrator of eCommons. For more information, please contact [mschlange1@udayton.edu](mailto:mschlange1@udayton.edu), [ecommons@udayton.edu](mailto:ecommons@udayton.edu).

**MORPHOLOGY DEVELOPMENT OF LAYERED SILICATE EPOXY BASED  
NANOCOMPOSITES**

Dissertation

Submitted to

The College of Engineering of the

UNIVERSITY OF DAYTON

In Partial Fulfillment of the Requirements for

The Degree

Doctor of Philosophy in Materials Engineering

by

Tia Benson Tolle


UNIVERSITY OF DAYTON

Dayton, Ohio

May, 2005

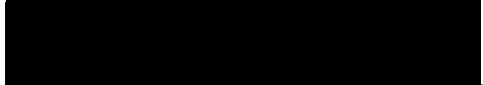
# MORPHOLOGY DEVELOPMENT OF LAYERED SILICATE EPOXY BASED NANOCOMPOSITES

## APPROVED BY:



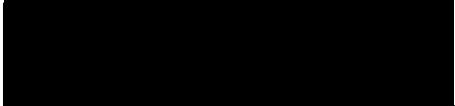
---

Jill S. Ullett, Ph.D.  
Advisory Committee Chair  
Professor, Materials Engineering  
Department



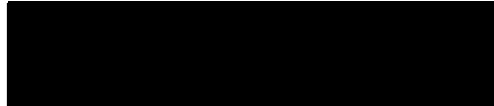
---

James A. Snide, Ph.D.  
Committee Member  
Professor, Materials Engineering  
Department




---

Charles E. Browning, Ph.D.  
Committee Member  
Air Force Research Laboratory



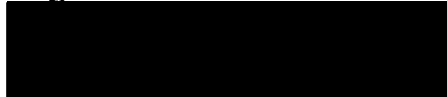
---

Gerald Shaughnessy, Ph.D.  
Committee Member  
Professor, Mathematics Department



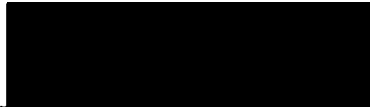
---

Donald L. Moon, Ph.D.  
Associate Dean  
Graduate Engineering Programs &  
Research  
School of Engineering



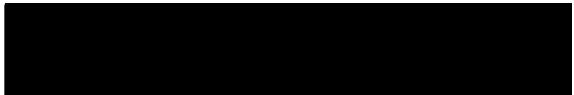
---

David P. Anderson, Ph.D.  
Committee Member  
University of Dayton Research  
Institute



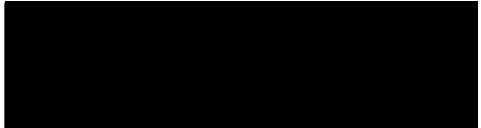
---

Gordon Sargent, Ph.D.  
Committee Member  
Vice President, Research



---

Joseph P. Gallagher, Ph.D.  
Committee Member  
Aeronautical Systems Center



---

Joseph E. Saliba, Ph.D.  
Dean, School of Engineering

## **ABSTRACT**

### **TITLE OF THESIS: MORPHOLOGY DEVELOPMENT OF LAYERED SILICATE EPOXY BASED NANOCOMPOSITES**

Name: Benson Tolle, Tia Hall  
University of Dayton, 2005

Advisor: Dr. J.S. Ullett

Nanotailoring of polymeric materials offers the opportunity for unprecedented multifunctional properties and classical material property trades. Significant improvements to thermoplastics have been demonstrated over the past decade stimulated by the pioneering work of Kojima, Usuki, and Okada. The ability to translate such improvements to epoxy-based composites will undoubtedly impact multiple aerospace and non-aerospace applications. However, the thermodynamically and kinetically competing processes inherent to thermosetting systems represent significant challenges for the development of controlled nano-scaled morphologies in epoxies. Before ultimate control of morphology and material design can be achieved, fundamental understanding of how morphologies of various scales develop with processing parameters must be developed through careful examination of model systems. This research produced a single material system capable of developing two distinct morphologies through controlled room-temperature resin-advancement. Integrated analysis techniques were utilized to provide understanding of the effects of

processing parameters and to capture both nano-scale and micron-scale morphologies. The results of unique real-time processing studies and the development of process-morphology and morphology-property relationships, as described in this dissertation, demonstrates that layered silicate epoxy nanocomposites are not classical two-phase systems but rather multiphase systems in which subtle intra-gallery chemistries can dictate ultimate morphologies and properties. Through morphology-property and fracture study results this dissertation demonstrates that ordered nano-scale morphologies in which intercalated regions exist on a large enough scale to interact with propagating cracks represent a more effective morphology for improving toughness than highly dispersed, exfoliated morphologies.

## **ACKNOWLEDGMENTS**

To Ralph, my partner in the adventure of life; my family, my steadfast supporters; and my parents, who provided the foundation for who I am.

## **PREFACE**

A large body of recent research into nanocomposites has been performed, primarily focusing upon the unique benefits imparted to thermoplastic polymers. Advanced composite materials have become an engineering material of choice for aerospace applications through development spanning the past three decades. Composites today still offer the most opportunity for the materials community and aerospace applications, as they are truly the first generation of 'engineered materials'. Nanotailoring of composites can provide materials with new capabilities. Many aerospace applications could benefit by using nanotailored composites, but rely upon composites based on thermosetting polymers such as epoxy. The work described in this dissertation was performed to bring nanotailoring into the advanced composites community and to address their specific needs.

## TABLE OF CONTENTS

ABSTRACT.....	iii
ACKNOWLEDGMENTS.....	v
PREFACE.....	vi
LIST OF FIGURES.....	ix
LIST OF TABLES.....	xvi
CHAPTER	
I. INTRODUCTION.....	1
II. BACKGROUND.....	5
Constituent Materials: Organically Modified Layered Silicates	
Early Nanocomposites	
Processing Routes for Layered Silicate Nanocomposites	
Epoxy Nanocomposites	
Toughening Mechanisms and Particles	
III. EXPERIMENTAL METHODS.....	32
Materials and Processing	
Characterization Techniques	
Error Analysis	
IV. RESULTS.....	55
<i>In situ</i> SAXS Study results	
Temperature as a Variable in Morphology Development	
Temperature Rate as a Variable in Morphology Development	
Role of Organoclay Selection on Morphology Development	

Material Preconditioning as a Variable  
 Role of Variability: Degas and Hydration of OLS  
 Result of Cure Agent Variations  
 Volume Fraction Variation  
 Thermal Analysis Results  
 Mechanical Characterization and Fractography  
 Chemical Characterization

V.	DISCUSSION.....	96
VI.	SUMMARY AND CONCLUSIONS.....	174

#### APPENDICES

Appendix A:	Scattering Data for Isothermal Temperature Processes.....	180
Appendix B:	Scattering Data for Non-Isothermal Temperature Processes....	188
Appendix C:	Scattering Data as a Function of Material Preconditioning.....	195
Appendix D:	Scattering Data for Cure Agent Studies and of Constituents....	208
REFERENCES.....		218

## LIST OF FIGURES

2-1.	Crystalline structure of smectite mineral.....	7
2-2.	Schematic diagram of the structures of kaolinite and montmorillonite .....	11
2-3.	Representative conceptual 'idealized' morphologies for layered silicate polymer nanocomposites.....	14
2-4.	Structure of diglycidyl ether of bisphenol A or DGEBA Epoxy.....	22
2-5.	Crack tip particle interactions: rigid particle and nano particle.....	29
3-1.	Chemical structure of: (a) Epon 828 epoxy and (b) cure agent m-phenylenediamine (mPDA).....	33
3-2.	Structure of Cure Agent: (a) W and (b) T-403.....	35
3-3.	Differential Scanning Calorimetry (DSC) of Epon 828/mPDA showing reaction onset temperature occurs at approximately 126°C.....	39
3-4.	Dynamic mechanical data for Epon 828/mPDA showing storage modulus ( $G'$ ) and $\tan\delta$ , the ratio of storage to loss modulus ( $G''$ ).....	40
3-5.	Beamline X-27C at Brookhaven National Laboratory (a) view looking towards beam source and showing programmable oven, (b) view looking towards detector, and (c) close up view of sample cell holder and oven.....	44
3-6.	Representative data curves for idealized nanocomposite morphologies... ..	46
4-1.	Time-dependent small angle x-ray scattering data for 5 % I.30E/Epon 828 with mPDA at isothermal temperature of 60°C after 1, 10, 20, 30, 45 and 60 minutes (intensity data offset for clarity).....	58
4-2.	Time-dependent small angle x-ray scattering data for 5 % SC18/Epon 828 with mPDA at isothermal temperature of 70°C after 1, 5, 10, 15, 20, 30 and 45 minutes.....	59

4-3.	Time-dependent small angle x-ray scattering data for 5 % SC18/Epon 828 with mPDA at isothermal temperature of 80°C after 1, 5, 10, 15, 20, 30 and 45 minutes.....	59
4-4.	Time-dependent small angle x-ray scattering data for 3 % SC18/Epon 828 with mPDA at isothermal temperature of 100°C after 1, 10, 20, 30 and 45 minutes. ....	60
4-5.	Time-dependent small angle x-ray scattering data for 5 % I.30E/Epon 828 with mPDA at heating rate of 2°C/minute.....	62
4-6.	Time-dependent small angle x-ray scattering data for 5 % I.30E/Epon 828 with mPDA at heating rate of 10°C/minute.....	62
4-7.	Time-dependent small angle x-ray scattering data for 5 % SC18/Epon 828 with mPDA at heating rate of 5°C/minute.....	63
4-8.	Time-dependent small angle x-ray scattering data for 5 % SC18/Epon 828 with mPDA at heating rate of 10°C/minute.....	63
4-9.	Time-dependent small angle x-ray scattering data for 5 % SC18/Epon 828 with mPDA at heating rate of 12°C/minute.....	64
4-10.	Time-dependent small angle x-ray scattering data for 5 % I.30E/Epon 828 with mPDA at isothermal temperature of 80°C.....	66
4-11.	Time-dependent small angle x-ray scattering data for 5 % SC18/Epon 828 with mPDA at isothermal temperature of 80°C.....	66
4-12.	Time-dependent small angle x-ray scattering data for 5 % mixture of SC18+I.30E/Epon 828 with mPDA at isothermal temperature of 80°C.....	67
4-13.	Time-dependent small angle x-ray scattering data for 5% I.30E/Epon 828 with mPDA at isothermal temperature of 80°C, no advancement (repeat of Figure 10).....	68
4-14.	Time-dependent small angle x-ray scattering data for 5 % I30E/Epon 828 with mPDA at isothermal temperature of 80°C after advancement for 4 weeks.....	68
4-15.	Time-dependent small angle x-ray scattering data for 5 % I30E/Epon 828 with mPDA at isothermal temperature of 80°C after advancement for 18 weeks.....	69

4-16.	Time-dependent small angle x-ray scattering data for 5 % SC18/Epon 828 with mPDA at isothermal temperature of 80°C.....	71
4-17.	Time-dependent small angle x-ray scattering data for 5 % SC18/Epon 828 with mPDA without degas step at isothermal temperature of 80°.....	71
4-18.	Time-dependent small angle x-ray scattering data for 5% SC18/Epon 828 with no cure agent at isothermal temperature of 80°C (intensity data offset for clarity).....	73
4-19.	Time-dependent small angle x-ray scattering data for 5 % SC18/Epon 828 with mPDA at isothermal temperature of 80°C (intensity data offset for clarity).....	74
4-20.	Time-dependent small angle x-ray scattering data for 5 % SC18/Epon 828 with T403 at isothermal temperature of 80°C (intensity data offset for clarity).....	74
4-21.	Time-dependent small angle x-ray scattering data for 5 % I30E/Epon 828 with mPDA at heating rate of 5°C/minute (intensity data offset for clarity).....	75
4-22.	Time-dependent small angle x-ray scattering data for 5 % I30E/Epon 828 with T403 at heating rate of 5°C/minute (intensity data offset for clarity) .....	76
4-23.	Time-dependent small angle x-ray scattering data for 5 % I30E/Epon 828 with Epi-cure W at heating rate of 5°C/minute (intensity data offset for clarity) .....	76
4-24.	Time-dependent small angle x-ray scattering data for 5 % I30E/Epon 828 with mPDA at isothermal temperature of 80°C (intensity data offset for clarity) .....	77
4-25.	Time-dependent small angle x-ray scattering data for 5 % I30E/Epon 828 with Epi-cure W at isothermal temperature of 80°C (intensity data offset for clarity) .....	78
4-26.	Time-dependent small angle x-ray scattering data for 1 % I.30E/Epon 828 with mPDA at isothermal temperature of 80°C (intensity data offset for clarity) .....	79
4-27.	Time-dependent small angle x-ray scattering data for 7 % I.30E/Epon 828 with mPDA at isothermal temperature of 80°C (intensity data offset for clarity) .....	80

4-28.	DMA storage modulus data comparing 828/mPDA, 5% I.30E/Epon 828/mPDA baseline and mixture advanced nanocomposites cured via standard recommended cure process. ....	82
4-29.	DMA loss modulus data comparing 828/mPDA, 5% I.30E/Epon 828/mPDA baseline and mixture advanced nanocomposites cured via standard recommended cure process. ....	83
4-30.	DMA sub-ambient storage modulus data comparing 828/mPDA, 5% I.30E/Epon 828/mPDA baseline and mixture advanced nanocomposites cured via standard recommended cure process.....	84
4-31.	DMA sub-ambient loss modulus data comparing 828/mPDA, 5% I.30E/Epon 828/mPDA baseline and mixture advanced nanocomposites cured via standard recommended cure process. ....	84
4-32.	DMA sub-ambient tan $\delta$ data comparing 828/mPDA, 5% I.30E/Epon 828/mPDA baseline and mixture advanced nanocomposites cured via standard recommended cure process.....	85
4-33.	Photo of the fracture surface of failed compact tension specimens. White arrow identifies the fracture surface, black arrow identifies the machined surface (notch).....	88
4-34.	Scanning electron microscope (SEM) image of the fracture surface of 828/mPDA no OLS (sample B4). ....	89
4-35.	(A) SEM image of the fracture surface of 5% I.30E/828/mPDA baseline process (sample A5). (B) Increased magnification of (A). White arrows identify anomalies on the fracture surface as compared with neat resin fracture. Black arrows identify resin-rich areas. (C) Increased magnification of (B). Scale bars = (A) 100 micrometers, (B) 50 micrometers, (C) 10 micrometers.....	90
4-36.	(A) SEM image of the fracture surface of 5% I.30E/828/mPDA “advanced” (sample D9). (B) Increased magnification of (A). Anomalies shown by white arrows. Resin-rich areas shown by black arrows. (C) Increased magnification of (B). Scale bars = (A) 100 micrometers, (B) 50 micrometers, (C) 10 micrometers.....	91
4-37.	(A) SEM grey scale image of 828/mPDA. (B) EDS map of aluminum. (C) EDS map of silicon. Scale bars = 11 micrometers.....	92

4-38.	(A) SEM grey scale image shown in Figure 35 (A), 5% I.30E/828/mPDA baseline process. (B) EDS map of aluminum. (C) EDS map of silicon. Scale bar = 50 micrometers.....	92
4-39.	Transmission electron microscopy of I.30E/828/mPDA nanocomposites.....	94
5-1.	Time-dependent small angle x-ray scattering data for SC18/Epon 828 with mPDA at isothermal temperature.....	98
5-2.	d-spacing of two organoclays after 45 minutes at an isothermal temperature as a function of temperature shows that systems reach higher gallery sizes for higher temperatures.....	100
5-3.	Differential Scanning Calorimetry for 828/mPDA and 5% I.30E/828/mPDA shows that the addition of the OLS advances the onset of reaction. Data taken at 10°C/minute in nitrogen. ....	101
5-4.	Differential Scanning Calorimetry for 5% I.30E/828 shows that the OLS reacts with the epoxy at high temperature. Data taken at 10°C/minute in nitrogen.....	101
5-5.	Initiation of exfoliation in epoxy-silicate nanocomposite occurs faster with increasing temperature .....	106
5-6.	Scattering data development for the epoxy/I.30E system at q associated with intercalated peak ( $q \sim 0.18\text{\AA}^{-1}$ ) shows trend of morphology development with time at isothermal temperature (90°C).....	112
5-7.	Exfoliation process as evidenced by loss of peak associated with initial intercalated morphology at $q \sim 0.18\text{\AA}^{-1}$ for epoxy/I.30E system occurs faster at higher temperatures.....	114
5-8.	d-spacing of two organoclays after 45 minutes at temperature ramps of 2, 5, 6, 10 and 12 degrees/minute as a function of temperature rate.....	115
5-9.	Morphology development occurs at higher temperatures with increased heating rate for epoxy/I.30E system.....	116
5-10.	Morphology development occurs at higher temperatures with increased heating rate for epoxy/SC18 system.....	117
5-11.	Change of scattering intensity associated with exfoliated and intercalated morphologies as a function of time (isothermal temperature 110°C, epoxy/I.30E).....	118

5-12.	Time-dependent small angle x-ray scattering data for 5% I.30E/Epon 828 with mPDA at isothermal temperature of 80°C after mixture advancement for 16 weeks (intensity data offset for clarity).....	122
5-13.	Time-dependent small angle x-ray scattering data for baseline (no advancement) 5% I.30E/Epon 828 with mPDA at isothermal temperature of 80°C (intensity data offset for clarity).....	122
5-14.	Differential Scanning Calorimetry for 828/mPDA, baseline processed, and advanced 5% I.30E/828/mPDA shows that advancement minimizes the catalytic effect of the OLS. Data taken at 10°C/minute in nitrogen.....	126
5-15.	TEM images of 5% I.30E/828/mPDA nanocomposites show (a) flexibility of OLS layers and (b) greater expansion on edge of tactoid. ....	129
5-16.	Small angle x-ray data for baseline material (a) and mixture-advanced materials (b) show similar behavior initially (1 minute) but differ significantly in the low q region slope and Bragg peaks after 45 minutes at 80°C.....	134
5-17.	Low q slopes for materials versus time show earlier onset of slope stabilization for mixture-advanced materials.....	135
5-18.	Time for loss of scattering intensity of initial Bragg peak [~28 minutes for baseline (a), ~17 minutes for mixture advanced (b)] corresponds with onset of stabilization of low q slopes. (Difficulty in fitting peak breadth causing scatter in data.).....	136
5-19.	TEM images of representative tactoids.....	138
5-20.	Schematic of various proposed models with associated SAXS.....	141
5-21.	Time-dependent small angle x-ray scattering data comparison of a) 5 % I.30E/Epon 828 with Epi-cure W and b) 5% I.30E/Epon 828 with T-403 at heating rate of 5°C/minute (intensity data offset for clarity) .....	145
5-22.	Dynamic mechanical data, DMA torsion, performed at 2°C/minute, 100 rad/sec, 0.1% strain, shows storage modulus for 828/mPDA and 5% I.30E/828/mPDA processed via baseline and mixture advancement processes.....	148
5-23.	Dynamic mechanical data, DMA torsion, performed at 2°C/minute, 100 rad/sec, 0.1% strain, sub-ambient loss modulus data comparing	

828/mPDA, 5% I.30E/Epon 828/mPDA baseline and mixture advanced nanocomposites cured via standard recommended cure process.....	151
5-24. SEM image of the fracture surface of 3% I.30E/828/mPDA (magnified 214 times) and 5% I.30E/828/mPDA (magnified 255 times).....	155
5-25. SEM image of the fracture surface of 3% I.30E/828/mPDA (magnified 428 times) and 5% I.30E/828/mPDA (magnified 510 times).....	155
5-26. Tensile properties of Epon 828/mPDA, 5% I.30E/Epon 828/mPDA, and 3% I.30E/Epon 828/mPDA (two difference processes).....	162
5-27. SEM image of the fracture surfaces of (A) 5% I.30E/828/mPDA and (B) 5% I.30E/828/mPDA “advanced” materials show rough fracture surfaces.....	163
5-28. SEM image of the fracture surfaces of (A) 5% I.30E/828/mPDA and (B) 5% I.30E/828/mPDA “advanced” materials show rough fracture surfaces.....	165
5-29. SAXS data for 3% I.30E/828/mPDA nanocomposite show effect of horn sonication step on tactoid order.....	168
5-30. TEMs of 3% I.30E/828/mPDA nanocomposite show horn sonication (Process A) during the mixing process has negligible effect on d-spacing within tactoids.....	169
5-31. Large field of view TEMs of 3% I.30E/828/mPDA nanocomposites show horn sonication during the mixing process produces more uniform dispersion and smaller groupings of organoclay layers.....	170
5-32. Compact tension fracture toughness test data shows processes that include horn sonication step (Process A, D) result in lower K <sub>q</sub> values.....	171
5-33. SEM image of the fracture surface of 3%I.30E/828/mPDA Baseline Process (magnified 214 times) and 3%I.30E/828/mPDA Process D which included horn sonication (magnified 228 times).....	171
5-34. SEM image of the fracture surface of 3%I.30E/828/mPDA Baseline Process (magnified 428 times) and 3%I.30E/828/mPDA Process D which included horn sonication (magnified 489 times).....	172

## LIST OF TABLES

2-1.	Average values of relative dimensions and unit charge for common clay minerals .....	12
2-2.	Toyota nanocomposite results demonstrate dramatic property improvements .....	15
2-3.	Examples of layered silicate nanocomposites with various polymer matrices and property improvements.....	18
3-1.	Variations in fabrication process of nanocomposites .....	37
4-1.	<i>In situ</i> SAXS Studies on Isothermal Temperature Processes versus Morphology Development for I.30E/828/mPDA Nanocomposites.....	60
4-2.	<i>In situ</i> SAXS Studies on Isothermal Temperature Processes versus Morphology Development for SC18/828/mPDA Nanocomposites.....	61
4-3.	<i>In situ</i> SAXS Studies on Heating Rate Processes versus Morphology Development for I.30E/828/mPDA Nanocomposites.....	64
4-4.	<i>In situ</i> SAXS Studies on Heating Rate Processes versus Morphology Development for SC18/828/mPDA Nanocomposites.....	65
4-5.	Summary of Advancement Effects at Isothermal Temperature of 80°C.....	69
4-6.	Summary of Processing Variations and Associated Scattering Data.....	72
4-7.	Summary of Cure Agent Variation Studies.....	78
4-8.	DSC data summary.....	81
4-9.	Summary of Ambient DMA Data.....	83
4-10.	Mixing Processes.....	86
4-11.	Fracture Toughness Data from Compact Tension Testing.....	86
4-12.	Tensile properties of neat epoxy and nanocomposites.....	87

4-13.	Energy dispersive spectroscopy analysis of fracture surfaces comparing baseline and mixture 'advanced' nanocomposites.....	93
5-1.	The d-spacings reached by I.30E/epoxy-mPDA at an isothermal temperature of 80°C are greater for greater mixture advancement.....	121
5-2.	DSC data for preconditioned epoxy/mPDA/I.30E materials.....	127
5-3.	Dynamic mechanical analysis data of the alpha transition of baseline and mixture advanced nanocomposites.....	149
5-4.	Fracture toughness of 5% I.30E/Epon 828/mPDA materials .....	156

## **CHAPTER I**

### **INTRODUCTION**

Polymeric nanocomposites offer exciting opportunities to explore new and enhanced material properties beyond those currently available in polymers and polymer matrix composites. Like other composites, nanocomposites are materials that are designed and processed from selected constituents. However, unlike typical advanced composites in which a reinforcing constituent is on the order of micrometers, nanocomposites utilize a constituent on the order of a few nanometers, which is on the same scale as the radius of gyration of a polymer. A composite material that can be tailored at this scale may open the door to significantly improved materials that could readily be transitioned into current processing practices.

Composite materials, those in which two or more constituents are combined to result in properties better than those of the individual constituents, represents the most mature, accepted class of engineered materials and are highly desired for aerospace applications. Key to this class of materials is the fact that each constituent retains its separate chemical, physical and mechanical properties; to date, they primarily rely on a (polymeric) matrix and microscopic reinforcing constituent. The ability to incorporate a nanoscopic

constituent will provide for much finer control of resulting properties by enabling tailoring of the polymer matrix, as well offer the opportunity to explore new properties and property trade spaces that result from tailoring on this scale. Significant effects on mechanical, thermal, and physical properties of polymeric materials through the addition of nanoconstituents have been observed over the past decade [1, 2]. It is not uncommon, for example, for a nanocomposite to have twice the elastic modulus of the base polymer. The potential to change typical property trade spaces has also been demonstrated and researchers have shown abilities to dramatically improve tensile strength, modulus and heat distortion temperature without decreasing impact resistance.

Unique to nanocomposites is the achievement of such property improvements through incorporation of nanoconstituents at volume fractions as low as 2-5%. Significant property improvements with such low volume fractions of reinforcement has not been achieved prior to current research into nanocomposites. While microscopic fillers such as talc or silica have historically been incorporated within epoxy resins to modify cure shrinkage, water absorption, thermal properties and to reduce cost, weight fractions as high as 20% to 50% were required to achieve the desired effects [3, 4]. Advanced fiber reinforced composites that are employed today for their extremely high specific properties and tailorability achieve their performance through the incorporation of structural (micron size) fiber reinforcements as high as 60% by volume. Such high volume fractions can dominate processability. Yet the incorporation into a polymer of constituents that are on the scale of nanometers and in the amount of only a few percent can have minimal impact on its viscosity. This in turn offers the potential for

nanotailoring existing polymer resins without requiring significant modification of existing processing techniques, providing for low-cost property improvements for commodity polymers and increased tailorability options for advanced composite matrices. This potential for increased tailoring and for new or modified properties without significantly altering the original structural property suite or existing processing techniques is the primary motivation for investigating polymeric nanocomposites for aerospace applications.

Before this promising class of materials can be fully exploited within aerospace applications, understanding and control of processing, morphology development, and morphology-property relationships must be developed. Control on the nanoscale has been investigated in polymer research with liquid crystal polymers and block copolymers, as well as sought after in many material fields. Much research conducted in the field of rubber-toughened epoxies (and to a lesser extent rigid particle filled epoxies) has demonstrated the importance of processing on morphology development for that specific class of materials. Yet the effect of particle size on some properties such as toughness is still inconclusive, and the ability to engineer or control materials at this scale that are composed of distinctly different constituents has not been undertaken in a broad sense.

Crucial to the ability to fully investigate nanocomposites is development of in-depth understandings of nanoscale morphologies and their evolution, much like what has been achieved for rubber-toughened epoxies. The nanoscale morphologies, e.g., the dispersion

of the nanoscopic constituent, are expected to play a key role in the resulting properties. Today many strive to develop materials in which the nanoscale constituent is completely dispersed in the polymer, motivated by the belief that such morphology will provide for the full realization of desired property improvements. Yet validation of this premise requires an ability of material process-morphology control that has not yet been achieved due to the limited understanding of how morphologies develop through processing.

Predictive morphology-property relationships for the material studied here, epoxy-based layered silicate nanocomposites, face unique challenges due to the complexities associated with network formation during cure. The objective of this research is to define the role of specific processing and material variables on morphology development for layered silicate epoxy nanocomposites so that morphology development models may be generated to guide material developers. New insight into morphology development under various processing conditions is provided. Processing approaches to alleviate some of the challenges faced in developing different morphologies are suggested. Observations are made on the ability of nanotailoring to improve toughness of epoxy and the role of the dispersion of the nanoconstituents on toughness.

## **CHAPTER II**

### **BACKGROUND**

This chapter is divided into several sections to provide both background and context for the research. A review of the constituent materials will cover the basic layered silicate system and organically modified layered silicates. Next, early work in polymeric nanocomposites will be reviewed, as will general processing routes for nanocomposites. The importance of epoxy-based nanocomposites leads into the motivation behind the selection of this material system for this research. Epoxy-based nanocomposites will be then reviewed specifically to establish the current state of the art. A discussion of epoxy curing is included to highlight the complexities associated when fabricating layered silicate epoxy nanocomposites. A brief review of toughness and predictive models will complete the chapter.

#### **Constituent Materials: Organically Modified Layered Silicates**

Organically modified layered silicates (OLS) are one of the most broadly researched constituents for polymeric nanocomposites. Their structure and chemistry play a significant role in how they may be combined with a polymer and the property enhancements that may result. The natural layered silicates have historically been

incorporated into polymers as fillers. They are hydrophilic by nature and incompatible with organic polymers so remain as immiscible micron-sized tactoid particles. The natural silicates must therefore be modified to render them organophilic so they can disperse into nanoscale particles. This section will discuss the layered silicates and how they are modified to enable their incorporation into polymers.

A large portion of polymeric nanocomposite research utilizes the mineral montmorillonite (MMT), a naturally occurring layered silicate that belong to the smectite group of clay minerals. Smectites are one of the 2:1 layer types of clay minerals that have the ability to expand and contract their structures while maintaining two-dimensional crystallographic integrity. The layers in these minerals consist of two silica tetrahedral sheets of tetrahedral units of oxygen atoms at the four corners surrounding a single silicon atom, and one alumina octahedral sheet, comprised of octahedral units consisting of six oxygen or hydroxyls enclosing an aluminum, magnesium, iron or other atom (Figure 2-1). The space between a given tetrahedral silica - octahedral alumina - tetrahedral silica unit layer and its next neighboring unit layer is defined as the gallery. In the gallery, oxygen layers of neighboring units are adjacent to each other, resulting in weak van der Waals bonds. Whereas the bonding between layers is weak, bonding within the unit layers is strong (covalent). Exchangeable cations may reside in the gallery, and it is into the gallery that molecules may penetrate or 'intercalate'<sup>1</sup>.

---

<sup>1</sup> Webster's 1913 Dictionary (via on-line) \n\*ter"ca\*late\, v. t. [imp. & p. p. {Intercalated}; p. pr. & vb. n. {Intercalating}.] [L.intercalatus, p. p. of intercalare to intercalate to intercalate; inter between + calare to call, proclaim. See {Calendar}.] 1. (Chron.) To insert, as a day or other portion of time, in a calendar. 2. To insert among others, as a verse in a stanza; specif. (Geol.), to introduce as a bed or stratum, between the layers of a regular series of rocks. Beds of fresh-water shells . . . are intercalated and interstratified with the shale. -Mantell (English geologist remembered as the first person to recognize that dinosaurs were reptiles (1790-1852) )

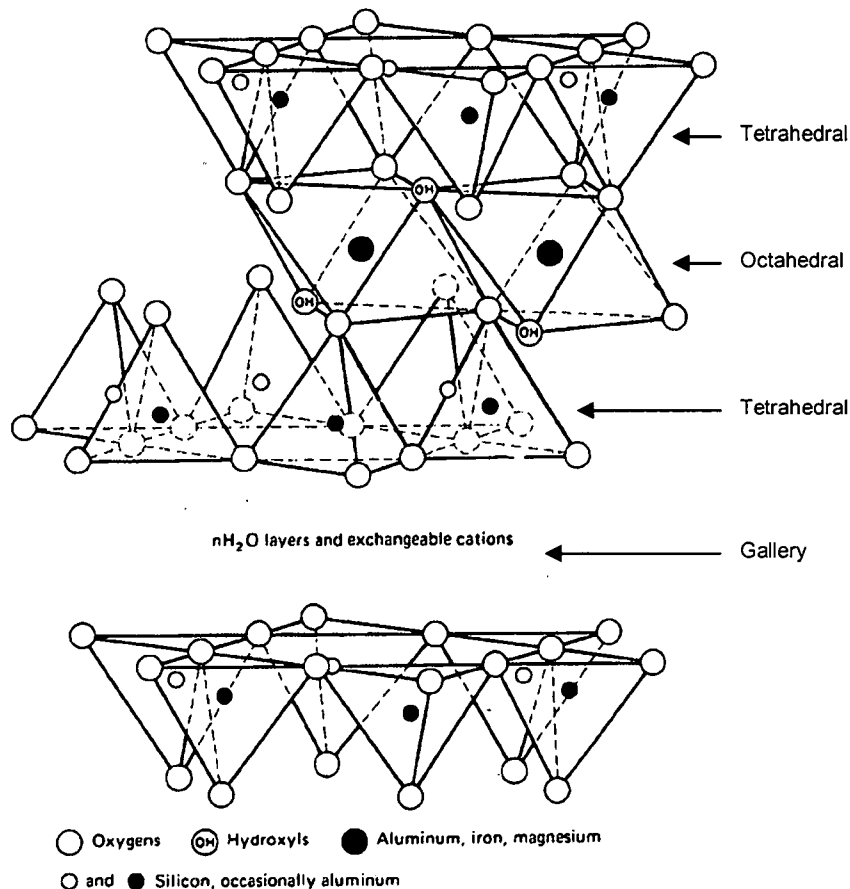


**Figure 2-1:** Crystalline structure of smectite mineral [7]

The exchangeable cations within the structure determine the silicate's behavior and are affected by the crystalline structure. The type of cation occupying the tetrahedral and octahedral sites is limited primarily by ionic size and coordination, resulting in opportunity for isomorphous substitution within these structures. The manner in which the octahedral positions are filled determines a smectite's subgroup, either trioctahedral or dioctahedral [6]. In trioctahedral smectite structures, all of the octahedral sites are occupied; in dioctahedral, only two-thirds of the sites are occupied. When fewer than all sites are occupied or when cations of similar size and coordination but of different

valency occupy one of the sites, an overall negative charge to the unit layer results. This charge can be compensated by sorption of exchangeable cations into the gallery. The amount of isomorphous replacements as well as the site determines the surface density of charge and the cation-silicate layer attraction. The edge surfaces are small relative to the plane surfaces, and the majority of the charge is on the plane surfaces. In most cases, cations are attracted to the surfaces, anions to the edges [5].

These minerals can have a very wide range of behaviors based on various substitutions such as described above. This attribute must be recognized when selecting them for use in nanocomposites. For example, when all of the octahedral positions are filled by  $Mg^{2+}$  ions, the resulting structure (talc) is electrically neutral and non-expanding. In the case where extensive isomorphous substitution occurs leading to very strong electrostatic attraction between the layers and the interlayer ions, such as what occurs with mica, it can lead to a loss of swelling ability [6].

Modification of the silicate through cation exchange is key for polymer compatibility, and as this research will show, silicate modification may play a role in morphology development. Cation exchange is brought about by processes which expose the clay to strong concentrations of single-cation solutions. Through such processing, cations within the galleries that are balancing the charge can be replaced by others. The amount of cations replaced is a measure both of the negative charge on a layer and the cation exchange capacity (CEC) of the silicate. CEC is used as a property of exchange capacity and is measured in terms of milliequivalents per gram or per 100 grams (me/100g). Its

study dates back to the very early soils literature, when in 1850 H. S. Thomson was credited with an in-depth study of ion exchange of soils [5]. It roughly matches the total charge, but since number of factors influence the CEC, no single value is characteristic of a given group of minerals; instead, the CEC is typically provided as a range. The CEC is influenced by broken bonds around the edges of the layer unit which would give rise to charge; the isomorphous substitutions within the lattice structure; and any hydrogen of exposed hydroxyls within the structure – all of which can be replaced by a cation which might be exchangeable [7]. The range in CEC of minerals is also due to variations in particle size, crystallinity, and the measurement environment and techniques (such as temperature and the nature of the cations).

### **Montmorillonite**

Dispersion of the individual layers within a polymer is a fundamental step in the fabrication process of layered silicate nanocomposites and relies on the intercalation of the organic phase into the galleries of the inorganic silicate. As previously noted, montmorillonite (MMT) is the current workhorse of layered silicate nanocomposites, and this is due to its structure and how well organic materials can be intercalated within it. There are many inorganic layered materials that exhibit intercalation capabilities, but the smectite group is quite strong in this characteristic, and it is into this group, specifically the dioctahedral subgroup of the smectite group, that MMT falls. In MMT as in other 2:1 minerals, an octahedral sheet is sandwiched between two silica sheets with the tips of the tetrahedrons combining with the hydroxyls of the octahedral sheet to form a single unit or

2:1 layer. The repeating unit layers of MMT are approximately 1 nm thick (0.96 nm); the areal dimensions are on the order of 10 to 100 times the thickness, but due to irregularity, are difficult to obtain. In MMT the substitution of  $\text{Al}^{3+}$  in the octahedral positions occurs, providing for a layer with a permanent negative charge. This charge is balanced by the absorption of exchangeable cations and/or water between the unit layers.

Montmorillonite can experience extensive interlayer expansion, exposing a large active surface area (700-800  $\text{m}^2/\text{g}$ ). It also has a high cation exchange capacity and can form interlayer complexes with a wide variety of organic molecules, hence has been the most widely used in industry for applications such as adsorbants for organic compounds [8]. MMT's CEC, typically 70-150 me/100g, is one of the highest relative to other minerals, as is its specific surface area, and many molecules can intercalate its galleries.

Comparison with other minerals further elucidates the selection of MMT for polymeric nanocomposites. Figure 2-2 compares kaolinite with MMT. Kaolinite is another layered silicate, but is a 1:1 mineral consisting of repeating layers of one silica tetrahedral sheet and one alumina octahedral sheet, with the tips of the silica sheet bonded to the octahedral sheet. Successive unit layers are held together by both van der Waals and hydrogen bonding between the hydroxyls of the octahedral sheet and the oxygens of the tetrahedral sheet. There is essentially no unbalanced charge, so no exchangeable cations reside in the gallery. Such strong interlayer bonding makes kaolinite very difficult to intercalate. Since the kaolinite unit layers are held together so strongly, the edges

represent 10-20% or so of the total crystal area of  $15\text{-}40\text{ m}^2/\text{g}$ , and with their active broken bonds become very important in any interactions.

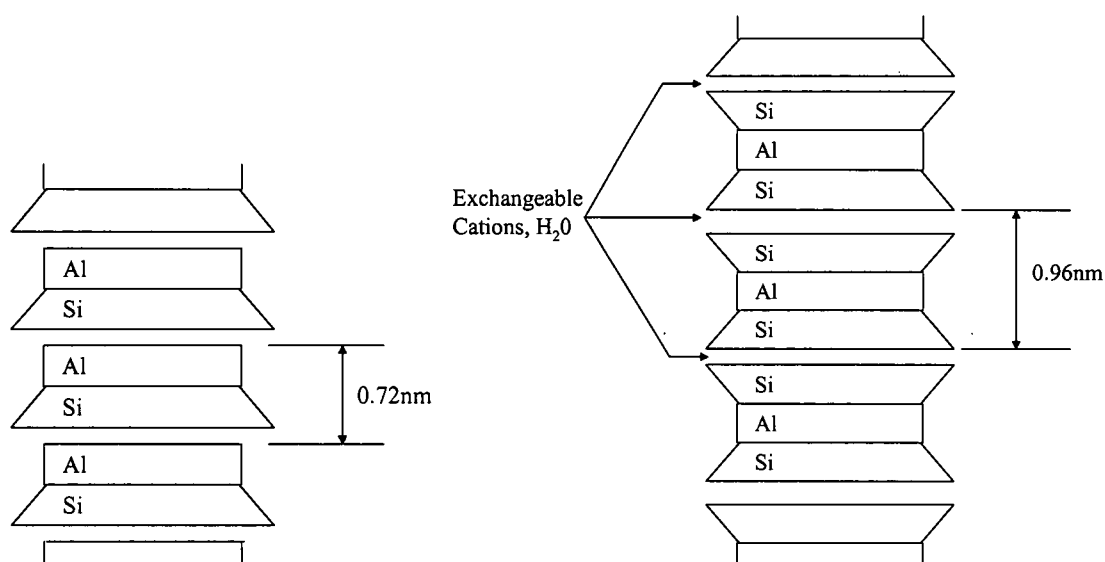


**Figure 2-2:** Schematic diagram of the structures of kaolinite (left) and montmorillonite (from [9])

In comparison, MMT with its net charge that results in exchangeable cations and weak van der Waals interlayer forces, is easy to intercalate. Its edges represent typically 2-23% of the total area of  $\sim 760\text{ m}^2/\text{g}$ , and the influence of the edges in sorption or anions, electron-transfer reactions, and influence on polymerization is less [8]. Further comparisons of some of the common clay minerals are captured in Table 2-1.

**Table 2-1:** Average values of relative dimensions and unit charge for common clay minerals (after data [7], [8], [9])

Mineral	Typical Thickness (nm)	Typical Diameter (nm)	Specific Surface (km <sup>2</sup> /kg)	Charge per Formula Unit (x)	CEC (me/100g)
Montmorillonite (2:1 Smectite Group)	1	100-1000	0.8	~0.25-0.6	70-150
Chlorite (2:1:1 Chlorite Group)	30	10,000	0.08	variable	10-40
Kaolinite (1:1 Kaolinite-serpentine Group)	50-2,000	300-4,000	0.015	~0	3-15

### Organic Modifications and Incorporation within Polymers

Though in its natural state the MMT unit layers are hydrophilic and incompatible with hydrophobic organic polymers, modifications through cation-exchange reactions render the layers organophilic, enabling polymer or monomer intercalation [5,8]. The resulting mineral is often termed an organoclay or organically modified layered silicate (OLS).

References to organophilic clays and successful intercalation of organic molecules through replacement of exchangeable inorganic cations with organic cations date back as far as the 1940s when it was found that octylammonium-montmorillonite solvated layered silicates and intercalation of organic molecules was possible [7]. Just as the selection of the particular smectite mineral can greatly affect a resulting combination within a polymer as discussed above, so can the various organic modifications as this research will show.

Two idealized morphologies are often used to describe the dispersion of OLS in polymers: (1) intercalated morphologies, which occur when a single or a few polymer chains enter the gallery of the silicate and the unit layers expand (typically on the order of 10's of Å over the original gallery height; for organically modified MMTs, often on the order of 30-40 Å), retaining their stack-like registry and association and (2) exfoliated morphologies, which result when the layers are highly separated (typically on the order of 100 Å or more) and are well dispersed and usually disordered within the polymer [10]. Most minerals in are immiscible in polymers if not organically modified, with no intercalation of polymer into the silicate thus no swelling of the silicate beyond its original gallery height (typically on the order of 10-20 Å for MMTs). Graphics of these idealized morphologies are shown in Figure 2-3. However, it is more common that layered silicate nanocomposites exhibit variations and combinations of these idealized morphologies such that morphology descriptions must not only take into account layer-to-layer associations (d-spacing) but also higher scale orders between colonies of intercalated tactoids<sup>2</sup> or ordered regions [11, 12, 13]. Thus, enhanced understanding of morphology development is often hampered by the challenge of adequate morphology characterization and description, not to mention the challenges in experimentally characterizing such small scale morphologies.

---

<sup>2</sup> **tactoid:** The colloidal sized aggregates of phyllosilicate clay particles that can form under certain conditions of exchangeable cations and ionic strength; intercalated or exfoliated clay platelets aligned parallel to each other..

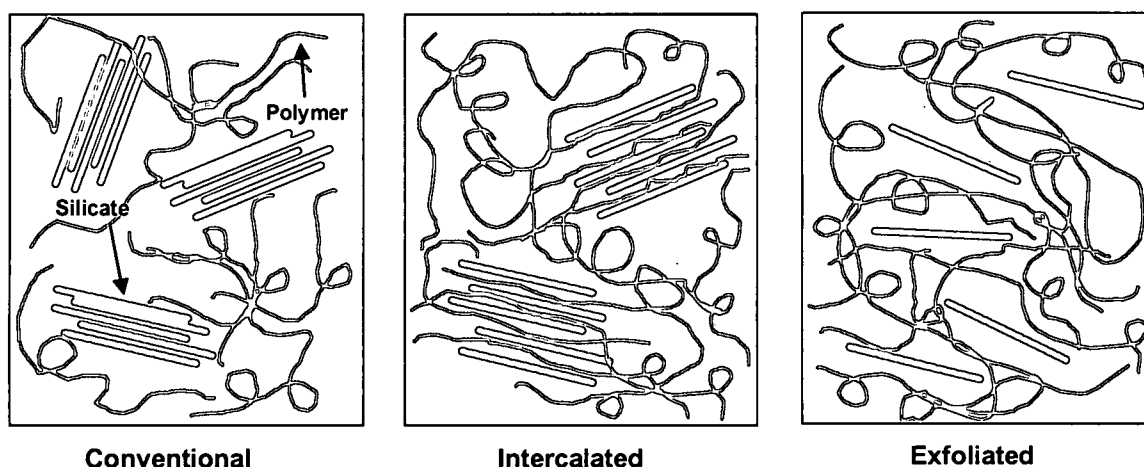


**Figure 2-3:** Representative conceptual ‘idealized’ morphologies for layered silicate polymer nanocomposites

### Early Nanocomposites

Although minerals have been utilized within polymers and composites for decades, it was the pioneering work of researchers at the Toyota Central Research Laboratories during the 1990s that is credited as the origin of polymer-organoclay nanocomposites. The Toyota work documented the first effort directed at integrating polymeric materials and minerals with the specific intent of dispersing the clays at the nanoscale [14, 15, 16]. The Toyota research was motivated by the hypothesis that unexpected or significantly enhanced mechanical properties might result if the dispersions of polymers and clays could be achieved “in the dimension of molecules [14].” This expectation was based on theory drawn from random, discontinuous fiber filled composites that suggested that the degree of reinforcement is a function of both the rigidity and aspect ratio of the filler as well as the interface [2]. This motivation was coupled with the recognition that the clay minerals represent a potential nanoscale additive if they could be dispersed at the unit layer level, and intercalated with organic molecules. Their successful fabrication of

organically modified montmorillonite-nylon 6 (polycaprolactam) based nanocomposites demonstrated dramatic improvements in properties at a surprisingly low weight fraction of 4% [17, 18]. Most significant, not only were the modulus and strength of the nanocomposite improved to an unexpected level over that of the nylon, but concomitant was the improvement of apparent toughness (impact strength), a property typically traded for improved modulus (Table 2-2).

**Table 2-2:** Toyota nanocomposite demonstrate dramatic property improvements [19,20]

Property	Nylon 6	Nanocomposite (4% OLS by wt)	Change
Tensile Modulus	1.1 GPa	2.1 GPa	+ 91%
Tensile Strength	69 MPa	107 MPa	+ 55%
Impact Strength	2.3 kJ m <sup>2</sup>	2.8 kJ m <sup>2</sup>	+ 22%
Heat Distortion Temp	65°C	145°C	+ 80°C
Water Absorption	0.87%	0.51%	- 41%
CTE	13 X 10 <sup>-5</sup>	6.3 X 10 <sup>-5</sup>	- 52%

An excellent recent review of this pioneering work can now be found in Kato and Usuki, and Yasue et al., chapters 5& 6 of [2].

Reports of the Toyota group's success stimulated a near-explosion of international research, and many nanocomposite systems have been investigated to date utilizing a variety of inorganic silicates or other nanoelements and a number of polymeric resins.

The motivation to achieve new properties without sacrificing others drove many efforts toward reproducing the Toyota group's achievement. In addition to the initial work with nylon 6, layered silicate-based nanocomposites have been fabricated using polypropylene, polystyrene, polyester, polyether, polyimides, poly(ethylene oxide) (PEO), poly(butylene terephthalate) (PBT), and elastomers such as polyurethane [21-30]. Equally impressive enhancements at low volume fractions have been reported for various properties and material systems, with increases in heat distortion temperature up to 87°C; increases in tensile strength of over 40%; and increases in tensile modulus of almost 70% not uncommon [18, 20, 31]. Thermal stability, decomposition behavior, and CTE have been shown to be positively impacted through nanotailoring [32]. And unique permeability, optical, and dielectric behaviors have been observed [26, 27, 33, 34].

Yet general trends and summaries have not yet been captured for layered silicate polymer nanocomposites. Direct comparisons of literature data are extremely difficult due to lack of consistency in characterization techniques as well as processing approaches. Full characterization of the d-spacing and morphology of layered silicate nanocomposites requires a description of the gallery height, the distribution of gallery heights, and the order or disorder of the distributed layers with respect to each other. This can only be accomplished through the combined use of tools such as transmission electron microscopy (TEM) and x-ray scattering. Only small angle scattering can assess average gallery heights greater than about 4.5 nm. In early research, and often even today, papers claim exfoliated morphology based only on the lack of a Bragg reflection peak in the wide angle x-ray diffraction (WAXD) data; in actuality, the only claim that can be made

with WAXD is that the average gallery height is beyond the capability of the machine. Many rely solely on high resolution TEM images, which are insufficient for assessment of global and local morphologies. Such challenges associated with morphology descriptions will be discussed in the following chapters. In addition, for direct comparisons within any given material system, processing routes must be understood. Yet often, research is performed and reported on nanocomposites that have been processed by such diverse cure profiles as a long, step-wise cycle taken from the advanced composites community, to a cycle of only a few hours at a given temperature. As this research will show, processing temperature and heating rates can greatly impact the resulting morphology. Cure agent selection alters initial morphology development as well. The role that the specific type of OLS, of which there are many, may play must also be taken into account, as will be discussed in following chapters.

To make the ultimate comparison of properties, suitable test methods must be employed. Toughness, for example, is a property that is often assessed by various tests which can greatly affect the resulting values. A polymer's yield strength and flow ability is time and temperature dependent, as is its relaxation and response to stress. Crack propagation behavior is therefore also time dependent, and this must be taken into account for high rate impact tests or low rate single edge notch type tests. Different test rates will illicit different response and crack propagation behavior within a polymer. Typically, high speeds (or low temperature) give brittle-stable crack growth; lower speeds (or increased temperatures) give brittle-unstable behavior). Therefore one cannot compare data obtained through impact tests such as Charpy or Izod with compact tension fracture

toughness tests. Moreover, comparisons between different material systems are difficult, as a number of material variables affect energy dissipation mechanisms and resulting fracture behavior. These variables include characteristics of the resin, such as being amorphous, crystalline, or crosslinked; those of the filler constituent; the volume fraction and interface as well as size and shape, and the distribution and morphology. Keeping the above cautions in mind, Table 2-3 shows a few examples of polymers other than nylon that have been used in layered silicate nanocomposites and some key observations.

**Table 2-3:** Examples of reported experimental data on layered silicate nanocomposites with various polymer matrices.

<b>Polymer</b>	<b>Observation</b>	<b>Reference</b>
Polypropylene	<ul style="list-style-type: none"> <li>- Gallery expanded from 2.3 nm to 3.5 nm</li> <li>- Improved tensile strength (26%), bending strength (39%) and modulus (40%), IZOD impact strength (70%), HDT 10°C</li> </ul>	Kurokawa et al., 1997 [21]
Polystyrene	<ul style="list-style-type: none"> <li>- Gallery on order of 2 nm</li> <li>- Increased glass transition temperature</li> <li>- Decreased toughness</li> </ul>	Moet et al., 1994 [22] Laus et al., 1998 [35] Manias et al., 1997 [24]
Polyimides	<ul style="list-style-type: none"> <li>- Gallery expanded from 2.97 nm to 3.2 nm</li> <li>- Reduced tensile strength; insignificant improvement or reduction of flexural modulus; improved Izod impact strength (0-400%)</li> <li>- Reduced gas permeability by 50%</li> </ul>	Park et al., 2001 [36]  Yano et al., 1993 [27]
Polyurethane	<ul style="list-style-type: none"> <li>- Gallery expanded from 1.79 nm to 3.7 through 5.08 nm</li> <li>- Tensile strength, modulus and strain-at-break increased by over 100%</li> </ul>	Wang and Pinnavaia, 1998 [30]
Polyester	<ul style="list-style-type: none"> <li>- Gallery expanded; primarily intercalated morphology</li> <li>- Decreased tensile modulus, reduced gas permeability.</li> </ul>	Bharadway et al., 2002 [12]

Implicit in the majority of layered silicate nanocomposite studies is the goal of achieving fully exfoliated morphologies and the expectation that such morphologies will provide for the maximum mechanical property improvements. The pioneering work that the Toyota group performed with nylon had this goal and did achieve good dispersion and generally exfoliated morphology. Yet it is not clear that all property improvements will be maximized by fully exfoliated morphologies. Indeed, some properties such as permeability or fracture toughness may require some degree of anisotropic morphology such as that provided by intercalated morphologies or aligned ordered morphologies. Morphology details on a larger scale such as groupings of intercalated morphologies may more effectively interact with crack tips. Although such control is not achievable today, this research is motivated by the premise that local morphologies must be assessed as a function of the desired property, and in particular that for toughness, fully exfoliated morphologies may not be optimum.

### **Processing Routes for Layered Silicate Nanocomposites**

Many processing routes have been investigated in the field, but most fall into three general approaches: (1) melt intercalation processing, in which the organoclay is combined with a polymer that has been heated to the molten state; the polymer intercalates within and expands the gallery of the layered silicate; (2) solvent assisted processes, in which both the organoclay and polymer are dissolved in a solvent; the solvent penetrates the galleries along with the dissolved polymer; the solvent is subsequently removed by evaporation; and (3) *in situ* intercalative polymerization, in which the organoclay is dispersed in a monomer (with or without solvent); the monomer

intercalates the galleries; then the monomer is subsequently polymerized in the presence of the organoclay. The first two approaches lend themselves to systems in which physical interactions dominate, such as thermoplastics; *in situ* polymerization lends itself to systems that involve chemical reactions, such as thermosets.

A general understanding of the correlation between nanocomposite processing and morphology development has yet to be developed, and is key to eventual control of morphology development and the study of morphology – property relationships.

Although this understanding is necessary for any effective material development, it is of critical importance for morphology-sensitive properties such as toughness, permeability, and absorption. It is specifically necessary for thermosetting resins like epoxies, for which properties such as toughness and moisture absorption have been key historical limitations to their increased use in many arenas, including aerospace structures.

### **Epoxy Nanocomposites offer Unique Opportunities and Challenges**

Although many thermoplastic nanocomposites have been investigated since the pioneering achievements of the Toyota group, research on thermosetting systems such as epoxies lagged that on thermoplastic systems. The challenges associated with such materials lies in the fact that, unlike thermoplastics, they undergo chemical reactions during their cure, and these reactions can be sensitive to the presence of additional constituents such as fillers. During cure, epoxies develop three-dimensional crosslinked networks, providing a dynamically changing environment that can significantly interfere with the expansion of the organoclay tactoids.

Epoxy resins represent one of the standard resins of aerospace composite applications as well as many other non-aerospace applications. Their broad use originates from the wide variety of chemical reactions that they can undergo in curing, the wide variety of materials that can be used to cure them, and the diverse properties that can result. Their processing can be performed over a wide range of temperatures, and the control of the degree of crosslinking can provide for a wide range of use temperatures and physical properties. Epoxies give off no volatiles during their cure, and have low shrinkage relative to resins such as unsaturated polyesters or acrylics that rearrange and reorient considerably in the liquid and semi-gelled phase. They react with little chemical structure rearrangement which, combined with the lack of volatiles evolved, results in good dimensional control throughout processing. Cured epoxies can offer good chemical resistance, high mechanical properties, good heat resistance, and high electrical resistance. Today there are many forms of epoxies and cure agents from which one can select to achieve specific, desired end properties. Nanotailoring this class of materials may find wide applications as well as provide for higher performance in existing applications.

### **Epoxy Cure Process**

In the general sense, the term epoxy refers to a chemical group consisting of an oxygen atom bonded to two other (carbon) atoms that are already united in some manner. The simplest chemical group, which is what will be discussed here, is a three membered ring referred to as a  $\alpha$ -epoxy or 1,2-epoxy, although there are resins that contain four and five

member rings. An epoxy resin is a molecule that contains more than one  $\alpha$ -epoxy group, and its functionality is determined by the number of epoxy end-groups that can react. The earliest epoxy resins were made through the reaction of epichlorohydrin and bisphenol A, which gives di-functional diglycidyl ether of bisphenol A or DGEBA. (Bisphenol A is produced from reacting phenol and acetone.) These resins can be synthesized in a wide range of molecular weights based on the ratio of epichlorohydrin to bisphenol A. Epoxy resins can be synthesized by reacting epichlorohydrin with other aromatic compounds, but DGEBA (as well as the diglycidyl ether of bisphenol F and tetraglycidyl methylene dianiline (TGMDA)) is representative of the most widely used epoxy resins in aerospace applications [37, 38]. While epoxies as a group can undergo a large variety of addition and polymerization reactions, all cure through reactions that involve the epoxy group ring opening and cross-linking (typically with the curing agent). Epoxy resins based on DGEBA will be discussed here (Figure 2-4).

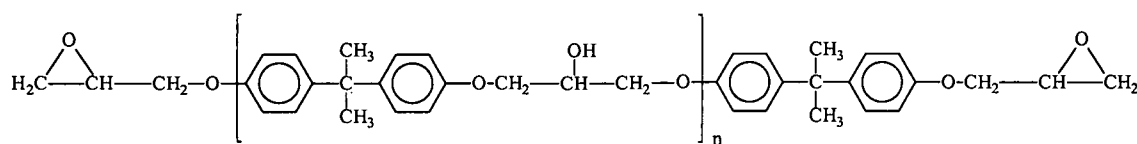


**Figure 2-4:** Structure of diglycidyl ether of bisphenol A or DGEBA Epoxy

Under the right environment the two epoxide rings open, each establishing a reacting point in the molecular chain, so the DGEBA molecule is di-functional. The specific reaction is a function of the selected cure agent and process. The cured structure may be a homopolymer (composed of epoxy molecules linked together through their own

reactive sites) or a heteropolymer (composed of epoxy molecules linked together through the reactive sites of the curing agent) or a mixture of these. The exact reaction depends on the location of the epoxy ring (e.g., terminal or internal).

One of the many variables in the curing of epoxies is the cure agent. The basic cure agents used for epoxies fall into the Lewis bases, inorganic bases, primary and secondary amines, and amides. Of these, the amines are most often employed in high performance structural materials. The type of amine plays a large part on final crosslink structure. Amines are defined as primary, secondary or tertiary, a classification defined by the number of hydrocarbon groups attached to the nitrogen. They are further defined by their functionality, the number of hydrogens available for reaction, which plays a major role in the way in which they react with epoxy. Cure via di-functional amines such as a single primary amine or two secondary amines results mainly in the formation of linear polymers. Functionality higher than di-functional is needed for highly cross-linked polymers. The reaction may also be catalyzed by various chemistries such as hydroxyls.

Amines are further categorized as aliphatic or aromatic. Primary aliphatic amines were the earliest used to cure epoxy resins. When used in stoichiometric proportions (i.e., one active amine hydrogen for each epoxide group) they provide for similar cured properties as a class. Aliphatic amine structures can be branched or linear. They typically react at low temperatures, which can ease processing requirements, but their use temperature is limited by their relative flexibility. Aromatic amines are defined as those in which the amine nitrogen is attached directly to an aromatic ring. Their use provides for improved

temperature capability, lower shrinkage, improved strength and chemical resistance compared to what is attainable with aliphatic amines and generally lower toughness. They require elevated temperature to fully react. The reaction of the epoxy groups with aromatic amines is generally slower than that with aliphatic amines due to their lower basicity and to steric factors of the aromatic ring. Aromatic amines are the preferred cure agents for aerospace applications.

The cure of epoxy resins is well known to be sensitive to temperature and temperature rate as well as the cure agent selection. Cure of epoxies as with all thermosetting resins is complex. The cure begins by formation and linear growth of the epoxy chains which then begin to branch and cross-link. As the reaction continues, the molecular weight increases rapidly and several chains eventually become linked together into networks of infinite molecular weight. This point is termed gelation or the gel point, and is a sudden and irreversible transformation from the viscous liquid to an elastic gel. This is a characteristic of thermoset cures and is critical as after this point the polymer no longer flows (although the reaction can continue). Another characteristic phenomenon of thermoset cures is vitrification of the growing chains or network. Vitrification is the transformation from a viscous liquid or elastic gel to a glass. Vitrification occurs as the glass transition temperature of the growing chains or network reaches the cure processing temperature. Although reversible, further cure reaction in this state is extremely slow and essentially stops. At vitrification the reaction changes from being chemically controlled to diffusion controlled. Near this point the kinetics are affected by the local viscosity, yet the local viscosity is in turn a function of the extent of reaction and the temperature [39,

40,41]. The interactions of the chemical kinetics and the changing physical properties can affect both the ability to reach a fully-developed network and the development of any second-phase morphology. An extensive body of literature on the effects of processing on the development of second phases within epoxies, such as rubber tougheners, provides insight into the challenges that such complexities pose [42, 43, 44]. Therefore the extension of the work of the Toyota group and the experiences with early nylon-based nanocomposites to epoxy-based layered silicate nanocomposites should be expected to confront unique obstacles.

### **Epoxy Nanocomposites**

Interest in layered silicate epoxy-based nanocomposites has increased but only relatively recently has research addressed epoxy nanocomposite morphology descriptions and models so critical in the development of process-morphology correlations and controlled systems [45, 46, 47, 48]. One of the specific challenges associated with describing epoxy nanocomposite morphology development is quantifying the role of the numerous processing variables that affect network development and thus morphology formation. These variables include time, temperature, and other process history such as shear [37, 49]. In addition to processing variables, many constituent variations can play a role in layered silicate nanocomposite morphology such as charge density of the silicate surface, compatibility between the silicate and the polymer, the nature of the polymer (polar or apolar), and chain length and structure of the cationic surfactant/modification [7, 8, 50-54]. Also, the organic modifications of MMTs affect the initial size of the gallery and may participate in the polymerization process [7, 8, 55, 56, 57]. Such numerous variables

suggest that morphology development in layered silicate epoxy nanocomposites will be quite complex. To date the understanding of its complexity, as evidenced by the literature and the effect of various processing and material variables, is limited. However, the ability to achieve morphologies that allow for improved toughness without the sacrifice of modulus provides motivation to continue to develop foundational understanding that will lead to morphology control.

The earliest reported work on epoxy-based nanocomposites is found in 1994-1996, when Lan and Pinnavaia reported the ability to form epoxy nanocomposites both in the glassy and rubbery state. They observed d-spacings on the order of 80-150 Å, and improvements of modulus and strength in the rubbery state though only marginally improved modulus and strength for the glassy state relative to that achieved in the rubbery state [58]. Messersmith and Giannelis also initiated the move toward epoxy, reporting similar levels of d-spacing (80-120 Å), and increased modulus (via DMA) but again much less in the glassy phase than in the rubbery phase [31]. This is not surprising, as it is well known that the effects of cross-links or fillers impact the rubbery modulus much more than glassy modulus. Pinnavaia et al. extended the work with epoxies, assessing the role of the organoclay's alkyl chains on morphology development, observing the ability of the organically modified layered silicates to polymerize epoxy, and mechanically and optically characterizing materials cured with amines that provided for rubbery materials [59, 56, 34, 58]. They also observed that the challenges associated with the fact that epoxies form cross-links during processing were significant, and suggested that the role of network formation both within the layered silicate galleries

(intragallery) and surrounding the layered silicate tactoids (extragallery) must be taken into account to achieve a desired exfoliated morphology [57].

Others have built on and extended this early work. Chin and Russell et al. employed small angle x-ray scattering to study morphology development [47]. Kornmann et al. observed that the nature of the cure agent and of the clays influenced the network formation and hence the ability to exfoliate the organoclays in epoxies [46, 53]. The role of cure temperature on morphology development addressed in this research has also been studied by Becker et al. [60]. Characterization of rubbery phase epoxies continued, but an emerging interest and focus was on finding an explanation of the development of exfoliated morphology within highly crosslinked systems.

### **Toughening Mechanisms and Particles**

During this period the quest for improved properties continued to provide motivation for further research. Data on fracture toughness of glassy epoxy based nanocomposites are still limited, and are difficult to assess due to the various materials, morphologies, and test methods employed to collect the data. So it is yet open as to which morphology will provide the greatest toughness enhancements. Fracture behavior of a material depends on the stress levels, presence of flaws, material properties, and available energy dissipation mechanisms. Morphology is a very important factor in fracture as well as in failure mechanisms, and can affect fracture behavior. Morphologies can cause inhomogeneous stress distributions about the crack tip which can either provide energy

dissipation and thus higher toughness or weaker locations for crack formation and thus lower toughness. Morphologies can also influence macroscopic material properties such as yield strength and thus indirectly affect fracture behavior. And morphologies, including those created through the use of second phases, can provide for mechanisms that provide for enhanced energy absorption through crack tip interactions that include those that deflect crack paths, pin crack fronts, fracture the second phase particle, and shield the crack tip from the full extent of the driving force. In traditional materials, typical morphological features are relatively large; grain boundaries in metals and ceramics vary from as small as one micrometer to as large as 10 mm. Although liquid crystal thermosets and co-polymers have morphologies on nanoscopic scales, traditional polymer toughening routes have relied on larger features [61]. With this understanding it is important to question the relative size effect of nanoscopic morphologies on fracture.

Specific to layered silicate nanocomposites is the question of the effectiveness of a single exfoliated silica layer in providing toughening mechanisms. A single layer may act as a brittle particle, whereas an intercalated set of layers may act as a tough 'composite' particle and more effectively interact with the crack not just due to size but due to overall composition (Figure 2-5). This question motivated one aspect of and is investigated in this research: the role of nanoconstituents in toughening.

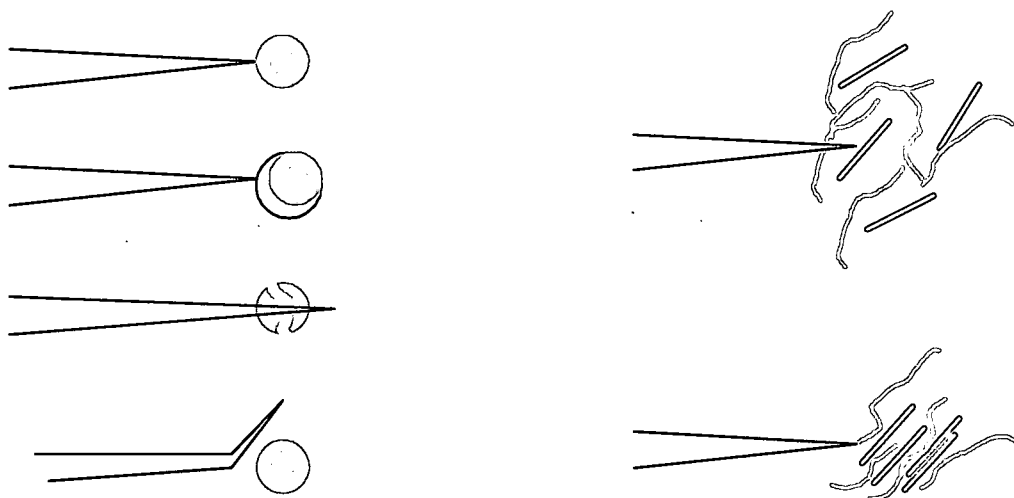


**Figure 2-5:** Crack tip particle interactions: rigid particle and nano particle [62].

This motivation was supported by the observation that early research provided conflicting data on whether or not nanotailoring improves properties and toughness [[63] vs. [64] for nylon; [30] vs. [65] for polyurethane]. In fact, some work focused specifically on fracture mechanisms generated data that showed a decrease in toughness with nanotailoring over that of neat polystyrene [24].

Limited data were available for thermosetting materials, which will both have different polymer toughening behavior as well as experience different toughening through second phase particles than thermoplastics due to the relative modulus of particle and resin. Even more limited were correlations between morphologies and properties. Harcup, Yee et al. suggested that the level of exfoliation may play a strong role in toughness due to the relative size of the ‘microstructure’ [66]. Zilg et al. characterized the fracture toughness of a series of epoxy nanocomposites based on various synthetic ion-exchanged

fluoromicas in an attempt to achieve controlled morphologies and to correlate performance with levels of exfoliation [67]. Their study generated fracture toughness data many formulations, yet any comparison of the varieties is difficult as one cannot state that the material system was held constant. As this research will demonstrate, the complexities of the composition within the gallery of layered silicate epoxy nanocomposites cannot be dismissed due to the role it may have on both the morphology and the material properties. Morphology characterization was often performed through TEM and/or WAXD alone, without any global assessment of large scale organization. As this thesis suggests, the hierarchical morphologies while not well understood, cannot be ignored.

More recently, Zerda and Lesser demonstrated significant toughness improvements through the incorporation of organically modified layered silicates in aliphatic-cured epoxy. The reported morphologies had mixtures of various regions of intercalation and neat resin, and they concluded that toughening is most improved through intercalated morphologies. However, they based this conclusion on the recognition of the complexity of the various and hierarchical morphologies; and thus the characterization of the morphology is inconclusive [68]. Kornmann et al. concluded that fracture properties are not substantially affected by nanomorphology based on a series of epoxy nanocomposites that had d-spacings on the order of 50 Å (which is not significantly expanded over the typical intercalated epoxy values of 25-35 Å) [69]. Becker et al. achieved glassy epoxy nanocomposites with improved toughness and modulus over the neat epoxy, with morphologies that were comprised of mixtures of intercalated and slightly expanded

'exfoliated' regions characterized by WAXD and TEM to be on the order of 50 Å [70]. A challenge that all of these recent developments share is the lack of ability to correlate the difference in d-spacing, or nanoscale morphology, with toughness. In addition the morphologies in these systems are mixed, with both intercalated OLS (d-spacings on the order of 50 Å) and minimally exfoliated (with d-spacings on the order of 100 Å). The morphologies are also often hierarchical in that there are both the d-spacing size as well as regions of given d-spacings and given orientations. The ability to achieve and work with systems in which that is the sole variable has not yet been appreciated, as this dissertation will further demonstrate.

A fundamental understanding of the morphology development events can provide researchers with the insight needed to control nanocomposite morphologies, hence to control morphology-sensitive properties and manufacturing processes. The many scales at which nanocomposite morphologies occur makes this a challenging endeavor, and the use of epoxy resins adds significant complexities due to the interaction of network formation and OLS expansion. The galleries of the OLS themselves, so important to morphology development, may also contain complex gradients of physical and chemical properties from silicate layer to silicate layer. This complexity must ultimately be recognized for control of processing, morphologies, properties, and model development. Ultimately, insight into the morphology development may provide guidance to material developers of future layered silicate epoxy nanocomposites. Relationships between the nanoscale morphologies and properties such as fracture toughness must follow.

## **CHAPTER III**

### **EXPERIMENTAL METHODS**

This chapter is divided into two sections. The first section, Materials and Processing, provides rationale for the selection of the materials and addresses the variables explored within the materials and the processes to gain insight into morphology development. The second section, Experimental Techniques, addresses the specific techniques used in data generation and analysis.

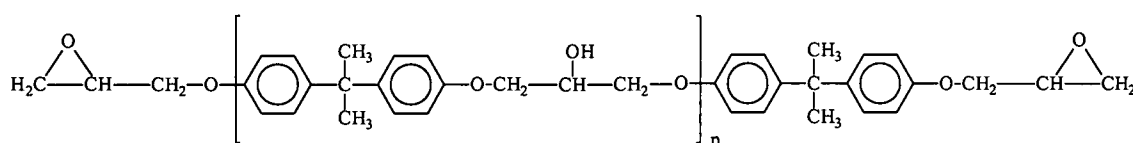
#### **Materials and Processing**

##### **Material Selection**

The epoxy selected for this study was Epon 828 (Shell Chemical Company), a diglycidyl ether of bisphenol A (DGEBA) (Figure 3-1a). This epoxy represents a model material as it is a widely-used base for many epoxy resins that has good physical characteristics when cross-linked, and a fairly low equivalent molecular weight (185 - 192) with minimal additives that could interact with or affect the behaviors being investigated. The cure agent selected was m-phenylenediamine (mPDA), (Sigma-Aldrich Chemical), a tetra-functional primary aromatic diamine-based cure agent as shown in Figure 3-1b with

an average molecular weight of 108, that can provide for highly cross-linked, high glass transition temperature epoxies. This selection was to ensure that the properties of the matrix and the nanoconstituents in the cured nanocomposites were representative of high performance aerospace resins. The selection of the specific epoxy and cure agent was also based on the fact that the amine-epoxy reaction is one of the most frequently studied thermoset reactions, and specifically, the reaction between DGEBA and mPDA has been extensively used as a reference system in the past and therefore represents a model system for the study of epoxy-based nanocomposites [71].

(a)



(b)

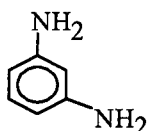


**Figure 3-1:** Chemical structure of: (a) Epon 828 epoxy and (b) cure agent m-phenylenediamine (mPDA).

The layered silicates utilized are based on organically modified montmorillonite for the reasons discussed in the Background Chapter. Two very similar organically modified layers silicates (OLS) were selected. One, I.30E, is a commercially available product from Nanocor (Arlington Heights, IL) with a cation exchange capacity (CEC) of approximately 145 meq/100g. The second, SC18, is a laboratory fabricated OLS provided by Dr. Chenggang Chen (of the University of Dayton Research Institute), which is made from the treatment of sodium montmorillonite with octadecylammonium chloride

through an ion-exchange reaction. SC18 has a CEC of approximately 92 meq/100g. Both are an OLS based on montmorillonite modified with a 18-carbon aliphatic chain with an ammonium end group.

### **Material Variations**

Variations in material preparation were included to explore the sensitivity of morphology development to material conditions. One set of variations explored the natural sensitivity of smectite layered silicates to moisture and the potential role of trapped moisture on morphology development [8]. Water uptake at various levels of humidity are greatly influenced by the nature of the interlayer cation, and interlayer water can either be directly coordinated to the interlayer cation, or indirectly linked to the cation through secondary coordination and more easily removed. Dehydration studies performed in mineralogical research has shown that considerable water loss is typically seen at 100°C or higher, depending on the nature of the absorbed ions, and free water can evolve above 40°C [7, 72]. The OLS was preconditioned with a drying step under vacuum at temperatures of 25°C, 60°C and 100° C for over 12 hours before mixing with the epoxy. These temperatures were selected to represent typical processing temperatures as well as the temperature range at which considerable dehydration might occur.

A variation in cure agent selection was performed to further explore the development of morphology as a function of steric hindrance to intercalation. Early studies on organic modifications structures in the mineralogical literature have determined relationships

between intercalation and the number of carbon atoms on the amine vs. basal spacing, and suggest that steric hindrance within the galleries may play a role in morphology development [7]. Epi-Cure Curing Agent W (diethyltoluenediamine (DETDA), Shell) a tetra-functional primary aromatic diamine with an average molecular weight of 178, and Jeffamine T-403, (polyoxypropylenetriamine, Huntsman), a hexa-functional primary aliphatic triamine with an average molecular weight of approximately 440 were selected to explore the effect of cure agent size and chemistry on morphology development (Figure 3-2).

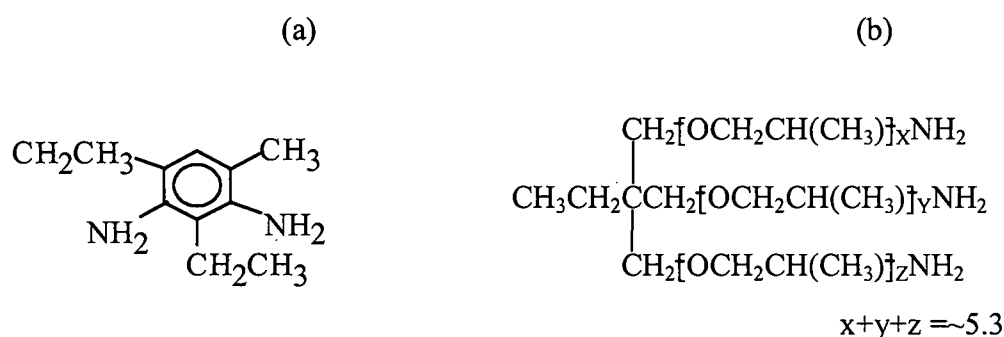


**Figure 3-2:** Structure of Cure Agent: (a) W and (b) T-403

### Processing of the Nano-tailored Epoxy

Preparation of the OLS-epoxy-cure agent mixture has several variables such as mixing technique and time. Various processing techniques were initially explored, including solvent assisted processing in which the OLS or resin was dispersed in a solvent (acetone) and mechanically stirred and sonicated prior to mixing with the resin or OLS to aid in dispersion. The solvent was stripped off via vacuum and temperature prior to the addition of the cure agent. Early investigations into various mixing techniques explored

the use of mechanical shear mixing and the use of an ultrasonic bath. Various stirring times were also investigated.

*In situ* polymerization was ultimately used as the baseline process. This process yielded predictable quality, is amenable to most fiber reinforced composite processing methods, and has become comparable to that used by others investigating epoxy nanocomposites. The epoxy was heated to approximately 60°C to both reduce viscosity and to take into account the melting point of the mPDA cure agent (~62°C) for its subsequent addition. OLS in the amount to achieve the desired final fraction by weight was added directly to the epoxy. Weight fractions of 1%, 3%, 5%, and 7% were investigated where weight fraction was defined by:

$$\text{Wt\%} = \text{weight OLC} / (\text{weight epoxy} + \text{weight cure agent} + \text{weight OLC}) \quad (1)$$

Care was taken to add the OLS slowly to the epoxy while stirring to ensure good mixing. The silicate-epoxy mixture was stirred with a magnetic stir bar at a medium high speed for one hour or more while maintaining the temperature at 60°C. In the baseline process, the mixture was then degassed under vacuum at 60°C, the cure agent was melted in the case of mPDA (in the range of 60 to 65°C), and then the appropriate amount of cure agent was blended well with the epoxy silicate mixture at 60 to 65°C (14 parts per hundred by weight (pph) of epoxy for mPDA; 26 pph for Cure W; and 42 pph for T-403).

One variation on the preparation process omitted the degas step of the epoxy-clay mixture. Preconditioning of the silicate-epoxy mixture was comprised of variations in the elapsed time between preparation of the silicate-epoxy mixture and the addition of the cure agent. This process, here called “advancing”, was achieved at room temperature for periods ranging from a few hours to a number of weeks to achieve distinct morphologies for subsequent testing.

Mixing variations were also performed in an attempt to provide distinct morphologies for mechanical testing. Initial intercalation of the epoxy into the OLS is facilitated by lowering its viscosity. This can be achieved either by heating or by the use of a solvent. In direct initial intercalation, the epoxy and OLS are mixed with a stir bar at temperature. In solvent-assisted initial intercalation, the OLS is initially mixed with acetone and then the epoxy is added. Once the OLS is dispersed in the epoxy, additional mixing is required to ensure maximum intercalation. The manner of additional mixing utilized stirring, high speed shear mixing, bath sonication, and high powered horn sonication in various combinations as summarized in Table 3-1. In all processes, degassing of the mixture was performed prior to cure.

**Table 3-1: Variations in fabrication process of nanocomposites**

<b>Process</b>	<b>Solvent Assisted Initial Epoxy-OLS Mixing</b>	<b>Stir Bar &amp; Temperature Initial Epoxy-OLS Mixing</b>	<b>High Speed Shear &amp; Bath Sonication</b>	<b>Horn Sonication</b>
Baseline	No	Yes	No	No
Process A	No	Yes	No	Yes
Process B	No	Yes	Yes	No
Process C	Yes	No	Yes	Yes
Process D	No	Yes	Yes	Yes

To obtain cured material for subsequent characterization and mechanical testing, plaques were cast between glass plates spaced 0.25 inches apart and cured in a programmable Blue M oven. The standard cure cycle was per manufacturer recommendation for the epoxy resin and selected cure agent, and consisted of heating the resin to 80°C at a rate of 5° per minute, a two hour hold at 80°C, a subsequent ramp to 150°C at rate of 5° per minute, followed by a two hour hold at 150°C and the cool-down to ambient temperature over two hours. This would likely be the process employed if the nano-modified thermoset resin were to be utilized as a matrix material for an advanced fiber reinforced composite.

### **Characterization Techniques**

#### **Thermal Analysis**

Differential scanning calorimetry (DSC) data gives valuable information about the thermal transitions of polymeric materials, providing a foundation for understanding the effects of material variability and compositions and processing history. The insight into the onset of polymerization is often employed in the development of process windows. A typical DSC curve is shown in Figure 3-3, plotting the measured heat capacity against temperature, from which one can determine the onset of the reaction and the degree of cure.

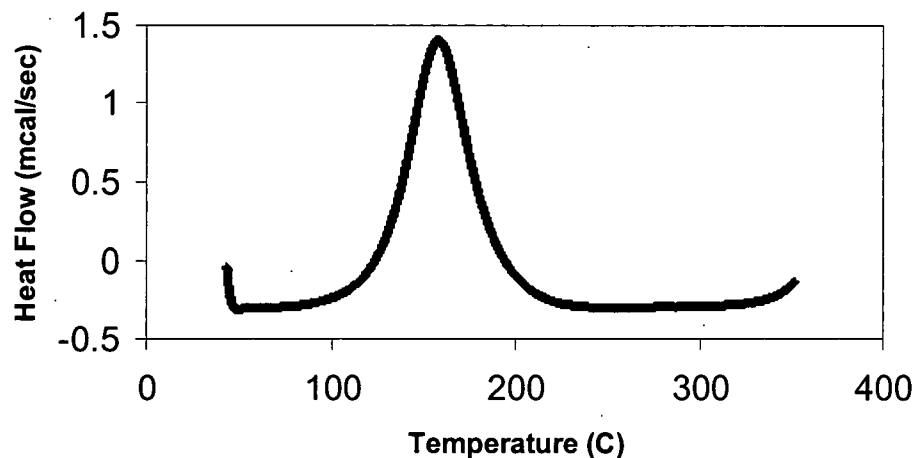


**Figure 3-3:** Differential Scanning Calorimetry (DSC) of Epon 828/mPDA showing reaction onset temperature occurs at approximately 126°C

DSC data was obtained on a Thermal Instruments Differential Scanning Calorimeter 2820 operated at a heating rate of 10°C/minute under nitrogen. Sample size was in the range of 10-20mg, sufficient to cover the bottom of the pan. Peaks related to the exothermic transitions were assessed providing valuable information on the range of temperature over which the curing reaction was completed and the heat of reaction to which degree of cure can be correlated. Heat of reaction was normalized for OLS content.

Dynamic mechanical analysis (DMA) measures the response of a material to a periodic force, providing information on the modulus and mechanical damping of a material. Dynamic mechanical parameters can provide information on transitions, relaxation spectra, crosslinking, and structural or morphological changes that result from processing. A typical data plot is shown in Figure 3-4;  $G'$  is defined as the storage modulus (in torsion), and  $\tan \delta$  as the ratio of the storage modulus,  $G'$ , to the loss modulus,  $G''$ .

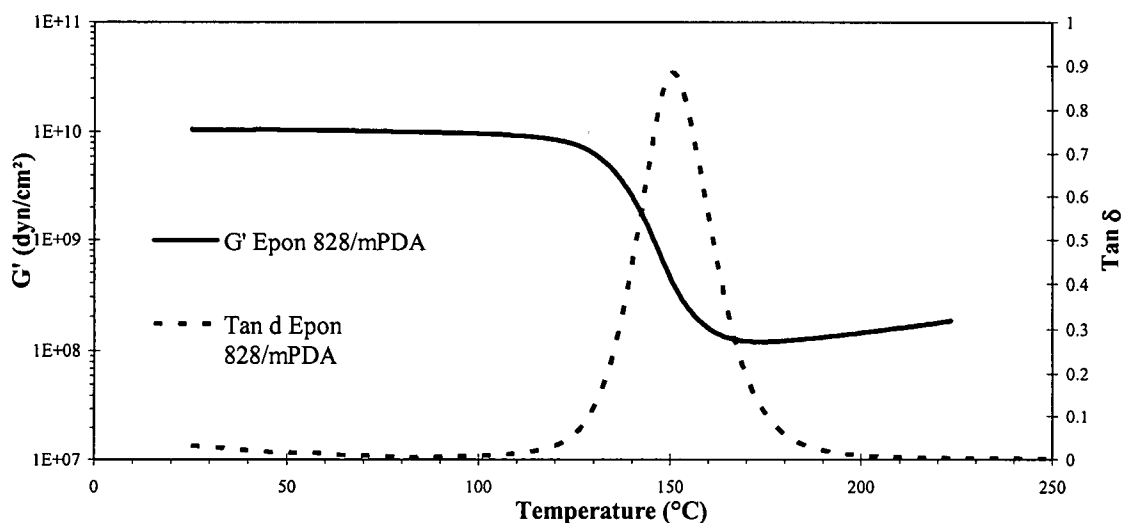


**Figure 3-4:** Dynamic mechanical data for Epon 828/mPDA showing storage modulus ( $G'$ ) and  $\text{Tan}\delta$ , the ratio of storage to loss modulus ( $G''$ ).

Modulus and glass transition temperature of cured nanocomposites were obtained on a Rheometrics Ares Dynamic Mechanical Analyzer in torsion mode at  $2^{\circ}\text{C}/\text{minute}$ , 100 radians/sec, 0.1% strain. The glass transition temperature, or  $T_g$ , is a second order transition in which the heat capacity undergoes a change from a lower value to a higher value. This change is not sharp, but occurs over a range of about 10 degrees.  $T_g$  measurements were determined from the DMA loss modulus peak as measured from 2.5 inch x 0.5 inch specimens. These transitions can also be defined by the inflection point of the change from the DSC data; the onset of the reaction extrapolated from this inflection point. Some subambient analysis was also performed in torsion mode by a continuous scan at  $5^{\circ}\text{C}/\text{minute}$  from  $-150^{\circ}\text{C}$  to  $200^{\circ}\text{C}$  to investigate other relaxations.

## X-ray Analysis

X-ray diffraction and scattering provides rapid globally averaged information on submicroscopic features of materials. X-ray analysis is uniquely suited to the study of crystalline structures and mineral based compositions such as layered silicate nanocomposites, and has been used historically for the identification of clay-minerals since the 1930s. Information about the number of OLS sheets in registry, the d-spacing or gallery height, and the relative order of the sheets within the epoxy can be gained from x-ray analysis of layered silicate nanocomposites [73-76].

Wide angle x-ray diffraction (WAXD) was initially performed for quick assessments of processing-morphology relationships in early investigations on a Rigaku X-ray Powder Diffractometer, with Cu K $\alpha$  radiation ( $\lambda = 1.5418 \text{ \AA}$ ). Samples were cast in silicone molds to provide specimens of 2 inch x 1 inch x 1/8 inch. A 0.5° divergent source slit was used. Generator power was set at 40 kV and 150 mA, and the scan mode was continuous at a rate of 0.8°/ minute, typically through 2° to 10°. Diffraction from the lattice of the layered silicates takes place according to Bragg's law,

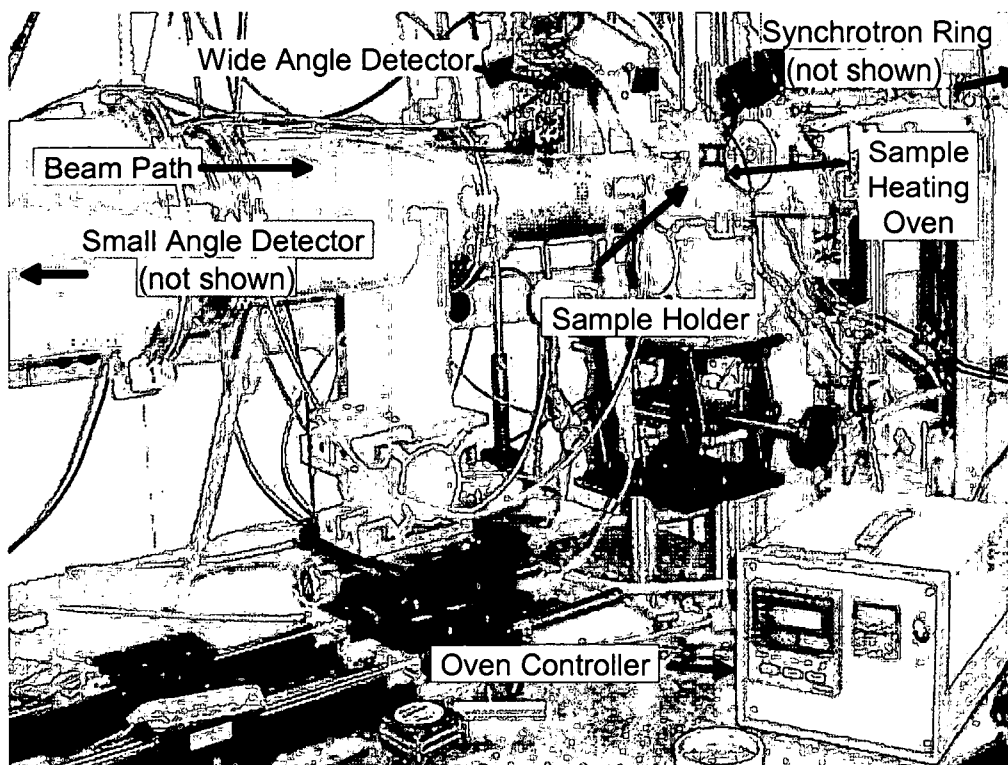
$$n \lambda = 2d \sin \theta \quad (2)$$

where  $n$  is the order of reflection, an integral value consistent with the number of wavelengths in the path difference between rays scattered by adjacent planes;  $\lambda$  is the wavelength of the incident x-ray beam;  $d$  is the spacing between adjacent planes of atoms in a crystalline phase (hence silicate layers that are parallel to one another); and  $\theta$  is the

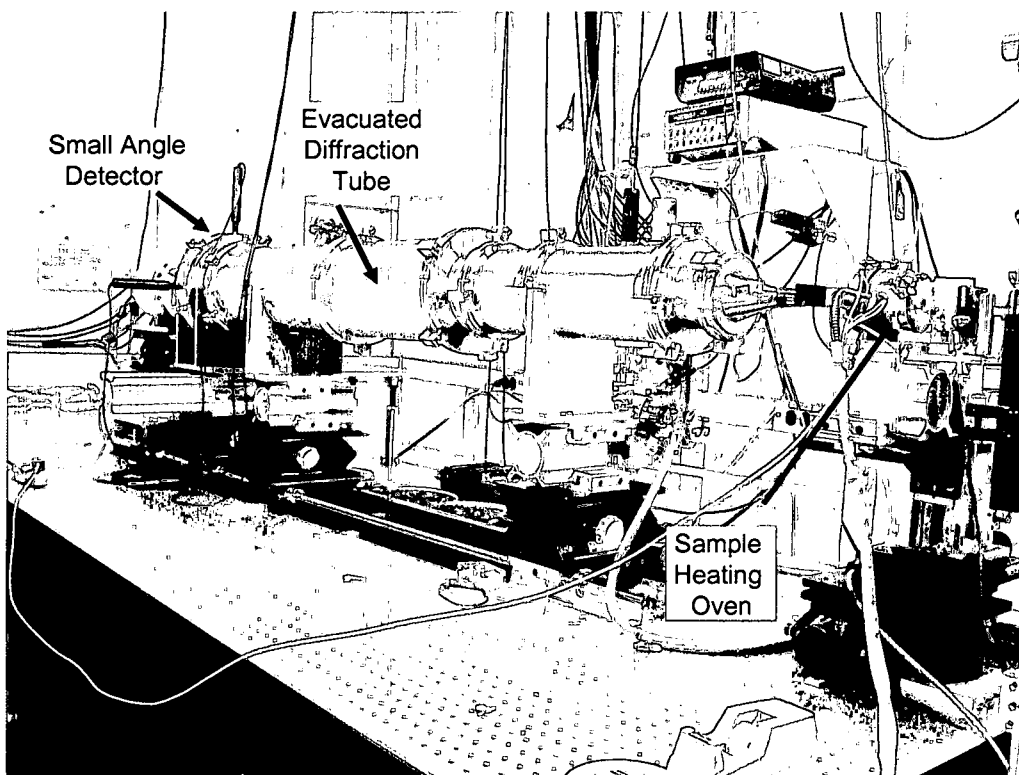
angle of incidence corresponding to a given  $\lambda$  and  $d$  at which diffraction occurs (corresponding to  $n = 1, 2, 3, \dots$ ). Detection down to  $2\theta$  of  $2^\circ$  allows for the characterization of basal spacings only up to  $44 \text{ \AA}$ , making WAXD a tool of limited use.

Small angle x-ray scattering (SAXS) measures scattering very near a highly collimated direct beam, providing data at smaller angles than is accessible with WAXD and hence an ability to detect large morphologies. SAXS therefore is a valuable tool for probing the higher basal spacings of exfoliated morphologies, and can be set up to capture information on structural features on the range of 10's of  $\text{\AA}$  (representative of OLS d-spacings) through 100's of  $\text{\AA}$  (representative of widely expanded or exfoliated OLS d-spacings). When coupled with synchrotron radiation sources, SAXS becomes a very powerful tool. Synchrotron radiation supplies a flux of x-rays much greater than that which can be obtained with conventional x-ray sources, enabling measurement of samples undergoing dynamic morphology evolution and the study of real-time morphology development.

*In situ* SAXS measurements were conducted at the National Synchrotron Light Source at Brookhaven National Laboratory on Beamline X27C utilizing a 1-D detector ( $\lambda = 0.1366 \text{ nm}$ ). Source-to-detector distances were typically on the order of 190 cm. Silver Behenate was used as a standard for calibration for the small angle scattering regions, and Aluminum Oxide ( $\text{Al}_2\text{O}_3$ ) was used as a standard for the wide angle scattering region. A programmable oven cell was placed within the x-ray beam for processing studies as shown in Figure 3-5.



(a)



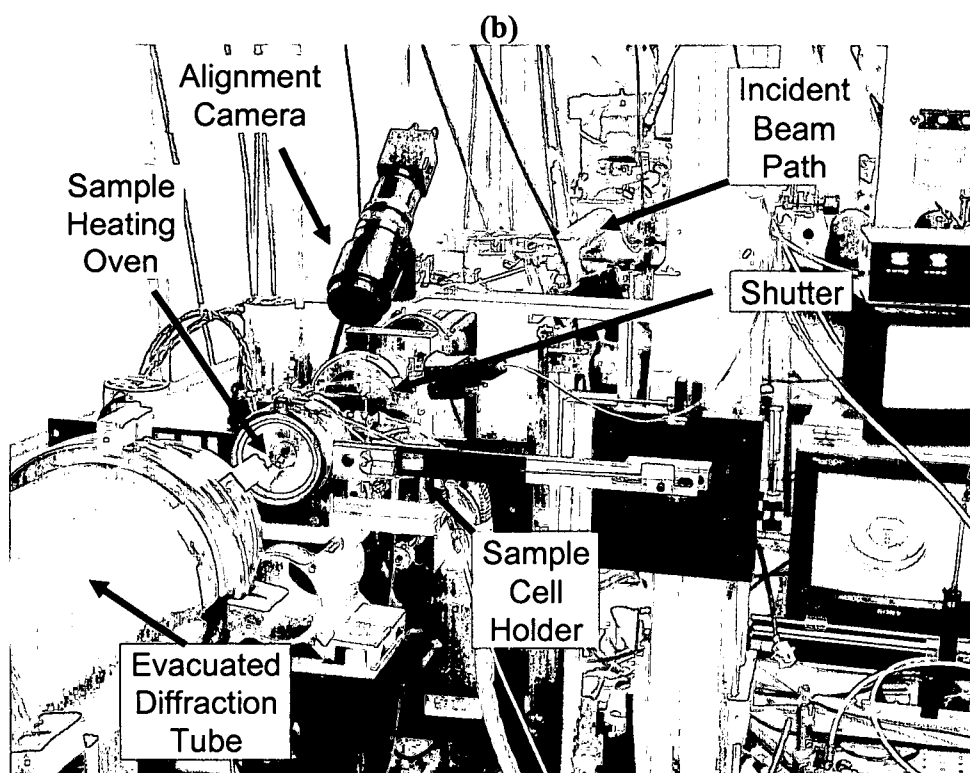


**Figure 3-5:** Beamline X-27C at Brookhaven National Laboratory (a) view looking towards beam source and showing programmable oven, (b) view looking towards detector, and (c) close up view of sample cell holder and oven.

Epoxy-silicate-cure agent mixtures were prepared and placed in a copper sample cell with Kapton tape windows. The sample cell was placed into the sample holder, which was then placed in the oven within the x-ray beam. The thickness of the sample thus formed was approximately 2 mm. Scattering data, comprised of intensity ( $I$ ) versus detector position, was collected and stored for subsequent analysis. A data scan was performed each minute. The scattering momentum transfer vector  $q$  was calculated from the calibrated detector position and is defined as

$$q = (4\pi/\lambda)\sin\theta \quad (3)$$

where  $\theta$  is half the scattering angle and  $\lambda$  is the wavelength of the incident beam.

Information on the development of layered silicate nanocomposite morphology can be obtained from analysis of small angle scattering data, ranging from the absence or presence of a Bragg peak; the evolution of the peak position with material composition and processing conditions; the breadth of the peak (which relates to degree of order); and power law decay at low  $q$  for large-scale organization information. The position of the initial peak provides information on the size of the developing structure through the relationship between the basal plane separation,  $d$ , and the scattering vector,  $q$ :

$$q = \frac{2\pi}{d} = \frac{4\pi}{\lambda} \sin \theta \quad (4)$$

The relative intensity provides information on the number of scattering structure. Peak breadth provides information on the scattering domains through the Scherrer equation:

$$L_{(hkl)} = \frac{K\lambda}{\beta \cos \theta} \quad (5)$$

where  $L$  is the crystallite dimension in angstroms perpendicular to the reflection plane (thickness),  $K$  is a constant approximately equal to 1, and  $\beta$  is the width of the peak at half height in radians. Broader peaks correspond to smaller scattering domains, sharper peaks to larger domains. Investigations of the  $q$  regions corresponding to the intercalated morphology and the exfoliated morphology were performed separately. An idealized

representative data set is shown in Figure 3-6 to illustrate the type of information that can be obtained through scattering methods.

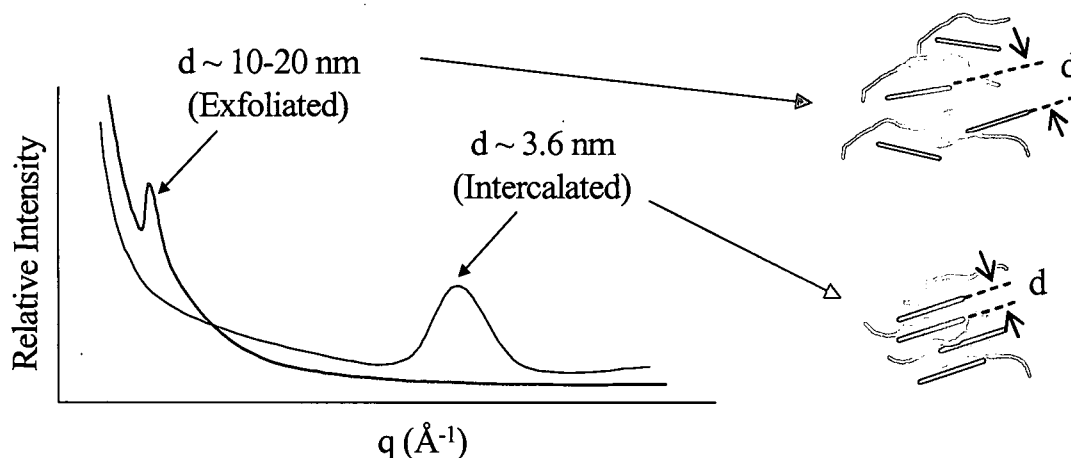


**Figure 3-6:** Representative data curves for idealized nanocomposite morphologies

Experiments were conducted at various heating rates and isothermal temperatures. To ensure that the nanocomposite was not significantly affected by the radiation during its cure within the high intensity x-ray beam, secondary post-cured readings on new areas of multiple samples were compared with final *in situ* readings. No difference in the primary basal plane reflections were observed, suggesting that any degradation that may have occurred in the material that was directly in the beam line during the curing process and data collection did not affect the final SAXS data. Scattering data were corrected for background and fitted through the use of PeakFit™ curve fitting software.

## Microscopy

X-ray studies are well suited to capturing averaged information about morphology, and in the case of synchrotron sources, to study real-time morphology development as a function of processing. Microscopy complements such studies with specific local morphology information. Neither method alone provides information on a sufficient volume of material from which to draw overall morphology conclusions, especially in light of the multiple combinations and scales on which morphologies can occur. Therefore their combined use is critical in the study of nanocomposites. This observation highlights a current challenge with this class of materials: the ability to probe and characterize at the nanoscale is limited by our current suite of tools. It is anticipated that this will change with time and accurate measurements of both constituent materials and interfaces in nanocomposites will become viable.

Transmission electron micrographs were obtained on cryomicrotomed samples prepared to minimize deformation-induced morphologies using a Reichert-Jung ultracut microtome equipped with a 45° diamond knife and mounted on 200 mesh copper grids. Bright field images were obtained on a Phillips CM200 transmission electron microscope with a LaB<sub>6</sub> filament operating at 200kV. Scanning electron microscopy (SEM) of gold coated fracture surfaces of cured nanocomposites was performed on JEOL JSM-6100. Gross energy dispersive spectroscopy (EDS) was performed on a ThermoNoran Voyager on fracture surfaces of cured nanocomposites to investigate elemental concentrations which could be correlated to morphology differences due to preconditioning.

### **Fourier Transform Infrared Analysis (FTIR)**

FTIR analysis was performed to assess effects of preconditioning on the polymerization reactions. Background spectra was run before each specimen spectrum. Infrared spectra were recorded using a Nicolet Magna-IR 560 Spectrometer in reflectance mode (Thunderdome attachment) at a resolution of  $4\text{ cm}^{-1}$  for 64 scans to obtain each spectra.

### **Mechanical Property Characterization**

Fracture toughness was calculated from compact tension specimens per ASTM Standard E399 under ambient conditions. Fracture toughness is a property that is sensitive to morphology, and one that has been shown to be modifiable by very small particles or second phases such as rubber. Cured specimens were cut to 0.75 inch x 0.75 inch on a diamond saw; a notch was cut into them with a diamond cutting wheel, then a pre-crack made by tapping a razor blade into the end of the notch. Specimens were loaded in a MTS frame at a displacement rate of 0.0009 inch/second. At the onset of cracking, the specimen was unloaded and the crack tip length measured. Specimen measurements were made on an Olympus light microscope, and both top and bottom surfaces were measured for the crack dimension and the values averaged for calculations. Statistical data were typically generated from three loadings per sample and multiple samples per material batch.

Calculations for fracture toughness were made following ASTM standard E399. This standard was developed for metallic materials and is based on linear elastic fracture mechanics (LEFM), defining the stress intensity factor by assuming a linear elastic

material in a state of plane strain. As thermoset materials are fairly brittle as compared to metallic materials (where  $K_{IC}$ 's can range from 30-40 ksi-inch<sup>1/2</sup> for aluminum alloys up to 65-185 ksi-inch<sup>1/2</sup> for steels; epoxies are in the range of 0.55-0.90 ksi-inch<sup>1/2</sup>), it is appropriate to assume that the plastic zone is small compared to the crack length and other geometric dimensions and hence that the behavior is linear-elastic. This will be discussed further in the Discussion Chapter.

The calculations provide a conditional result  $K_q$ , the value of the stress intensity factor where a material begins to crack significantly, from the following equation:

$$K_q = (P_q/bW^{1/2})(f(a/W)) \quad (6)$$

where  $P_q$  is the load (lbf) at crack propagation,  $b$  is the specimen thickness (inches),  $W$  the specimen width (inches), ' $a$ ' the crack length (inches), and  $f(a/W)$  is determined from

$$f(a/W) = (2+a/W)(0.866 + 4.64a/W - 13.32 (a/W)^2 + 14.72 (a/W)^3 - 5.6(a/W)^4)/(1-a/W)^{3/2}. \quad (7)$$

Slow stable crack growth may follow  $K_q$  until the critical stress intensity factor,  $K_c$  is reached.  $K_q$  and  $K_c$  have similar values and are also similar to the plane strain fracture toughness,  $K_{IC}$ , if the plastic zone is small compared to the specimen thickness and dimensions, which is when a state of plane strain can be assumed. In such a state, only limited slow-stable crack growth occurs, and  $K_{IC}$  represents a worst case value and can be

used for any material thickness. Since the behavior of the crack is affected by the plastic zone that forms at the crack tip, and since the plastic zone thickness is thickness dependent,  $Kq$  may decrease with increasing thickness. To ensure a state of plane strain, the thickness of the specimen must be sufficient and the requirement of

$$b \geq 2.5 (Kq/\sigma_{YS})^2 \quad (8)$$

where  $\sigma_{YS}$  is the material yield strength in tension as determined by a 0.2% offset is often employed. In the case where this thickness condition is satisfied, plane strain can be assumed, linear elastic fracture mechanics are applicable, and  $Kq$  can be assumed to be representative of the worst case value of  $K_{IC}$ . Published values for tensile strength and toughness for 828/mPDA are in the range of 8 ksi and 650 psi-in<sup>1/2</sup>. Based on these values, and assuming that the tensile and yield strengths are approximately equal for this brittle material system,

$$b \text{ selected as } 0.25 \text{ inch} \geq 2.5 (Kq/\sigma_{YS})^2 = 0.0164 \text{ inch}$$

Alternative specimen dimensions than those called out in the standard are acceptable as long as they have thickness and width such that  $0.5 W \geq b \geq 0.25 W$ , and therefore the miniature specimen size was utilized in this work to allow for fabrication of small batches of nanocomposite materials.

Yield strength (and modulus and strain to failure) was obtained from tensile specimens per ASTM D638 under ambient conditions. Although flexural test configurations can be used for small samples of materials, this tensile test method is most widely used to obtain data from advanced composites and other structural materials. It has also been suggested that when moduli are determined in flexure, properties at the surface are emphasized at the expense of the interior; for filled polymers, the surface may have a 'skin' which has a lower loading than the interior [44]. Cured specimens were machined to a tensile dog bone of 6.5 inch length with a center gage section of 2 inches, radius of fillet of 3 inches, gage widths of 0.5 inches, and tab width of 0.75 inches. The specimens were loaded in a MTS frame equipped with an extensometer and loaded to a strain rate of 0.05 inch/minute until failed. Tensile strength at failure and modulus were calculated from the loading results. The average properties were typically generated from testing at least three specimens where possible.

### **Uncertainty and Error Analysis**

Discussion of uncertainty and error is important for research in nanomaterials due to the small amounts of nanoconstituents used, the small size of material/specimens, and the current lack of understanding of the manner in which these materials behave. Error in this research could be introduced with physical measurements and weights. The digital calipers used for measuring dimensions were accurate to 0.001 inches; however, variation could be introduced depending on the consistency of pressure used during measurements.

Accuracy of the weights of epoxy, cure agent, and OLS depended on the scale that was being used; the scales used for weighing the cure agent and the OLS (dry ingredients) are accurate to within 0.0001 gram; the scale for weighing out the epoxy was accurate to 0.01 gram. For the standard material batch size of 100 grams epoxy, 6 grams OLS, and 14 grams cure agent, the error introduced by measurements would not be sufficient to significantly alter the stoichiometry. However, an additional source of error was introduced due to the difficulty of working with the mPDA cure agent, which must be melted at approximately 65°C and not allowed to re-crystallize during the period where it is poured into the epoxy-OLS mixture. It is very challenging to achieve an accurate measurement as a slight amount of mPDA typically experiences some minimal re-crystallization during the transport and introduced error up to 0.5 grams or 3-4%.

The intrinsic uncertainty associated with each instrument must be kept in mind. The thermal analysis equipment is accurate and repeatable to  $\pm 0.1^\circ\text{C}$  in the standard DSC mode, with constant calorimetry sensitivity of  $\pm 2.5\%$  from  $-100^\circ\text{C}$  to  $500^\circ\text{C}$ .

Uncertainty in data from mechanical testing is dominated by that found in the miniature compact tension testing for fracture toughness, a test that is known to have a degree of scatter. Variation in the initial starter crack is a potential source of error. The microscope on which the crack lengths were measured was accurate to 0.1 mm. Loads from the plotted data can be read to within 0.1 pounds. The MTS load frame used is capable of 5000 pounds and is used in the 500 pound range with accuracy of 0.001%.

This provides accuracy at the worst case of five pounds and at the best one-half pound.

The loads used in this study were in the range of tens of pounds.

In the case of the SAXS data, the uncertainty is not constant as the synchrotron x-ray source intensity decreases slightly over time. BNL's beamline is replenished every twelve hours, for during this time the x-ray beam current decreases by approximately 30%. Absolute intensity therefore changes by approximately 30%. Errors near higher  $q$  (larger distance between the beam center line and the detector position pixel) are less than those near lower  $q$ . For the experiments performed here, structures on the order of 35 to 100 angstroms were of interest. In this range, a pixel related to approximately a  $q$  value in the range of 0.0007 to 0.0009 or approximately 40 pixels to an angstrom providing resolution on the order of an angstrom. At  $q$  associated with structures of 100 angstroms, a change of  $q$  of 0.0005 results in a change of five angstroms; at  $q$  associated with structures of 35 angstroms, a 0.0005  $q$  translates to a change of one angstrom.

The raw diffraction data, intensity versus pixel location on the detector, is corrected by calibration with a reference material for which the crystallographic distances are known. This converts the raw pixel intensity data to  $q$ , the scattering vector, which relates to distance. Background intensities, caused by scattering from the sample cell's Kapton windows, from the window of the detector vacuum chamber, and from the beam stop, were determined by separate measurements on empty sample cells and subtracted. Background scattering is an additional source of error for absolute intensity. However,

for this research, the  $q$  value was the important parameter, and it did not vary with the intensity.

The various measurements and experiments represent sources of error in this research, yet the findings of this research provide important observations and trends that can be used in the development of morphology models and insight into the role of morphology on toughening mechanisms.

## CHAPTER IV

### RESULTS

This chapter provides representative results of the various experiments performed for subsequent analysis and discussion. Full data sets are included for reference in the Appendices, including those taken to support or corroborate observations and conclusions.

Approaches were explored to develop materials in which only the nanoscale morphology varied to assess the role of morphology – intercalated or exfoliated – on fracture toughness. The ability to fabricate controlled morphologies is a significant challenge for epoxy-based nanocomposites, as this research shows. Characterization of both final morphology and real-time morphology development was therefore performed to determine how processing variables affect morphology. *In situ* SAXS studies provided valuable insight into material and process subtleties that may play a role on ultimate morphology development. Thermal analysis was performed to assess the impact of epoxy cure on morphology development.

Two different OLS were utilized to explore the sensitivity of morphology development on materials. This was extended to explore material pre-conditioning variations and cure agents to further investigate the manner in which exfoliated morphology develops. For the SAXS, data exist for every minute of each experiment which in some cases extend over a period of several hours. Data shown in this chapter are selected to represent the significant trends and events only. Where appropriate, however, all of the data were analyzed for interpretation and discussion.

Process-morphology and morphology-property relationships have been well-established for rubber toughened epoxy systems and show that there may be multiple, potentially competing or sequential reactions, and phase separations during the transformation of the low molecular weight material to a glassy network. Yet for nanocomposites, not only is the effect of dimension not well understood, but approaches that focus on the role of processing on morphology as well as the role of morphology on properties are not yet routine. And unlike classical rigid particles that have been incorporated into polymers, organically modified layered silicates are an active player in network formation as this and other research shows. The results from the thermal and x-ray analyses couple to provide new insight into morphology development paths. These contributions to the understanding of how morphology develops with processing are critical for eventual control of morphologies for desired property enhancements.

## **In situ SAXS Study Results**

### **Temperature as a Variable in Morphology Development via SAXS**

*In situ* SAXS data show that morphology development can be greatly affected through use of different processing temperatures. For isothermal processing, higher temperatures result in more rapid onset of gallery expansion and a larger final gallery or d-spacing. This trend was consistent for both the I.30E and SC18 systems. *In situ* SAXS data for selected isothermal processes are shown in Figures 4-1 through 4-4. Scattering data from various times within a process are selected to show significant events and trends, and offsets are adjusted for clarity and to provide easy comparison of trends.

At low temperatures, the peak associated with d-spacing of the initial epoxy-intercalated gallery, seen in the data scan at one minute, shows negligible change in intensity or d-spacing over a 60 minute period as seen in Figure 4-1. There appears to be minimal change in morphology at this temperature, with d-spacing increasing from the initial 33 Å only on the order of 1 Å.

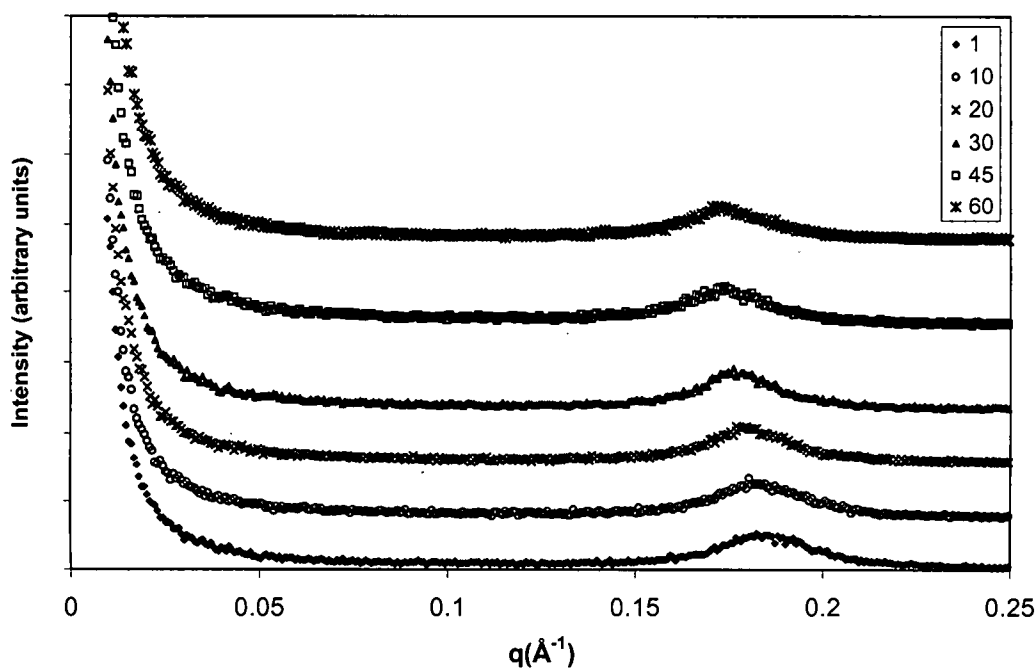


**Figure 4-1:** Time-dependent small angle x-ray scattering data for 5% I.30E/Epon 828 with mPDA at isothermal temperature of 60°C after 1, 10, 20, 30, 45 and 60 minutes (intensity data offset for clarity).

At higher temperatures the peak associated with initial d-spacing broadens, reduces in intensity and shifts to lower  $q$  (higher d-spacing), and eventually disappears as seen in Figures 4-2 and 4-3. The time for this peak to disappear is shorter at higher temperatures. A peak at low  $q$  is observed to develop with time, indicative of ordered d-spacing of higher values. This peak is seen to emerge more quickly at higher temperatures.

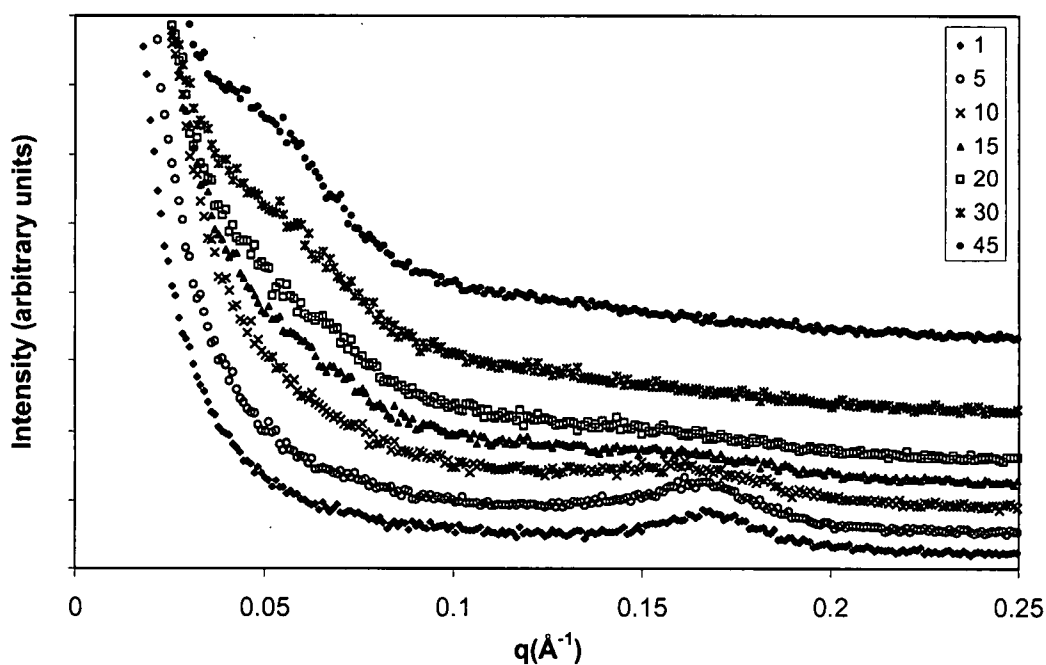


**Figure 4-2:** Time-dependent small angle x-ray scattering data for 5% SC18/Epon 828 with mPDA at isothermal temperature of 70°C after 1, 5, 10, 15, 20, 30 and 45 minutes.

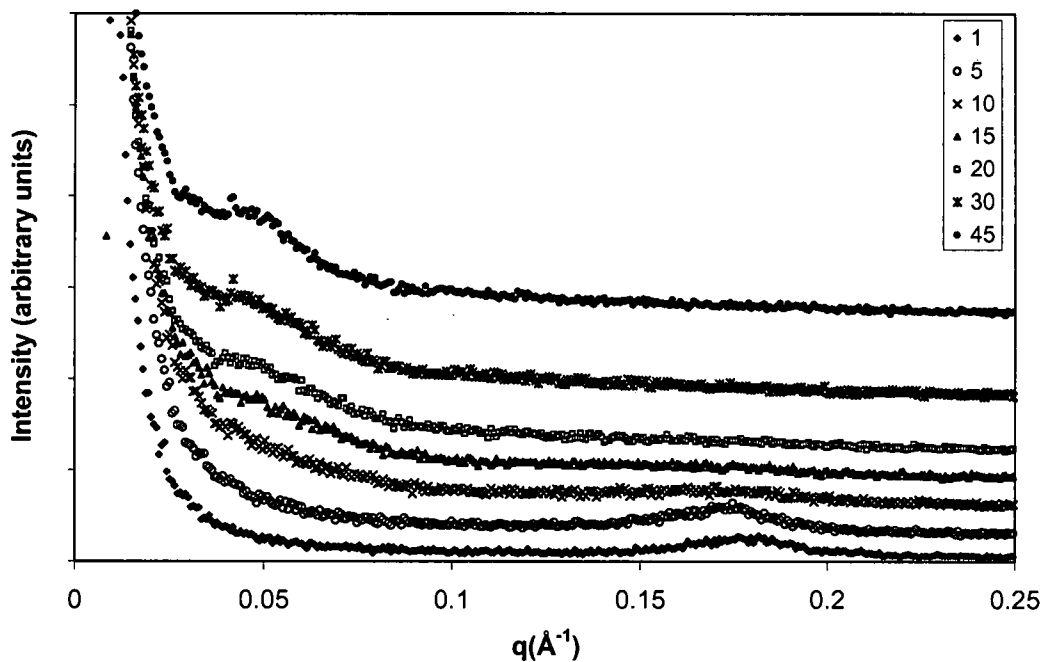


**Figure 4-3:** Time-dependent small angle x-ray scattering data for 5% SC18/Epon 828 with mPDA at isothermal temperature of 80°C after 1, 5, 10, 15, 20, 30 and 45 minutes.

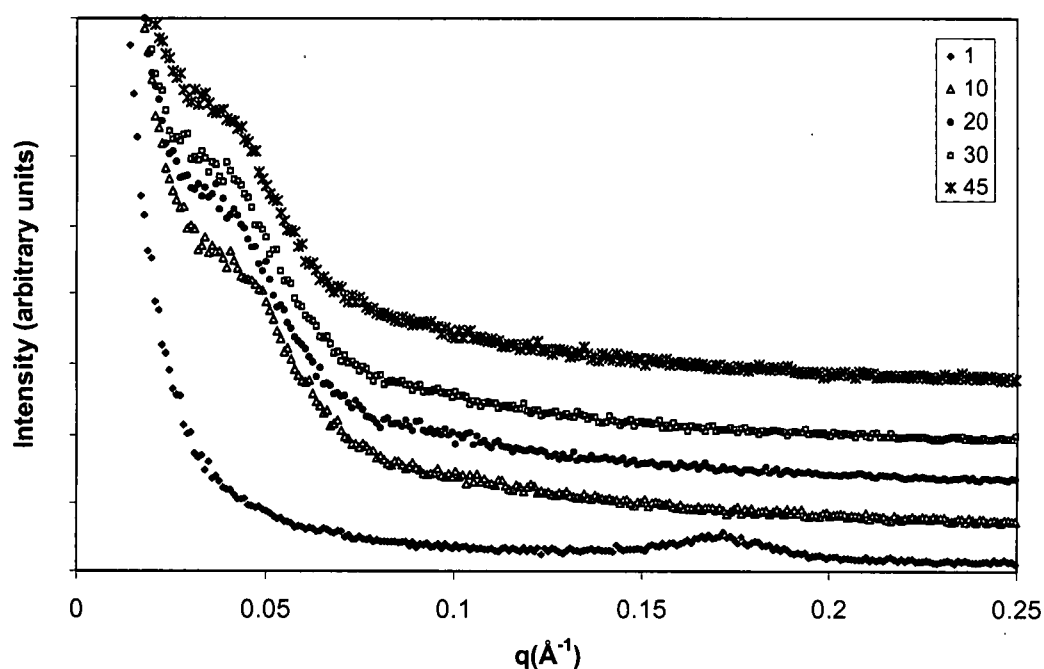


**Figure 4-4:** Time-dependent small angle x-ray scattering data for 3% SC18/Epon 828 with mPDA at isothermal temperature of 100°C after 1, 10, 20, 30 and 45 minutes.

Tables 4-1 and 4-2 summarize pertinent morphology information that has been drawn from the analysis of the scattering data and will be discussed in the next chapter.

**Table 4-1:** *In situ* SAXS Studies on Isothermal Temperature Processes versus Morphology Development for I.30E/828/mPDA Nanocomposites

Silicate	Isothermal Temperature (C)	Initial d-Spacing (Å)	Loss of Intercalation Peak (Minutes)	Final d-Spacing (Å) <sup>a</sup>
I.30E	60°	33 Å	168	33 Å
I.30E	70°	38 Å	> 45 <sup>b</sup>	38 Å
I.30E	80°	34 Å	22	42 Å
I.30E	90°	34 Å	19-20	140 Å
I.30E	100°	35 Å	15	140 Å
I.30E	110°	35 Å	9-10	150 Å

<sup>a</sup> Final Time: 45 Minutes

<sup>b</sup> Duration of run 45 minutes; exfoliation not initiated within run duration

**Table 4-2: *In situ* SAXS Studies on Isothermal Temperature Processes versus Morphology Development for SC18/828/mPDA Nanocomposites**

Silicate	Isothermal Temperature (C)	Initial d-Spacing (Å)	Loss of Intercalation Peak (Minutes)	Final d-Spacing (Å) <sup>a</sup>
SC18	60°	36 Å	85	46 Å
SC18	70°	37 Å	28	140 Å
SC18	80°	36 Å	10	125 Å <sup>b</sup>
SC18	90°	36 Å	8	153 Å
SC18 <sup>c</sup>	100°	37 Å	5	180 Å
SC18 <sup>c</sup>	110°	37 Å	3	185 Å

<sup>a</sup> Final Time: 45 Minutes

<sup>b</sup> Final Time: 15 Minutes

<sup>c</sup> Data on 3% weight fraction of silicate

### Temperature Rate as a Variable in Morphology Development via SAXS

Heating rates are observed to affect morphology development. Unlike the isothermal process, all of the heating rate processes provided for significant expansion of the galleries as evidenced by development of peaks at low  $q$  values associated with high final d-spacings. Higher heating rates drive faster disruption of the initial morphology as seen by the broadening and loss of the peak associated with the initial intercalated d-spacing. Final d-spacings appear to be greater for the higher heating rates as well. *In situ* SAXS data for heating rate processes are shown in Figures 4-5 through 4-9. Scattering data selected to show significant events and trends is depicted for various heating rates, from 2 degrees/minute through 12 degrees/minute. Summaries of key data are provided in Tables 4-3 and 4-4.

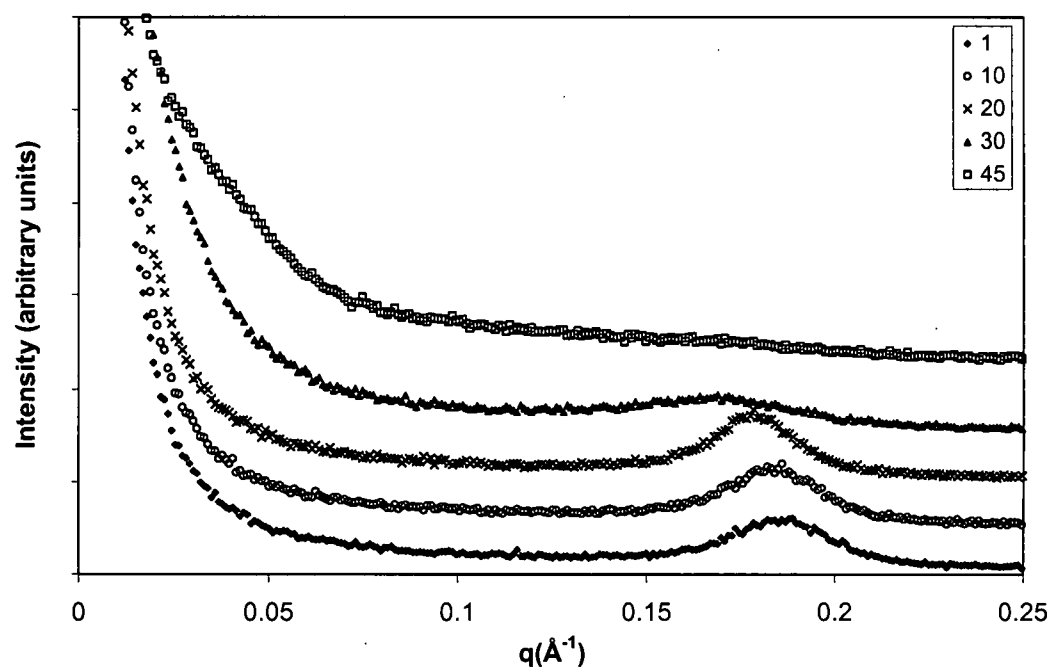


**Figure 4-5:** Time-dependent small angle x-ray scattering data for 5% I.30E/Epon 828 with mPDA at heating rate of 2°C/minute.

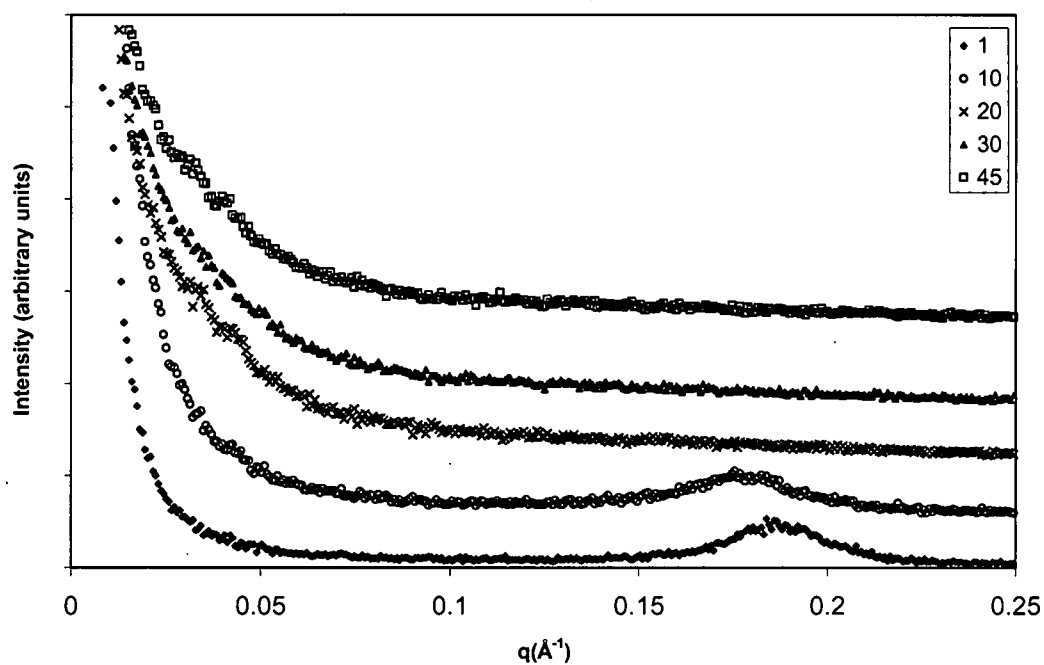


**Figure 4-6:** Time-dependent small angle x-ray scattering data for 5% I.30E/Epon 828 with mPDA at heating rate of 10°C/minute.

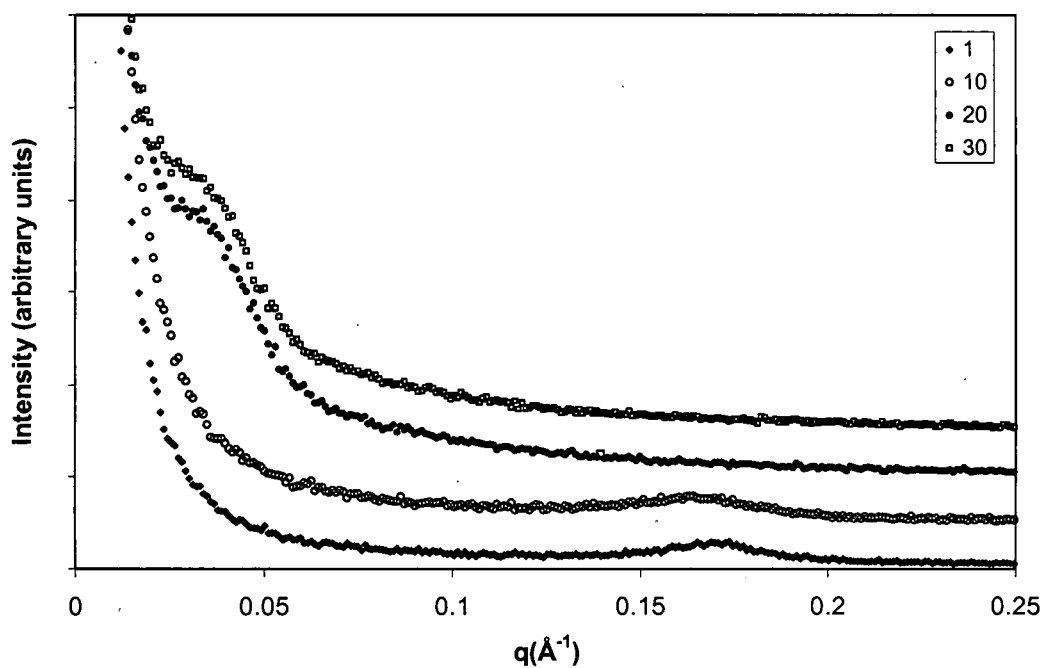


**Figure 4-7:** Time-dependent small angle x-ray scattering data for 5% SC18/Epon 828 with mPDA at heating rate of 5°C/minute.

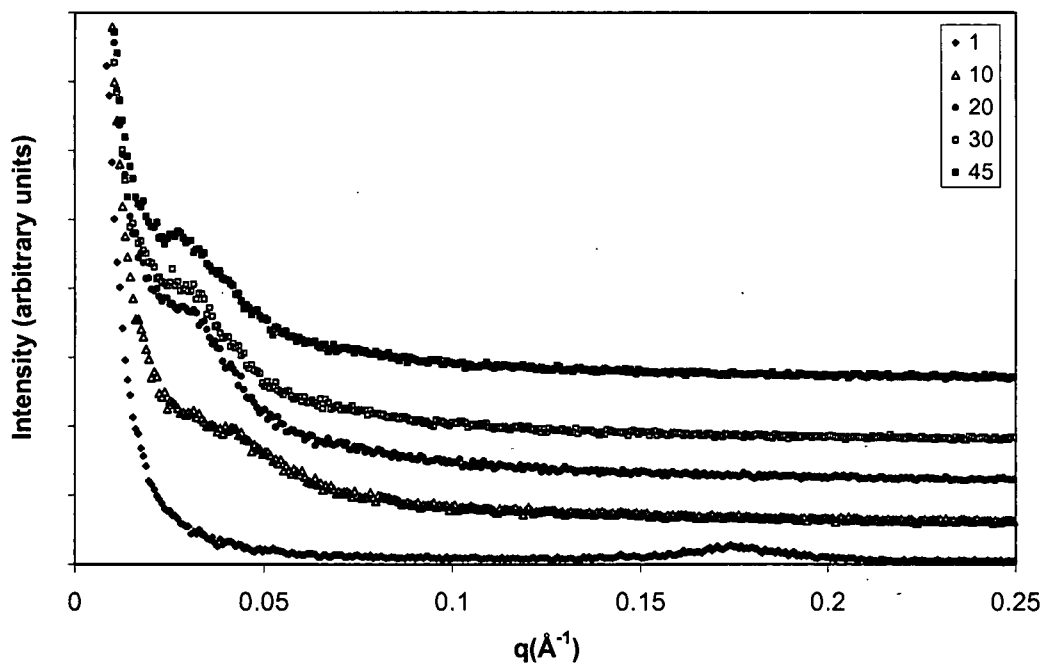


**Figure 4-8:** Time-dependent small angle x-ray scattering data for 5% SC18/Epon 828 with mPDA at heating rate of 10°C/minute.

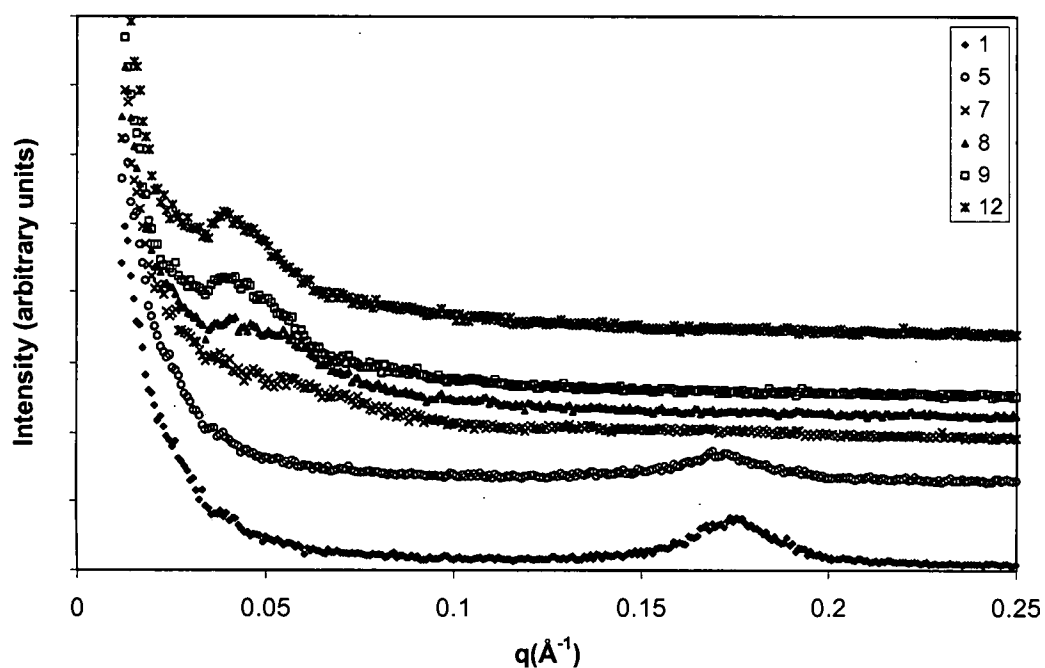


**Figure 4-9:** Time-dependent small angle x-ray scattering data for 5% SC18/Epon 828 with mPDA at heating rate of 12°C/minute.

**Table 4-3:** *In situ* SAXS Studies on Heating Rate Processes versus Morphology Development for I.30E/828/mPDA Nanocomposites

Silicate	Temperature Profile	Initial d-Spacing (Å)	Loss of Intercalation Peak (minutes)	Final d-Spacing <sup>a</sup> (Å)
I.30E	2°/Min Ramp	33 Å	36	155 Å
I.30E	5°/Min Ramp	33 Å	16	216 Å
I.30E	5.3°/Min Ramp	34 Å	15	225 Å <sup>b</sup>
I.30E	6°/Min Ramp	35 Å	10	180 Å <sup>c</sup>
I.30E	10°/Min Ramp	34 Å	12	216 Å
I.30E	12°/Min Ramp	34 Å	10	210 Å <sup>c</sup>

<sup>a</sup> Final Time: 45 Minutes

<sup>b</sup> Final Time: 30 Minutes

<sup>c</sup> Final Time: 25 Minutes

**Table 4-4:** *In situ* SAXS Studies on Heating Rate Processes versus Morphology Development for SC18/828/mPDA Nanocomposites

Silicate	Temperature Profile	Initial d-Spacing (Å)	Loss of Intercalation Peak (minutes)	Final d-Spacing <sup>a</sup> (Å)
SC18	2°/Min Ramp	36 Å	17	300 Å
SC18	5°/Min Ramp (5/01)	35 Å	9-10	210 Å
SC18	5°/Min Ramp (5.3)	37 Å	12	180 Å
SC18	10°/Min Ramp	36 Å	10	225 Å
SC18 <sup>2</sup>	12°/Min Ramp	36 Å	7	166-170 Å <sup>b</sup>

<sup>a</sup> Final Time: 45 Minutes

<sup>b</sup> Final Time: 13 Minutes

#### Role of OLS on Morphology Development via SAXS

For any given isothermal or heating rate experiments, the SC18 system was observed to undergo morphology development more quickly than the I.30E systems. The SC18 systems also reached higher d-spacings than the I.30E systems at a given time under similar temperature profiles. These data can be seen in the preceding Tables. Figures in the Appendices are also plotted for each condition and clearly depict this difference between the two organoclays studied. Figures 4-10 and 4-11 illustrate a comparison that is exemplary of the key differences in morphology development that are seen in all of the comparisons of the two OLS for a given process. In these figures, scattering data for set times under isothermal heating at 80°C are selected to show significant events and trends.

Mixtures of the two organoclays were observed to develop morphology similar to the slower developing system, I.30E, as shown in Figure 4-12.

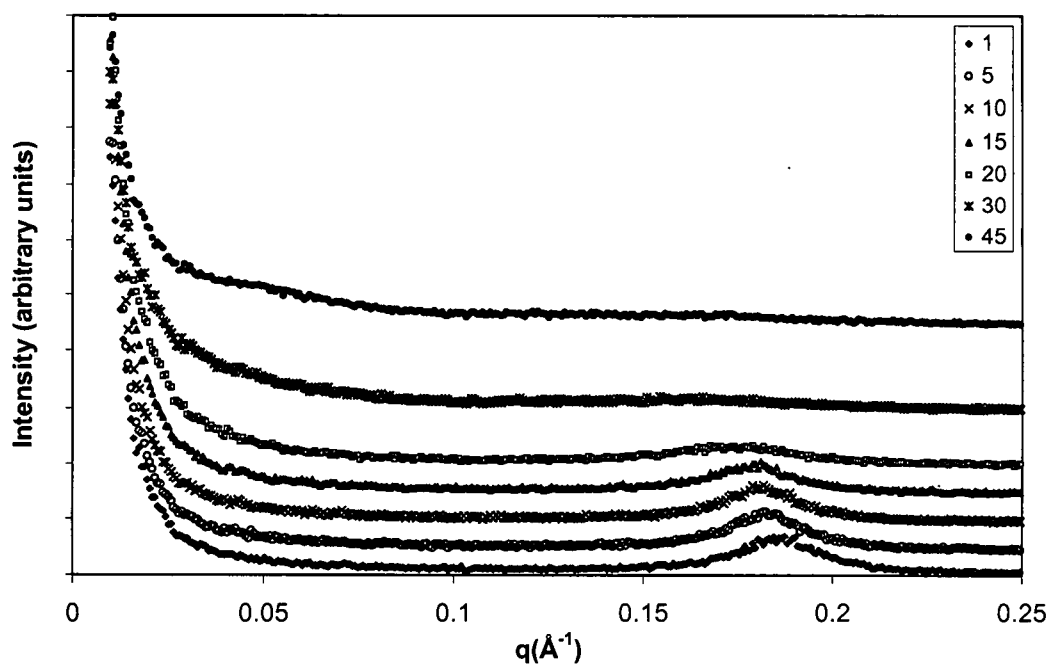


**Figure 4-10:** Time-dependent small angle x-ray scattering data for 5% I.30E/Epon 828 with mPDA at isothermal temperature of 80°C.

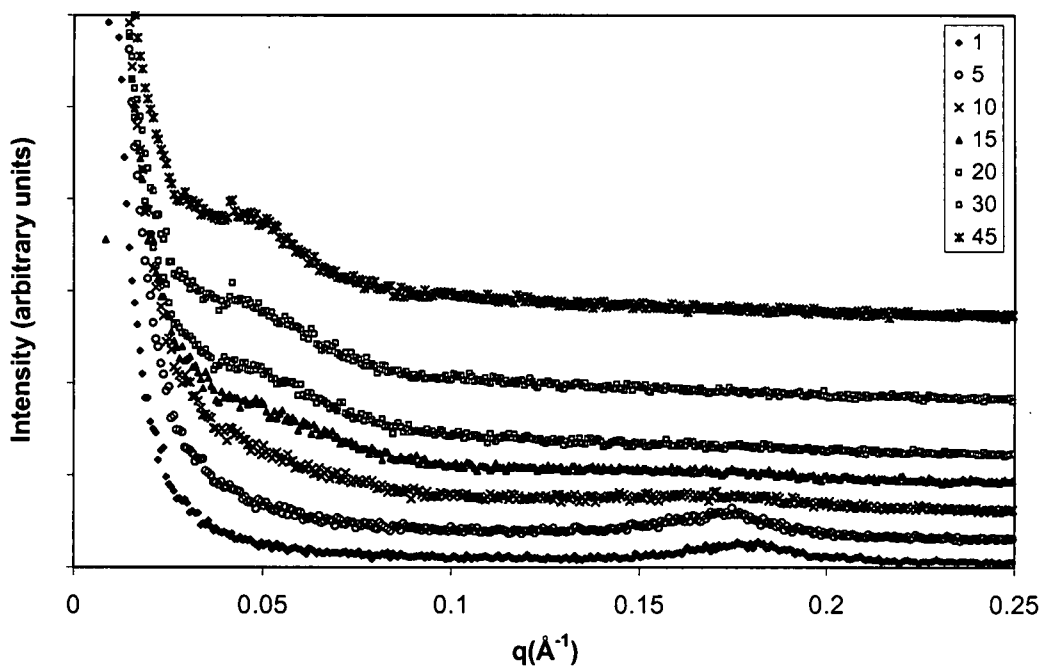


**Figure 4-11:** Time-dependent small angle x-ray scattering data for 5% SC18/Epon 828 with mPDA at isothermal temperature of 80°C.

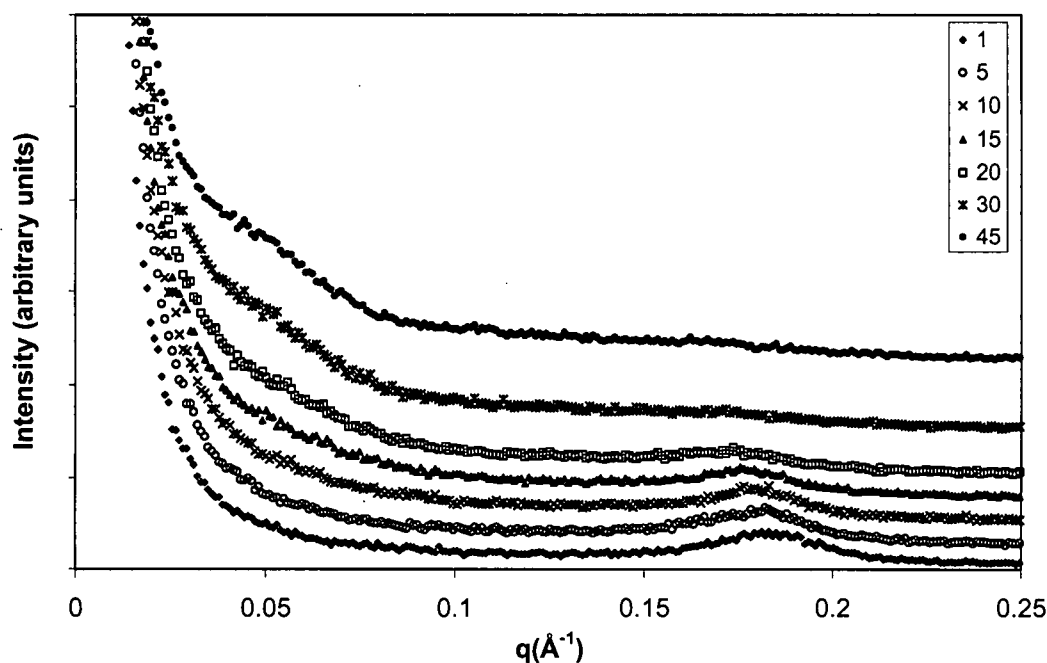


**Figure 4-12:** Time-dependent small angle x-ray scattering data for 5% mixture of SC18+I.30E/Epon 828 with mPDA at isothermal temperature of 80°C.

### **Material Preconditioning as a Variable in Morphology Development via SAXS**

The materials that underwent an aging of the OLS-epoxy mixture prior to the addition of cure agent and subsequent thermal processing, or ‘advancement’, are seen to develop morphology in quite a different manner than the baseline materials. These samples developed clear peaks at low  $q$  associated with well expanded galleries, unlike the baseline materials. The advanced resins also exhibited initiation of gallery expansion in significantly shorter times as evidenced by the loss of the peak associated with the initial intercalated morphology. This trend is illustrated in Figures 4-13 through 4-15; full data sets are described in Appendix C and will be discussed in the next chapter. Studies were performed at an isothermal temperature of 80°C and selected heating rates for comparison with the other data sets collected and are reported in Table 4-5.

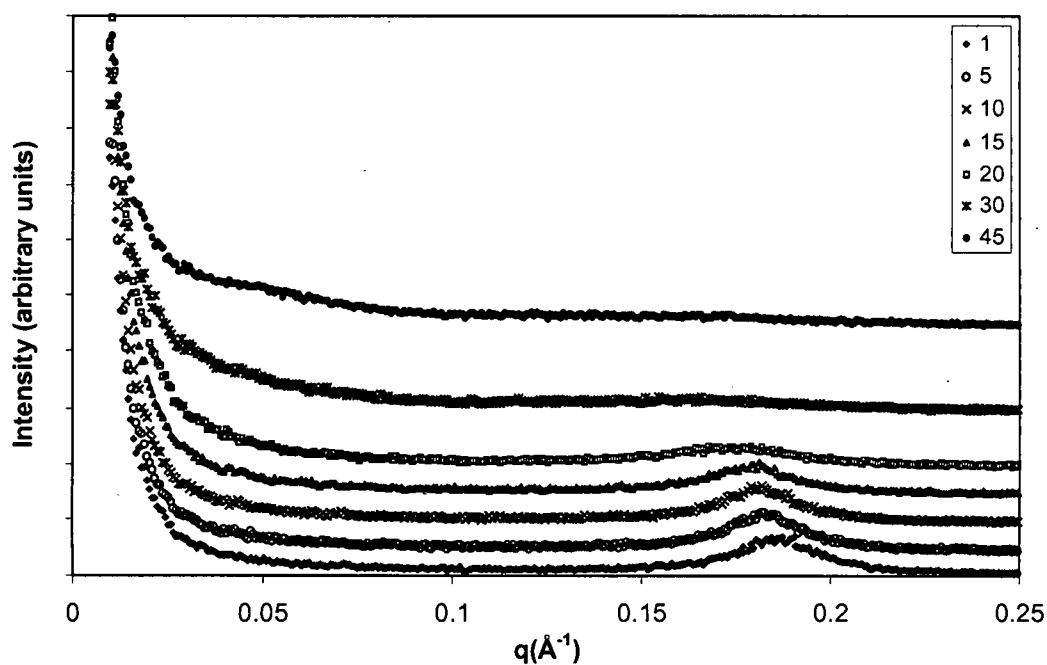


**Figure 4-13:** Time-dependent small angle x-ray scattering data for 5% I.30E/Epon 828 with mPDA at isothermal temperature of 80°C, no advancement (repeat of Figure 10).

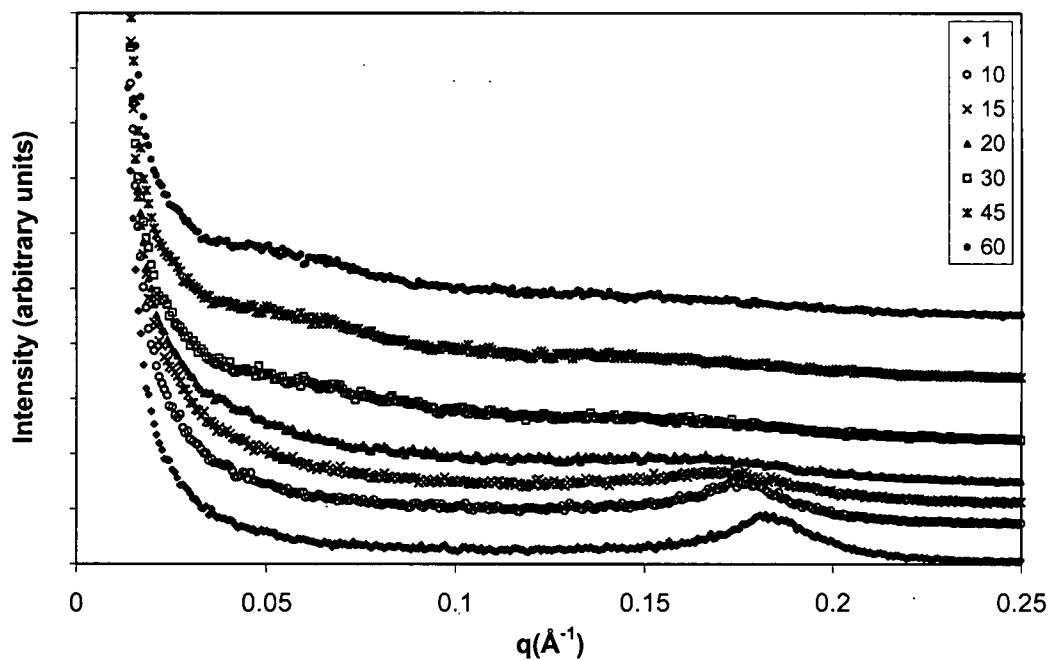


**Figure 4-14:** Time-dependent small angle x-ray scattering data for 5% I30E/Epon 828 with mPDA at isothermal temperature of 80°C after advancement for 4 weeks.

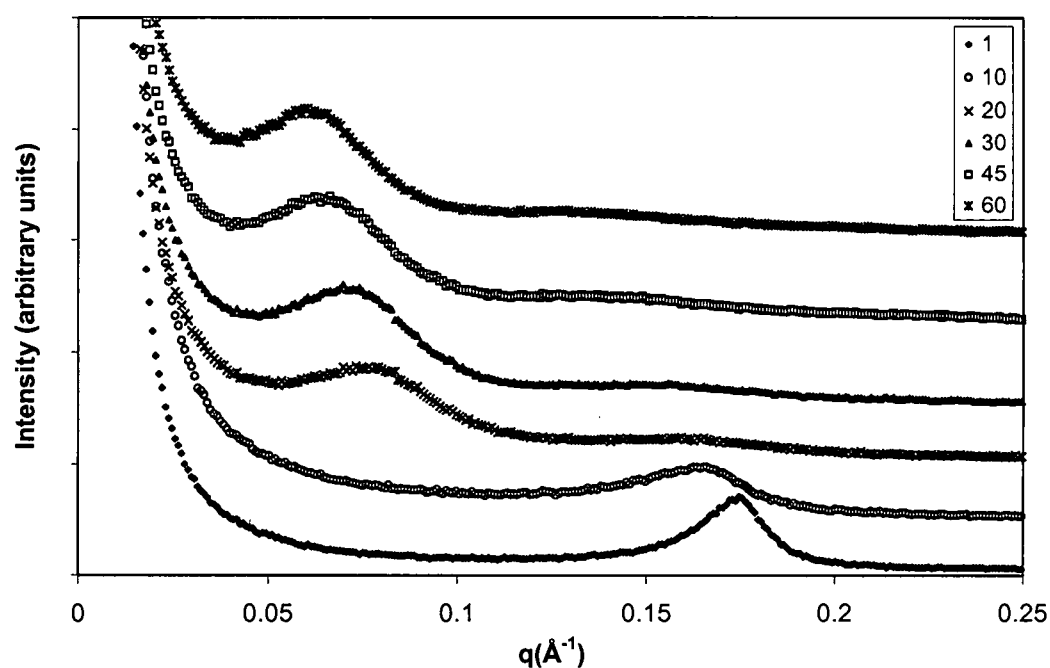


**Figure 4-15:** Time-dependent small angle x-ray scattering data for 5% I30E/Epon 828 with mPDA at isothermal temperature of 80°C after advancement for 18 weeks.

**Table 4-5: Summary of Advancement Effects at Isothermal Temperature of 80°C.**

Weight Fraction I.30E	Fabrication Process	Initial d-spacing (Å)	d-spacing at 60 minutes (Å)
5%	Baseline	34	42 <sup>a</sup>
5%	Epoxy-silicate mixture advanced 1 week	34	45
5%	Epoxy-silicate mixture advanced 4+ weeks	36	104
5%	Epoxy-silicate mixture advanced 8 weeks	35	105
5%	Epoxy-silicate mixture advanced 18 weeks	36	110
7%	Baseline	33	37
7%	Epoxy-silicate mixture advanced 18 weeks	35	106

<sup>a</sup> Final Time: 45 Minutes

### **Role of Variability: Degas and Hydration of OLS on Morphology Development**

The degas step of the material fabrication process is necessary for removal of entrapped air which can become locked into the resin on gelation (dramatic increase of liquid resin viscosity). Such voids can serve as the initiation site for fracture, and therefore it is typical in advanced composite fabrication to limit void content of the cured composite to less than 2% to maximize mechanical properties. The omission of the degas step does not appear to significantly impact the nanoscale morphology development, as illustrated in Figures 4-16 and 4-17, although in some cases appeared to possibly cause earlier initiation of gallery expansion.

Whereas pristine clays such as montmorillonite are known to be sensitive to hydration, these results show that organoclay preconditioning through drying does not provide for different initial gallery heights. However, subtle effects on morphology development are observed, and the trends are not conclusive between the two OLS types. When the I30E OLS underwent drying steps prior to integration with the epoxy and subsequent processing, initiation of morphology development occurred more slowly relative to the non-dried systems. For the SC18 system, morphology development initiation occurred slightly sooner than for the non-dried systems. However, taking into account the small differences and the potential for variation within such a small sample set, these differences were not seen as providing information other than the confirmation that the OLS is a much more robust constituent in varying humidity environments than is natural montmorillonite. Complete *in situ* SAXS data are included in the Appendix C and are summarized in Table 4-6.

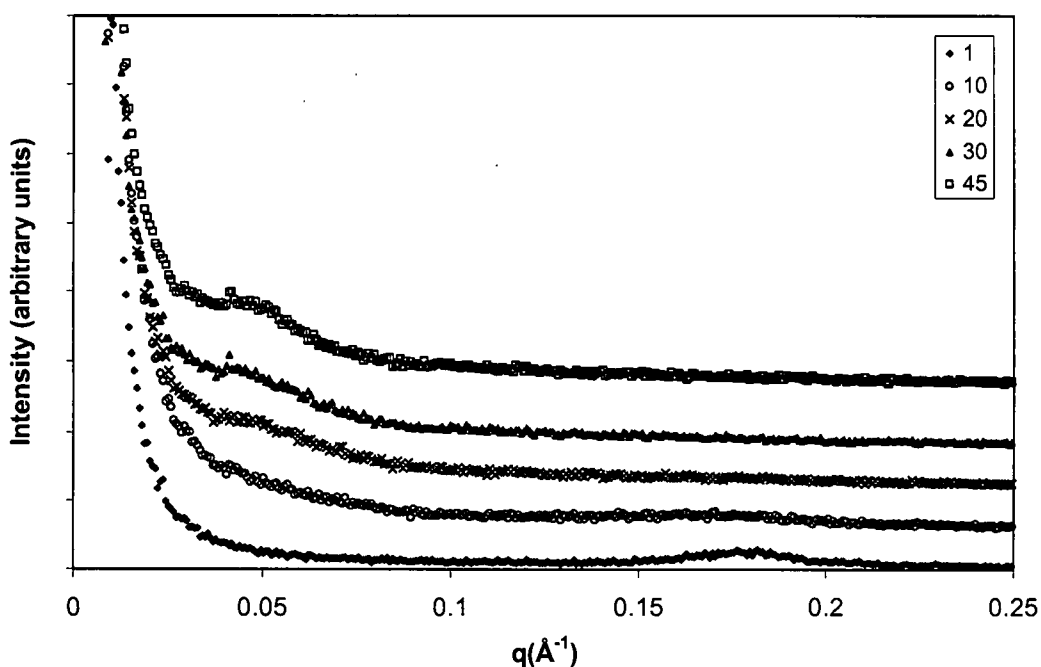


**Figure 4-16:** Time-dependent small angle x-ray scattering data for 5% SC18/Epon 828 with mPDA at isothermal temperature of 80°C.

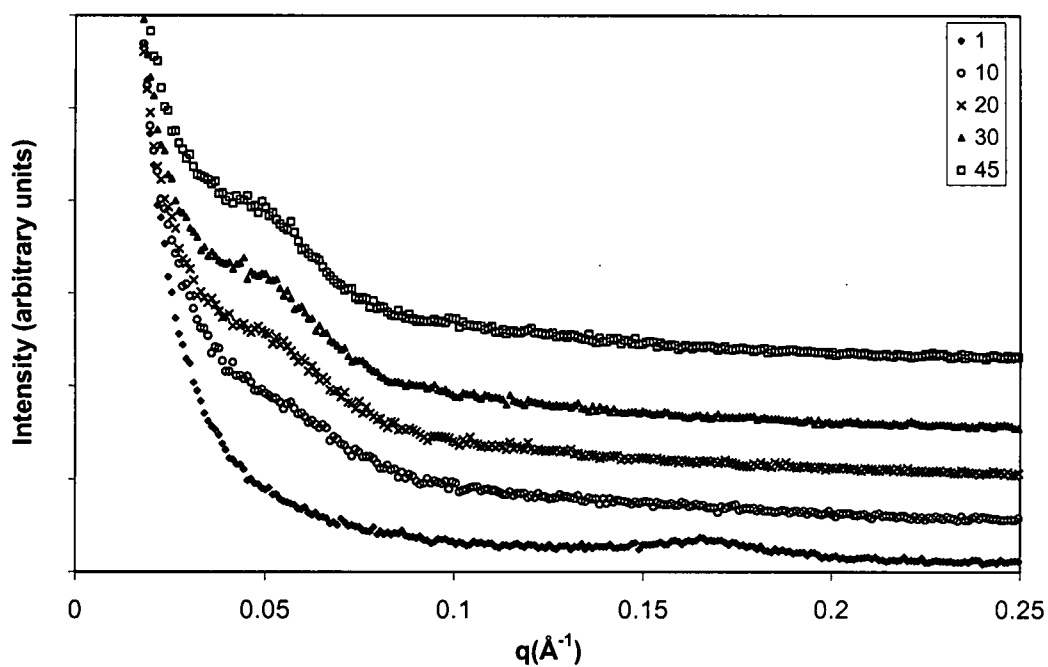


**Figure 4-17:** Time-dependent small angle x-ray scattering data for 5% SC18/Epon 828 with mPDA without degas step at isothermal temperature of 80°.

**Table 4-6: Summary of Processing Variations and Associated Scattering Data**

Silicate	Fabrication Process	Initial d-Spacing (Å)	Final d-Spacing (Å) <sup>a</sup>	Initiation of Exfoliation (minutes)
50%I30E, 50% SC18	Standard	34	42	20
I.30E	Silicate Dried at 25°C	33	36	25
I.30E	Silicate Dried at 100°C	33	35	28
SC18	Silicate Dried at 60°C	36	130	7-8
SC18	Silicate Dried at 100°C	36	131/153	9
I.30E	No Degas Step	34	43	17
SC18		38	155	4
I.30E	Standard	34	42	16
SC18	Standard	36	125/155	10

<sup>a</sup> Final Time: 45 Minutes

### Results of Cure Agent Variations vs. Morphology Development via SAXS

Three cure agents with differing structures allowed for the exploration of the role of steric factors and network formation on morphology development. Steric factors can impact the ability of the cure agent to infuse into the galleries, and also influence reactivity.

Therefore the rate of network formation as well as the ability to replenish epoxy into the galleries can be assessed, both of which can impede or drive morphology development.

The aliphatic amine, T403, provided for significantly different morphology development than the aromatic in that no initial SAXS peak was observed. In both of the aromatic amine systems, the addition of the cure agent did not change the peak associated with the intercalated epoxy. Clear peaks associated with initial d-spacing of approximately 35 Å were observed and persisted for a number of minutes, from 10-30, depending on the processing conditions. The addition of the T403 to the epoxy-OLS mixture resulted in

the loss of the original peak associated with the intercalated epoxy. This observation is clearly shown in Figures 4-18, 4-19 and 4-20, which compare data of epoxy-OLS (no cure agent), epoxy-OLS-mPDA, and epoxy-OLS-T403.

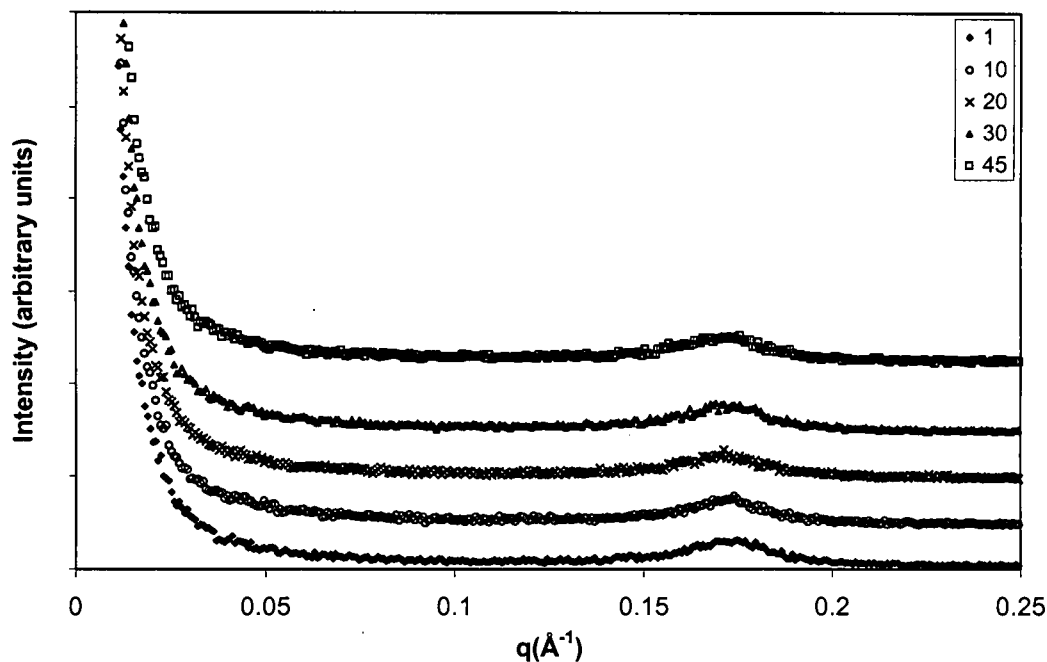


**Figure 4-18:** Time-dependent small angle x-ray scattering data for 5% SC18/Epon 828 with no cure agent at isothermal temperature of 80°C (intensity data offset for clarity).

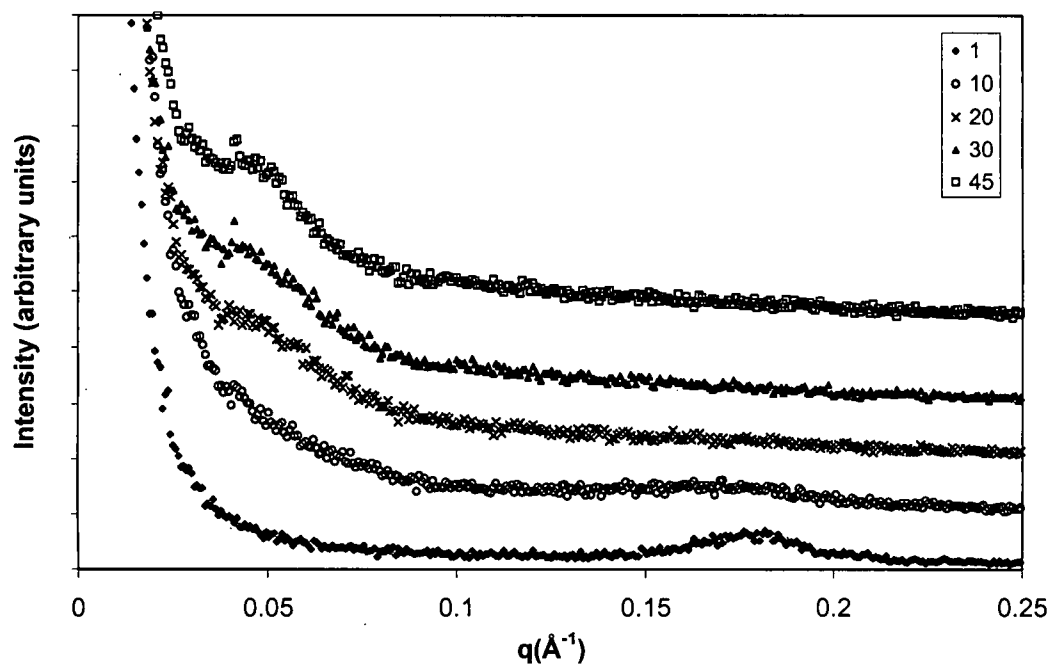


**Figure 4-19:** Time-dependent small angle x-ray scattering data for 5% SC18/Epon 828 with mPDA at isothermal temperature of 80°C (intensity data offset for clarity).

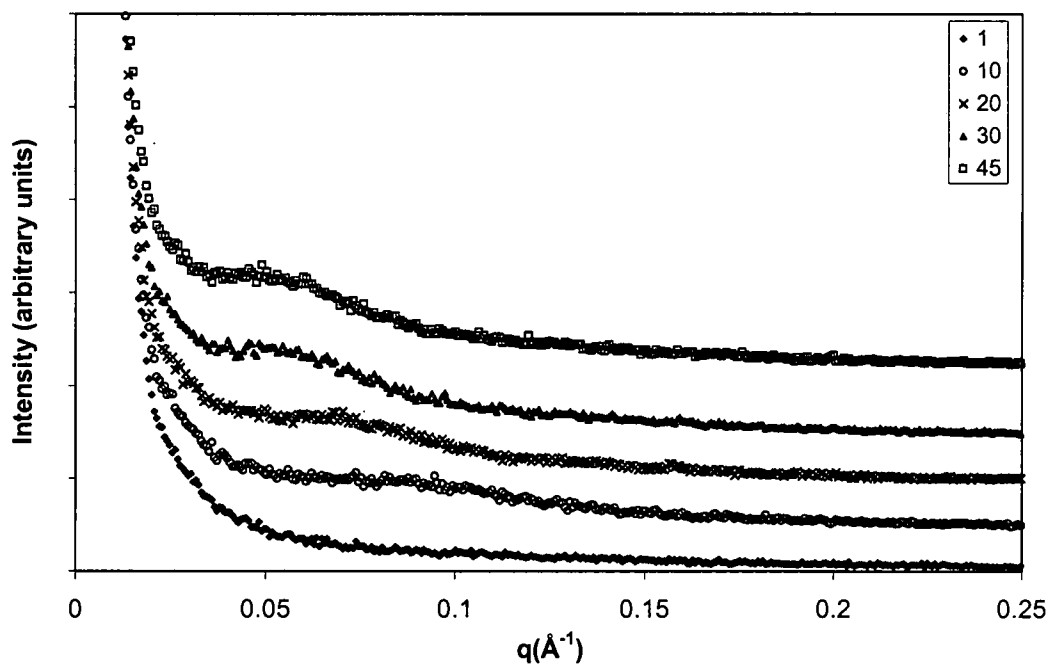


**Figure 4-20:** Time-dependent small angle x-ray scattering data for 5% SC18/Epon 828 with T403 at isothermal temperature of 80°C (intensity data offset for clarity).

Evolution of morphology, as evidenced by the change in peaks associated with various d-spacings, differed for all three cure agents. With the mPDA, the peak associated with the initial d-spacing disappeared within 15 minutes during processing of 5 degrees/minute. For the T403, there was no initial peak; for the Cure W, the initial peak was lost within 20 minutes at the same processing condition. The development of a low  $q$  peak associated with ordered, highly separated layers was unclear for the mPDA system; a bit clearer with the T403 system and evident by 20 minutes; and much clearer and evident by 30 minutes for the Cure W system. These trends can be seen in Figures 4-21, 4-22 and 4-23.

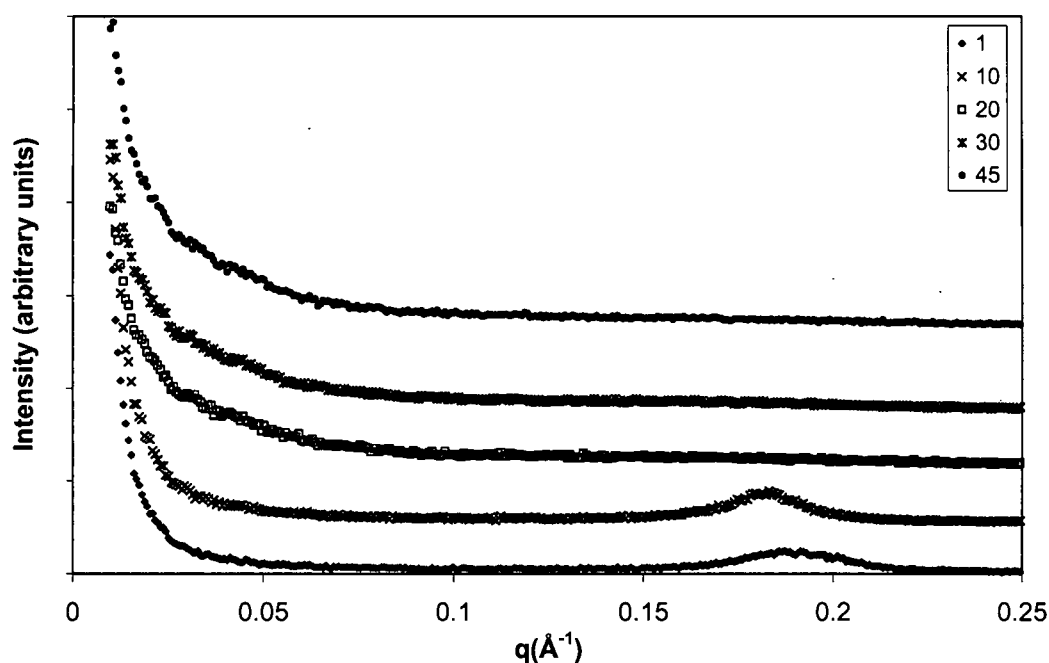


**Figure 4-21:** Time-dependent small angle x-ray scattering data for 5% I30E/Epon 828 with mPDA at heating rate of 5°C/minute (intensity data offset for clarity).

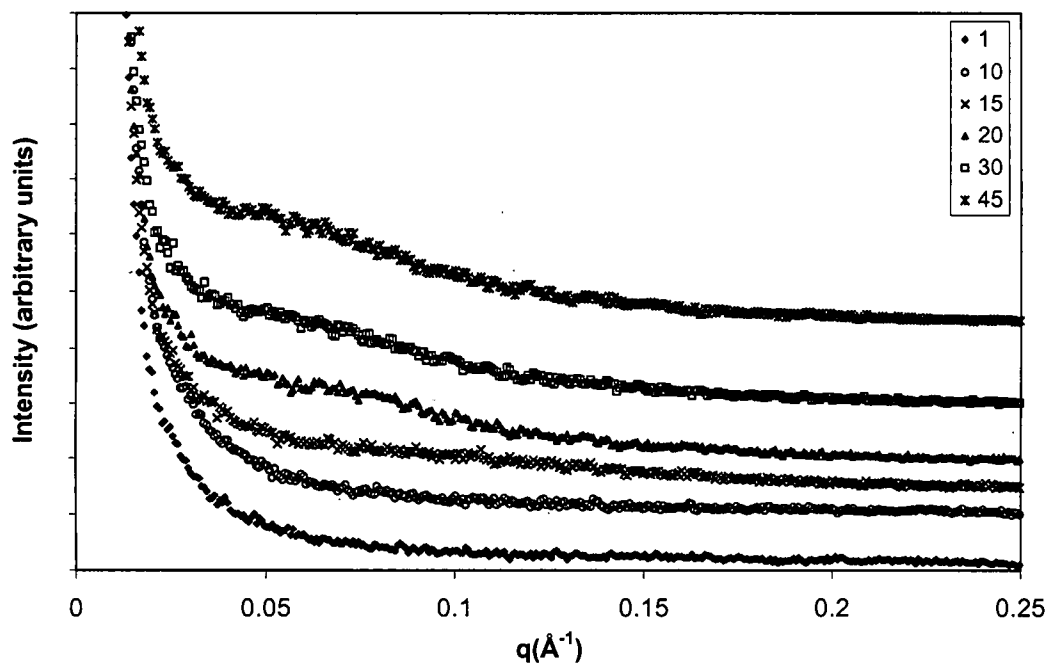


**Figure 4-22:** Time-dependent small angle x-ray scattering data for 5% I30E/Epon 828 with T403 at heating rate of 5°C/minute (intensity data offset for clarity).

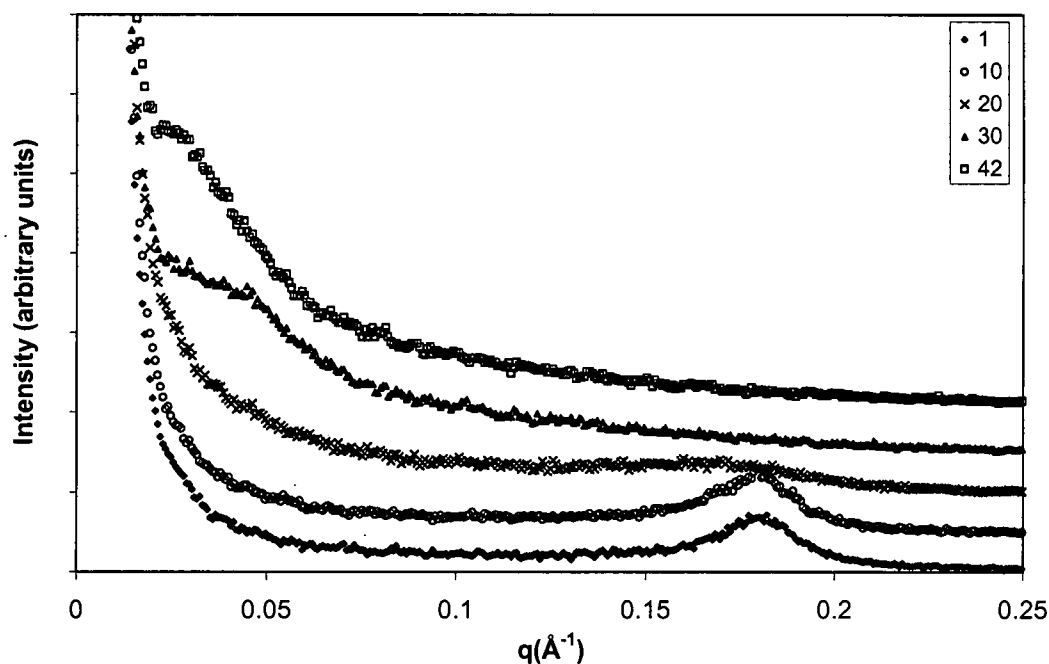


**Figure 4-23:** Time-dependent small angle x-ray scattering data for 5% I30E/Epon 828 with Epi-cure W at heating rate of 5°C/minute (intensity data offset for clarity).

The aromatic amines show different rates of morphology development (Figures 4-24, 4-25).

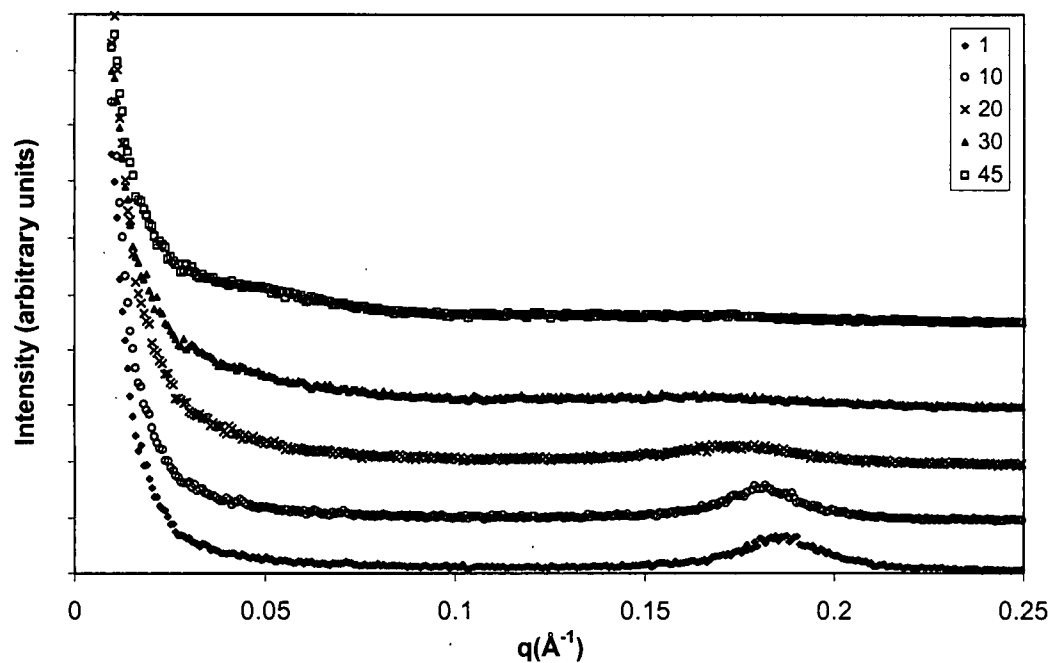


**Figure 4-24:** Time-dependent small angle x-ray scattering data for 5% I30E/Epon 828 with mPDA at isothermal temperature of 80°C (intensity data offset for clarity).

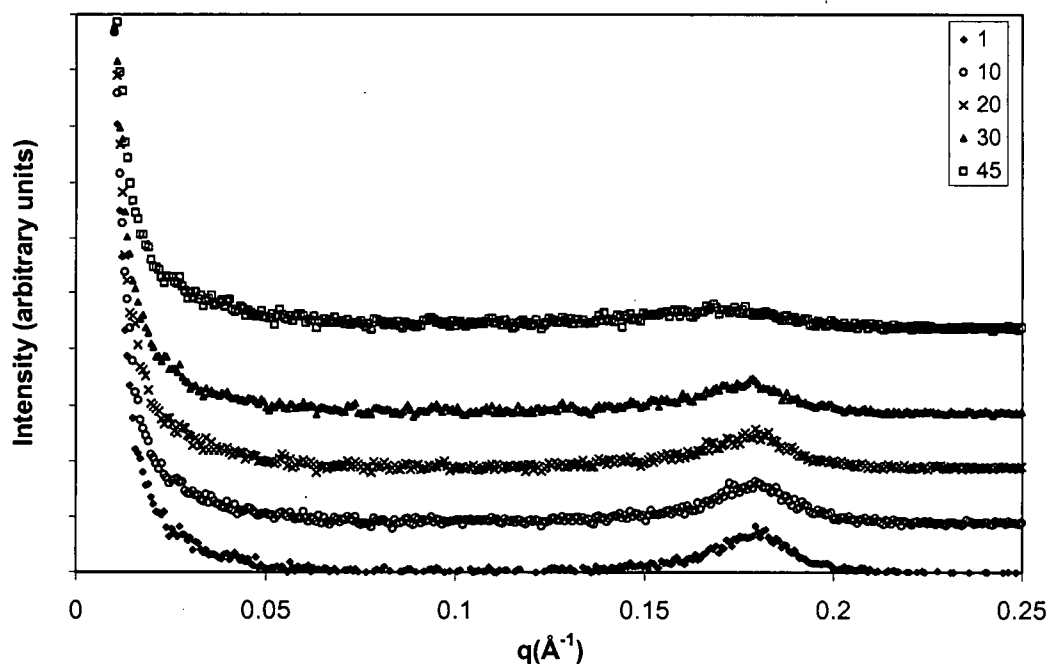


**Figure 4-25:** Time-dependent small angle x-ray scattering data for 5% I30E/Epon 828 with Epi-cure W at isothermal temperature of 80°C (intensity data offset for clarity).

**Table 4-7:** Summary of Cure Agent Variation Studies

Sample (5% by wt OLS)	Cure Agent	Process	Initial d-Spacing (Å)	Final d-Spacing (Å) <sup>a</sup>
I.30E/828	T403	Isothermal 80° C	None	peak~25 min <sup>b</sup>
I.30E/828	Epi-Cure W	Isothermal 80° C	35	37
I.30E/828	mPDA	Isothermal 80° C	34	39
I.30E/828	T403	5°/minute	None	broad ~150
I.30E/828	Epi-Cure W	5°/minute	35	268
I.30E/828	mPDA	5°/minute	33	broad~150
SC18/828	T403	Isothermal 80° C	None	~123
SC18/828	mPDA	Isothermal 80° C	36	125 <sup>c</sup>

<sup>a</sup> Final Time: 45 minutes

<sup>b</sup> data corrupted

<sup>c</sup> Final Time: 15 minutes

### Volume Fraction Variation via SAXS

Volume fraction studies were performed to determine the sensitivity of the observations as well as any effect on d-spacing. The intercalated value of weight fractions ranging from 1% OLS to 7% OLS differ little as seen in Figures 4-26 and 4-27. The initial d-spacing for 1%, 5% and 7% were within 1 Å, and final d-spacing at an isothermal heating of 80°C was within 5 Å. The lack of significant difference is supported by the fact that the theoretically-possible d-spacing for a given volume fraction is not reached with any of these systems (although processing did not drive them to high d-spacings). The clearer peak seen with the 7% system is due to the fact that there are more scatterers within the system. As will be discussed in the next chapter, the higher amount of OLS represents a high organic content due to the very large surface area of the OLS.

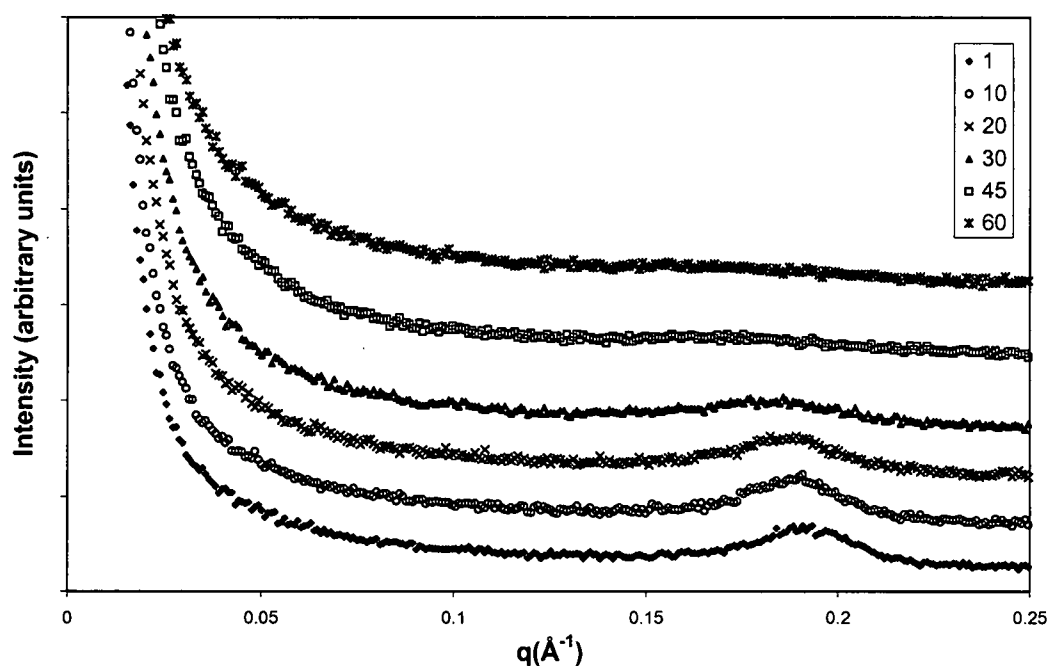


**Figure 4-26:** Time-dependent small angle x-ray scattering data for 1% I.30E/Epon 828 with mPDA at isothermal temperature of 80°C (intensity data offset for clarity).

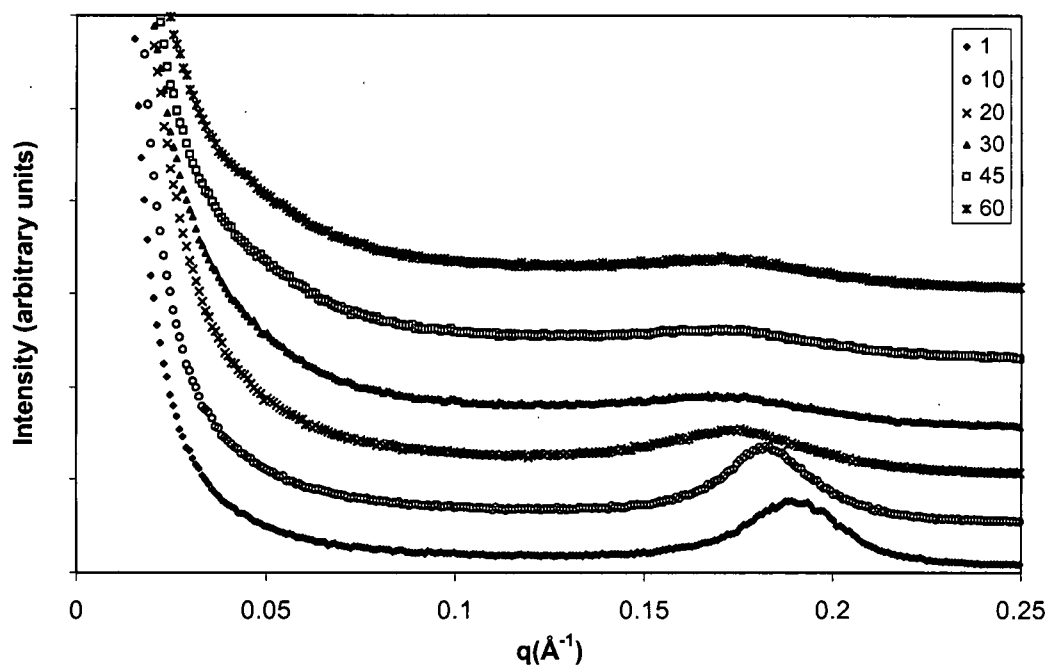


**Figure 4-27:** Time-dependent small angle x-ray scattering data for 7% I.30E/Epon 828 with mPDA at isothermal temperature of 80°C (intensity data offset for clarity).

### Thermal Analysis Results

Thermal analysis data shows the role that the OLS plays in polymerization and in network development, which is an important variable in the development of nanoscale morphology. The onset of reaction plays a role in the ability to achieve high d-spacings. Key thermal data from differential scanning calorimetry is summarized in Table 4-8.

**Table 4-8: DSC data summary.**

<b>Material</b>	<b>T<sub>onset</sub> (°C)</b>	<b>T<sub>max</sub> (°C)</b>	<b>ΔH<sub>rxn</sub> (cal/g)<sup>a</sup></b>
Baseline Material Information			
Epon 828	~300		
Epon 828/mPDA	126	158	106
Epon 828/I.30E 5%	205	215	108
Nanocomposite Systems			
Epon 828/mPDA/I.30E 5% baseline process	84	130	103
Epon 828/mPDA/I.30E 1% baseline process	111	155	80
Epon 828/mPDA/SC18 5% <sup>b</sup> baseline process	75	123	65
Epon 828/T403/I.30E 5% baseline process	72	125	67
Epon 828/I.30E 5% Dried 100°C	203	215	108
Mixture Advanced Materials			
Epon 828/mPDA/I.30E 5% baseline	84	130	103
Epon 828/mPDA/ I.30E 5% advanced 2 day	85	136	99
Epon 828/mPDA/ I.30E 5% advanced 1 week	87	136	101
Epon 828/mPDA/ I.30E 5% advanced 8 weeks	93	141	76
Epon 828/mPDA/ I.30E 5% advanced 16 weeks	107	154	96

<sup>a</sup> normalized to epoxy content

<sup>b</sup> average of multiple runs

Dynamic mechanical data on selected materials performed in torsion at 2°C/minute, 100 rad/sec, 0.1% strain are presented in Figures 4-28 through 4-32 and summarized in Table 4-9. Low temperature relaxations show effects of the processing methods and material conditions.

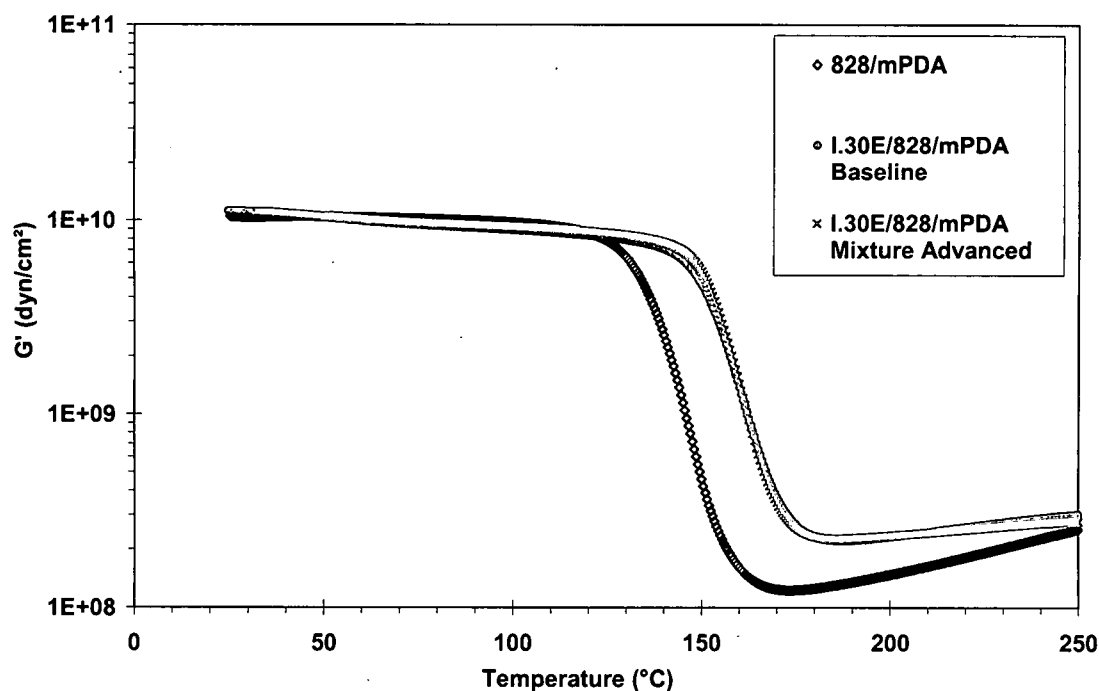


**Figure 4-28:** DMA storage modulus data comparing 828/mPDA, 5% I.30E/Epon 828/mPDA baseline and mixture advanced nanocomposites cured via standard recommended cure process.

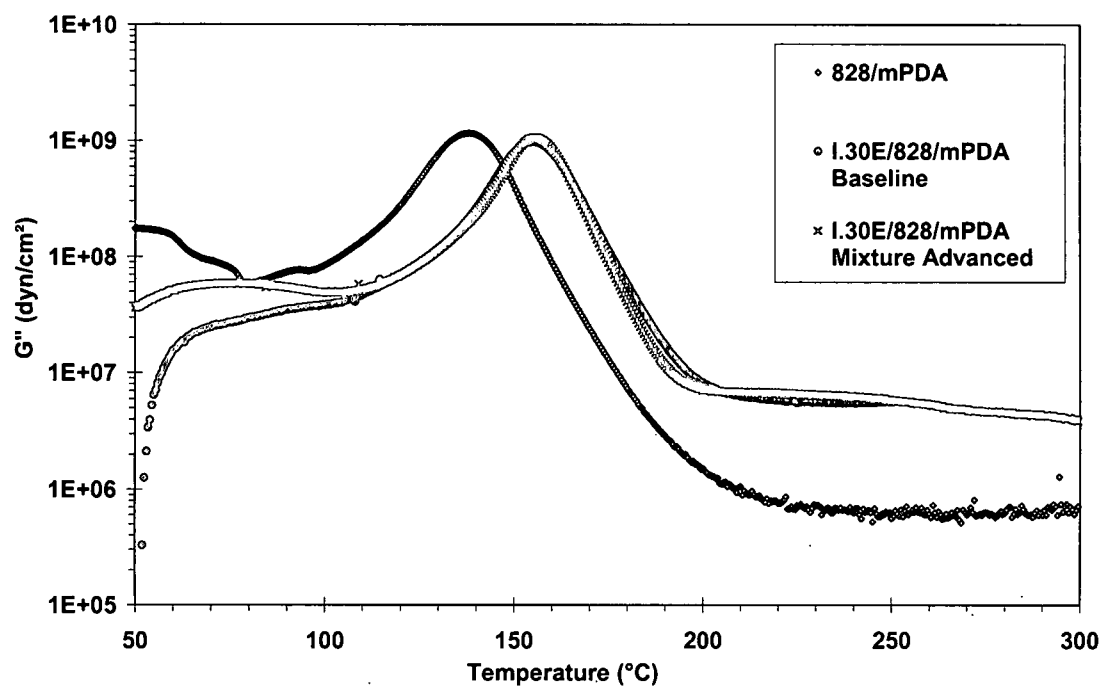


**Figure 4-29:** DMA loss modulus data comparing 828/mPDA, 5% I.30E/Epon 828/mPDA baseline and mixture advanced nanocomposites cured via standard recommended cure process.

**Table 4-9: Summary of Ambient DMA Data**

Material	Tg (G'/G''), °C
Epon 828/mPDA Standard Cure Process	132/138
Epon 828/mPDA/I.30E 5% Standard Cure Process	145/155
Epon 828/mPDA/I.30E 5% Mixture advanced 2 months	148/155

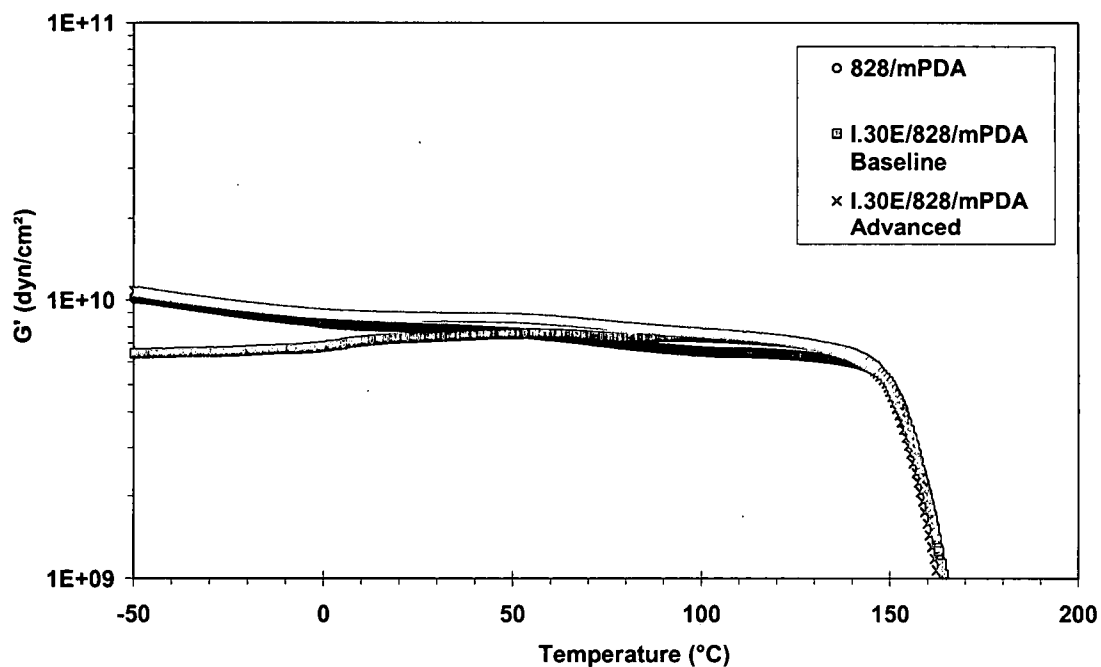


**Figure 4-30:** DMA sub-ambient storage modulus data comparing 828/mPDA, 5% I.30E/Epon 828/mPDA baseline and mixture advanced nanocomposites cured via standard recommended cure process.

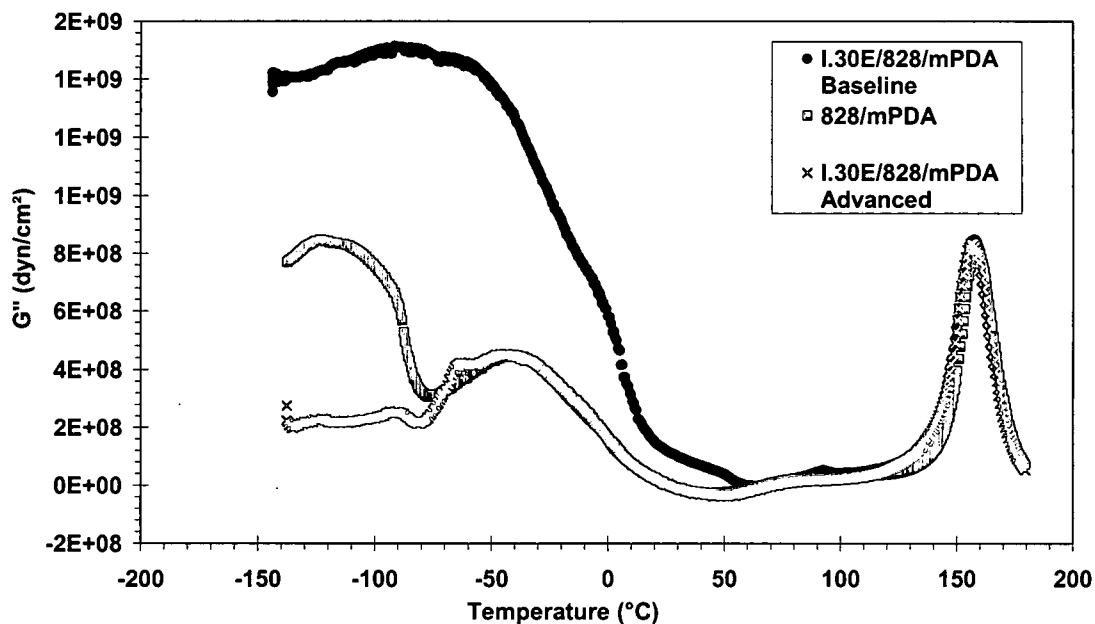


**Figure 4-31:** DMA sub-ambient loss modulus data comparing 828/mPDA, 5% I.30E/Epon 828/mPDA baseline and mixture advanced nanocomposites cured via standard recommended cure process.

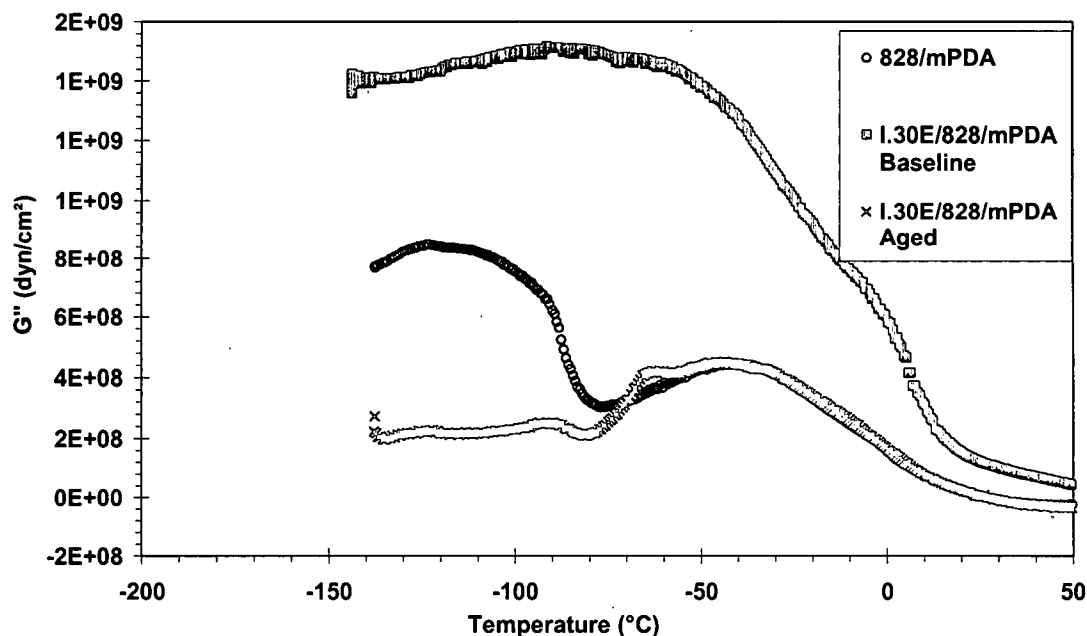


**Figure 4-32:** DMA sub-ambient  $\tan \delta$  data comparing 828/mPDA, 5% I.30E/Epon 828/mPDA baseline and mixture advanced nanocomposites cured via standard recommended cure process.

Thermal gravimetric analysis (TGA) was performed on some of the samples of OLS during the investigation of the role of moisture. Weight loss trends between the baseline OLS and the OLS pre-dried at 100°C were essentially the same and therefore no further TGA was performed.

### Mechanical Characterization and Fractography

Fracture data from compact tension specimens tested in Mode I opening (tensile) mode is summarized in Table 4-10. Effects of morphology on mechanical behavior is observed. Data reported is based on multiple specimens and measurements tested at ambient conditions.

**Table 4-10: Mixing Processes**

	Stir intercalate epoxy into OLS	Ultrasonic bath, high shear mixing, acetone into OLS	Ultrasonic bath, high shear mixing, acetone with OLS and epoxy	Horn sonicate, acetone with OLS and epoxy	Degas
Baseline	X				X
Process A	X			X	X
Process B	X		X		X
Process C		X	X	X	X
Process D	X		X	X	X

**Table 4-11: Fracture Toughness Data from Compact Tension Testing**

Material & Process	K <sub>q</sub> (psi-in <sup>0.5</sup> )
Epon 828/mpDA (no OLS)	646 ± 270 <sup>a</sup>
5% I.30E/Epon 828/mpDA baseline	913 ± 148 <sup>b</sup>
5% I.30E/Epon 828/mpDA advanced 4 mo	1,121 ± 343 <sup>b</sup>
3% I.30E/Epon 828/mpDA baseline process	1,028 ± 82
3% I.30E/Epon 828/mpDA Process C	1,172 ± 329
3% I.30E/Epon 828/mpDA baseline new 828	1,530 ± 217
3% I.30E/Epon 828/mpDA new 828 Process A	1,188 ± 112
3% I.30E/Epon 828/mpDA new 828 Process B	1,531 ± 260
3% I.30E/Epon 828/mpDA new 828 Process D	1,138 ± 224
1% I.30E/Epon 828/mpDA baseline process	661 ± 85 <sup>c</sup>
5% SC18/Epon 828/mpDA baseline process	1,121 ± 195 <sup>c</sup>
1% SC18/Epon 828/mpDA baseline process	756 ± 151 <sup>c</sup>
1% I.30E/Epon 828/mpDA baseline process, ambient prior to testing <sup>d</sup>	568 ± 135 <sup>c</sup>
5% SC18/Epon 828/mpDA baseline process, ambient prior to testing <sup>d</sup>	1,140 ± 195 <sup>c</sup>
1% SC18/Epon 828/mpDA baseline process, ambient prior to testing <sup>d</sup>	437 ± 171 <sup>c</sup>

<sup>a</sup> Data from 3 loadings per sample, 10 samples per material, 2 batches of material

<sup>b</sup> Data from 3 loadings per sample, 10 samples per material

<sup>c</sup> Data from 1 loadings per sample, 10 samples per material

<sup>d</sup> Samples typically stored in desiccators prior to testing; these were not

Tensile strength data was obtained to assess the validity of the fracture toughness testing. Specimen thickness must meet the specification requirements as discussed in the Experimental Chapter, in which tensile strength is a variable. Testing must also assure that the crack does not wander more than ten degrees out of the centerline crack plane; that there is no ductile tearing; and that the crack loading not be too high ( $K_{\max}$  (precrack)/  $K_q > 0.6$ ).

Tensile properties of samples are summarized in Table 4-12. Yield strength is the stress value associated with a 0.2 percent offset of strain. Values for fracture toughness data were valid per the requirements, and  $K_q$  representative of toughness. Specimens of varying thickness were not fabricated to conclusively demonstrate that  $K_q$  represented a worst case value for all thickness. However, as discussed in the Background Chapter, it is proposed that the plastic zone is small compared to the specimen thickness and dimensions, a state of plane strain is assumed, and the comparison of  $K_q$  across samples valid and similar to the plane strain fracture toughness  $K_{IC}$ .

**Table 4-12:** Tensile properties of neat epoxy and nanocomposites

<b>Material</b>	<b>Tensile Modulus (ksi)</b>	<b>Tensile Strength at Break (ksi)</b>	<b>Yield Strength (ksi)</b>
Epon 828/mPDA (no OLS)	$483.3 \pm 49.1^a$	$11.4 \pm 1.68^a$	$7.90 \pm 0.12^a$
5% SC18/Epon 828/mPDA Baseline Process	$456.7 \pm 20.7^a$	$9.08 \pm 0.68^a$	$6.50 \pm 0.42^a$
3% I.30E/Epon 828/mPDA Baseline Process	$481 \pm 9.9^b$	$10.2 \pm 0.26^b$	$7.89 \pm 0.20^b$
3% I.30E/Epon 828/mPDA Process A	$226^c$	$10.3^c$	7.14

<sup>a</sup> Data from 4 samples per material, 2 batches of material

<sup>b</sup> 3 samples tested with one failed in grip; data in table based on 2 samples

<sup>c</sup> only one good test sample

Fracture surfaces were analyzed with scanning electron microscopy to gain qualitative insight into the morphology effects on the fracture event and on the microscopic mechanisms of cracking. Epoxy resin failure typically occurs in a brittle manner, exhibiting relatively flat fracture planes with little evidence of permanent material deformation (similar to brittle failure in metals). The brittle fracture provides flat, smooth surfaces, and arced bands indicative of the crack-front geometry (which are formed in response to pronounced changes in crack velocity – low crack velocities result in smoother, more reflective fracture surfaces). Representative images in Figures 4-33 through 4-36 show distinct differences between 828/mPDA without OLS, baseline I.30E/828/mPDA and mixture advanced I.30E/828/mPDA that will be discussed further in the next chapter.

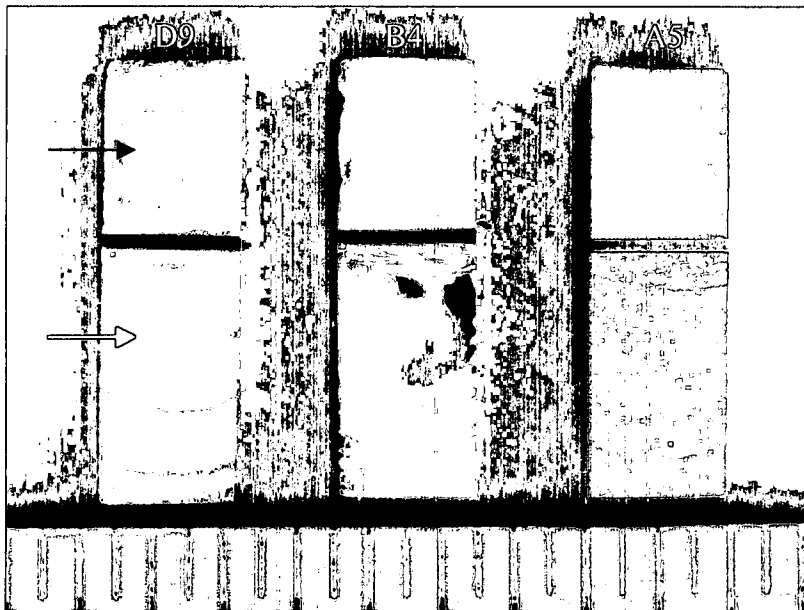


**Figure 4-33:** Photo of the fracture surface of failed compact tension specimens. White arrow identifies the fracture surface, black arrow identifies the machined surface (notch). Crack fronts from the multiple loads can be seen. A5: 5% I.30E/828/mPDA baseline process; B4: 828/mPDA (no OLS); D9: 5% I.30E/828/mPDA advanced. Scale bar minor division = 1/16 inch

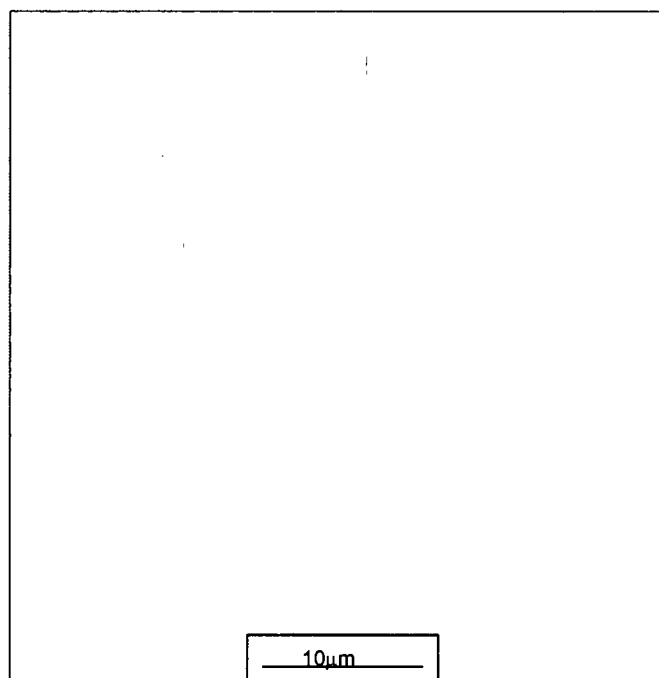


**Figure 4-34:** Scanning electron microscope (SEM) image of the fracture surface of 828/mPDA no OLS (sample B4).

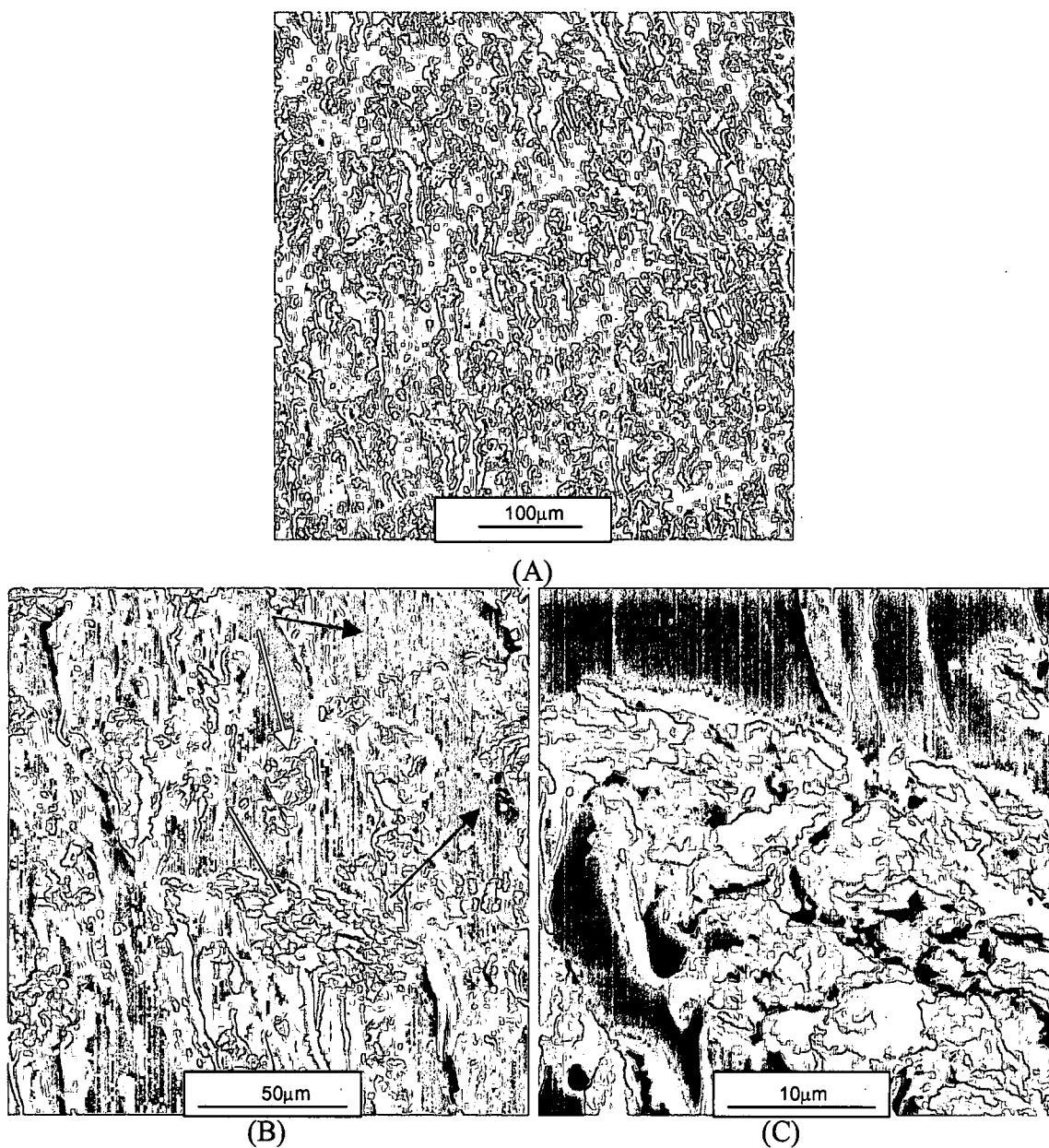


**Figure 4-35:** (A) SEM image of the fracture surface of 5% I.30E/828/mPDA baseline process (sample A5). (B) Increased magnification of (A). White arrows identify anomalies on the fracture surface as compared with neat resin fracture. Black arrows identify resin-rich areas. (C) Increased magnification of (B). Scale bars = (A) 100 micrometers, (B) 50 micrometers, (C) 10 micrometers.

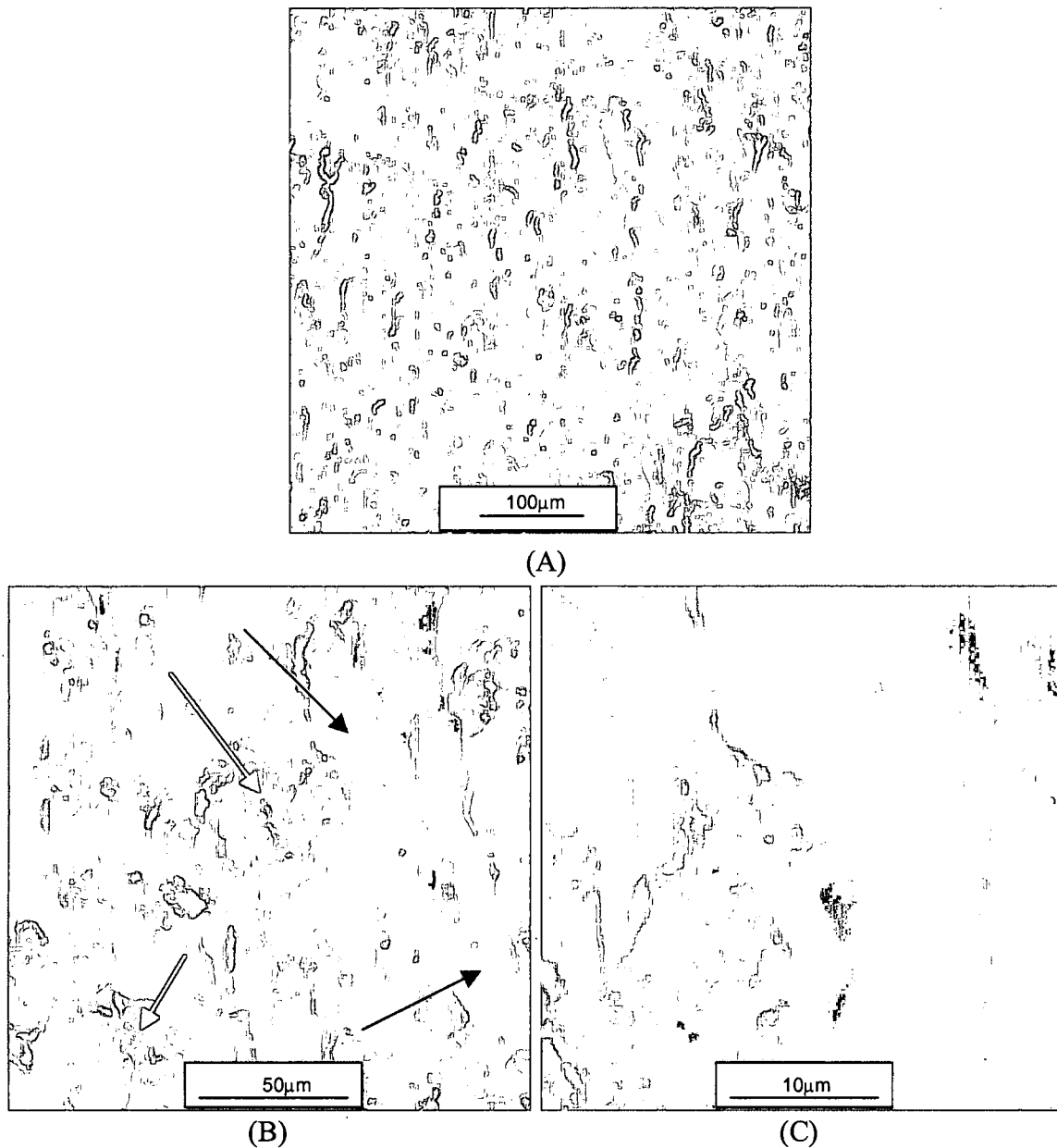


**Figure 4-36:** (A) SEM image of the fracture surface of 5% I.30E/828/mPDA “advanced” (sample D9). (B) Increased magnification of (A). Anomalies shown by white arrows. Resin-rich areas shown by black arrows. (C) Increased magnification of (B). Scale bars = (A) 100 micrometers, (B) 50 micrometers, (C) 10 micrometers.

Energy dispersive spectroscopy (EDS) analysis of fracture surfaces provides further information about local morphologies, mapping out locations of specific elements on the fracture surface which can be correlated with the OLS. Representative images are shown

in Figures 4-37 and 4- 38. The Figures show the SEM fracture surface (A), then color highlighting the location of aluminum (B) and silicon (C) concentration which is associated with the OLS. EDS data is summarized in Table 4-13.

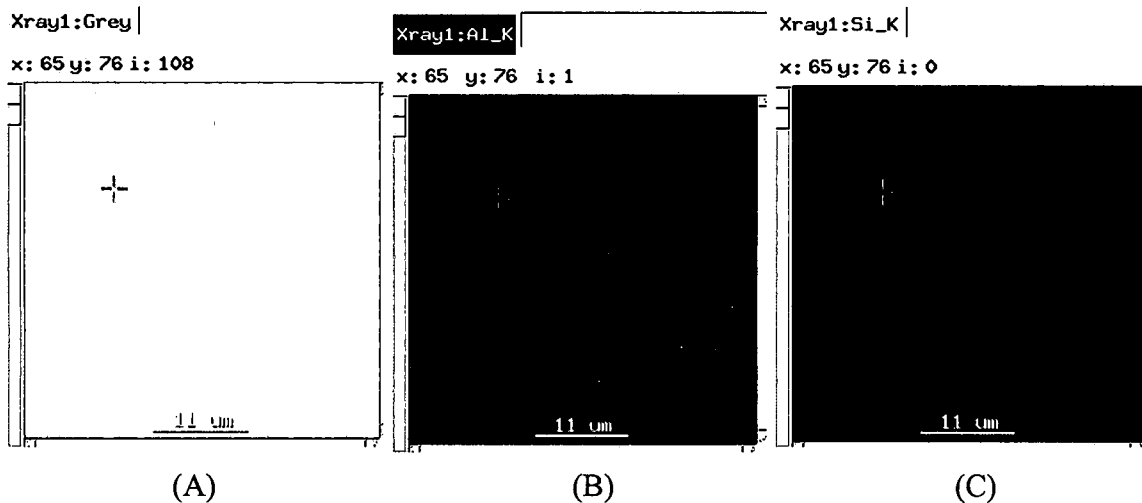


**Figure 4-37:** (A) SEM grey scale image of 828/mPDA. (B) EDS map of aluminum. (C) EDS map of silicon. Scale bars = 11 micrometers.

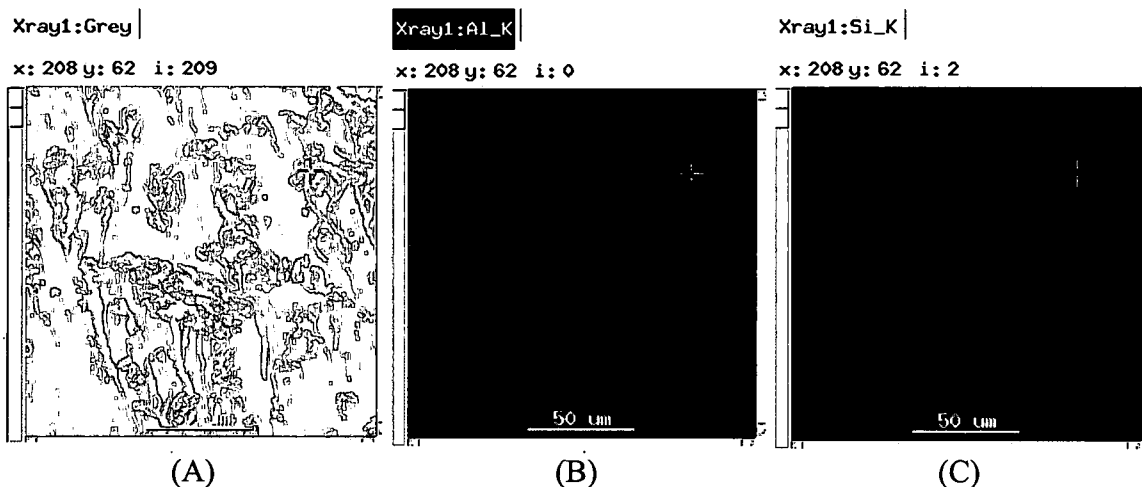


**Figure 4-38:** (A) SEM grey scale image shown in Figure 35 (A), 5% I.30E/828/mPDA baseline process. (B) EDS map of aluminum. (C) EDS map of silicon. Scale bar = 50 micrometers.

**Table 4-13:** Energy dispersive spectroscopy analysis of fracture surfaces comparing baseline and mixture ‘advanced’ nanocomposites.

Material	Area	Elemental Weight %				
		C	Si	Al	Fe	Mg
I.30E/828/mPDA Baseline	Tactoid	82.4	12.1	3.9	1.1	0.5
I.30E/828/mPDA Baseline	Matrix	97.1	2.2	0.2	0.4	0.1
I.30E/828/mPDA Advanced	Tactoid	85.1	10.2	3.4	0.9	0.4
I.30E/828/mPDA Advanced	Matrix	99.5	0.4	0.1	0.0	0.0
828/mPDA	Matrix	99.6	0.3	0.0	0.1	0.0

Transmission electron microscopy as a complementary tool to the x-ray data provides specific local information about the hierarchical morphology of the cured nanocomposites. Tactoid order, relationships between tactoids, and d-spacing within tactoids can be imaged to provide a more sophisticated description of morphology. A few images, selected to best illustrate the range of information that was gathered, are shown in Figure 4-39.

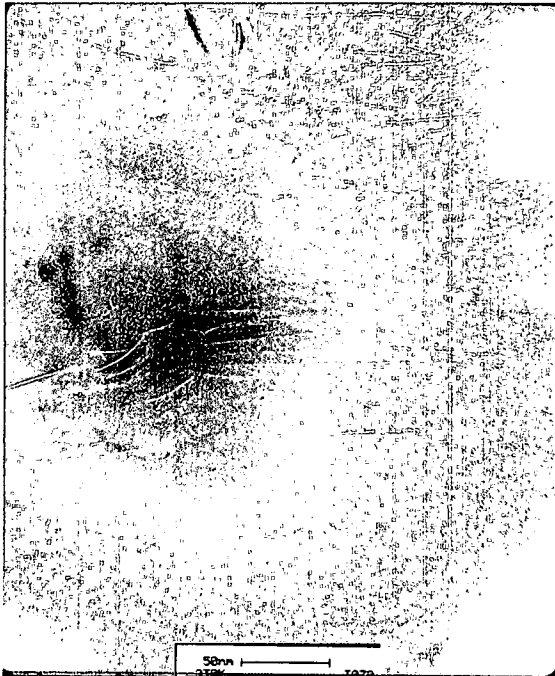


**Figure 4-39:** Transmission electron microscopy of I.30E/828/mPDA nanocomposites. Scale bars = 50 and 100 nanometers.

### **Chemical Characterization**

Chemical characterization was performed through FTIR to determine if any significantly different reactions had taken place with the various material systems. The system of materials that were based on the OLS that had been dehydrated was analyzed. A very slight decrease in the OH peaks around 3100-3300 were observed with the dried OLS; possibly H-bonded water reduced. A slight shift of the Si-O double peak at 1007 and 1023 was observed which was concluded to be negligible. FTIR is sensitive and can pick up reduction in the epoxy with cure. The mixture advanced samples were also analyzed to determine if slight differences in the amounts of epoxy could support the advancement of reaction that was indicated by thermal analysis. However, in this research, FTIR was not sensitive enough to detect significant differences in the materials.

## **CHAPTER V**

### **DISCUSSION**

Recall that the objective of this research is to provide a description of morphology development in layered silicate epoxy nanocomposites and to assess the role of nanoscale morphology on fracture toughness for glassy epoxy systems representative of those used in the aerospace community.

Characterization of morphologies is necessary for the development of morphology-property relationships, yet remains a challenge for nanocomposites. This is partially due to the lack of understanding of the mechanisms of morphology development and partially due to the lack of process-morphology relationships in these relatively new materials. Information about the relationships between morphology development, material selection and processing is crucial to our general understanding of how these materials develop and for ultimate control and design at the nanoscale. As this research shows, the complexities associated with morphology development of nanocomposites based on epoxy and organically modified layered silicates (OLS) are significantly more challenging than those associated with thermoplastic based nanocomposites.

True descriptions of nanoscale morphology are also difficult to capture with current characterization tools, and more than one approach is required to gain sufficient insight on which to base descriptions and models. Small angle x-ray scattering (SAXS) studies are uniquely suited to capturing averaged information about both intercalated and exfoliated states and, in the case of synchrotron sources, to study real-time nanoscale morphology development. Insight into the development of layered silicate nanocomposite morphology can be obtained from analysis of SAXS data, ranging from the absence or presence of a Bragg peak; the evolution of the peak position with material composition and processing conditions; the breadth of the peak (which relates to degree of order); and power law decay at low  $q$  (scattering momentum transfer vector) for large-scale organization information. Real-space imaging such as transmission electron microscopy (TEM) complements SAXS data with specific local morphology information. Neither method alone provides information on a sufficient volume of material from which to draw overall morphology conclusions, especially in light of the multiple combinations and scales on which morphologies can occur. Therefore, their combined use is critical.

The scattering data of many of the systems studied in this research is representative of what has become typically observed for epoxy-based nanocomposites. Clear Bragg peaks associated with initial epoxy-intercalated morphology are observed which shift to marginally lower  $q$  and broaden with time as the organoclay tactoids expand and lose order; these peaks disappear; and finally the subsequent appearance and development of a low  $q$  peak associated with the higher, exfoliated  $d$ -spacing is observed [47, 77].

Representative data are shown in Figure 5-1. It is important to note for this discussion that as mentioned in the background, the definition of ‘exfoliation’ can be broad and has evolved with our increasing understanding of nanocomposites. For this part of the discussion it will be used to indicate d-spacings that have reached spacings greater than 100 Å, and hence strictly describes the gallery expansion but does not suggest any information on the degree of order/disorder or higher level morphology.

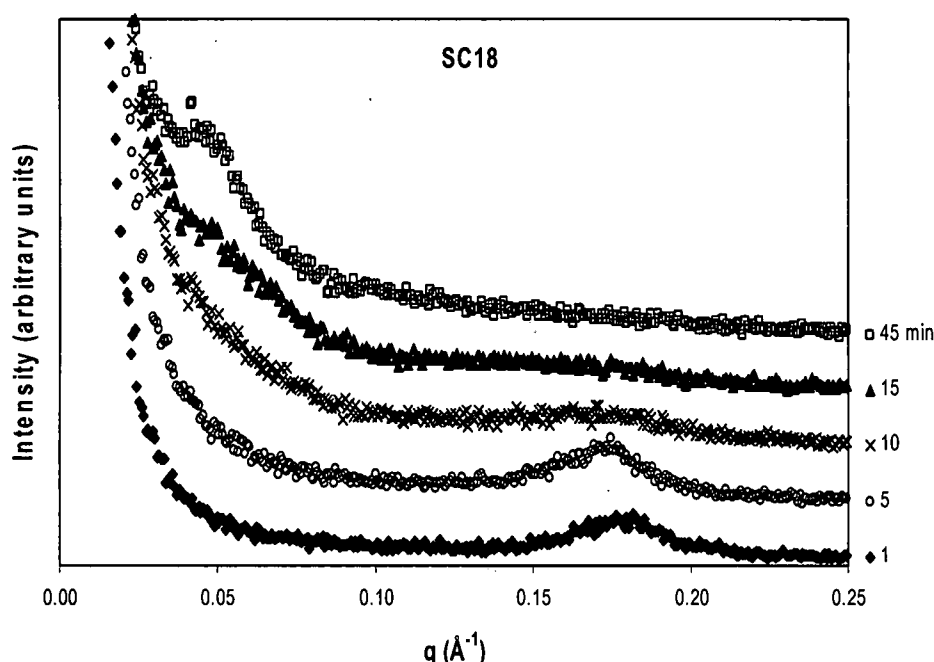


**Figure 5-1:** Time-dependent small angle x-ray scattering data for SC18/Epon 828 with mPDA at isothermal temperature of 80°C (intensity data offset for clarity).

*In situ* studies of real-time morphology development provides a foundation for describing the manner in which OLS tactoids exfoliate. Current understanding of morphology development in epoxy-based nanocomposites is limited. Lan and Pinnavaia’s proposal that the balance of the rates of network formation within and around the tactoid may play a role in the tactoid’s ability to exfoliate has stood as the primary model for this class of

nanocomposites [78,79]. However, as the *in situ* SAXS studies in this research show, there are multiple mechanisms at play. Relative network formation is indeed an important variable, but it is dependent on many contributing factors. The development of morphologies is shown to be significantly affected by material and processing parameters.

### **Role of Organoclay Selection on Morphology Development**

Both organoclays studied in this work were effectively intercalated with the epoxy resin on mixing, with average d-spacings on the order of 35 Å. There appears to be a possibility of slightly larger initial d-spacings for the SC18 organoclay on the order of one or two angstroms. However, the data are not statistically sufficient and this difference is not suggested to be significant.

*In situ* SAXS processing investigations show distinctly different morphology development with time and temperature for the two organoclays. Isothermal heating at 60°C, 70°C, 80°C, 90°C, 100°C, and 110°C shows a different magnitude of d-spacings at 45 minutes, as well as different times for initiation of tactoid expansion as shown in Figure 5-2. The I.30E remained effectively intercalated (expanding no more than up to 7 Å over initial d-spacings) at isothermal temperatures up to 90°C, at which it achieved d-spacings over 100 Å. The SC18 system achieved d-spacings well over 100 Å at all temperatures except 60°C.

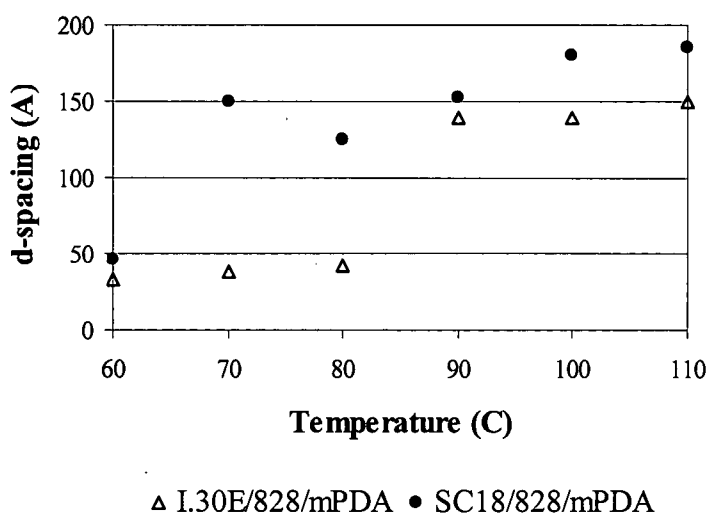


**Figure 5-2:** d-spacing of two organoclays after 45 minutes at an isothermal temperature as a function of temperature shows that systems reach higher gallery sizes for higher temperatures.

Morphologies reached d-spacings above 100 Å for processing temperatures that are higher than the onset of reaction temperature. As the network formation process is of great importance in this discussion of morphology development, thermal analysis can provide support for a more complete and integrated explanation of the observations. Differential scanning calorimetry (DSC) provides information regarding the extent and rate of chemical conversion and hence reactions. The addition of the OLS used in this study results in a significantly earlier onset of polymerization as compared with that for the epoxy-cure agent alone. The onset temperature for the reaction of the epoxy-cure agent alone is 126°C, for the I.30E (5%)-epoxy-cure agent the onset temperature is 84°C (Figure 5-3). Polymerization of the epoxy with 5% I.30E but without cure agents occurs at 205°C (Figure 5-4). The epoxy alone does not polymerize until ~300°C.

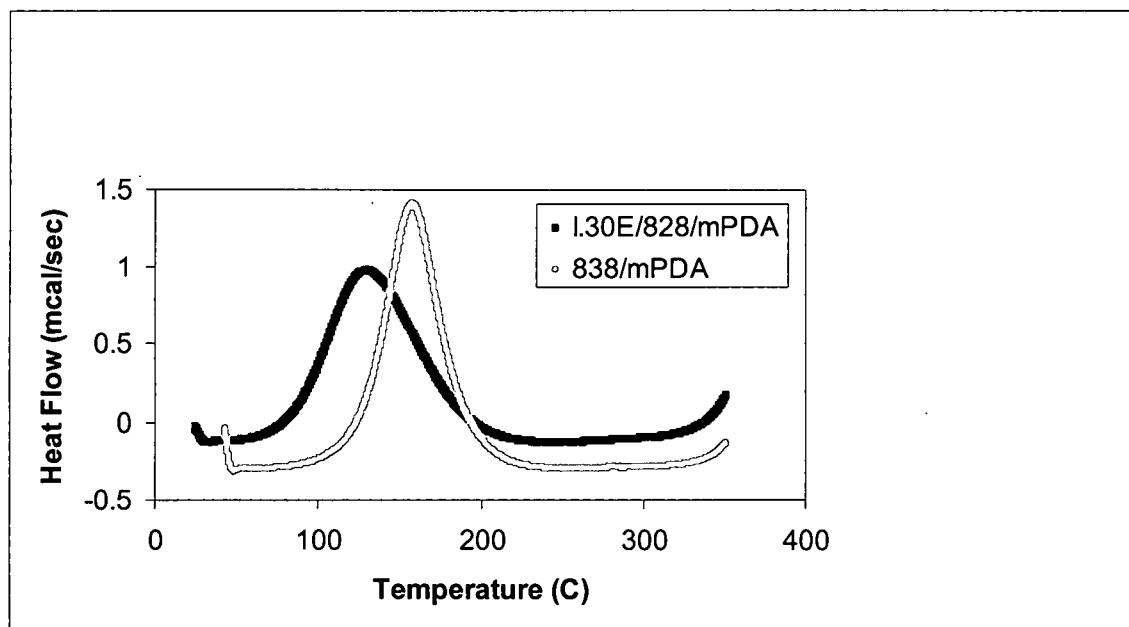


**Figure 5-3:** Differential Scanning Calorimetry for 828/mPDA and 5% I.30E/828/mPDA shows that the addition of the OLS advances the onset of reaction. Data taken at 10°C/minute in nitrogen.

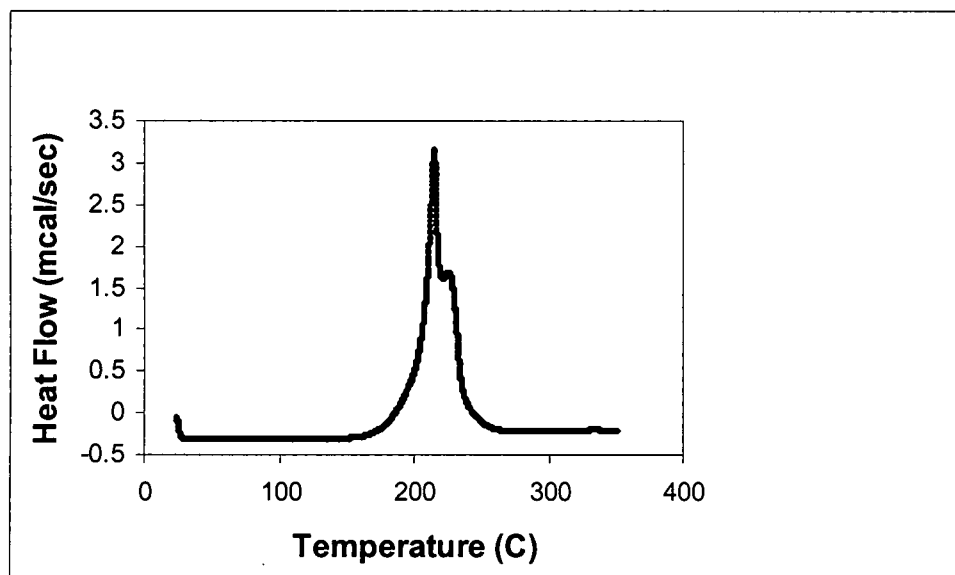


**Figure 5-4:** Differential Scanning Calorimetry for 5% I.30E/828 shows that the OLS reacts with the epoxy at high temperature. Data taken at 10°C/minute in nitrogen.

DSC analysis of the epoxy and I.30E without the primary cure agent shows that the silicate accelerates the epoxy homopolymerization reaction as well; however, homopolymerization with or without I.30E occurred at temperatures much higher than those studied in the scattering experiments, thus early reaction onset is not believed to be a homopolymerization reaction.

DSC, like the TEM and scattering data, recognizes the complexity of morphology, at times exhibiting a slight exotherm after the main cure exotherm observable in some of the systems which may be due to non-uniform network formation. Ranade et al. observed a second small peak after the primary peak and concluded that it indicated the presence of polymer that is not confined in the galleries of the OLS [80]. TEM images both in that study and this suggest that there may indeed be some galleries that are initially not intercalated. However the referenced conclusion that the two exotherms are representative of transitions of confined and non-confined material may not always be the case, but rather, that the addition of OLS and the processing of the nanocomposite may result in excess epoxy. In this study, as discussed earlier under Error Analysis, it is possible that less than stoichiometric amounts of cure agent resulting in un-reacted epoxy which would result in DSC data consistent with these observations. The slight secondary exothermic peak was not always observed in the DSC. When present it varied in intensity with various OLS-828-mPDA samples and occurred at 221 to 226°C. DSCs of combinations of the components show that the reaction of 828 with mPDA initiates at 126°C with a peak occurring at 158°C; the reaction of 828 and I.30E occurs at approximately 205°C and the exotherm peak max is at 213-215°C. DSCs of 828 and

I.30E were accompanied by a second peak at 225°C confirming two reactions between the OLS and epoxy. If confinement were the cause of the second reaction, then secondary peaks should occur in all of the OLS-828-cure agent DSCs in this research. This was not the case. It is more likely that the second peak represents a reaction between un-reacted epoxy and the OLS due to non-uniformity of the mixtures. Lan et al. attributed two peaks to two separate compositions. The first peak was suggested to be the polymerization of the intercalated epoxy within the galleries, which would have a high ratio of epoxy-ammonium, and the second peak due to the polymerization of the extragallery epoxy which may migrate to the surfaces of the OLS [81]. This explanation is more supportive of the relatively lower temperature secondary exotherms observed in this study. Thus it is suggested that while DSC is indeed sensitive to non-uniform network formation due to a variety of causes such as confined polymers, in the case where one has multiple reactions as can occur in certain layered silicate epoxy nanocomposites, multiple peaks in DSC data may be more indicative of the nature of the stoichiometry of the various reactants – be they cure agent, epoxy, or organoclays – than that of confined polymer transitions.

The reactivity of clays with organic materials goes back as early as 1908 when people became aware that oils and clays reacted by observing color changes [7]. The catalytic effect of clays was observed as early as 1933 by Gayer and is captured in extensive literature [82, 8]. Yet the specific reactions between MMT and organics were still being discussed as late as 1963. One postulation was that the presence of hydroxyl OH groups on the surface accounts for the organic reactions [83]. It has also been suggested that

residual adsorbed water on the clay may cause hydrolysis of the organic reactions and the resulting products of the hydrolysis may physically adsorb on the clay.

This catalytic behavior has been observed in layered silicate epoxy nanocomposite systems [84, 85, 31, 55]. Earlier postulations also focused on the role of hydroxyl groups, which as well documented to accelerate the amine-epoxy reaction, suggesting that they may be either generated during the epoxy reaction or resident on the organoclay [71, 55, 31]. However, there is evidence of OLS-epoxy nanocomposites in which the onset of reaction is not accelerated [55, 86]. As discussed in the Background Chapter, MMT has very few exposed hydroxyl groups at its edges and hence would not be expected to accelerate polymerization (nor hydrogen bond) due to active edges. This raises some question as to the role of hydroxyl groups from the OLS in the acceleration of the epoxy reaction.

It has been suggested that the acidity of the ammonium group for the organoclay may cause catalytic effects [51, 81]. The organoclays in this research have been treated with n-octadecylammonium ( $C_{18}H_{37}NH_3^+$ ). The reaction of ammonia and epoxy is also well understood, and can result in the opening of the epoxide ring and products that can include primary amines, which can react with epoxy to form secondary amines and tertiary amines [38]. Lan et al. investigated a series of montmorillonites treated with primary, secondary, tertiary and quaternary ammonium exchange ions to observe the role of acidity of the alkylammonium on the epoxy-OLS reaction. Their DSC data showed no reaction occurred when the OLS does not contain acidic protons associated with an

alkylammonium. Based on the literature data and on that generated here, it appears clear that the catalytic effect of the OLS is due to the acidity of the ammonium and not due to hydroxyl generation.

Comparison of the thermal analysis data and the SAXS provides insight into the role of the reaction in the development of exfoliated morphology. DSC shows that the onset of reaction and hence network formation for epoxy nanocomposites based on I.30E occurs at approximately 84°C. For the SC18 system, the onset temperature is approximately 65-70°C. The time at which the clear SAXS peak associated with initial intercalated morphology ( $q \sim 0.18 \text{ \AA}^{-1}$ , d-spacing  $\sim 35 \text{ \AA}$ ) disappeared was also recorded from the *in situ* SAXS data for the isothermal heating processes to provide an indication of the rate of morphology development with temperature. Both systems display similar trends in their initial loss of ordered intercalated morphology. Higher temperatures result in a faster rate of disorder and expansion. The time for this loss approaches a constant value following a power trend, with a marked reduction in rate change at 80°C and above. The accelerated initiation of network formation corresponds well to the rapid loss of initial intercalation order, and can be assumed to play a strong role in the disorder and expansion of the tactoids. The loss of initial order for the SC18 nanocomposites occurred at lower temperatures as seen Figure 5-5 again providing evidence that the initiation of network formation plays a role in the initial disruption of order. The onset of the epoxy-cure agent- organoclay reaction corresponds well to the knee in the curve plotting the initiation of exfoliation with increasing temperature.

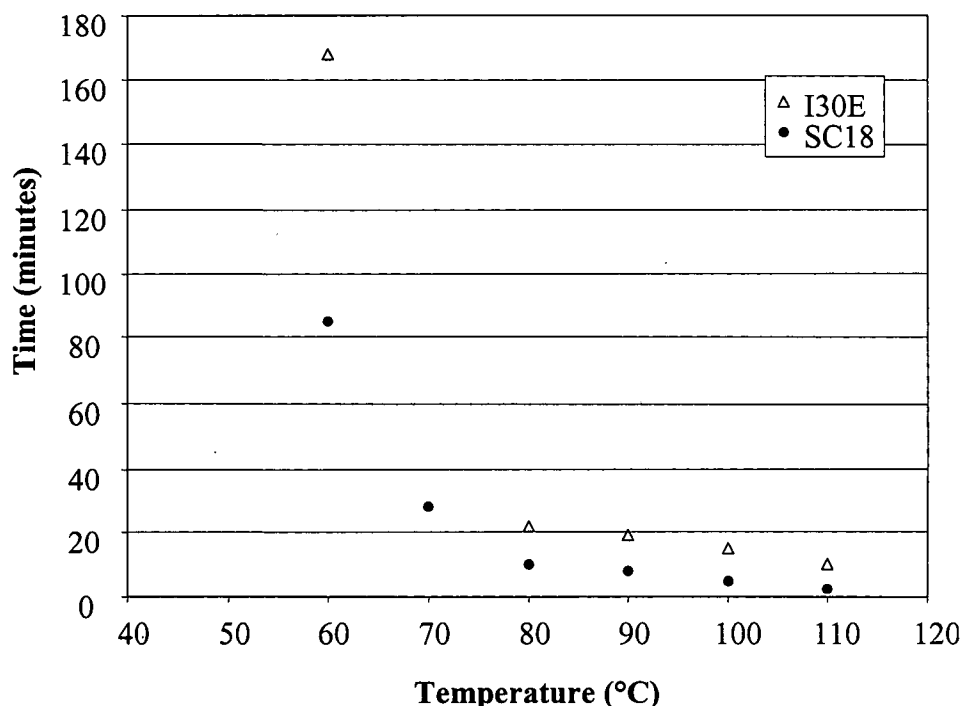


**Figure 5-5:** Initiation of exfoliation in epoxy-silicate nanocomposite occurs faster with increasing temperature. (Data for I.30E at 70°C omitted as the duration of run was 45 minutes and exfoliation not initiated within run duration. Data for SC18 at 100°C and 110°C on 3% vs. 5%; however, since this is the initiation one does not expect the trend to be significantly affected by volume fraction.)

Differences in d-spacing development with time between the I.30E- and SC18-based nanocomposites may be partially explained by the OLS synthesis process and by the cation exchange capacity (CEC), a property of exchange capacity measured in terms of milliequivalents per gram or per 100 grams. These two OLSs differ in that the SC18 OLS fabrication process is well controlled and completely washes out excess surfactant, which is not the case for the commercially produced I.30E material [87, 88]. These two silicates also represent opposite extremes of CEC typically exhibited by natural montmorillonite minerals, which range from 80 to 150 meq/100 g [7]. I.30E has a higher CEC of about 145 meq/100g, and SC18 a CEC of about 92/meq/100g. As intragallery

packing density of the intercalated organic modifications parallels the CEC of the host silicate, the I.30E would be expected to have a higher number of surfactant chains.

Order and orientation of these organic modifier chains, affected by their confinement within the silicate layers, are higher with higher intragallery packing density as shown by Vaia et al. [89]. The additional intragallery material of the I.30E could hinder the intercalation of the epoxy resulting in less initial intragallery epoxy in the I.30E than in the SC18. This could cause the following: a smaller initial d-spacing for the higher CEC organoclay due to less intercalated epoxy; and a smaller final d-spacing due again to the lower fraction of intercalated epoxy and cure agent. Such different amounts of surfactant and states of order promote different levels of mobility of the intercalating monomer and cure agent and may bias the balance between intra- and extragallery network formation towards the latter. As expected, initial silicate basal spacings are smaller for the higher exchange capacity system, I.30E, on the order of 34-35 Å, as compared with those of the SC18 which are on the order of 36-37 Å. The final spacings reached by the SC18 systems were consistently higher than those reached by the I.30E systems.

The high CEC of the I.30E could also result in relatively more of the ammonium group  $\text{RNH}_3^+$  in the gallery of the I.30E than in that of the SC18. The greater amount of the ammonium group within the I.30E system (and lesser relative fraction of epoxy) provides for different reactant ratios impeding exfoliation as compared to the SC18 system. These differences in morphology due to subtle variations in similar constituents reinforce the

importance of material and process history and variations in investigations of nanocomposite morphology.

This study strongly demonstrates that the selection of OLS, even when based on similar natural silicates and similar surface treatments, plays a strong enough role in morphology development to be accounted when determining models or descriptions of exfoliation. Comparisons of nanocomposites based on different OLS must be performed cautiously. For OLS with similar base silicates and surface treatments, a lower CEC favors monomer/oligimer penetration which may result in morphologies with more expanded tactoids.

The effect of volume fraction has been well studied by others in the layered silicate nanocomposites field, with particular emphasis on property trends as a function of volume fraction. A rigorous study therefore is not included in this work. However, a discussion here of volume fraction, particle size, and interparticle spacing can lend insight into the current ability to control and fully exfoliate layered silicate epoxy nanocomposites.

Weight fractions of OLS were used in this research, but can be converted to volume fractions through the use of reported density of the I.30E OLS of 2.5 – 3 g/cc [90]. Thus, 5 percent by weight equates to approximately 1.7 – 2 percent by volume.

If it is assumed that the tactoid order is retained for a given volume fraction, with individual layers of the OLS of thickness  $t$  are all stacked and in registry, and that the gallery is completely filled with epoxy, then the volume fraction ( $V_f$ ) of the OLS will be

$$V_f = t/(t+d) \quad (9)$$

where  $d$  is the maximum d-spacing that the expanded gallery can achieve for a given volume fraction [47]. The individual layer thickness of MMT is reported to be 0.96 nm; that of I.30E on the order of 1 nm. The calculated maximum d-spacing for a 2% volume fraction nanocomposite (or ~5% weight fraction) would be 490 Å; for 1.2% volume fraction (~3% weight fraction) 823 Å. These values are much higher than what has been achieved to date in this research or reported in the literature.

If a single silicate layer is assumed to be free to rotate in space, as would be the case for randomly oriented, maximally dispersed morphology, then the possible space that it can occupy can be modeled as a sphere having a diameter equal to the length of the individual layer. Using the concept of atomic packing factor from crystallography, the face-center cubic structure provides the closest atomic packing factor and thus the highest volume fraction for a sphere-based model. The lattice constant,  $a$ , is related to the atomic radius,  $r$  by

$$a = 4r/(2^{1/2}) \quad a = 4r/\sqrt{2} = 2\sqrt{2}r. \quad (10)$$

For a given volume fraction, the theoretical intersphere spacing can be calculated. For spheres of diameter 100 nm, the intersphere spacing is calculated at 41.4 nm; for 500 nm, 207 nm; and for 1,000 nm, 414 nm. If we assume that the average individual silicate sheet has an edge dimension of 1,000 nm, then by this discussion the maximum randomized inter-plate spacings for a volume fraction of 2% should be on the order of 400 nm before some sort of interparticle interaction would constrain the orientations and impart order on the morphology.

The above discussion suggests that completely exfoliated epoxy-based nanocomposites have yet to be achieved either in this or other current research. This underscores the effect of particle size on interparticle spacing, again highlighting the unique aspect of the nanoscale in that the spacing for a given volume fraction is approaching the size of polymers. With such small spacing, the polymer acts much more like a constrained interface/interphase than as typical bulk polymer. The surface area of the silicate is very high and hence the role of the organic modifications (relative amount, type) is significant for OLS-epoxy systems.

### **Role of Processing Temperature Variations on Morphology Development**

Experiments that study temperature and temperature rate, which are defining variables for cure cycles for epoxy-based composites, identify challenges to processing controlled nanoscale morphologies. Temperature affects cure rate, viscosity and phase separation.

Mass transport, such as required for cure agent migration, is controlled by the localized properties and molecular weight gradients. The incorporation of nanoscale OLS within thermosetting resins presents unique challenges compared with OLS modified thermoplastic resins.

Curing of thermosetting resins involves the interaction of chemical kinetics and the changing physical and mechanical properties. Near vitrification, the kinetics are affected by the local viscosity. The viscosity, in turn, is a function of the temperature and the extent of the reaction. In two-phase systems, different morphologies can arise from different processing routes due to the influence of temperature on the competition between thermodynamic (phase separation) and kinetic (mass transport) factors. In thermal cures of nanocomposites the level of exfoliation of the silicate layers may be impacted by the competition between the growing network formation, which will tend to impede the ability of the silicate layers to separate, and the lower viscosity, which will tend to ease physical separation of the silicate sheets. Once crosslinking proceeds on a macro scale the molecular weight of the resin and the viscosity increase, both of which will impede silicate mobility and hence exfoliation. This is a phenomena not encountered with thermoplastic nanocomposites, for which morphology development studies can focus primarily on thermodynamic factors. Time-temperature relationships have been studied extensively for rubber-toughened thermosets [40]. This research will highlight the additional complexities associated with OLS-epoxies associated with the role of the OLS.

A series of isothermal and non-isothermal temperature experiments were performed and *in situ* SAXS data collected to provide insight into morphology development. General trends were observed in all temperature experiments as were exemplified by Figure 5-1. Figure 5-6 shows reduced scattering data for the I.30E system at an isothermal temperature of 90°C, illustrating the trend through plots of relative peak intensity, peak breadth and basal plane separation associated with and directly measured at  $q = 0.18 \text{ \AA}^{-1}$ .

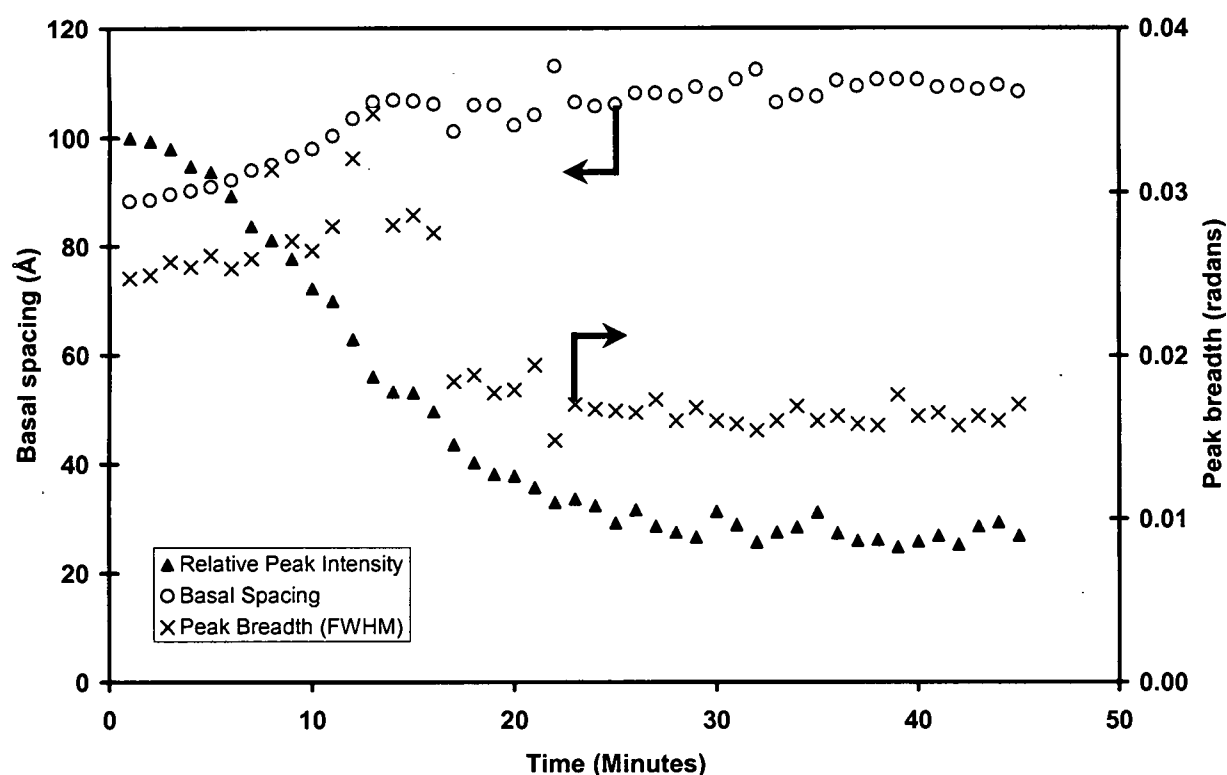


**Figure 5-6:** Scattering data development for the epoxy/I.30E system at  $q$  associated with intercalated peak ( $q \sim 0.18 \text{ \AA}^{-1}$ ) shows trend of morphology development with time at isothermal temperature (90°C).

A fairly broad peak associated with basal plane separation of approximately 34 Å is initially observed, representing the initial intercalated morphology of d-spacing of 34 Å.

Morphology at this point is primarily intercalated. Shortly thereafter, on the order of the first few minutes, the intensity of the peak increases slightly with minimal change in peak width. This may be due to the fact that some OLS galleries may not have been effectively intercalated with the epoxy and with time and temperature become so in the first few minutes. This conclusion is supported by TEMs that show an occasional gallery with d-spacing of the OLS prior to intercalation ( $\sim 20 \text{ \AA}$ ). The peak position then shifts to slightly lower  $q$ , indicative of slight expansion of the gallery. Then the peak intensity begins to decrease rapidly and steadily with a corresponding increase in width and shift in peak position. At some point, the width increases and intensity decreases very rapidly, the peak position shifts very rapidly to lower  $q$ , then the peak associated with the intercalated morphology ( $d \sim 34 \text{ \AA}$ ) disappears. These data are representative of a loss of the number of ordered scatterers (decreased intensity), a loss of the order (increased breadth), and eventual loss of the general intercalated morphology.

At some time after this point, a fairly narrow peak at low  $q$  associated with exfoliated morphology ( $d > 100 \text{ \AA}$ ) begins to develop (not shown in Figure 5-4). Finally the peak at low  $q$  develops into a distinct, single peak in the scattering data.

Although these are general trends, this morphology development is seen to be directly affected by temperature. The intensity of the peak at the  $q$  corresponding with the initial intercalated morphology ( $q \sim 18 \text{ \AA}^{-1}$ ) is followed with time for different isothermal temperatures in Figure 5-7 for the I.30E silicate system. The rate at which the silicate

layers start to separate and develop an exfoliated morphology is seen to be directly impacted by higher temperature.

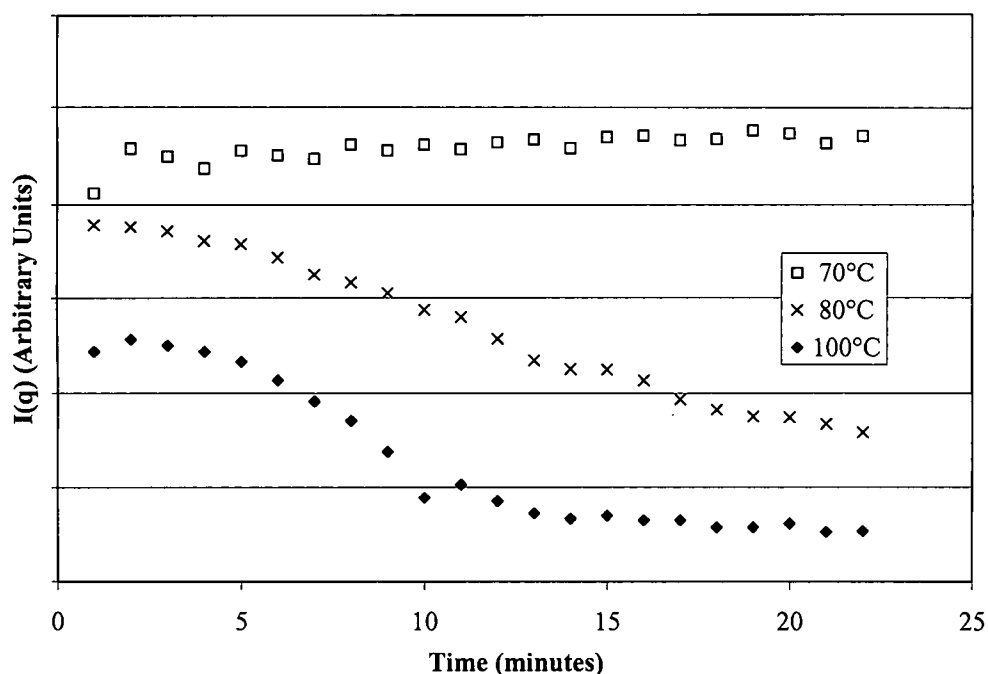


**Figure 5-7:** Exfoliation process as evidenced by loss of peak associated with initial intercalated morphology at  $q \sim 0.18 \text{ \AA}^{-1}$  for epoxy/I.30E system occurs faster at higher temperatures.

Heating rates affect the kinetics of the morphology development as well as the cure of the epoxy resin. *In situ* scattering data for both silicate systems at heating rates of 2, 5, 10 and 12 degrees/minute show that increased heating rates result in the development of exfoliated morphologies in shorter times. All heating rates resulted in a similar degree of exfoliation development ( $d > 150 \text{ \AA}$ ) within the 45-minute duration of scattering data collection (Figure 5-8).

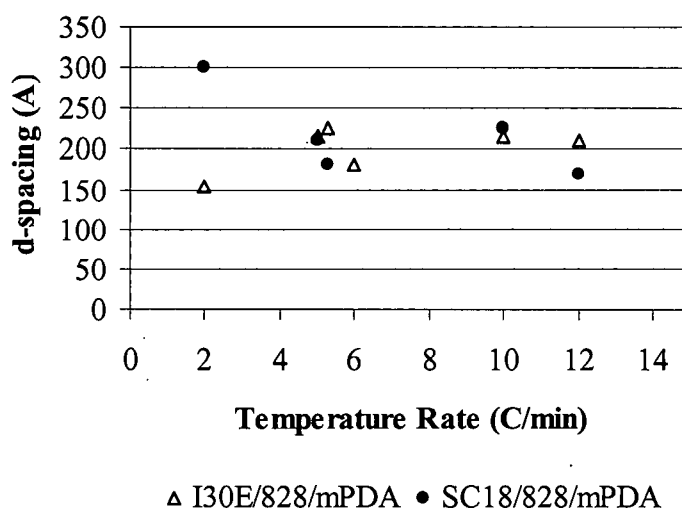


**Figure 5-8:** d-spacing of two organoclays after 45 minutes at temperature ramps of 2, 5, 6, 10 and 12 degrees/minute as a function of temperature rate.

For the I.30E system, the highest heating rate resulted in the onset of exfoliation at a significantly higher temperature as compared with the lowest rate. At 6° per minute, exfoliation did not initiate until the sample cell reached 130°C, as compared to 110°C for the 2° per minute rate (Figure 5-9)<sup>3</sup>. Although developed at different temperatures, the final degree of exfoliation between these two extremes was similar. Since temperature lags occur between the driving temperature and the measured temperature (which is that of the fixture), and differences exist between the measured temperature and the actual nanocomposite, the only observation that can be made with certainty is that the heating rate during processing affects the onset of exfoliated morphology development.

<sup>3</sup> Even accounting for a lag between the temperature that was being driven by the oven and the temperature measured, an effect is observed.

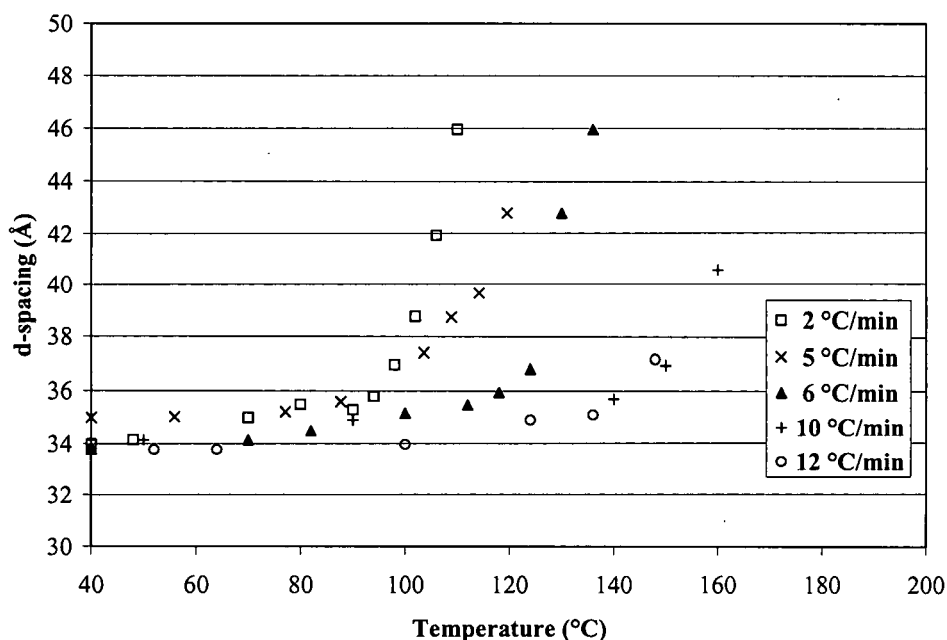


**Figure 5-9:** Morphology development occurs at higher temperatures with increased heating rate for epoxy/I.30E system.

The SC18 silicate system followed a similar trend in that the onset of exfoliation occurred at higher temperature and in shorter times at the higher heating rates (Figure 5-10). Here at the 2° per minute rate, the initiation of exfoliation occurred at a driving temperature of 72°C and within 16 minutes; at the 5° per minute rate, this occurred at about 100°C driving temperature and within 12 minutes. At the 12° per minute rate, the initiation of exfoliation occurred at a driving temperature of approximately 125°C and within 7 minutes.

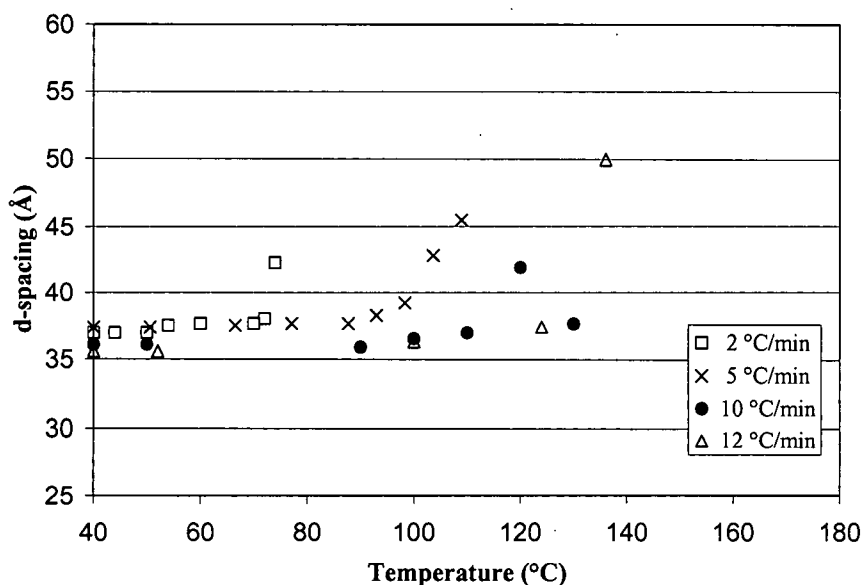


**Figure 5-10:** Morphology development occurs at higher temperatures with increased heating rate for epoxy/SC18 system.

A comparison with the standard recommended cure for the epoxy-mPDA system lends insight. The I.30E with the standard cure resulted in a morphology with d-spacings on the order of 150 Å. The SC18 silicate reached a similar exfoliated state with d-spacings on the order of 120 Å. The various heating rates resulted in composites with similar d-spacing, suggesting the heating rate primarily affects the rate of morphology development.

*In situ* SAXS provides data to construct descriptions or models of morphology development. For these systems, the initial development of exfoliated morphology occurs at a similar rate to that of the loss of intercalated morphology (Figure 5-11). A stable exfoliated morphology is reached in the same timeframe or slightly after the completion of the loss of intercalated morphology. This trend is seen in the majority of the isothermal temperature experiments with the exception of the higher temperatures in

combination with the SC18 silicate. In these cases, the loss of intercalated morphology as indicated by the scattering data occurs well before the development of the exfoliated morphology is completed.

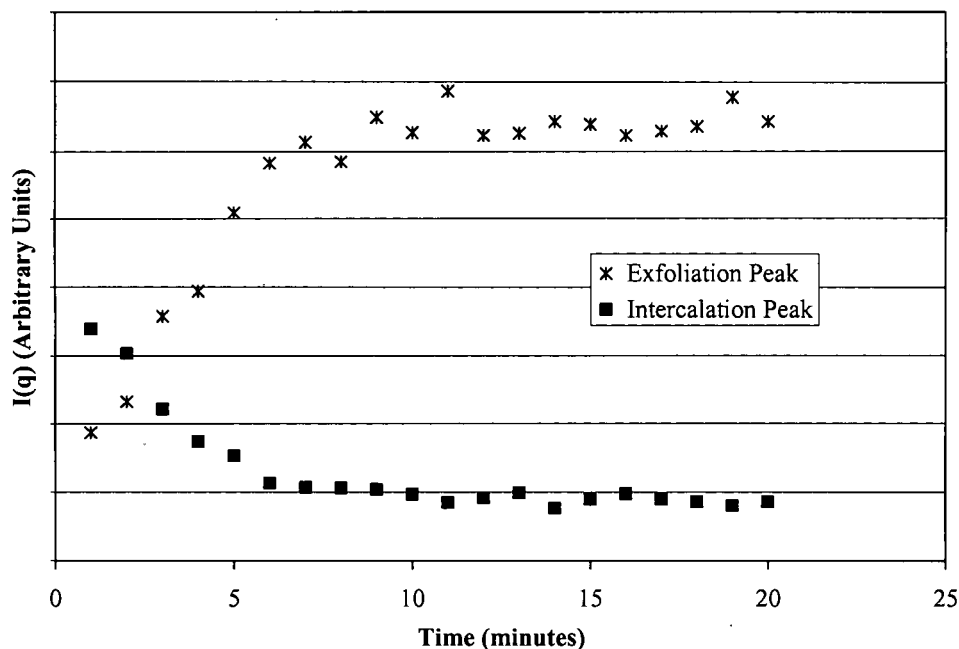


**Figure 5-11:** Change of scattering intensity associated with exfoliated and intercalated morphologies as a function of time (isothermal temperature 110°C, epoxy/I.30E)

It has been shown here that the temperature and the temperature heating rate play a large role in the control of morphology development of layered silicate epoxy nanocomposites. Temperature controls both the cure kinetics – network formation – as well as the diffusion rate of the cure agent and additional epoxy monomer into the galleries. Temperature also affects phase separation, as with slow cures large localized differences in molecular weight may occur which can further interfere with tactoid expansion. Large d-spacings are achieved when an isothermal cure temperature is selected that is greater

than the temperature for the onset of polymerization of the layered silicate-epoxy-cure agent system. When cured at an isothermal temperature below the onset temperature, the morphology remains intercalated with minimal gallery expansion (up to only  $\sim 10$  Å beyond the initial epoxy-intercalated value). When processed at an isothermal temperature above the onset temperature, d-spacings reach greater than 100 Å. A slight and continued trend of increasing d-spacing with increasing isothermal temperature is seen. The interaction between network formation and mobility is important for this class of nanocomposites. The development of high d-spacings is at least partially dependent on the rate of network formation.

Heating rate affects the rate of OLS expansion. The ultimate d-spacing achieved at all heating rates was greater than 150 Å. The development of expanded, exfoliated morphology occurs more quickly at higher heating rates. The temperature at which exfoliation began during heating rates was not related to the onset temperature. These findings are augmented with those of Kornmann in which processing temperature is suggested to have a role in morphology development as it affects both the kinetics of network formation and the diffusion of cure agent into the galleries [46]. Molecular mobility and reactivity of the epoxy-cure agent selected are parameters which influence the morphology development by affecting the reaction and network formation, which will be discussed further later in this chapter. Becker et al. more recently demonstrated similar effects of higher processing temperatures driving greater gallery expansion which agree well with the results of this study [60].

## **Role of Material Variations on Morphology Development**

Preconditioning of the silicate-epoxy mixture was comprised of variations in the elapsed time between preparation of the silicate-epoxy mixture and the addition of the cure agent. This process, here called “mixture advancing” or “advancing” was achieved at room temperature for periods ranging from a few hours to a number of weeks. This process is not unusual in the composites industry, and is often used to increase shelf life of carbon fiber reinforced thermoset prepregs through ‘advancing’ the cure of the resin by partial curing or ‘staging’ to the point that the glass transition temperature,  $T_g$ , is near or above room temperature<sup>4</sup>. The build-up of molecular weight in epoxies can be separate from three-dimensional network formation, which provides an additional complexity or process control variable that can be exploited in morphology development.

In the OLS-epoxy mixture used here, the OLS serves to catalyze reactions and therefore advances the epoxy over time with no addition of cure agent. Variations on the advancement of I.30E epoxy mixtures were explored through SAXS as well as through thermal analysis.

SAXS data shows that advancement of the epoxy results in dramatically different morphologies and exfoliation development behaviors (Table 5-1). Duration of mixture

---

<sup>4</sup> For co-reactants of difunctional and trifunctional reactants, cure starts with A-stage or uncured monomers and oligomers; proceeds via simultaneous linear growth and branching to an increasingly more viscous B-stage material below the gel point; continues with formation of a gelled but incompletely cross-linked network; and ends with the fully cured, C-stage thermoset.

advancement is seen to be directly related to d-spacing: longer durations result in higher d-spacings.

**Table 5-1:** The d-spacings reached by I.30E/epoxy-mPDA at an isothermal temperature of 80°C are greater for greater mixture advancement.

<b>Weight Fraction I.30E</b>	<b>Fabrication Process</b>	<b>Initial d-spacing (Å)</b>	<b>d-spacing at 60 minutes (Å)</b>
5%	Baseline	34	42 <sup>a</sup>
5%	Epoxy-silicate mixture advanced 1 week	34	45
5%	Epoxy-silicate mixture advanced 4+ weeks	36	104
5%	Epoxy-silicate mixture advanced 8 weeks	35	105
5%	Epoxy-silicate mixture advanced 16+ weeks	36	110
7%	Baseline	33	37
7%	Epoxy-silicate mixture advanced 16+ weeks	35	106

<sup>a</sup> Final Time: 45 Minutes

*In situ* studies of materials that had undergone long-term mixture advancement prior to addition of cure agent exhibited distinctly different features related to morphology as compared with samples that underwent the baseline fabrication process. Figure 5-12 shows scattering curves from materials which had been mixture advanced for 16 weeks; significant differences in scattering can be seen in comparison to the baseline material shown in Figure 5-13.

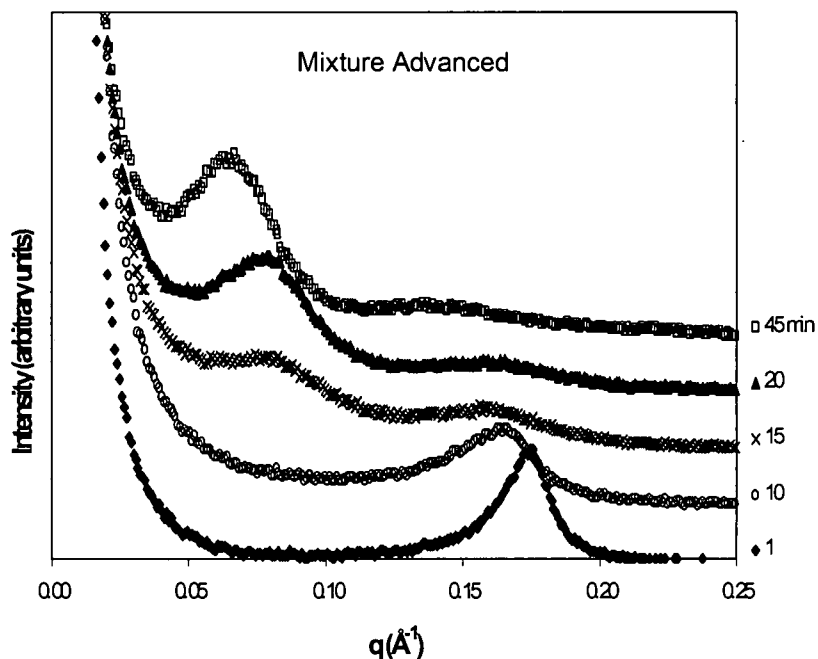


**Figure 5-12:** Time-dependent small angle x-ray scattering data for 5% I.30E/Epon 828 with mPDA at isothermal temperature of 80°C after mixture advancement for 16 weeks (intensity data offset for clarity).

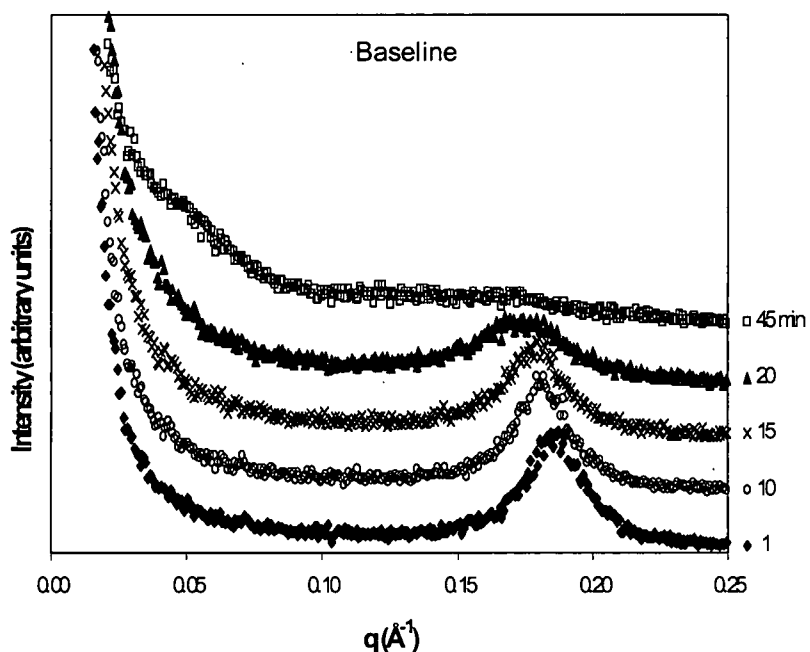


**Figure 5-13:** Time-dependent small angle x-ray scattering data for baseline (no advancement) 5% I.30E/Epon 828 with mPDA at isothermal temperature of 80°C (intensity data offset for clarity).

Mixture-advanced samples exhibited initiation of gallery expansion in significantly shorter times as evidenced by the loss of the peak associated with the initial intercalated morphology. With isothermal heating at 80°C, peak intensity associated with intercalation ( $q \sim 0.18 \text{ \AA}^{-1}$ , d-spacing  $\sim 35 \text{ \AA}$ ) for the material that underwent the longest mixture advancement time reached half of its initial intensity within 10 minutes as compared to 20 minutes for baseline samples. Peak breadth, an indication of the size of the scatterer domains, was narrower for the mixture-advanced materials, implying less disorder and a longer range persistence of the dominant scattering morphology. Most significant was the difference in scattering in the range of  $q$  0.05 to  $0.1 \text{ \AA}^{-1}$ , or structures  $>63\text{-}125 \text{ \AA}$ , with mixture-advanced samples exhibiting a clear and gradual development of a Bragg peak within 45 minutes at 80°C. Note that the baseline material did not clearly develop such peaks within this time period.

The manner in which such a peak develops with time differs from that of the baseline as well. In previous studies of epoxy nanocomposites both in this study as well as in the literature, trends on the loss of peaks associated with intercalated morphology and the development of peaks associated with exfoliated morphology have been observed to occur as if through a transition, with pertinent peaks appearing to be mutually exclusive (Figure 5-12) [77, 87]. Such observations suggest a rapid loss of intercalated morphology and subsequent development of exfoliated morphology. The lack of clear Bragg peaks during this period may be due to a loss of initial registry and order through network formation. Extragallery network formation may occur closely thereafter and limit mobility before the layers are fully expanded and reach more ordered states. This

would provide a model in which minimal low  $q$  peak development occurs prior to gelation. Yet for the mixture-advanced materials, the development of Bragg peaks associated with exfoliated morphology occurs simultaneously with the loss of peaks associated with intercalated morphology. Two distinct and ordered morphologies co-existed during the process, which is clearly seen in Figure 5-13. This behavior was reproduced and the change in the real-time morphology development is seen to occur gradually with mixture advancement (full data in Appendix C).

The mixture advanced process raises the question of the possibility of settling of the OLS over time and the effect it would have on morphology development. Scattering data at the same processing temperature for I.30E in weight fractions of 1%, 5% and 7% were compared and all exhibit the same trend in which the peak associated with the epoxy intercalation gradually decreases in intensity, broadens, and shifts to slightly lower  $q$  representative of an expansion of the gallery on the order of a few angstroms over a period of 60 minutes. Settling of the OLS would reduce the number of scatterers and provide only for a peak intensity and breadth reduction, but not for the SAXS data observed. Thermal analysis also proves that the observed variations are not due to settling as will be discussed later.

### **Mechanisms of Exfoliated Morphology Development**

A postulation on the role of the balance between intragallery and extragallery network formation on exfoliation in layered silicate epoxy nanocomposites has been developed

over the past several years [46, 78, 79]. The generally accepted model proposed by Lan et al. in which intragallery crosslinking rates must be higher than extragallery rates to allow for the development of exfoliation has become a dominant reference as interest in epoxy-based nanocomposites has increased [47, 54, 60, 78, 91, 92]. However, comparisons often lack complete characterization of morphologies and appreciation for the role of OLS and processing variables.

### **Role of Organoclay Participation in Reaction**

In the baseline material, the acceleration of the reaction and network formation within the vicinity of the organoclay may have resulted in less cure agent able to intercalate the galleries due to network formation around the edges of the tactoid which could effectively constraining a gradual expansion. This explanation would be supportable if the catalytic effect was due in some manner to the edges of the individual silicate layers. However, as it is the ammonium groups on the surface that are active, it is more plausible that the accelerated network formation within the gallery may have resulted in an effective blockage to the continued infusion of new epoxy and cure agent necessary to continue network formation and resulting gallery expansion.

With the variations in time that the mixture advanced epoxy-organoclay systems experienced prior to the addition of cure agent and the demonstration that the OLS reacts with the epoxy, it is reasonable to expect that final polymerization may have occurred in a different manner base on different mixture compositions.

In the mixture advanced materials, the catalytic effect is not observed to the extent seen in the baseline materials (Figure 5-14). Preconditioning through mixture advancement discussed previously minimizes the advancement of reaction onset, or more accurately, may be slowly advancing the molecular weight of the epoxy locally with respect to the organoclay. Slow advancement of molecular weight over time can occur and is documented. Such advancement will affect the heat of reaction measured as well, with a decreased heat of reaction reflective of the reduced amount of epoxy remaining/available for reaction (Table 5-2). Such an increase in molecular weight may also result in higher temperatures necessary for mobility, and the possibility that the DSC is not capturing the catalytic activity as effectively.

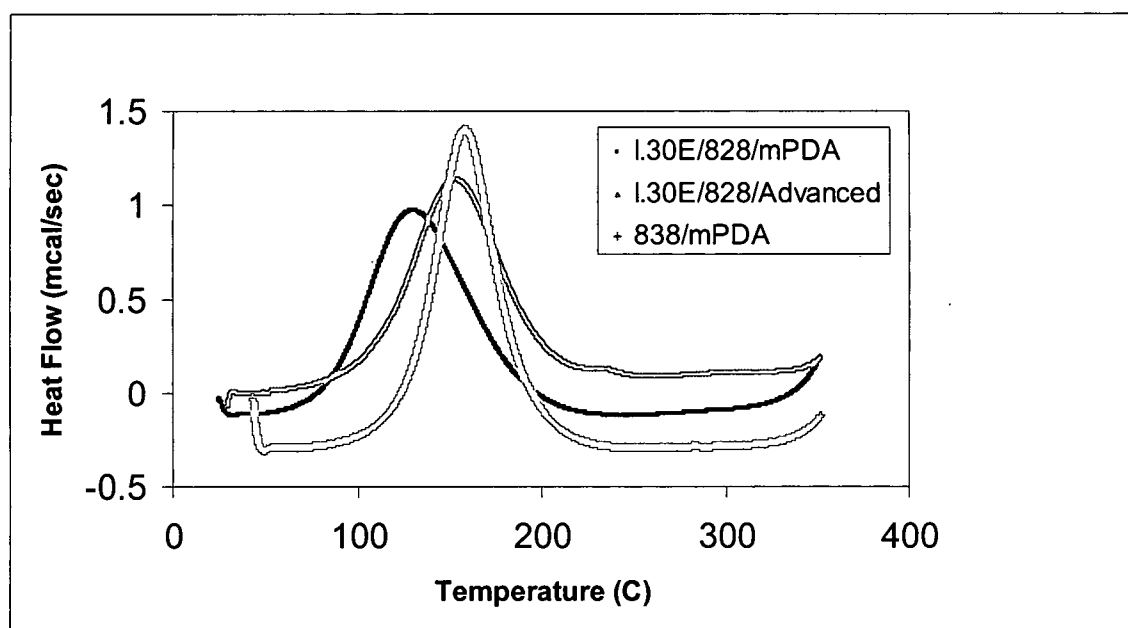


**Figure 5-14:** Differential Scanning Calorimetry for 828/mPDA, baseline processed, and advanced 5% I.30E/828/mPDA shows that advancement minimizes the catalytic effect of the OLS. Data taken at 10°C/minute in nitrogen.

**Table 5-2:** DSC data for preconditioned epoxy/mPDA/I.30E materials.

<b>Material</b>	<b>T<sub>onset</sub> (°C)</b>	<b>T<sub>max</sub> (°C)</b>	<b>ΔH<sub>rxn</sub> (cal/g) (normalized to epoxy content)</b>
Epon 828/mPDA	126	158	106
Epon 828/mPDA/I.30E baseline	84	130	103
Epon 828/mPDA/ I.30E advanced 2 day	85	136	99
Epon 828/mPDA/ I.30E advanced 1 week	87	136	101
Epon 828/mPDA/ I.30E advanced 8 weeks	93	141	76
Epon 828/mPDA/ I.30E advanced 16 weeks	107	154	96

If the edges of the silicate layers were responsible for the catalytic effect, then cross-linking of the epoxy would have radiated out from the tactoids in a linear manner over the time of mixture advancement, which would have resulted in an increased viscosity of the bulk material. This model would also then result in less ability for the tactoids to expand on addition of mPDA and through processing as the tactoid would be surrounded by some degree of cross-linked epoxy, and the higher resulting viscosity would both constrain its expansion as well as prevent the infusion of cure agent and fresh epoxy into the gallery. However, if the catalytic effect occurs within the galleries, the mixture advanced materials would have maintained viscosity as is observed. In the mixture advancement process, the ammonium group is partially consumed prior to the addition of the amine cure agent, so the reaction between the cure agent and epoxy is not catalyzed to the extent that occurs in the baseline process. The diffusion of cure agent and replenishment of epoxy into the galleries is allowed to occur over a longer period of time, with less competition between crosslinking and diffusion, allowing the galleries to expand uniformly and to a greater extent before extragallery network formation reduces any additional expansion. The DSC data coupled with the SAXS and TEM observations

suggests that accelerated network formation due to the OLS hinders tactoid expansion, perhaps through the limitations that are put on the infusion of additional epoxy and cure agent into the gallery. The forces required to expand the gallery must come from within and here are due to the infusion of additional material within the gallery.

### **Role of Network Formation and Infusion into the Galleries**

This research provides evidence that factors other than balance of intra-and extragallery network formation affect morphology development. *In situ* SAXS studies provides unique signatures of real-time morphology development which can be used to develop phenomenological models. If the balance of network formation were the only factor in tactoid expansion, *in situ* SAXS data would reflect an initial peak that remains constant until the onset of reaction, then shift to lower  $q$  as galleries expand under situations in which the intragallery polymerization is faster than that of the bulk. Intensity, indicative of number of layers in the tactoids and of the order (registry), would not change significantly. This is shown to not be the case by results of this research. SAXS data shows an initial peak that broadens and reduces in intensity corresponding to loss of number of scatterers (layers) and loss of order (breadth at half max) during first phase of morphology development. This behavior occurred irrespective of the temperature. The SAXS suggests that the gallery expands on the order of 1-2 Å for some period of time then loses order, rather than expand consistently over time.

For the majority of the materials studied, the intragallery can be assumed to have higher polymerization rates catalyzed by the OLS (as shown by thermal analysis). In the baseline system, at isothermal heating of temperatures below the reaction onset temperature, the initial intercalated spacing undergoes about a 10 Å or 25% increase in d-spacing over 45 - 60 minutes. As crosslinking occurs in the gallery, epoxy is consumed and more material from outside the tactoid ingresses into the gallery. As it enters the tactoids from the edges, the tactoid may become distorted providing the resulting broader and weaker peak. The flexibility of the individual OLS layers is evidenced in TEM here and in other research (Figure 5-15). The outer layers of the tactoid would expand initially as they have more freedom to do so (less constrained by other layers and by the driving force of network formation in the galleries). The crosslink density in the gallery may become so great due to the accelerated effect that the OLS has that new epoxy infuses in from the edges cannot displace the center material, distorting the tactoids and losing the peak at 35 Å. The initial d-spacing is eventually lost. This occurs as if in stages, with the two peaks appearing to develop in a transition that has been noted in recent research (86, 93, 94).

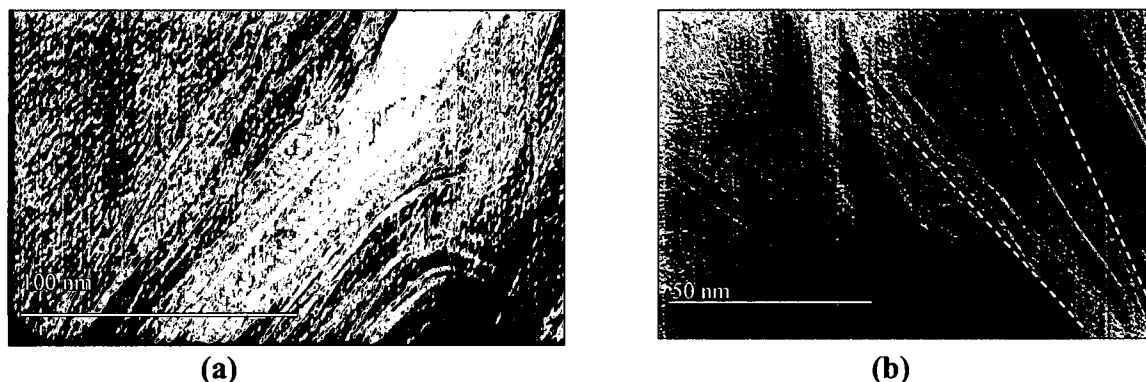


**Figure 5-15:** TEM images of 5% I.30E/828/mPDA nanocomposites show (a) flexibility of OLS layers and (b) greater expansion on edge of tactoid.

However, when the temperature is greater than that of the onset of reaction, a peak indicative of large d-spacings develops. The epoxy reaction plays a role in enabling dramatic gallery expansion. The rapid network formation and consumption of epoxy and cure agent cause infusion of additional material into the gallery, providing some force to expand the galleries. As the reaction is exothermic, the heating that results may both reduce local viscosity and enable more mobility so that the tactoids may more easily expand via polymer intercalation. The ability of new monomer and cure agent to diffuse into the gallery is an important factor in morphology development. If constrained by localized network formation, the tactoid will not expand significantly beyond its intercalated state.

The gallery expansion behavior of the mixture advanced materials further suggests that rate of network formation is not the only factor. In these materials we assume that the catalytic effect of the OLS on reactions occurs over the time periods prior to addition of the cure agent. At the time the cure agent and temperature are added to induce polymerization, the ratio of epoxy, cure agent and catalyzing organic modifications within the gallery is similar to the ratio outside the gallery. The role of the OLS is diminished in the amine-epoxy reaction, hence once polymerization via the primary cure agent is initiated it occurs at close to the same rate both within and without the tactoid. As epoxy is consumed within the gallery, it is replaced with infusing extragallery epoxy and there is a gradual expansion of the tactoids. This expansion occurs quickly since the flow of epoxy/cure agent into the galleries is not impeded by a cross-link density gradient

within the tactoid. Deformation of the OLS layers induced by the resistance that infusing epoxy meets due to the accelerated network within the gallery may be reduced as compared to the baseline materials. Registry is also much better maintained, and clear peaks that move to lower  $q$  associated with large  $d$ -spacing develop. The SAXS data suggest a loss of scatters (decreasing intensity) as if layers are removed from the tactoid one at a time. This 'peeling' off of layers, whether with registry maintained as for the mixture advanced materials or with out-of-plane deflection and deformation as for the baseline materials. This behavior has been suggested for molecular dynamics of semicrystalline thermoplastics [95]. TEMs show some evidence of graduated gallery size in tactoids, and also of retention of registry. For this system, at an isothermal temperature below that of the reaction onset temperature, the  $d$ -spacing increases from 35 Å to 110 Å or about 300% over 45 minutes.

The role of diffusion of epoxy monomer and of cure agents and the nature of the general composition of the material within the gallery is suggested here to be an equally important controlling variable. Normal extragallery network formation would be expected for the materials studied here on addition of the cure agent, with primary differences being acceleration effects and network formation within proximity of the silicates. Chin et al. observed exfoliation with the same materials studied in this work only under suppression of extragallery crosslinking through the use of less than stoichiometric amounts of cure agent and elevated temperatures [47]. The systems studied here provided a well-ordered development of structure similar to that reported by Chin with no cure agent at high temperature, with the exception of the manner in which

the peaks developed. Normal extragallery network formation would be expected for the materials studied here on addition of the cure agent, with primary differences being acceleration effects and network formation within proximity of the OLS tactoids. The different behaviors observed here suggest that the role of the zone within close proximity of the silicate is important to morphology development as is the recognition of the nonhomogeneity of intragallery and interfacial regions. These subtleties may result in different network formation around the tactoid which could serve to hinder its expansion and the development of exfoliated morphology by establishing cross-linked network barriers to the infusion of additional epoxy and cure agent into the gallery.

### **Scattering Data and Microscopy Analysis of Higher Order Morphologies**

Scattering coupled with microscopy highlight the hierarchical and mixed morphologies in OLS-epoxy nanocomposites. A characteristic feature of scattering from disordered and fractal systems is a power law relationship; in regions where

$$q \cdot a \gg 1,$$

then

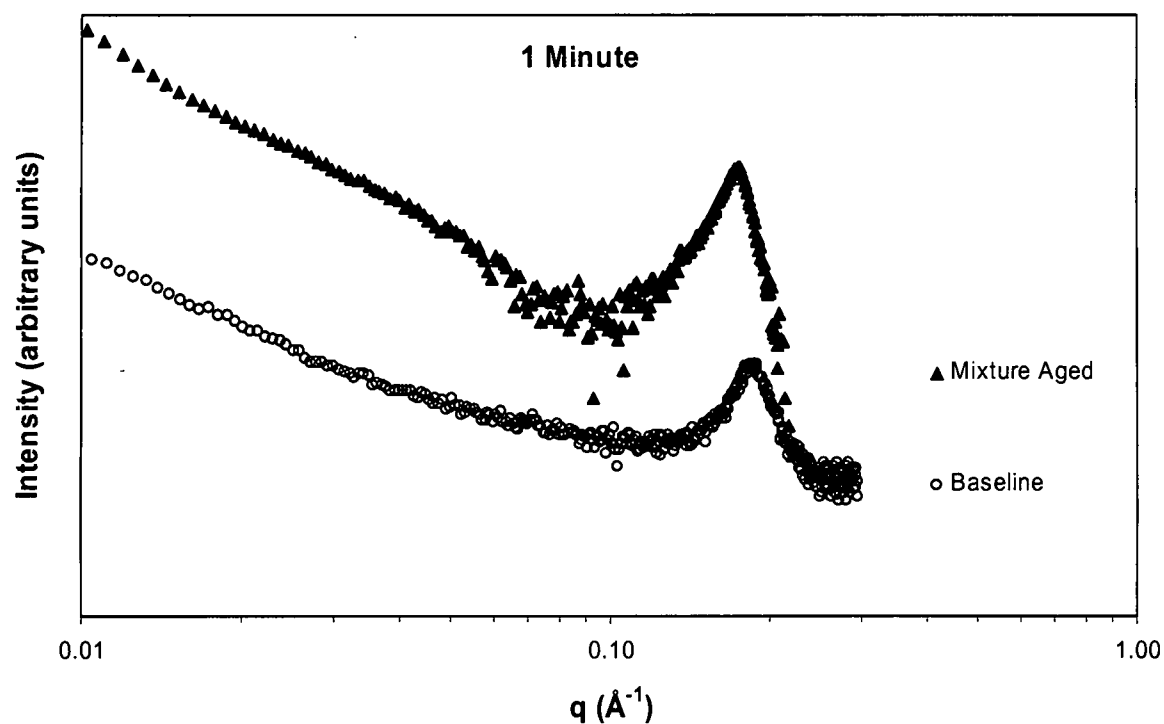
$$I(q) \sim q^{-\alpha} \quad (11)$$

Where 'a' is a characteristic length of the scatterer [96, 97]. For well-defined, simple geometric particles, it has been shown that  $\alpha$  reflects the dimensionality of the object (4 for three-dimensional objects such as spheres; 2 for quasi-two-dimensional bodies such as disks of negligible thickness; and 1 for quasi-one-dimensional elements such as thin

rods). More complex structures, or 'mass fractals', can be similarly characterized but with non-integral exponents.

Differences in the low  $q$  power law behavior, an indicator of more global structure and morphology at a scale on the order of hundreds of Å, are observed between baseline and mixture-advanced materials (Figure 5-16). Both baseline and mixture-advanced materials follow  $I(q) \sim q^{-2.5}$  initially, then tend towards  $I(q) \sim q^{-1.9}$ , with time at 80°C. These power law behaviors, though not quantitative, show a trend towards sparser structures if a mass fractal interpretation is used [98]. The various power law slope regions, which are indicative of morphologies, as well as the breaks in the slopes, which are indicative of length scales, also differ. The low  $q$  slope trend with time, depicted in Figure 5-17, shows a strong dependence on the mixture advancement condition of the materials. The time at which the slope undergoes a significant transition occurs sooner for the material that underwent the longest advancement, at approximately 16 as compared to 23 minutes. Once past the knee in the curve, the slope continues to increase slightly with time for the advanced materials, whereas the slope for the baseline materials appears to stabilize. The slope trend goes towards more two-dimensional scatterers for the mixture advanced material, possibly indicative of tactoid development through gallery expansion. The knees in the curve correspond well with the minimum intensity of Bragg scattering from the initial intercalated structures of 34 Å d-spacings (Figure 5-18). At this point, the initial well-ordered intercalated morphology no longer dominates the material.

(a)



(b)

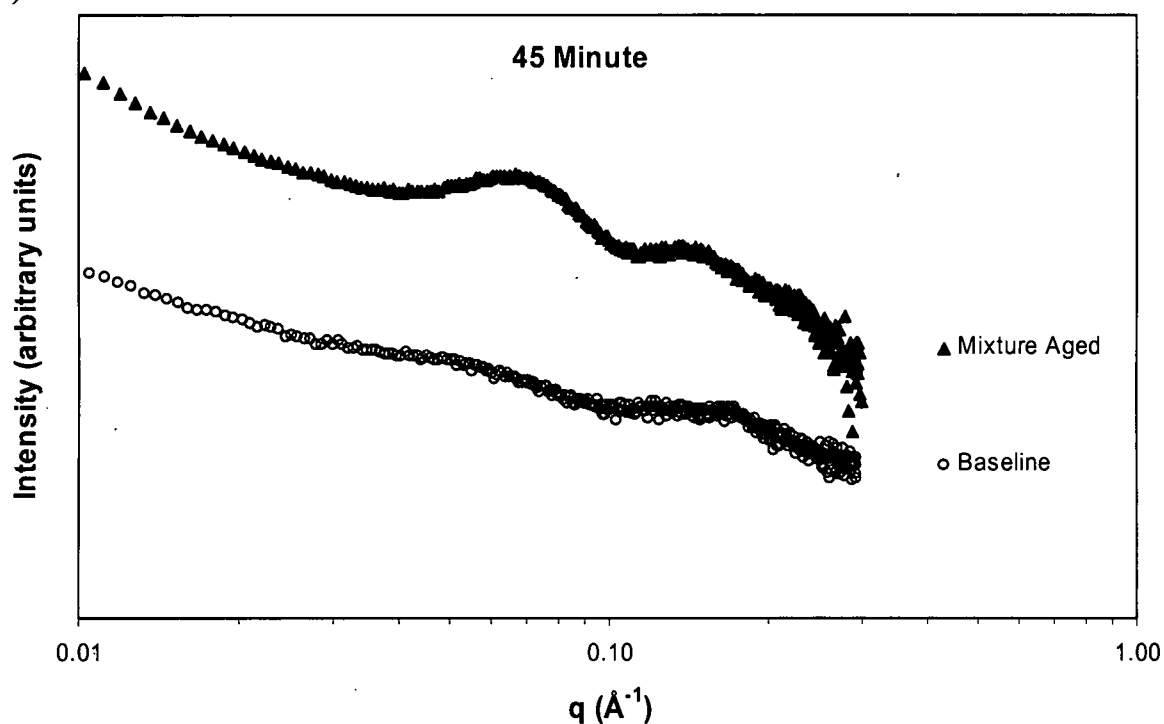


**Figure 5-16:** Small angle x-ray data for baseline material (a) and mixture-advanced materials (b) show similar behavior initially (1 minute) but differ significantly in the low  $q$  region slope and Bragg peaks after 45 minutes at 80°C.

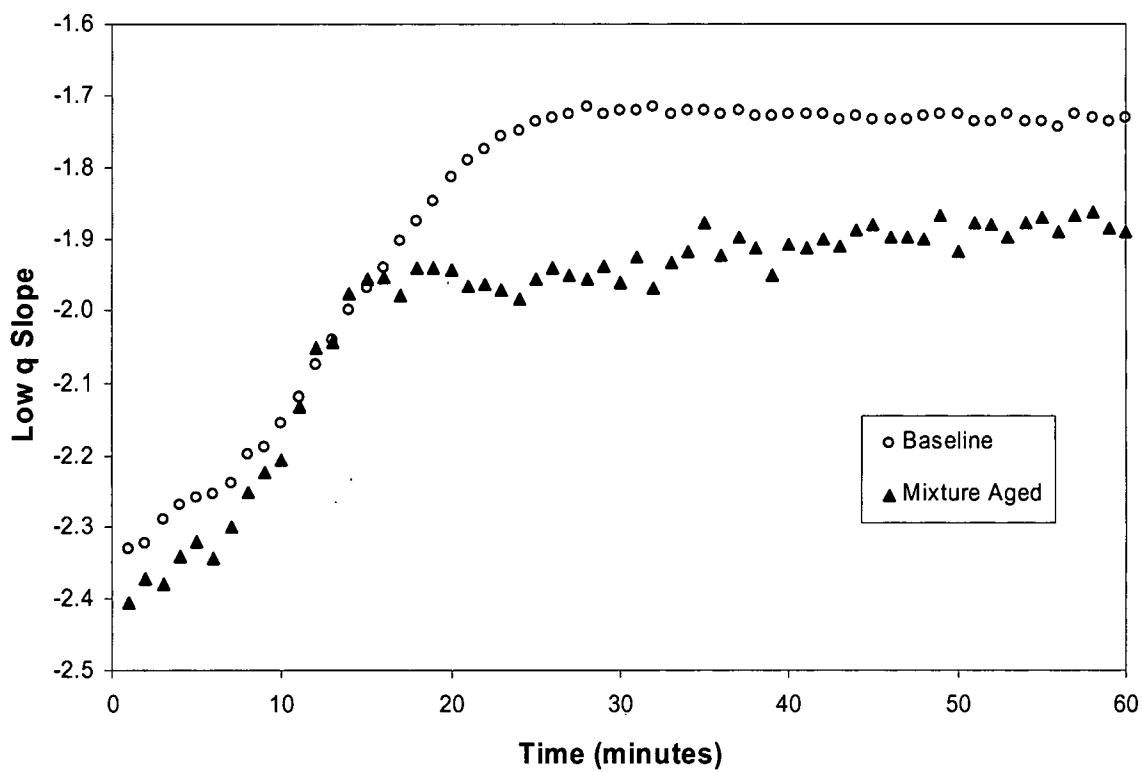
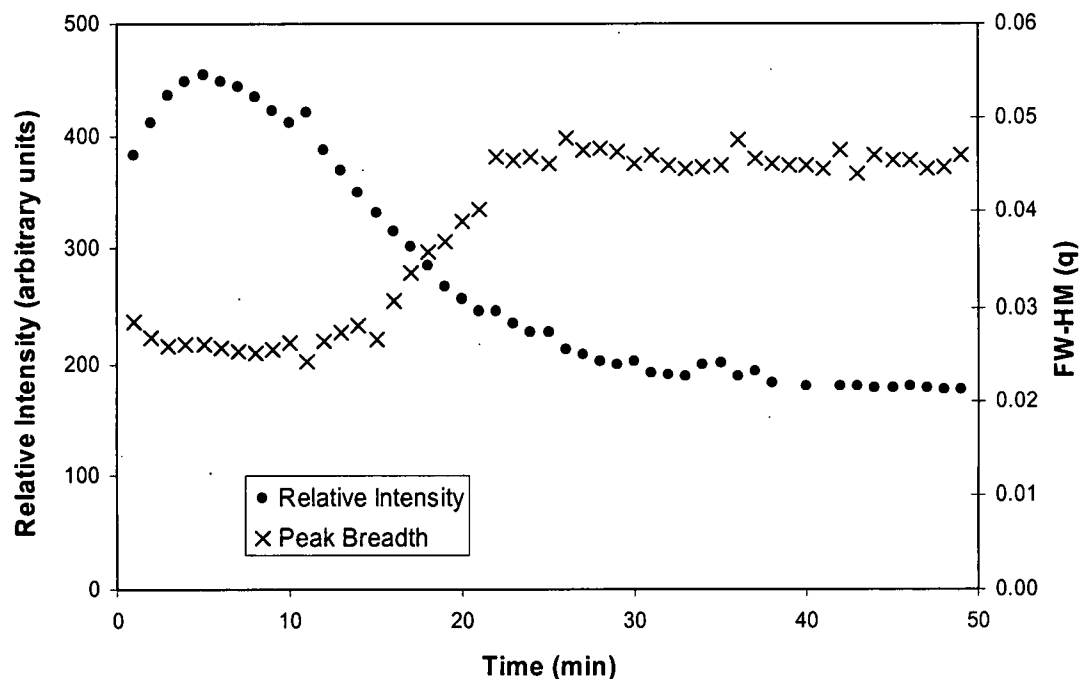


**Figure 5-17:** Low q slopes for materials versus time show earlier onset of slope stabilization for mixture-advanced materials.

(a)



(b)

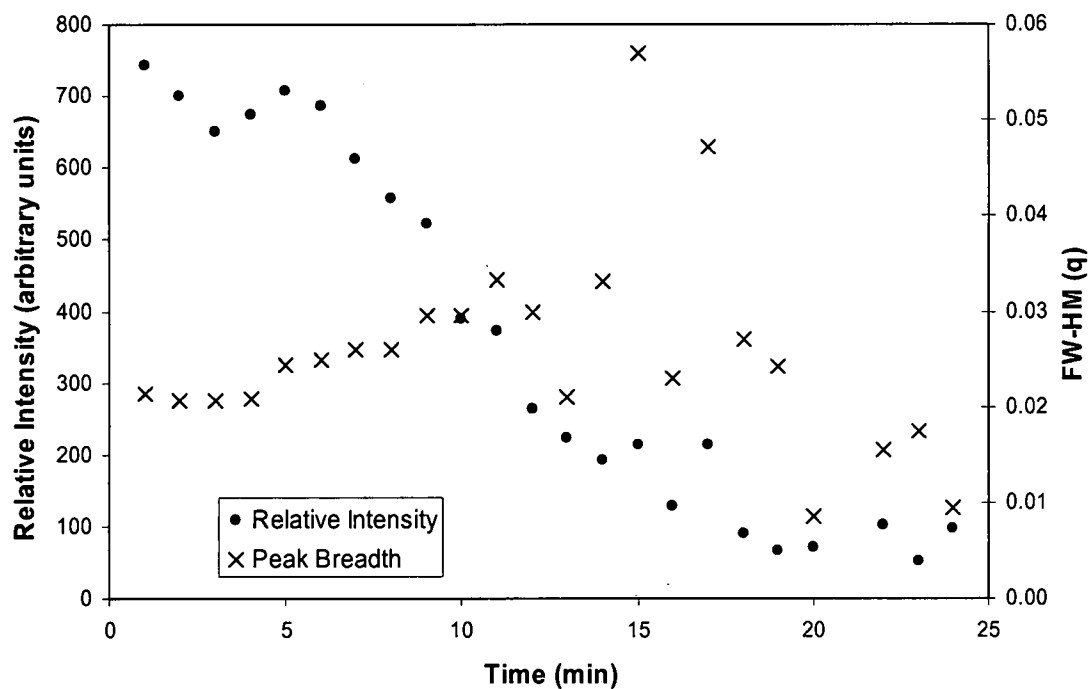


**Figure 5-18:** Time for loss of scattering intensity of initial Bragg peak [ $\sim 28$  minutes for baseline (a),  $\sim 17$  minutes for mixture advanced (b)] corresponds with onset of stabilization of low  $q$  slopes. (Difficulty in fitting peak breadth causing scatter in data.)

The significant differences in morphology states between these two conditions are depicted clearly in TEM images (Figure 5-19). Although it is possible to distinguish multiple as well as hierarchies of morphologies within a single TEM image, analysis of multiple images reveals a dominant morphology in the baseline materials that are intercalated, with straight OLS layers separated typically by constant spacings of 25 to 75 Å and associated in tactoids of 5 to 9 layers. On a higher scale, tactoids are generally parallel to each other or at small angles and are separated by 50 to 150 Å. The dominant morphology for the materials that underwent mixture advancement included ordered tactoids in packs of 4 OLS layers with spacings of approximately 80 Å. Tactoids are generally parallel, separated by 75 Å through over 600 Å. Some tactoids also exhibited gradient spacings in which layers were separated by increasing distances through a tactoid. For both material systems, multiple levels and mixtures of intercalated and exfoliated morphologies can be found (as well as some silicates that are not intercalated). In general, mixture advancement results in a more expanded tactoid morphology state with smaller colonies of tactoids; the baseline material shows an ordered intercalated morphology with longer range registry both within and between tactoids.

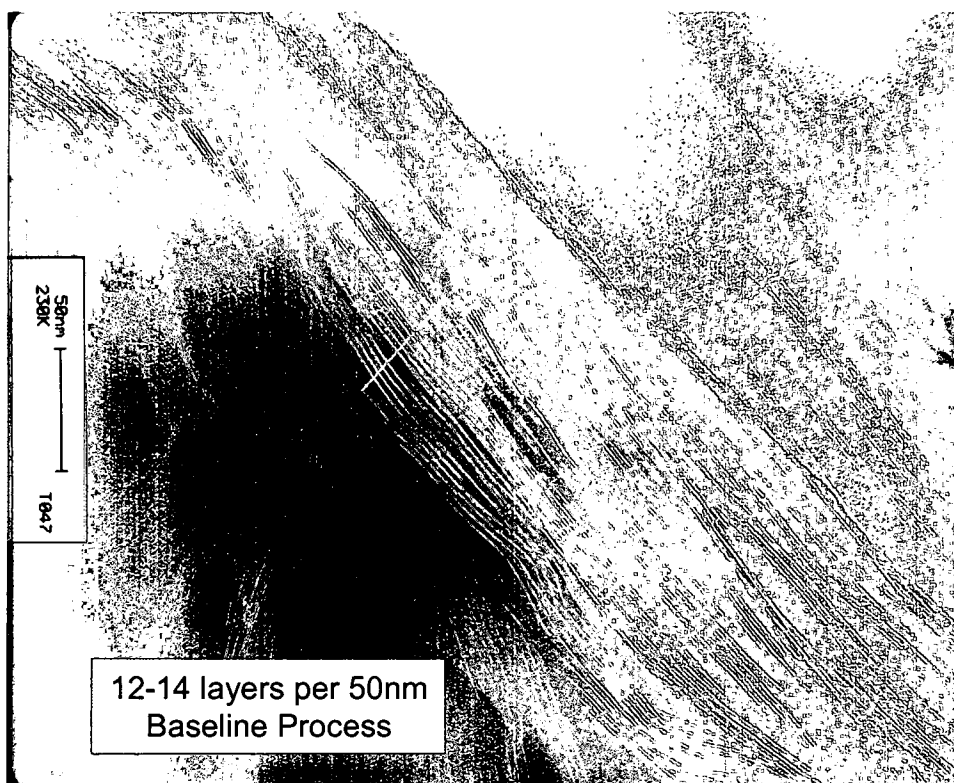
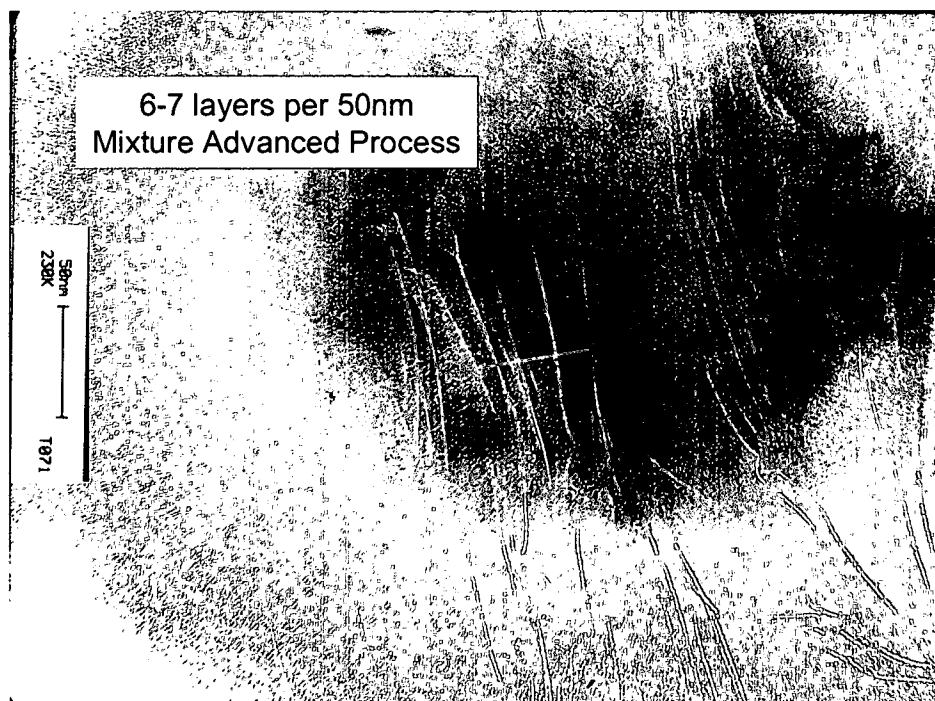


**Figure 5-19:** TEM images of representative tactoids.

The discussion to this point highlights differences observed by *in situ* SAX and DSC due to the material preconditioning studied here which can be used to support an extended phenomenological-based model of morphology and exfoliation development and offer motivation for the recognition of unexpected complexities in layered silicate thermoset nanocomposites due to material and process variations. Such models are of great interest now that nanocomposite research is focusing on epoxies and thermosetting polymers. Chen, and Ober et al. propose that the exfoliation mechanisms in epoxy nanocomposites consists of three stages: first, interlayer expansion occurs to a level sufficient to overcome any network development that might bridge the silicate layers and effectively bind the tactoids; second, steady increasing of expansion, and third, a slowing and stopping of such expansion [99]. This model rests again on the general thought that the intragallery cross-linking rate must be higher than that of the extragallery, but does not capture the data generated in this research. Kong and Park also identify a stepwise exfoliation approach, in which expansion of the galleries is due first to polymerization catalyzed by the protonated organoclay amine cation and then by the expansion due to the driving force due to the crosslinking from the primary cure agent in the gallery [100]. More recent work suggests that the role of forces exerted by cross-linked epoxy within the galleries is the key mechanism for exfoliation and concludes that higher intragallery polymerization is not necessary for exfoliation [101].

The research performed here concludes that

- the general make-up of the inner gallery chemistries is important and slight differences can be significant – that is, the ratios of epoxy monomer,

organoclay modifier, and cure agent at a minimum must be well understood for control of morphology development;

- with n-octadecylammonium ( $C_{18}H_{37}NH_3^+$ ) modified montmorillonite, the acidity of the ammonium is the primary catalyst to the epoxy-amine reaction;
- key factors controlling the development of exfoliated morphologies include temperature, temperature rates, and diffusion rates of intercalation of epoxy and curing agent [77, 93]. Recent work by Wang provides additional support for this premise, finding that although the relative cross-linking rates govern the development of exfoliation, other parameters such as cure temperature may have a role [106].

These observations suggest that the role of network formation within the galleries and its impact on mass transport and phase separation is a more important variable in morphology development than is the network formation outside the gallery and its impact on the mobility of the individual OLS layers.

Review of the differences observed in the real-time scattering data from this study suggest that a more general phenomenological model be offered to encompass the above observations. As the epoxy and amine react, intragallery epoxy is consumed and epoxy and cure agent from outside the tactoid infuse into the galleries from the tactoid edges. If the intragallery polymerization is catalyzed by the OLS ammonium, intragallery network builds up quickly and may hinder infusion, causing the tactoid to become distorted or

expand in a disordered manner. This provides for the resulting broader and weaker peak. At some point gelation occurs within the gallery, after which infusion of fresh epoxy and cure agent may be hindered such that continued expansion in a general sense ceases.

If the intragallery polymerization is not highly catalyzed, polymerization via the primary cure agent occurs at close to the same rate within and outside the tactoid. As epoxy is consumed within the gallery, it is replaced with infusing extragallery epoxy and cure agent and causes a gradual and ordered expansion of the tactoids. The force exerted by the network forming inside the galleries serves to expand the tactoid's outer layers first. Expanded structures can be achieved even when the rates of intra- and extragallery polymerization is matched. This gradual expansion occurs fairly quickly, as the flow of epoxy/cure agent into the galleries is not impeded by a cross-link density gradient.

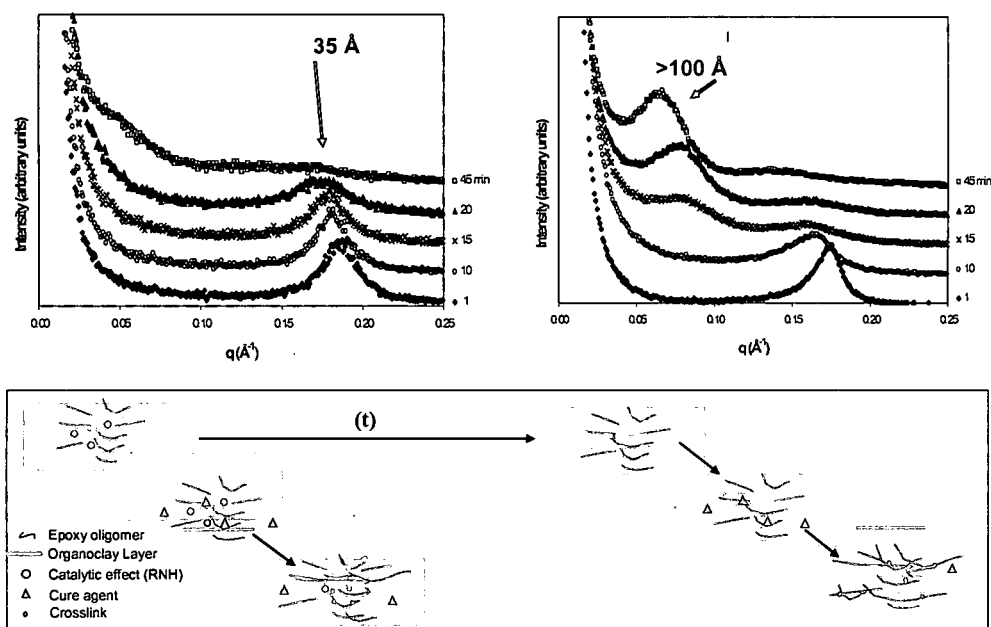


**Figure 5-20:** Schematic of morphology development for catalyzed systems (left) and non-catalyzed systems (right).

### **Role of Cure Agents on Morphology Development**

As shown by the previous section, factors other than the balance of intragallery and extragallery network formation rates must be included to explain exfoliated morphology development phenomena in OLS-epoxy systems. Differences in the types of reactants may play a role in the development of exfoliated morphology. In reactions of epoxy with aromatic amines, network development occurs through the initial formation of linear polymer molecules of high molecular weight, which then crosslink to form a network, with some remaining uncrosslinked. In contrast, with aliphatic amines network development initiates with the formation of branched, low molecular weight polymer molecules, which then link to form a highly crosslinked network [37]. It is reasonable to expect unique interaction of the OLS with the oligomer and the process of polymerization due the fact that most of the polymer sees OLS surfaces.

A variation in cure agent chemistry was the focus of selected studies. Epi-Cure Curing Agent W (diethyltolouenediamine, Shell) another aromatic amine with an average molecular weight of 181, and JeffamineT-403, (polyoxypropylenetriamine, Huntsman), an aliphatic amine with an average molecular weight of approximately 440 were selected in addition to the mPDA to explore the effect of cure agent size and mobility on morphology development. Cure W and mPDA, both fairly rigid molecules of similar size, could be expected to offer similar molecular diffusivity under similar processing conditions. T-403 represents not only a much larger molecule, but also a flexible structure.

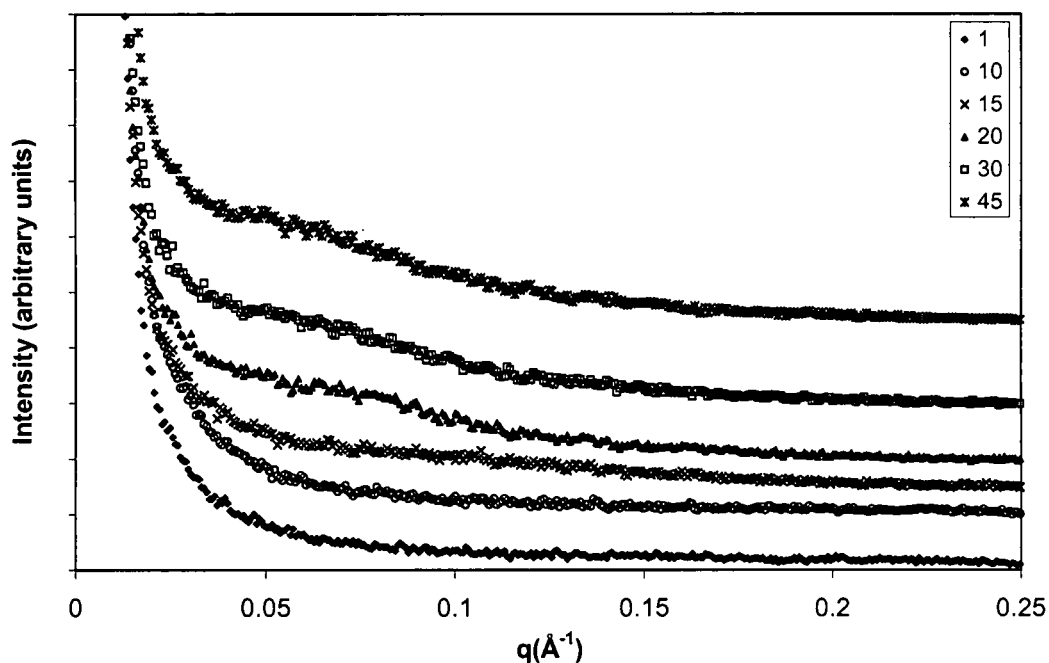
Aromatic amine cure agents affect not only the rate of cure but the network geometry and morphology. The shape, size and chemistry of the cure agent may affect how it interacts with the OLS. Kornmann et al. characterized cured samples of 828 epoxy with D-230, a aliphatic diamine curing agent, with WAXD and found that an intercalated morphology on the order of 88 Å when cured three hours at 75°C [46]. According to the material supplier, T-403 undergoes reactions typical of primary amines and closely related to their JEFFAMINE D-230 cure agent. Kornmann concluded that the nature of the curing agent has a major effect on the ability to exfoliate epoxy nanocomposites, primarily through the impact on the balance of reaction rates between the intragallery and extragallery polymerization. Want et al. also studied the exfoliation process with different curing agents [92]. Yet it is very difficult to compare the data from this research to the conclusions drawn in the literature, as we have shown that the temperature of curing as well as heating rate affects the morphology development. Comparisons of a morphology gained at 3 hours at 75°C by Kornmann with different systems and different processing does not provide insight; this challenge also underscores the need to fully characterize material systems at various processing conditions and with various tools for true understanding of morphology development. It has also been shown that a difference of polymerization rates is not the sole factor in morphology development of nanocomposites.

Cure agents not only are capable of determining network formation paths, but are also small molecules that can diffuse into the galleries. Early studies on organic modifications in the mineralogical literature have observed relationships between intercalation and the

number of carbon atoms on the amine vs. basal spacing suggest that steric hindrance within the galleries may play a role in morphology development [7, 58]. Therefore, at these scales, it is reasonable to expect that morphology development may be affected by cure agent selection for additional reasons beyond its specific network formation.

Jeffamine T-403 provided for significantly different morphology development than did the aromatic amines mPDA and Cure W as shown by *in situ* SAX studies. Upon mixing with the epoxy-OLS, the T-403 immediately intercalated and disrupted the tactoid as evidenced by the complete lack of a scattering peak associated with the intercalated epoxy-organoclay (Figure 5-21). In comparison, on addition of the aromatic amines to the epoxy-organoclay mixture the peak associated with this intercalated ordered structure remains strong.

a)



b)

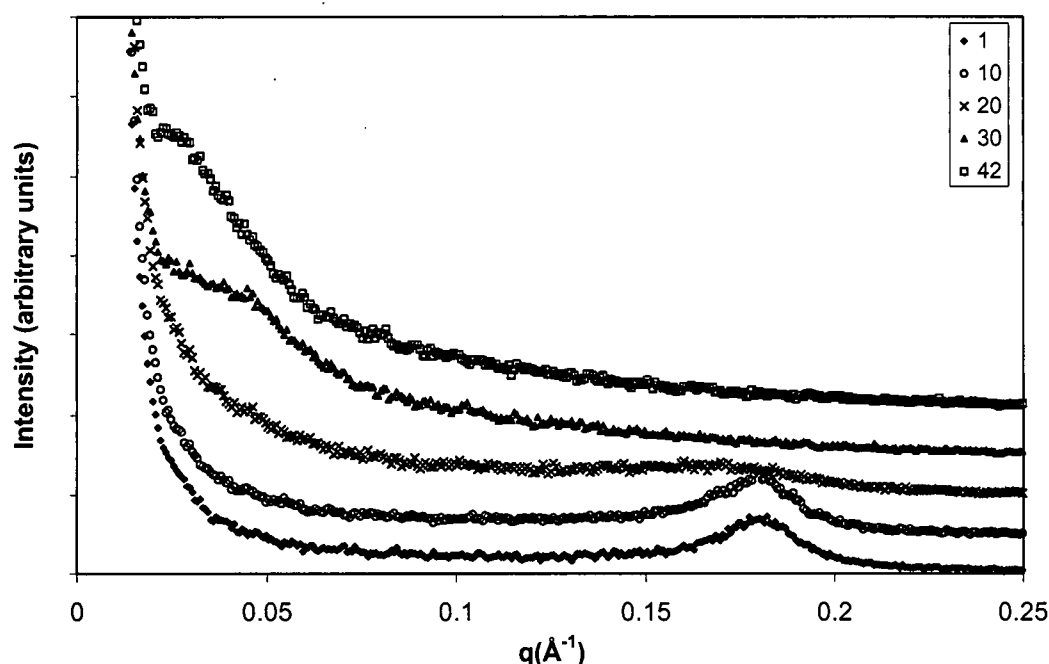


**Figure 5-21:** Time-dependent small angle x-ray scattering data comparison of a) 5% I.30E/Epon 828 with Epi-cure W and b) 5% I.30E/Epon 828 with T-403 at heating rate of 5°C/minute (intensity data offset for clarity).

The SAXS data suggest that there are significant differences between the manner in which these cure agents interact with the initial epoxy-intercalated OLS. Chemical compatibility and steric hindrance may play a role. Size, concentration and structure all offer insight into the differences observed in the morphology development behavior via SAXS data. Although not a rigorous study, these observations serve to add to the ability to assess the major variables of morphology development. T-403 is a larger molecule than the mPDA or Cure W, and geometric factors may play a role in the general disruption of the tactoid order. The epoxy-filled gallery prior to addition of cure agent is approximately 35 Å. mPDA is on the order of 4-5 Å; Cure W on same order; T-403 on order of 20 Å. The T-403 is over half the size as the space into which it will intercalate,

whereas the aromatic amines are on the order of one seventh the size of the gallery. The stoichiometric ratios for each cure agent increase with increasing size: mPDA – 14 pph (by weight) epoxy; Cure W – 26 pph epoxy; and T-403 – 42 pph epoxy. Thus the relative size and higher concentration of T-403 could displace more of the intercalated epoxy and result in the initial disruption of tactoid registry as observed in the scattering data.

However, the molecular structure of the T-403 is more flexible than those of the aromatic amines, and may adopt more positions within the gallery and thus be less hindered in its intercalation within the galleries. Chemical compatibility between the T-403 and the organoclays may also play a role. T-403, like the n-octadecylammonium ( $C_{18}H_{37}NH_3^+$ ) treatment on the montmorillonite, is an aliphatic amine. It is likely more chemically compatible with the OLS than the aromatic amines, as like dissolves like either in terms of similar chemical groups or similar polarities. Final d-spacings for the difference cure agents were not significantly different.

These cure agents should all result in a three dimensional crosslinked network as all are primary amines. The ultimate network formations and reaction rates will differ based not only on the difference between aromatic vs. aliphatic, but perhaps also due to functionality. Reaction efficiency of the reaction is related to how accessible the epoxy groups are to the reactive parts of the cure agent. The molecules' rotational and translational freedom affects its chance to form primary bonds with adjacent epoxy groups, so again, mobility and flexibility may play a role. Reaction mechanisms must

also be considered, as both rates and directions differ with different cure agents, but are not explored in depth here. Further investigation of the role of solubility of cure agents and OLS is suggested for future work, but the fact that compatibility and mobility can play such a drastic role on initial morphology underscores the complexities that must be taken into account when suggesting models for morphology development in aerospace epoxy-based nanocomposites. And of course, the ultimate application of nanocomposites and required physical and mechanical properties will largely dictate the selection of cure agent.

### **Polymer Mobility in Cured Nanocomposites**

The effects of the OLS on network formation and ultimate network density must be accounted for not only within the morphology of the OLS constituent but also for the polymer itself. The ring-opening reaction of epoxies are well known to be sensitive to steric hindrance, and in nanocomposites the scale of the OLS is on the order of the oligomers so could be expected to affect network formation and local network density (polymer molecular weight between two points of crosslinking) [37, p 286].

Conventional fillers have also been observed to decrease the local concentration of the crosslinking agent, thus disrupting the crosslinking process and decreasing the network density in the composite compared to the neat resin [4, 102]. Network formation through curing determines the level of all physical properties for thermosets (modulus, thermal expansion, conductivity, etc) and is very important for thermoset composite materials.

Dynamic mechanical analysis (DMA) can provide insight into molecular mobility and the

polymer network, and allows the exploration of subtle differences that may not be readily apparent but could manifest themselves in eventual physical properties and behavior.

DMA data shows that the incorporation of OLS results in very slight to insignificant changes to the glassy storage modulus value, however, it does shift the glassy behavior to a slightly higher temperature (Figure 5-22). This data is consistent with what others have found with OLS epoxy-amine systems [103]. The very slight improvement in storage modulus in the glassy region is seen with no improvement in the tan delta damping peak, even a slight decrease. Impact in the rubbery region is much higher as would be expected, as the effect of filler, crosslink density or other such structures impacts the rubbery modulus to a much greater extent than the glassy modulus for polymers.

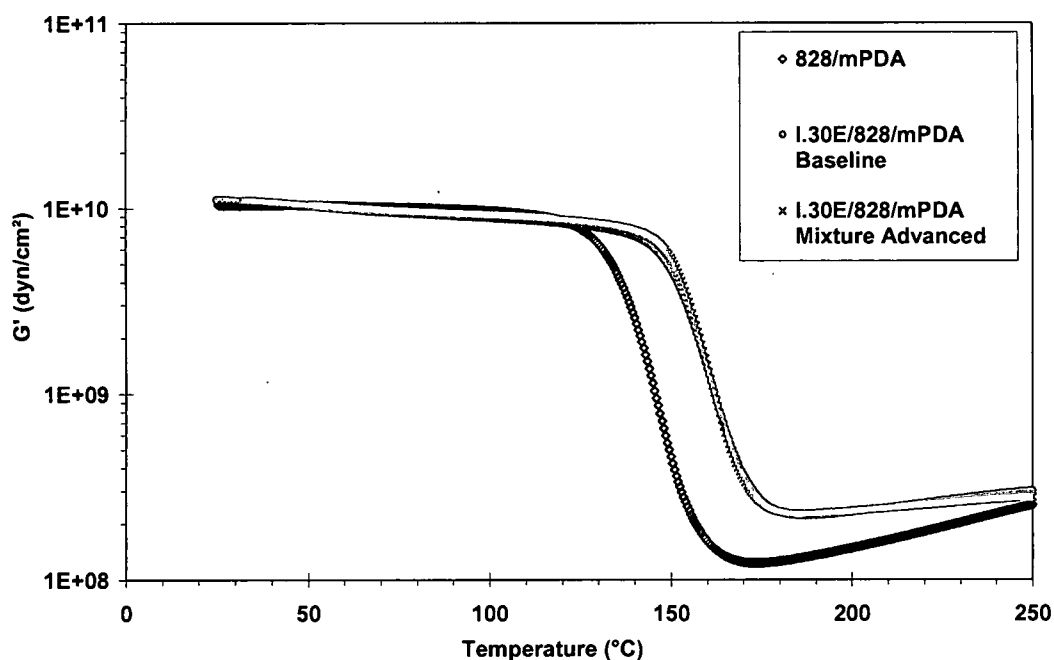


**Figure 5-22:** Dynamic mechanical data, DMA torsion, performed at 2°C/minute, 100 rad/sec, 0.1% strain, shows storage modulus for 828/mPDA and 5% I.30E/828/mPDA processed via baseline and mixture advancement processes.

Additional information about relaxations and hence structure can be obtained through DMA. There are three well-documented relaxation processes in amino-cured epoxies: the  $\alpha$  transition - the onset of long-range, coordinated molecular motions; the  $\beta$  relaxation observed at about  $-60^{\circ}\text{C}$  as a result of the motions of the hydroxypropylether units together with the flips of the benzene rings of the DGEBA; and the  $\gamma$  relaxation at approximately  $-150^{\circ}\text{C}$  due to motions of the flexible central parts of long aliphatic sequences [39, 102]. The loss modulus and  $\tan \delta$  (defined as the ratio between the loss and storage moduli) display maxima at the alpha transition and are typical characteristics of a polymer. The area under the peaks is related to the chemical structure of the polymer and provide insight at the molecular level [103]. The  $\tan \delta$  peaks (plotted with a linear y axis) were automatically fitted using PeakFit and a linear baseline subtracted, and data summarized in Table 5-3.

**Table 5-3:** Dynamic mechanical analysis data of the alpha transition of baseline and mixture advanced nanocomposites

Material	Area	T <sub>Max</sub> ( $^{\circ}\text{C}$ )	T <sub>ave</sub> ( $^{\circ}\text{C}$ )
828/mPDA	14.0	171	119
I.30E/828/mPDA Baseline Process	13.0	169	120
I.30E/828/mPDA Mixture Advanced	12.8	167	120

The area under the curve appears the same for both the mixture advanced and baseline nanocomposites; this suggests that the chemical structure of the polymer is the same. The area is slightly less for the nanocomposites than for the neat resin, suggesting that an effect to the network due to the incorporation of the nanoscopic elements may be

possible. It has been suggested that the behavior of a constrained polymer behave may shed insight into nanocomposites, as the dynamics of polymers under confinement is manifested by a behavior dramatically different from the bulk in local relaxation and mobility [105]. Specifically, cooperative motion is expected to decrease as polymers are confined. In the case of the materials studied here, the monomers and resulting polymers are confined in gaps that are on the order of a few nanometers (intercalated d-spacing), which compared to the size of a monomer or resulting crosslinked polymer is quite small.

Subambient transitions were analyzed to further explore differences in the network formation due to the addition of the organoclay and the effect of mixture advancement (Figure 5-23). The neat resin exhibits a broad peak at approximately  $-40^{\circ}\text{C}$ <sup>5</sup>. The addition of OLS processed in the standard method resulted in a significant broadening of the peak with perhaps a slight reduction in temperature. Yet the mixture advanced nanocomposite exhibited a  $\beta$  relaxation very similar to that of the neat resin.

---

<sup>5</sup> (the rate used in the DMA tests were likely too high which could cause the higher beta transition than expected).

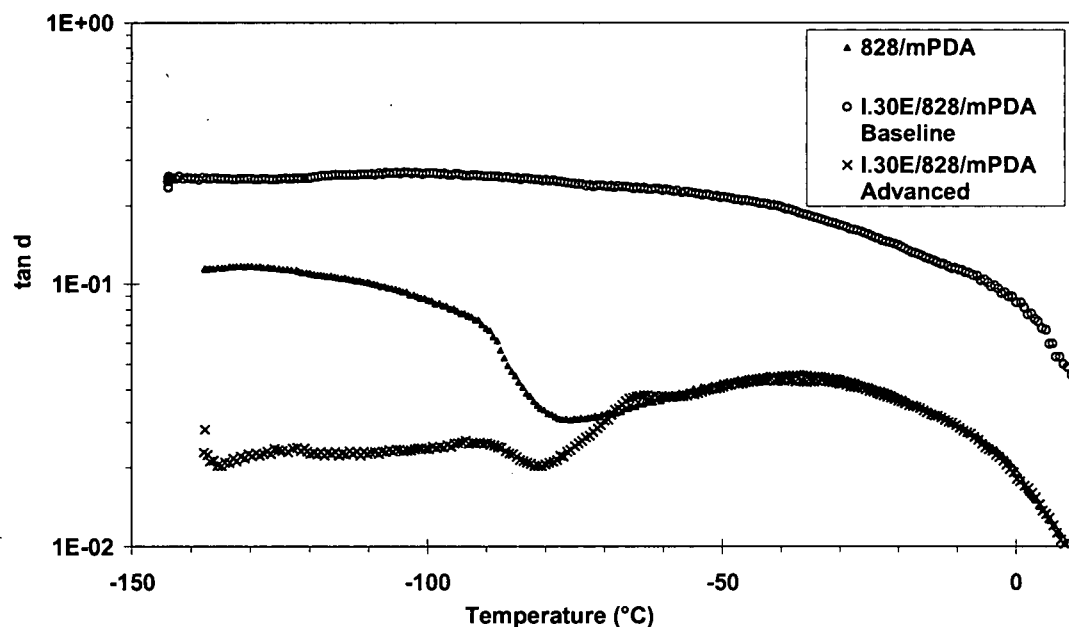


**Figure 5-23:** Dynamic mechanical data, DMA torsion, performed at 2°C/minute, 100 rad/sec, 0.1% strain, sub-ambient loss modulus data comparing 828/mPDA, 5% I.30E/Epon 828/mPDA baseline and mixture advanced nanocomposites cured via standard recommended cure process.

The  $\beta$  relaxation has been attributed to cooperative motions involving a minimum number of epoxy-amine repeat units necessary to provide a crankshaft rotation of the main-chain cross-linking segments [39, 102]. The broadening of this relaxation proves that the nanoscopic organoclays influence the cooperative motions of the epoxy. The OLS interferes to such an extent with the network formation that a wide variety of cooperative motions are allowed reflecting a wide breadth of local network structures. The individual organoclay plates represent a element that can significantly interact with much of the network formation, with a thickness roughly on the order of an epoxy monomer and a plane roughly the order of a polymer (10-100 nm). As discussed earlier,

at this size for a given volume fraction a very large percentage of the monomer/polymer will be in contact with the OLS. They may therefore effectively break up the minimum number of groups in succession necessary or crankshaft motions, and provide for a wide distribution of polymer chain segment lengths and rotations between crosslinks. The mixture advanced material has relaxation behavior close to that of the epoxy-mPDA alone; reflective perhaps of the benign chemical participation of the OLS in this material. In this case, the network is not disrupted. The catalytic effect of the OLS in the baseline process may serve to provide for more gradient and varied network structures. These data serve to underscore the complexities associated not just with the size of the OLS but their participation in the polymerization process.

### **Fracture Behavior**

The potential of nanomodifications to achieve an improved toughness-stiffness balance was the instigation of much research, yet general trends have not been conclusively demonstrated [67, 107]. The ability to alter toughness of a polymer through the addition of a second phase such as particles is attractive in that this route generally does not affect the mechanical properties of the polymer at elevated temperatures. Although the understanding of both rubber and rigid particle toughening of thermosetting polymers was greatly extended in the 1980s due to the historical engineering limitations of inherent brittleness of these important materials, extension of this base of understanding to the nanoscale has yet to be performed [43].

It is not necessarily to be expected that nanoscale particles will provide for the same toughening mechanisms as conventional toughening techniques, due to the size of the nanoelement and the nanoscale morphology as compared with the mechanisms which typically control fracture toughness. Of the many existing variables that can affect energy dissipation mechanisms and apparent toughness results, morphologies on various scales are of well-known importance. And although many of the trends for rigid particle toughening of epoxies at the micron scale are well understood, the effect of size on fracture, though determined to be a secondary influence, has not yet been conclusively defined [108, 109, 110]. For nanoscale particles, much of the early exciting property improvements were achieved in thermoplastics or rubbery epoxies. Research based on layered silicate epoxy nanocomposite materials is still less extensive than that based on thermoplastic materials; and to date not only do epoxies offer significant processing challenges as discussed earlier, but property enhancements have been less impressive<sup>6</sup>. Yet the potential payoff of nanotailoring epoxies for physical property enhancement while minimally modifying traditional processing routes offers significant opportunities for many aerospace applications. Therefore one goal of this research was to characterize layered silicate epoxy nanocomposites in which the sole variable was d-spacing of the nanomorphology so as to assess the role of morphology at this scale on toughness. The lack of processing control and process - morphology relationships as

---

<sup>6</sup> Yet it must be pointed out that it has been well understood by the polymers community that the addition of small fillers can significantly increase the rubbery modulus of a polymer but that the effect is minimal in the glassy modulus region. This expectation is understood by the mechanics community as well and documented in theoretical equations for modulus. E.g., the Mooney Equation holds for rubber with rigid fillers, but does not agree well when matrix is rigid. The Halpin-Tsai equations recognize the importance of the relative moduli of the matrix and filler for dynamic mechanical properties.

well as the many complexities beyond the exfoliation of the tactoid that must be taken into account. However, distinct morphologies from the same constituents and same cure process were fabricated which provides new experimental evidence of the role of nanoscale morphology on toughness.

The majority of testing was performed on nanocomposites with 5% by weight OLS, and to a lesser extent 1% by weight. Later processing studies utilized 3% by weight samples to provide data at an intermediate weight fraction to complement earlier data. Plane strain fracture toughness results for the nanocomposites fabricated in this research exhibit higher toughness than the epoxy alone. The mixture-advanced materials exhibit higher toughness than the baseline materials. The modified processes that included horn sonication resulted in lower toughness than the baseline process. The materials based on SC18 OLS had higher toughness than those based on the I.30E OLS. For these materials, more effective toughening will be shown to be associated with more ordered morphologies.

The later-investigated baseline 3% mixtures resulted in increased toughness values compared with the 5% mixtures. Although initially surprising, this can be explained. Visual inspection suggest that the dispersion in the 5% materials is not as good nor on as small a scale as that in the 3% materials, for the 3% materials are significantly more transparent than the 5% materials. If the OLS were dispersed on the order of single layers, their small size would provide for a transparent nanocomposite. The SEMs of fracture surfaces support that finer dispersions were achieved in the 3% materials and that

greater surface area was created to move the crack front forward (Figures 5-24 and 5-25). This correlates well with the higher values from the compact tension tests. Past rigid particle filler research has observed plateaus in  $K_{Ic}$  with volume fraction for particles of very small size [44].<sup>7</sup> Overall, it will be shown that an ordered nanoscale morphology is a more effective toughener than a dispersed morphology.

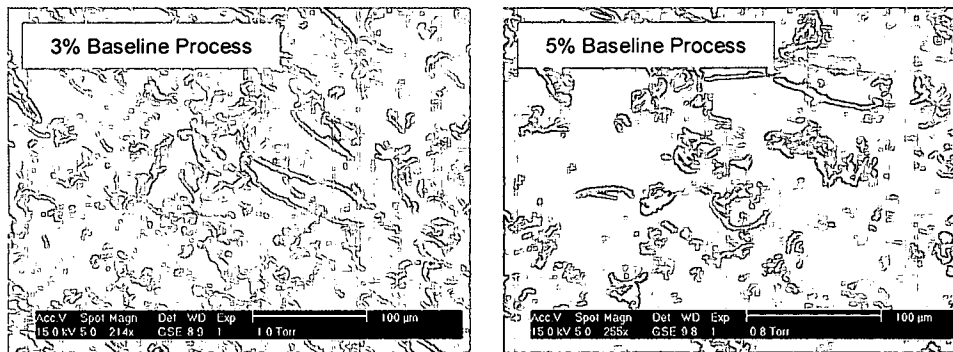


**Figure 5-24:** SEM image of the fracture surface of 3% I.30E/828/mPDA (magnified 214 times) and 5% I.30E/828/mPDA (magnified 255 times).

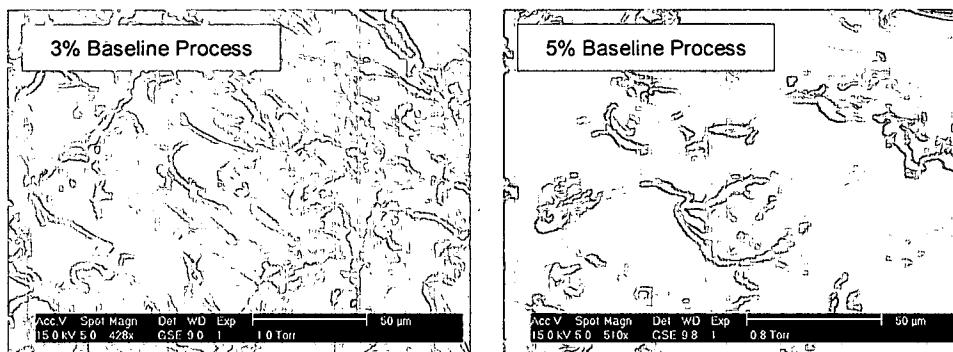


**Figure 5-25:** SEM image of the fracture surface of 3% I.30E/828/mPDA (magnified 428 times) and 5% I.30E/828/mPDA (magnified 510 times).

<sup>7</sup> Evan's crack pinning theory and its extension by Green for brittle particle reinforced composites provides a relationship between the stress required to propagate a crack in a composite and the ratio of the particle diameter ( $d_p$ ) to the interparticle separation ( $D_p$ ). Based on calculations of the stresses required to propagate a crack through a matrix reinforced by an array of particles, they determined that increasing  $d_p/D_p$  tends to provide increasing critical stress intensity factors  $K_{Ic}$ . For a given particle size, an increase in volume fraction provides for an increase in the ratio  $d_p/D_p$ , which would provide for an increase in  $K_{Ic}$ . This discussion is not meant to suggest the applicability of their theories to nanoscale second phases, but rather to shed light into the fact that particle size can play a role in the trend observed here.

Table 5- 4 summarizes the fracture toughness data for the baseline and mixture-advanced materials, with the mixture-advanced material marginally tougher than the baseline material.

**Table 5-4:** Fracture toughness of 5% I.30E/Epon 828/mPDA materials (data from 3 loadings per sample, 10 samples per material with the exception of Epon 828/mPDA (no OLS), in which case data is additionally on two batches of material).

Material	$K_q$ (psi-in <sup>0.5</sup> )
Epon 828/mPDA (no OLS)	646 ± 270
Epon 828/mPDA/5% I.30E baseline	913 ± 148
Epon 828/mPDA/5% I.30E advanced 16 weeks	1121 ± 343

The baseline and advanced materials represent different morphologies as discussed earlier. The morphologies of the mixture-advanced materials appear to be dominated by smaller, more ordered tactoids with larger d-spacings than the tactoids in the baseline materials. The role of both size and dispersion can be investigated with the materials developed and studied here.

Toughness should be expected to be sensitive to the nature of the OLS morphology, be it intercalated or more widely separated or exfoliated. Lan et al. suggested that fully, disordered exfoliated morphologies provide slightly better modulus and strength [45]. However, based on classical rigid fillers one would question the effect of size of individual layers on toughness. (Much research into rubbery toughening of epoxies was performed in the 1980s and 1990s, and while it provides a foundation to explore the

processing challenges of epoxy nanocomposites, is not directly applicable to toughening with organoclays due to the ratio of modulus between the rubber and the epoxy and the size and the nature of the silicate particles). One can also expect different trends for rubbery particle toughening and for rigid particle toughening as the resulting toughening mechanisms due to a dispersion of a second phase that is rubbery will be different from those in which the second phase is rigid [111].

Work with rigid particle filled (glassy) epoxy suggests that one can generally expect the following effects due to the particles:

- increase in tensile modulus with increasing volume fraction of particles (if there exists a good interface between the particle and matrix)
- decrease in room temperature tensile strengths (although some improvement may be obtained at elevated temperature)
- typically decreased toughness, or increase to a maximum then decreasing with increasing volume fraction. This is partially due to the fact that the modulus increases continuously with volume fraction, and therefore fracture reflects both changes in toughness and in modulus
- Secondary if any effects due to particle size with the exception of tensile strength, as it is a flaw-dominated property and stress fields near smaller particles affect a lower volume of polymer, so provide for smaller area of stress concentration [4, 38, 42].

Toughness is very sensitive to morphology such as a second phase, which can influence both macroscopic material properties (such as yield strength) and thus indirectly affect fracture; can cause inhomogeneous stress distributions about the crack tip which can provide energy dissipation and thus higher strengths or can provide weak locations for crack formation and thus lower fracture strengths; and can determine the fracture path through mechanisms that enhance energy absorption during fracture.

The relationship between the crack tip front, plastic zone, and the nanocomposite morphology can be assessed to postulate on the ability of the morphology to interact with the crack tip. Fracture energy comes partially from the localized plastic deformation at the crack tip; to increase toughness it is necessary to introduce energy dissipating mechanisms such that the overall volume of material near the crack tip involved in plastic deformation is increased. During fracture, it is assumed that the energy dissipation processes at the crack tip are sufficiently local that the specimen can be treated as an elastic body. As the epoxy is a brittle material and as discussed in the Experimental Chapter, sample geometry was such that the crack tip material was in a state of plane strain, and the linear elastic parameter  $K$  can be used to calculate crack tip driving forces. The local process zone where the plastic energy is dissipated, the crack tip plastic zone, can be approximated at a level of stress intensity,  $K_I$ , and yield strength,  $\sigma_{YS}$ , by

$$2r_y = (1/3\pi) (K_I/\sigma_{YS})^2 \quad (12)$$

for plane strain conditions. For most glassy thermosets this crack tip zone is small, with a diameter on the order of  $\sim 50\text{ }\mu\text{m}$ , so again specimens of the geometries analyzed here can achieve plane strain conditions which allow for the calculation of toughness [112]. For the materials used in this study the plastic zone is on the order of ten to thirty micrometers (or 10,000 to 30,000 nanometers). If fully exfoliated, the individual layers of the OLS are on the order of one nanometer thick by 100's of nanometers on each side. This kind of particle presents the crack tip with a two dimensional plate that, depending upon its orientation with respect to the crack propagation, may span as much as one-tenth to one-hundredth of the plastic zone but little of the volume. If, however, the tactoid has expanded galleries that have retain some registry with each other, a significantly different type of particle is available for interaction with the crack tip. For tactoids of five layers in good registry with average gallery heights of 10 nanometers, the resultant particle would a more three-dimensional composite of epoxy and OLS layers of approximately 55 nanometers by a few hundred nanometers. This resulting particle is much larger than the single OLS layer. Although for a given OLS volume fraction the silicate layers will take up the same volume whether they are individually dispersed or associated in tactoids, the tactoids that remain in registry will also directly affect inner-gallery polymer hence have a larger overall impact on the local plastic zone. Such ordered particles would provide more energy dissipation opportunity due to its size and ability to interact with the crack front. It also represents a tougher particle in general due to its laminated structure.

The data from this research do not probe the ability of individually dispersed silicate layers to toughen the epoxy as such a system was not achieved. However, the data do

support the premise that ordered tactoids provide effective toughening, and is supported by the above argument. Recent research by Zerda and Lesser supports the findings reported here [68]. Comparison of the two OLS used in this research also agrees well. In all cases, the SC18 OLS provided for higher fracture toughness data when compared with the I.30E (reference Table 4-11). In all cases the SAXS data suggested a more ordered morphology for the SC18 systems. SAXS data of the various materials show that the mixture advanced I.30E had the most order, followed in turn with decreasing order by the baseline processed SC18, the baseline processed I.30E, and the various modified processed I.30E. systems. The fracture toughness results show that the SC18 and mixture advanced I.30E had the highest toughness, followed by the baseline I.30E process and the advanced processes. Although not comprehensive, this too supports the relationship between ordered morphologies and toughness.

The observed increase in toughness may be attributed to factors other than the morphology of the tactoids. Since fracture occurs through breaking of primary covalent bonds in the epoxy, it is likely that the strength of the polymer will be affected by the density of main-chain bonds crossing the fracture plane as well as the energy absorbing processes that take place during fracture. As discussed earlier, the epoxy network itself may be modified through the mixture advancement process. However, the body of epoxy research to date has found that a small fraction of the fracture energy is accounted for by the energy necessary for bond rupture and is generally unaffected by variations in the average molecular weight between cross-links, even though glass transition temperature drops markedly with increasing molecular weight between cross-links and effects have

been observed in Charpy and notched Izod impact strengths<sup>8</sup> [42]. Yee and Pearson found that a large decrease in cross-link density of DGEBA epoxies produce only modest increases in fracture toughness, although they found toughenability to be a strong function of inherent matrix ductility which is partially a function of cross-link density [113]. Based on the body of work in epoxies, the previous discussion of particle size and morphology, and the data observed here, it is suggested that morphologies that have more ordered, registered tactoids provide for more energy dissipation and increased toughness in OLS epoxy nanocomposites.

General properties such as modulus and strength may also affect toughness. Although DMA showed a slight increase of the storage and loss moduli ( $G'$ ,  $G''$ ) of the nanocomposites, tensile testing revealed no significant impact to modulus due to the inclusion of the OLS with differences within one standard deviation (Figure 5-26). Tensile strengths were reduced by twelve to twenty percent over the baseline epoxy strength. This is not surprising as strength is typically expected to be reduced through the introduction of rigid particles. Strength is also a flaw-dominated property and the interface between the OLS and the epoxy is uncertain. The tactoids may also introduce slightly more entrapped air which may serve as flaws.

---

<sup>8</sup> for brittle thermosets less than 10% (10 J/mm) of the fracture energy is accounted for by the energy necessary to rupture chemical bonds [43].

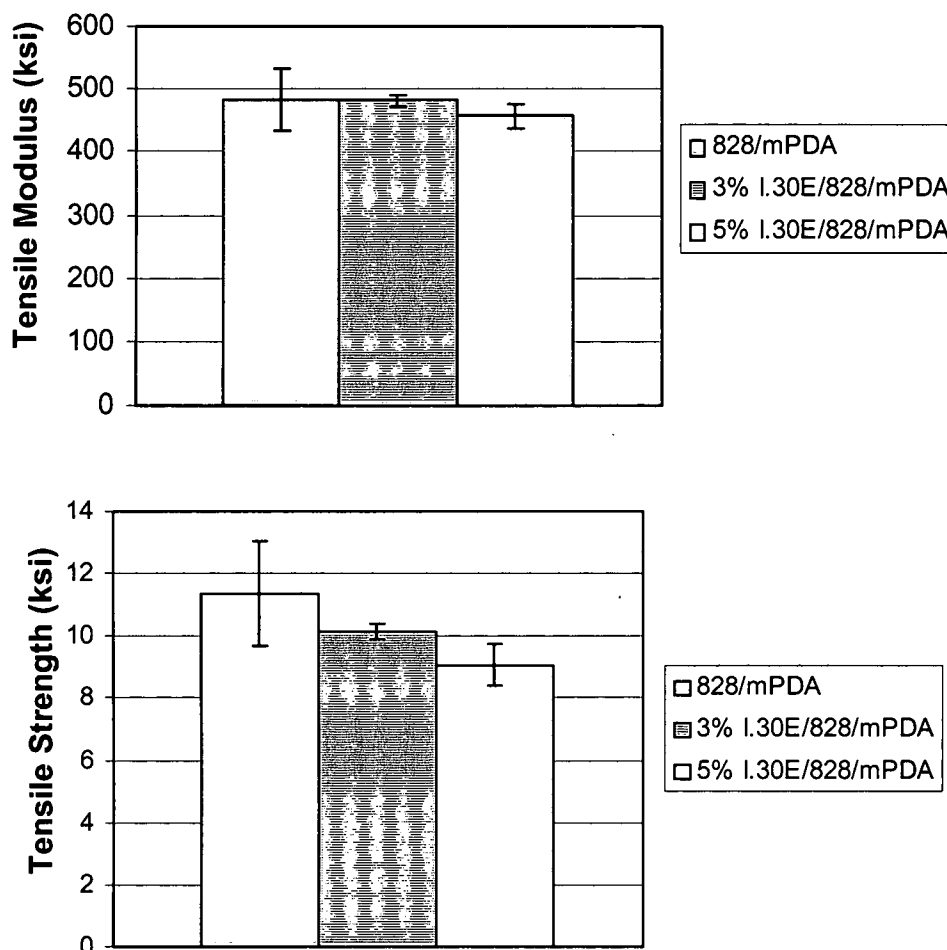


**Figure 5-26:** Tensile properties of Epon 828/mPDA, 5% I.30E/Epon 828/mPDA, and 3% I.30E/Epon 828/mPDA (two different processes).

These data suggest that the increased toughness is not due to macroscopic property enhancements such as global matrix strengthening but rather due to the OLS as a distinct second phase and also possibly due to its disruptive nature on the local network.

Fractography provides additional insight into morphology's effect on toughening. SEMs of the neat resin shows typical cohesive resin fracture with the characteristic flat fracture planes with very little evidence of permanent material deformation (Figure 5-27). The overall surface topography exhibits pronounced 'river markings' or branching lines. The

direction of their coalescence corresponds with the direction of the crack front. The fairly featureless fracture surface is typical of brittle glass materials, with river mark patterns perpendicular to the crack front [114, 115].

The nanomodified samples exhibit considerable surface roughness as compared with the neat resins. Studies have suggested that the amount of strain energy involved in a fracture is considered to be proportional to the area of fracture surface created and the amount of plastic deformation at the crack tip, and the increased surface roughness seen in the nanomodified samples is a qualitative indicator of higher toughness [114]. The many planes visible on the fracture surface of the nanomodified epoxy indicate that greater surface area was created to move the crack front forward. This correlates well with the higher fracture toughness values from the compact tension tests.

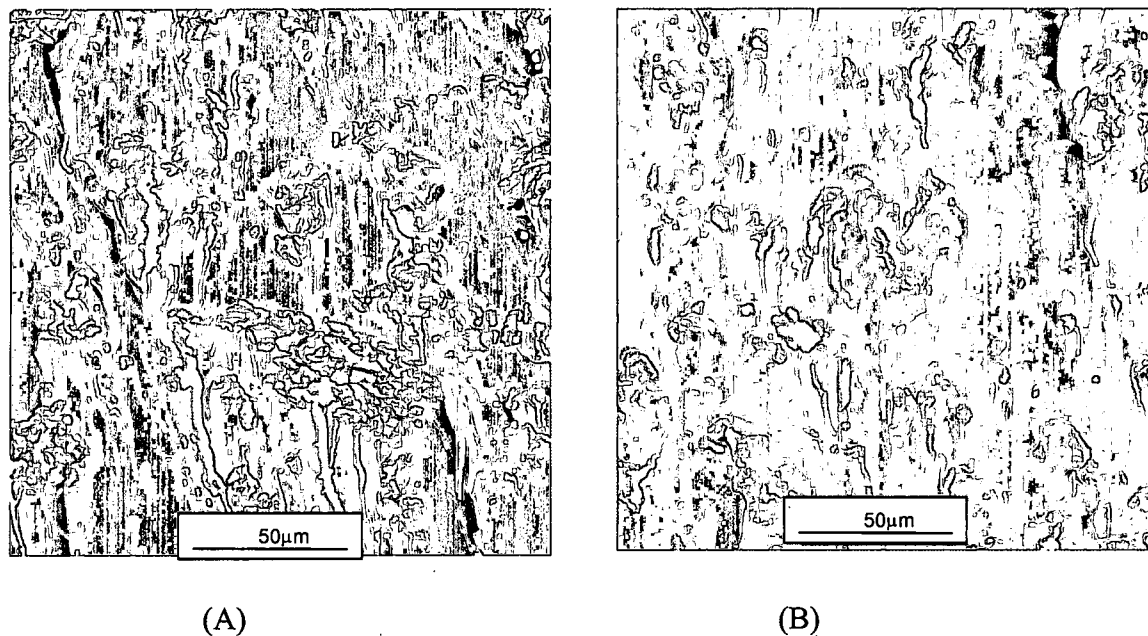
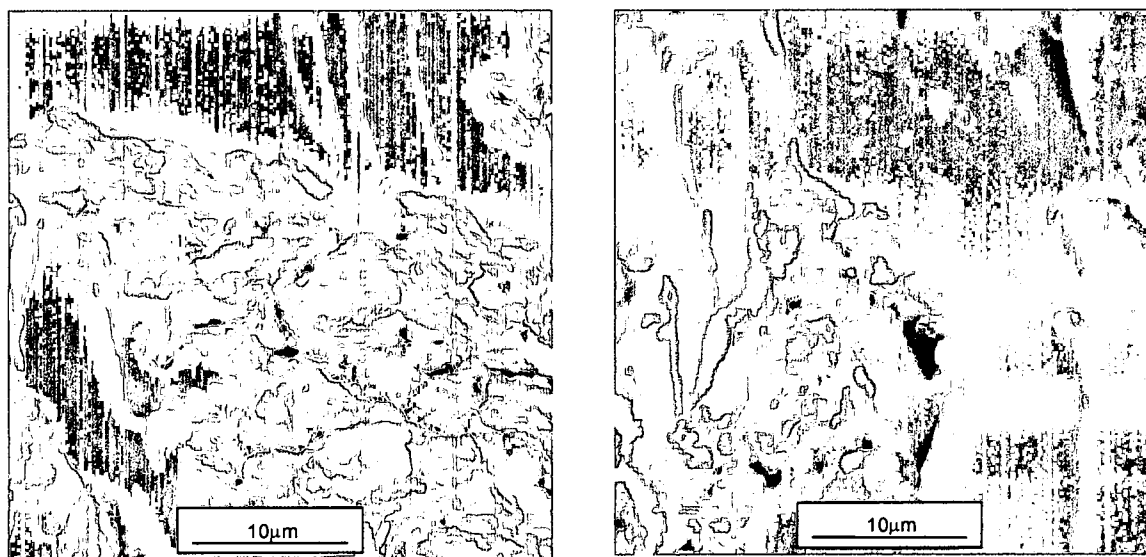


**Figure 5-27:** SEM image of the fracture surfaces of (A) 5% I.30E/828/mPDA and (B) 5% I.30E/828/mPDA “advanced” materials show rough fracture surfaces.

The fracture surfaces suggest that the crack was propagated through the particles. However, some weak level of particle-matrix bond may exist, for if the particles were easily broken, the crack face would be expected to show flat fracture surfaces across the particulate areas. The tougher regions for the baseline material appear to be slightly larger and more irregular than those in the advanced material, which agrees with the TEM descriptions of generalized morphologies. It is difficult to assess the cavitation and debonding potential for these small regions; however, SEMs of rubber toughened materials from the literature appear similar [43].

Higher magnification SEM of the two nanocomposites highlights the regions of rougher areas as clusters on the order of 25-50 micrometers (Figure 5-28). These regions are on the order of the crack tip radius for epoxy as discussed earlier. The regions of clusters appear slightly larger for the baseline than for the advanced material. Step and ridge formation appears, which leads to an increase in surface area requiring extra energy during fracture. Diffuse shear yielding of the matrix is not observed and no conclusion can be drawn on this micro-deformation process. Shear banding of the matrix is also not observed; however, for highly crosslinked epoxies shear deformation is not expected to occur. This is consistent with other filled epoxy research [116]. Particle cavitation or debonding is one of the typical micro-deformation processes that may dissipate strain energy; although often observed in glass bead filled epoxies, this mechanism was unclear with the nanocomposites. This may be due to the small size and complex makeup of the OLS tactoids [110].



(A)

(B)

**Figure 5-28:** SEM image of the fracture surfaces of (A) 5% I.30E/828/mPDA and (B) 5% I.30E/828/mPDA “advanced” materials show rough fracture surfaces.

Energy dispersive spectroscopy (EDS) analysis and mapping of the fracture surfaces revealed that the rough clusters contained high concentrations of aluminum (Al) and silicon (Si), confirming that these more tortuous fracture surfaces were tactoids of the OLS. These tougher regions of tactoids were likely the primary toughening mechanism contributing to the overall improvement of toughness. EDS analysis of the two distinct fracture surfaces observed (tactoids regions and more resin rich regions) revealed that in general the advanced samples had slightly less of the Al, Si, Mg and Fe – possibly suggesting a lower volume fraction due to settling. However, the ratios of the elements did not all follow the same trend: whereas the Al and Fe were much less by weight percent in the advanced material, the other elements that were assessed (C, Si, Mg) were very close in value. In general, the tactoids of the aged and baseline materials had similar compositions. The so-called bulk material (resin rich regions) also displayed a rougher

surface suggestive of higher fracture energy, and likely also played a role as a mechanism of the improved toughness over the neat resin. However, no obvious differences between the aged and baseline materials in these regions were observed through EDS to help explain the higher toughness of the aged material.

It is well known for polymers that in general, the volume fraction of the secondary toughening phase has a primary dominant effect on fracture toughness. Relative moduli of the matrix and the secondary toughening phase plays a role as well. One can expect different effects for particles within a glassy rigid material and within a rubbery material. These data provide experimental evidence that ordered nanoscale morphologies may provide for better toughening of epoxies than more exfoliated, disordered nanoscale morphologies as postulated by this research as well as by Kornmann [107], Zilg, [67] and Miyagawa and Drzal [117]. To date, the nanocomposites studied here provide the closest comparison of varying morphology within a given OLS-epoxy material system. This elimination of other variables is necessary to eliminate the effects of different constituents and processing routes on morphology and ultimate properties.

### **Mixing Process Variable Effects**

Although chemistry and reactions play a strong role on the development of morphology in epoxy-based nanocomposites, the role of shear and mechanical means of generating forces that assist in the exfoliation of layered silicates is not a new concept and has been

suggested in the clays and rheological additives literature [7, 118, 119]. The research into mixture advancement performed here coupled with the successful exfoliations achieved in thermoplastics suggest that the ability of the liquid in which the OLS are mixed to impart force to the tactoids may assist to some degree the intercalation and subsequent expansion of the tactoids. Larger molecular weight entities such as thermoplastic polymers and advanced thermoset oligomers may impart force on the OLS layers during mixing more effectively than monomers.

In a limited part of the overall thesis study, the addition of high speed shear mixing and bath sonication of the epoxy-OLS mixture did not appear to affect the final nanocomposite morphology as evidenced by SAXS and TEM. The incorporation of horn sonication, however, appears to slightly impact the hierarchical morphology and fracture behavior.

SAXS data show that the 3% I.30E based materials fabricated by various mixing processes all developed similar low  $q$  range peaks associated with high  $d$  spacing on the order of 150 Å. Figure 5-29 shows offset SAXS data for the processing variations in log-log format to emphasize the pertinent peaks. All samples have a low- $q$  peak at  $q = 0.0425 \text{ Å}^{-1}$  associated with large  $d$ -spacings of approximately 150 Å. Data for the baseline process and Process B show evidence of a mid- $q$  peak associated with intercalated morphology. Data for Process A and D, both which included horn sonication, show no mid- $q$  peak associated with intercalated order.

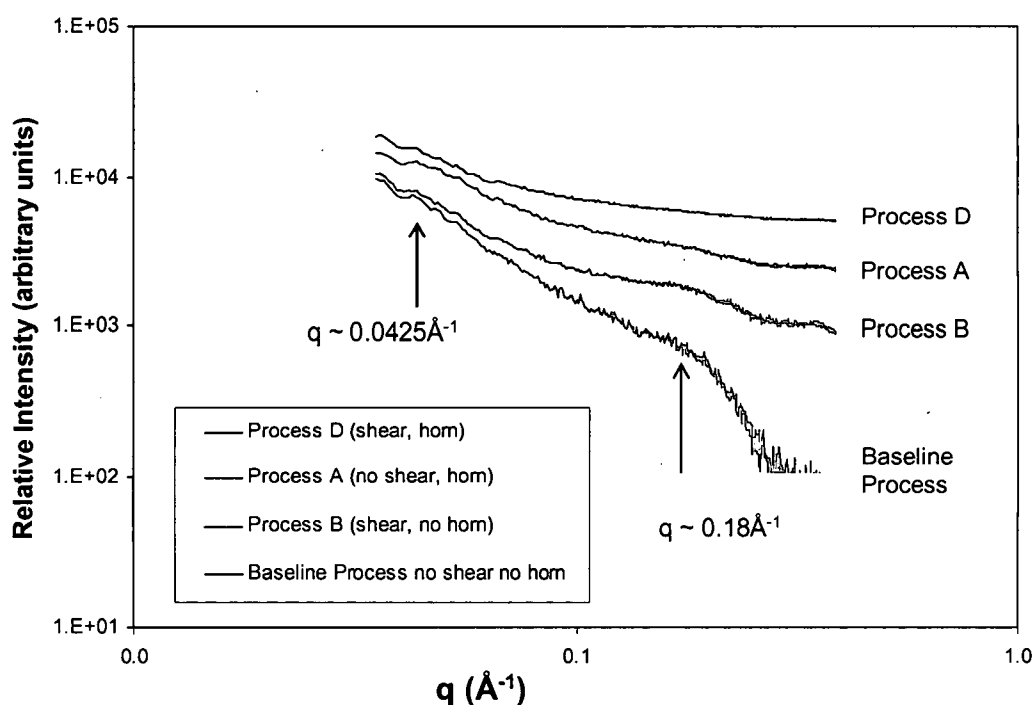


**Figure 5-29:** SAXS data for 3% I.30E/Epon 828/mPDA nanocomposites show effect of horn sonication step on tactoid order. Log-log plot to highlight the peaks.

Closer examination shows sharper low- $q$  peaks for the baseline and Process B, as compared with broader low- $q$  peaks for materials from Process A and Process D. These observations suggest that the addition of horn sonication breaks up the tactoids more effectively than mixing processes that rely only on stirring or high shear mixing, resulting in few to no ordered intercalated morphologies and more disorder at the low- $q$  morphologies.

The low  $q$  range slope, indicative of morphologies/order, supports this premise. Data from nanocomposites fabricated without horn sonication (Processes A and D) are similar, with slopes in the range of -3 to -4 possibly more indicative of a polymer or three dimensional scatterer, such as tactoids. The much higher slopes of the horn sonication

process is not understood. The breaks in the slopes, which relate to length scales, all occur at about the same location. The use of solvent or high shear mixing does not appear to strongly affect the morphology.

TEMs of local tactoid and higher order morphology supports the conclusion that horn sonication assists in breaking up tactoids. Large and small fields-of-view highlight the hierarchical morphology necessary to capture tactoid size, and tactoid-tactoid separation as well as the d-spacing within tactoids. Tactoids appear to be smaller for the horn processes, with the largest in range of 1-5 micrometers as compared to 5-10 micrometers for the non-horn processes. The majority of composite appears to have more finely and regularly dispersed OLS layers and less pure epoxy regions. Representative TEMs are shown in Figures 5-30 and 5-31.

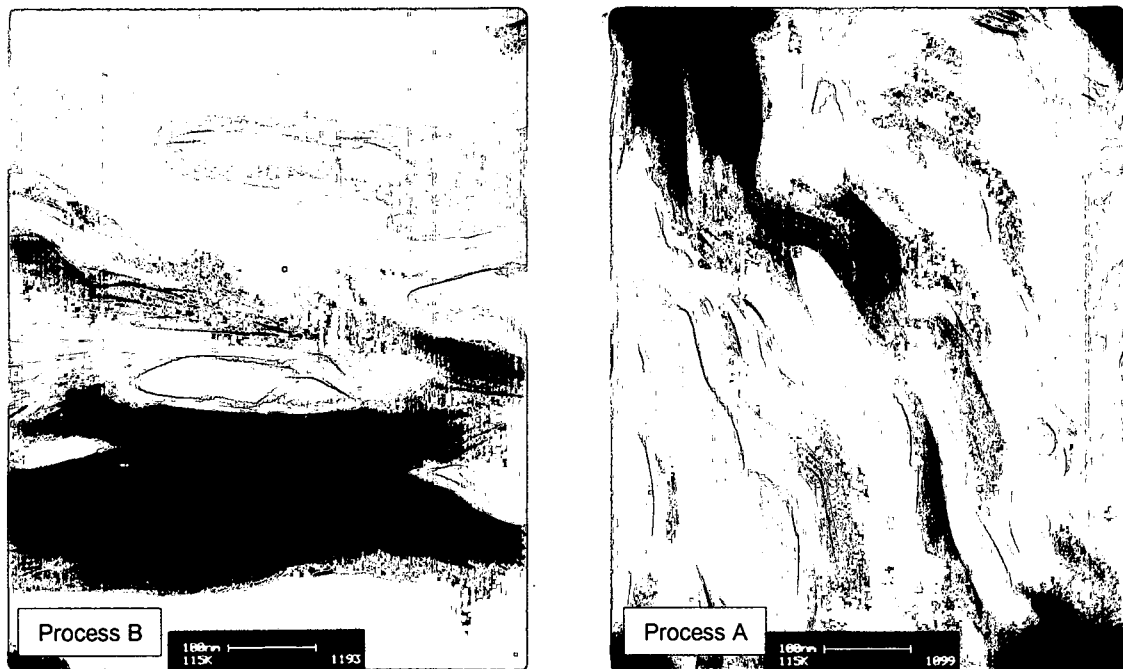


**Figure 5-30:** TEMs of 3% I.30E/Epon 828/mPDA nanocomposites show horn sonication (Process A) during the mixing process has negligible effect on d-spacing within tactoids.

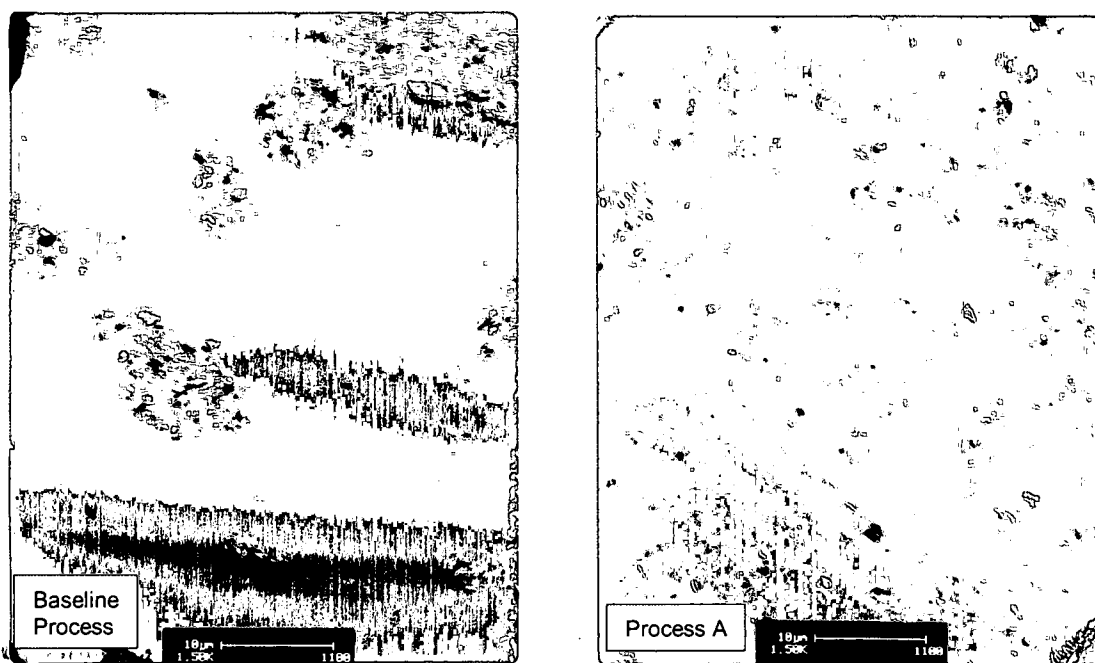


**Figure 5-31:** Large field of view TEMs of 3% I.30E/Epon 828/mPDA nanocomposites show horn sonication during the mixing process produces more uniform dispersion and smaller groupings of organoclay layers.

Comparing the effect of varying mixing processes within this sample of materials, it can be seen that Processes A and D, those that utilized horn sonication, provided for  $K_q$  values roughly 77% of what was obtained with the baseline process and Process B (Figure 5-32)<sup>9</sup>. From TEM and SAXS, it is concluded that these processes that provided for more effective dispersion of the OLS resulted in lower fracture toughness. These data coupled with the mixture-advanced data all support that an ordered nanoscale morphology is a more effective toughener than a dispersed morphology.

<sup>9</sup> As previously noted, these 3% OLS by weight samples had relatively high  $K_q$  values, likely due to the combination of newer epoxy material, different batch of OLS material, and possibly better skill at fabrication as they were fabricated at a significantly later date than the set of 5% samples.

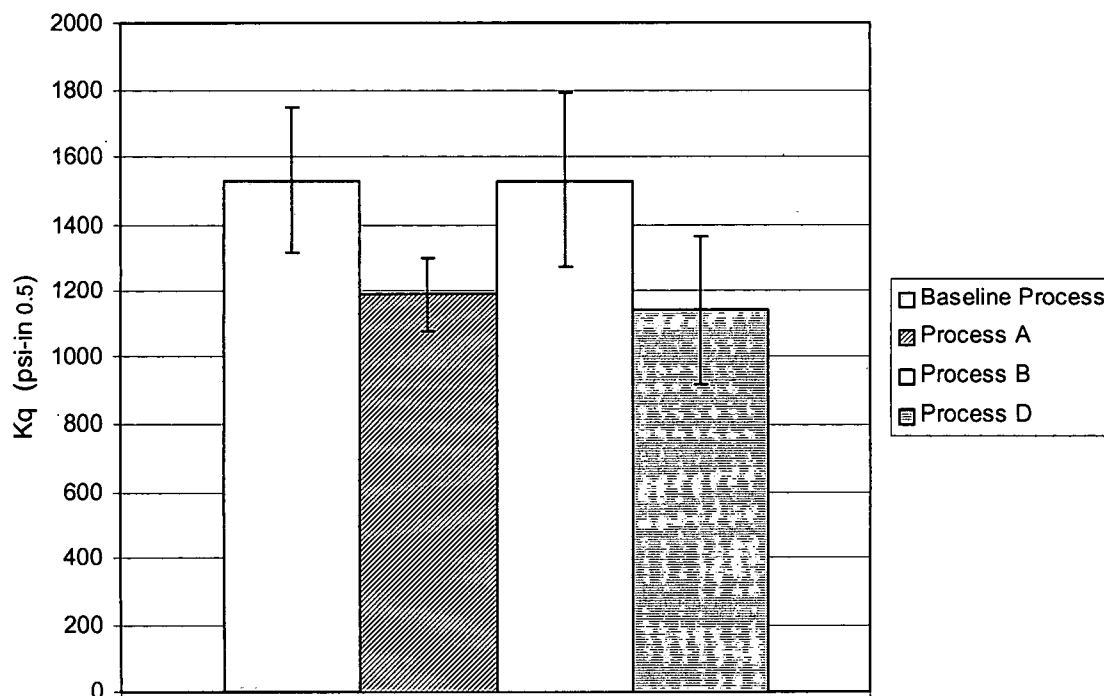


**Figure 5-32:** Compact tension fracture toughness test data shows processes that include horn sonication step (Process A, D) result in lower Kq values.

Fracture surfaces of the baseline process and a horn sonication process provide evidence of the increased toughening occurring with the more ordered morphologies. Figure 5-33 and 5-34 provides comparisons at low and high magnifications.

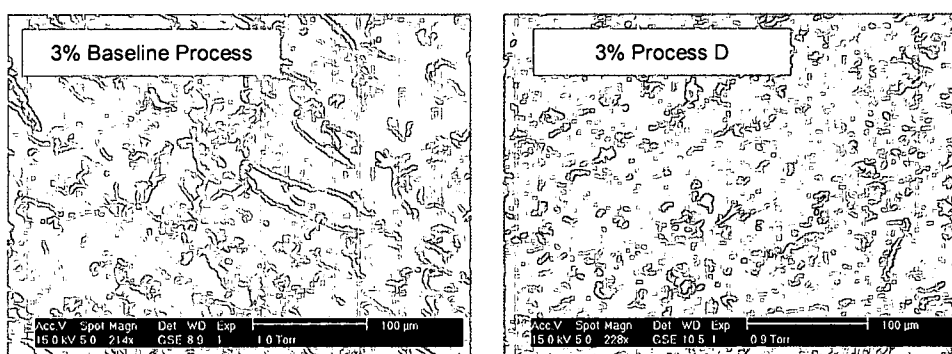


**Figure 5-33:** SEM image of the fracture surface of 3% I.30E/828/mPDA Baseline Process (magnified 214 times) and 3% I.30E/828/mPDA Process D which included horn sonication (magnified 228 times).

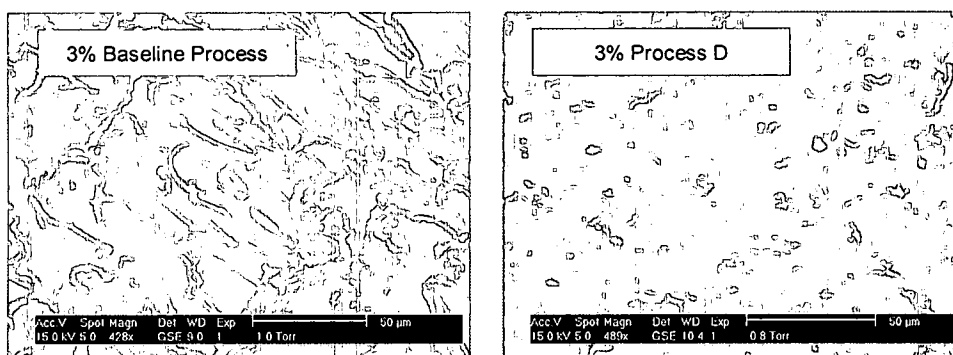


**Figure 5-34:** SEM image of the fracture surface of 3% I.30E/828/mPDA Baseline Process (magnified 428 times) and 3% I.30E/828/mPDA Process D which included horn sonication (magnified 489 times).

The fracture surface of the material processed with horn sonication is much more uniform and exhibits finer rough texture and more numerous fracture planes and increase in surface area requiring extra energy during fracture.

More ordered morphologies are observed to provide for higher fracture toughness.

Nanoscale morphologies, the separation of the tactoid plates, can be examined effectively with SAXS and TEM. Higher order morphologies can be examined by TEM and SEM.

Mixture advanced materials achieved higher nanoscale order at high d-spacings over those that underwent the baseline process. Materials based on the SC18 OLS achieved more ordered tactoid expansion over those based on I.30E OLS. And materials that were fabricated with processes based on stirring and shear mixing developed morphologies that were more ordered than those based on processes that included horn sonication. All of the more highly ordered morphologies provided for more effective toughening of the nanocomposite as compared with more dispersed morphologies. This suggests that the

goal of completely exfoliated nanoscale morphologies that many seek is not the appropriate morphology for improving fracture toughness of epoxies.

## CHAPTER VI

### CONCLUSIONS AND RECOMMENDATIONS

#### Conclusions

Nanocomposites based on epoxy resins offer a new materials choice for many applications and markets, such as aerospace. These materials, once understood to a level where controlled morphologies can be obtained, can be used as matrices for advanced carbon fiber reinforced composites and offer new properties without sacrifice of the existing properties and processes. Achieving optimized properties repeatedly in a production environment will require an understanding of material/process interactions.

This research provides processing-morphology and morphology-property information that significantly extends the understanding of morphology development in layered silicate epoxy nanocomposites and that is critical for eventual morphology control. The approach of starting from the understanding of toughened epoxies and of epoxy processing has provided a unique foundation for effectively creating materials with improved mechanical properties and more specifically fracture toughness. Sensitivity to

temperature, temperature rate, organoclay selection, cure agent, and molecular weight has been characterized through innovative *in situ* SAXS studies.

In systems where reactions other than the epoxy-amine reaction occur or in which the epoxy-amine reaction is catalyzed, processing at isothermal temperatures above the onset temperature of the reactions results in high d-spacings. Processing at temperatures below the onset temperature result in intercalated morphologies. For systems in which the amine-epoxy reaction is not catalyzed, intra-gallery and extra-gallery polymerization rates are similar and intra-gallery network formation does not hinder epoxy infusion into the OLS tactoid. For these systems ordered exfoliation occurs at temperature below the onset temperature. Heating rates provide for high d-spacing, and the development of exfoliated morphology occurs more quickly at higher heating rates. The chemically compatible, flexible aliphatic amine cure agent immediately intercalated and disrupted the tactoid when added to the epoxy-OLS mixture; the aromatic amines resulted in an ordered intercalated initial morphology. The laboratory fabricated low CEC OLS provided more ordered morphologies than the high CEC commercial OLS.

This dissertation research has demonstrated that simple models of morphology development cannot be compared across different material systems, nor across differing processes or conditions for a given material system. Physical and chemical variables can greatly affect final epoxy layered silicate nanocomposite morphology. Cure temperature profiles, cure agent, organoclay type, fabrication and chemistry affect the morphology development and ultimate structure. Advancing the epoxy resin and mitigating the

catalytic effect of the organoclay provides for significantly different morphology development. Techniques for initial mixing of epoxy and organoclays can result in differing morphology development through the cure process.

The epoxy-amine reaction cannot be ignored in processing of this class of nanocomposites. The onset of the amine-epoxy reaction can be catalyzed by the ammonium of the organoclay surface. The level of catalyzation plays a strong role in morphology development. The reactions of specific constituents must be kept in mind when comparing systems. The reaction is an important factor in obtaining expanded morphologies. The development of morphology is affected by the network formation, the relative ratios of epoxy and cure agent within the galleries, and the ease by which additional epoxy and cure agent can infuse the tactoid during the polymerization reaction.

This dissertation research has developed a single model material system capable of achieving two distinct morphologies under the same processing conditions. Such a controlled comparison enabled a focused study of process-morphology and morphology-property relationships.

Nanomodified epoxy exhibits increased toughness over the neat epoxy as evidenced by fractography and mechanical testing. Through processing and material variations it can be concluded that well dispersed morphologies are least effective at toughening epoxies. Larger d-spacings are observed to translate to slightly increased toughening, as evidenced by both comparison of the SC18 and I.30E systems and through mixture advancement.

The effect of advancing the epoxy-OLS mixture provided for a more ordered morphology and potential for higher fracture toughness. Process variations that resulted in more effective dispersions of the OLS as evidenced by scattering data and microscopy provided fracture toughness approximately 22% - 27% lower than baseline processes. Ordered expanded tactoid regions may more effectively interact with crack than individually dispersed organoclay layers. EDS and fractography suggest that OLS rich areas and tactoid regions provide for toughening.

The combined use of scattering data for nano-scale morphology investigations, microscopy for meso-scale investigations, and mechanical testing for bulk behavior assessments contributes an integrated approach to determination of morphology-property relationships. The coupling of process-morphology and morphology-property understanding provides a more complete picture of this material class than has been previously achieved and identifies the most effective morphology for improving toughness.

### **Recommendations**

All future research of epoxy and thermoset based nanocomposites should include complementary characterization techniques as well as *in situ* monitoring as was performed in this research to capture accurate descriptions of process-morphology relationships. Reliance on any single characterization technique with the current state-of-the-art tools severely limits the ability to accurately describe morphology.

A series of smectite clays that are not organically modified could be assessed to probe the effects of clay surface chemistry on the epoxy-amine reaction and enable a finer assessment of the role of d-spacing on toughness. Investigation of the potential for local or intragallery network gradients and the impact of such gradients on global properties could be studied by new high resolution atomic force microscopy tools.

It is recommended that interface chemistries and tools to assess interface strength be developed. This is important not only for tailoring nanocomposites for selected properties but also for enabling the assessment of viability of continuum based models for prediction of properties.

FTIR studies, while not conclusive in this research, should be continued and augmented with other chemical characterization techniques to determine if indeed the polymer phase is affected by the nanotailoring. Degree of conversion of reactive groups could be studied through the use of chemical tagging. Evolution of spectroscopic tools with improved resolution over AFM and indentors will allow for the direct measurement of modulus of the polymer phase and provide more conclusive evidence of polymer modification. Information combined from such studies will determine whether or not the polymer constituent properties are modified when combined with nanoconstituents, which will be critical to eventual modeling efforts.

Nanomodified epoxies should be extended to fiber reinforced composites, and full characterization of morphology determined as a function of processing. The effect of nanoconstituents in epoxies is not expected to translate directly to systems with micron size carbon fibers. The toughening mechanisms for the nanotailored fiber reinforced composites should be studied.

## **APPENDIX A: SCATTERING DATA FOR ISOTHERMAL TEMPERATURE PROCESSES**

Characterization of real-time morphology development was performed to provide insight into what processing variables might enable controlled morphologies. In-situ SAXS studies were performed to gain insight into morphology development paths, and provided valuable insight into material and process subtleties that may play a role on ultimate morphology development.

SAXS data exists for every minute of each experiment which in some cases extends over a period of several hours. Data to be shown here were selected to represent the significant trends and events only. Where appropriate, however, all of the data were analyzed for interpretation and discussion. Experiments were performed on two different organoclays. Plots of significant trends for the two OLSs at a given temperature are grouped for comparison. Offsets are adjusted for clarity and to provide easy comparison of trends. Table 1 summarizes pertinent morphology information that has been drawn from the analysis of the scattering data.

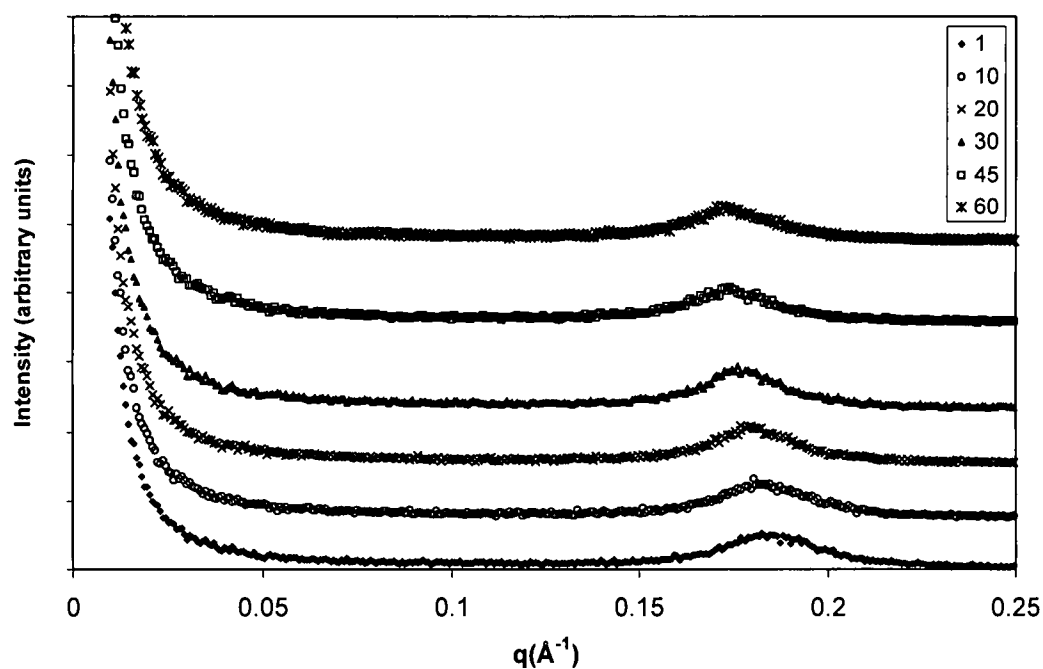


**Figure A-1:** Time-dependent small angle x-ray scattering data for 5 % I.30E/Epon 828 with mPDA at isothermal temperature of 60°C (intensity data offset for clarity).

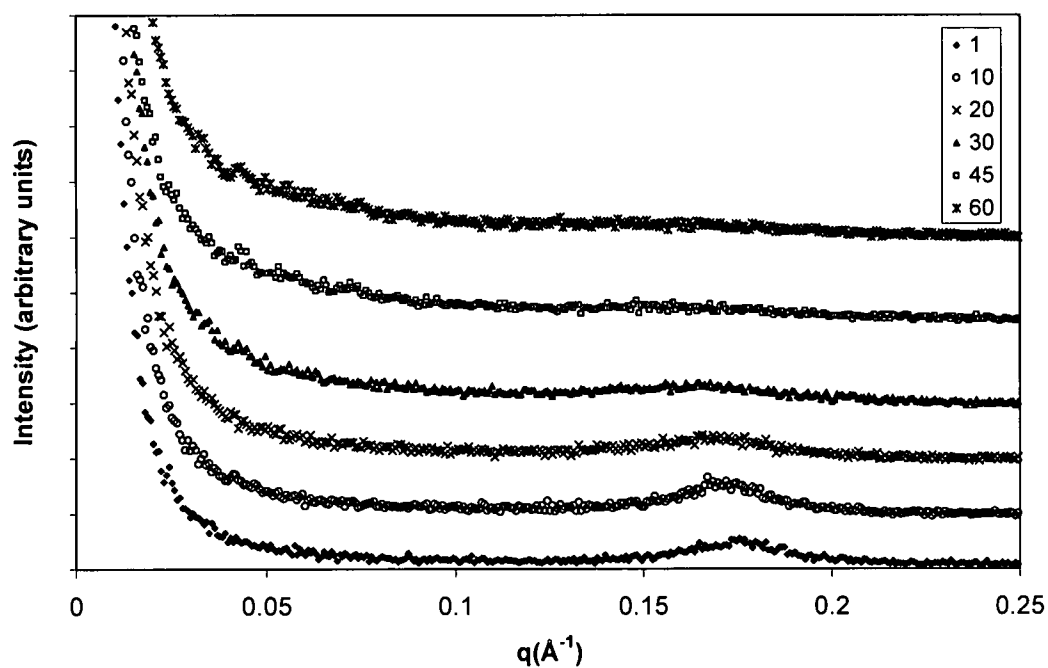


**Figure A-2:** Time-dependent small angle x-ray scattering data for 5 % SC18/Epon 828 with mPDA at isothermal temperature of 60°C (intensity data offset for clarity).

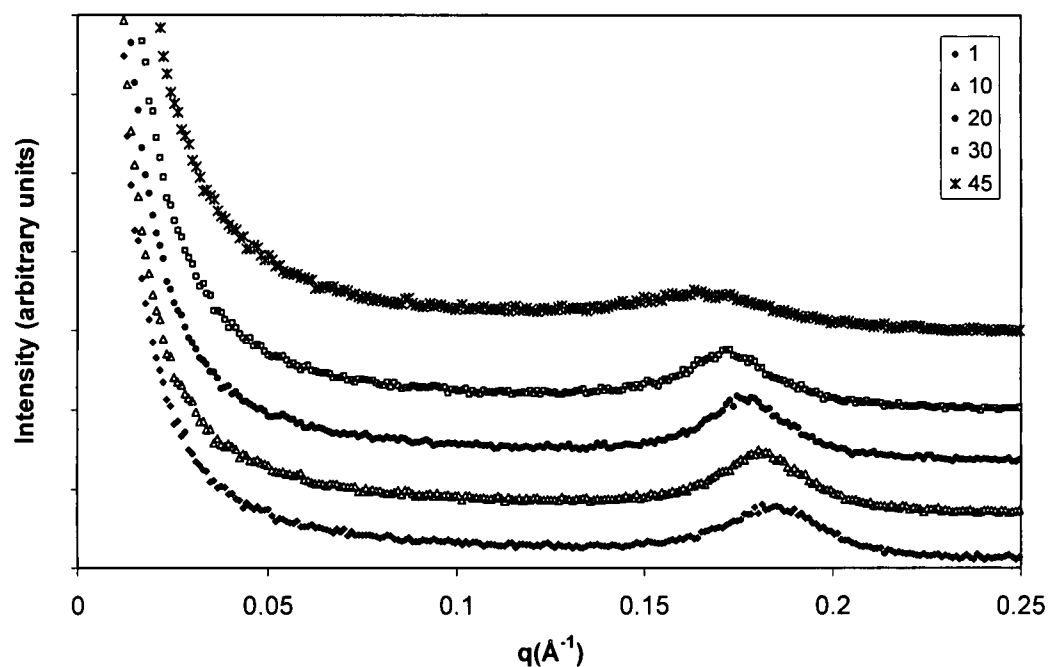


**Figure A-3:** Time-dependent small angle x-ray scattering data for 5 % I.30E/Epon 828 with mPDA at isothermal temperature of 70°C (intensity data offset for clarity).

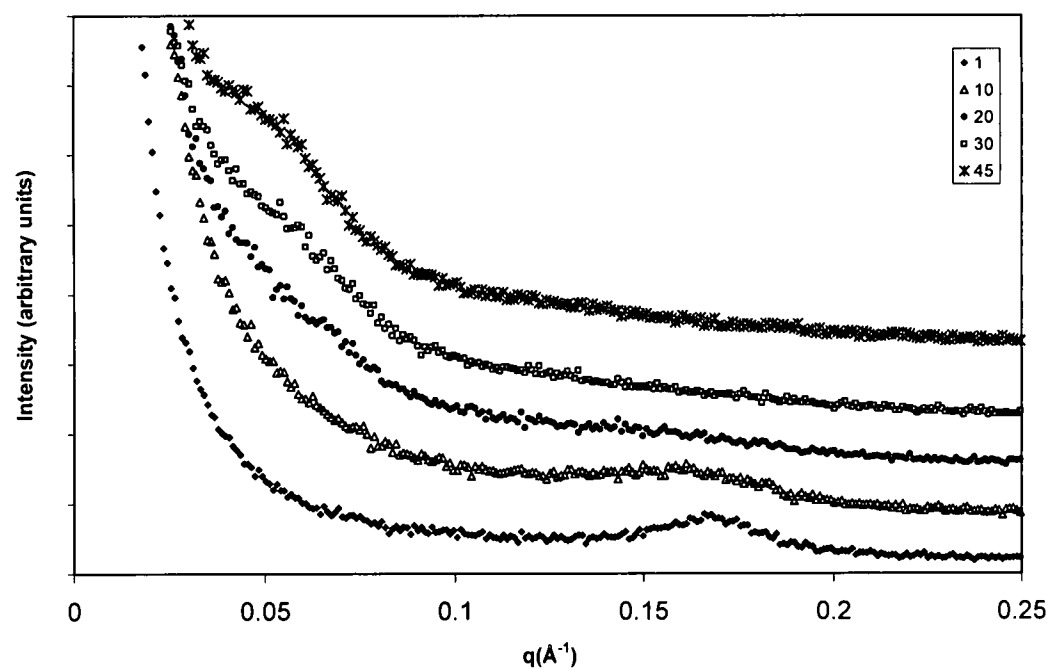


**Figure A-4:** Time-dependent small angle x-ray scattering data for 5 % SC18/Epon 828 with mPDA at isothermal temperature of 70°C (intensity data offset for clarity).

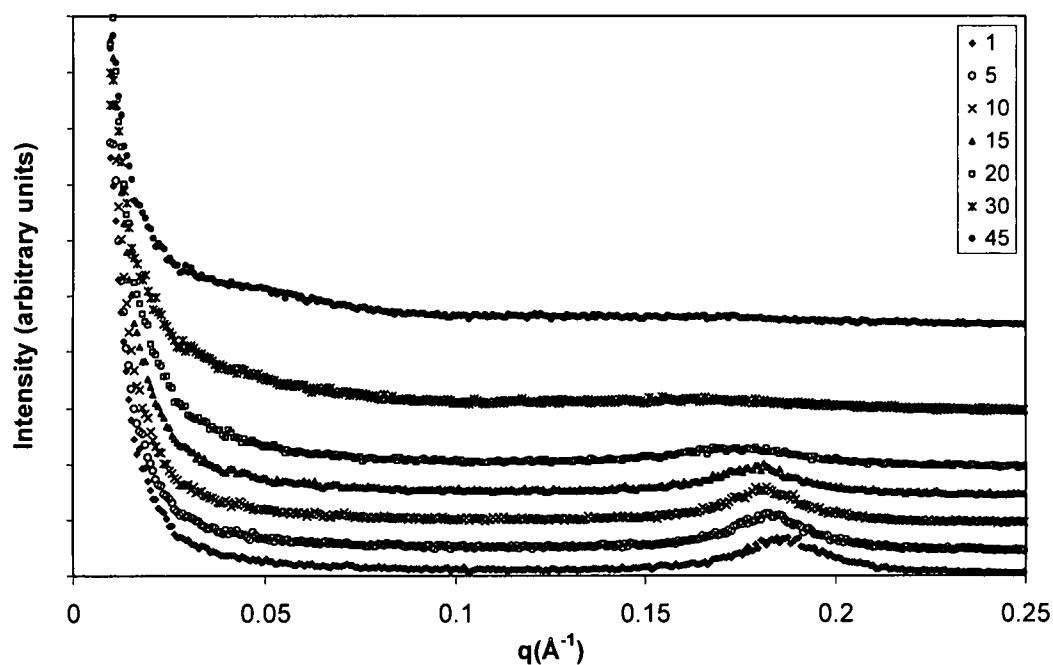


**Figure A-5:** Time-dependent small angle x-ray scattering data for 5 % I.30E/Epon 828 with mPDA at isothermal temperature of 80°C (intensity data offset for clarity).

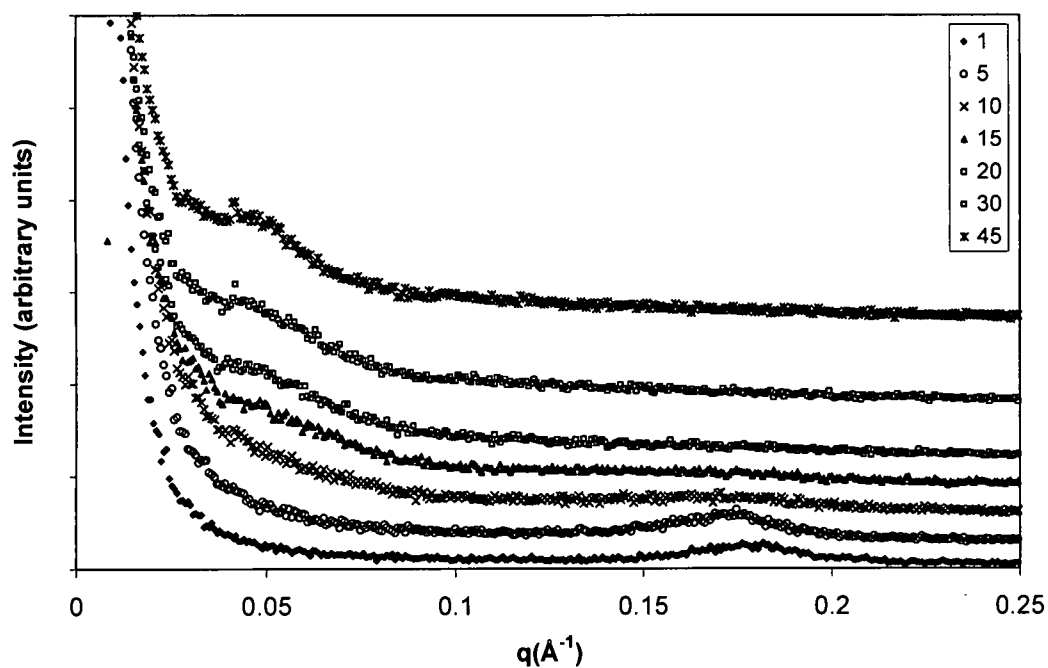


**Figure A-6:** Time-dependent small angle x-ray scattering data for 5 % SC18/Epon 828 with mPDA at isothermal temperature of 80°C (intensity data offset for clarity).

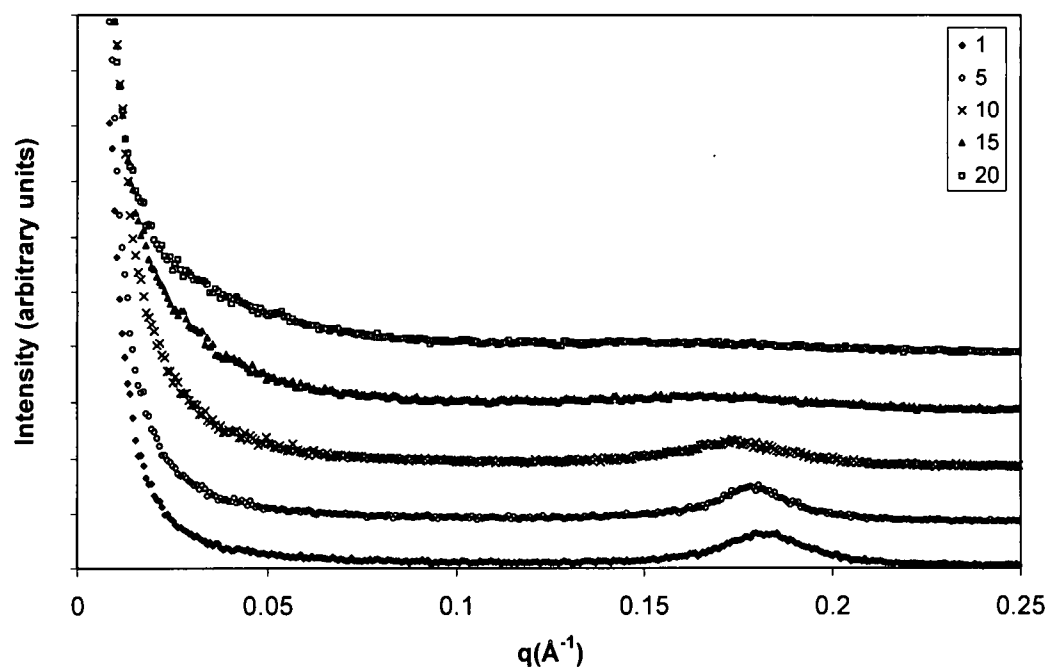


**Figure A-7:** Time-dependent small angle x-ray scattering data for 5 % I.30E/Epon 828 with mPDA at isothermal temperature of 90°C (intensity data offset for clarity).

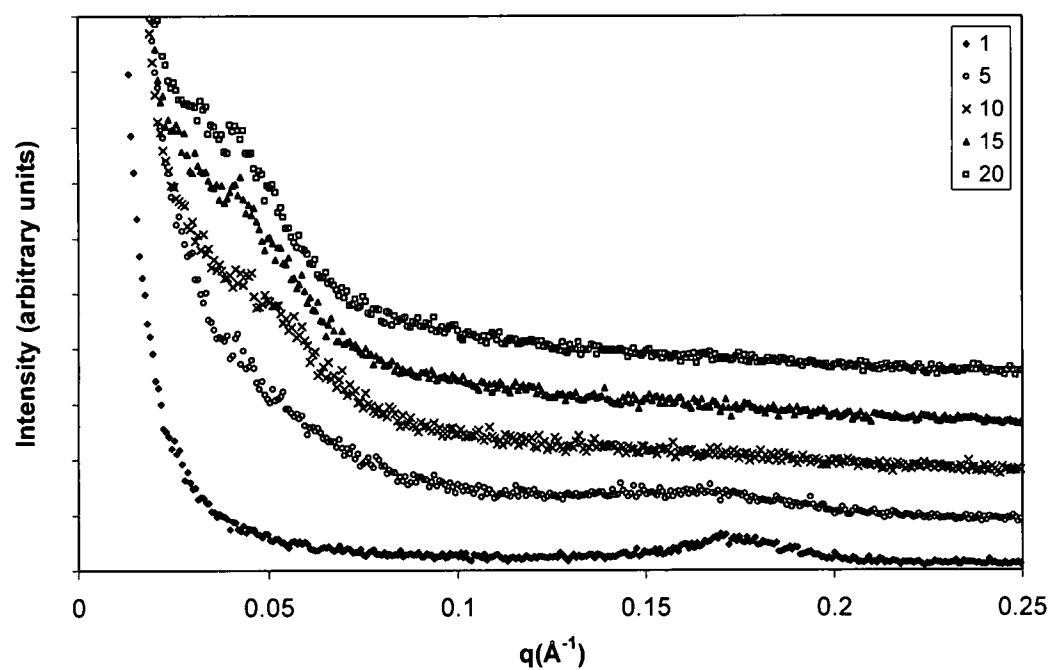


**Figure A-8:** Time-dependent small angle x-ray scattering data for 5 % SC18/Epon 828 with mPDA at isothermal temperature of 90°C (intensity data offset for clarity).

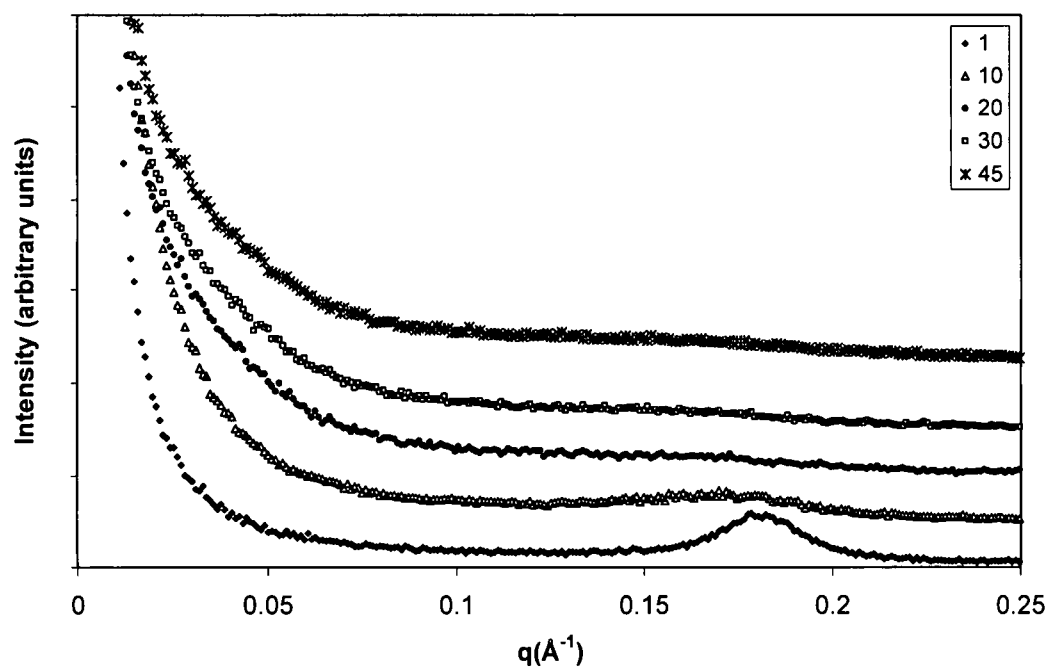


**Figure A-9:** Time-dependent small angle x-ray scattering data for 5% I.30E/Epon 828 with mPDA at isothermal temperature of 100°C (intensity data offset for clarity).

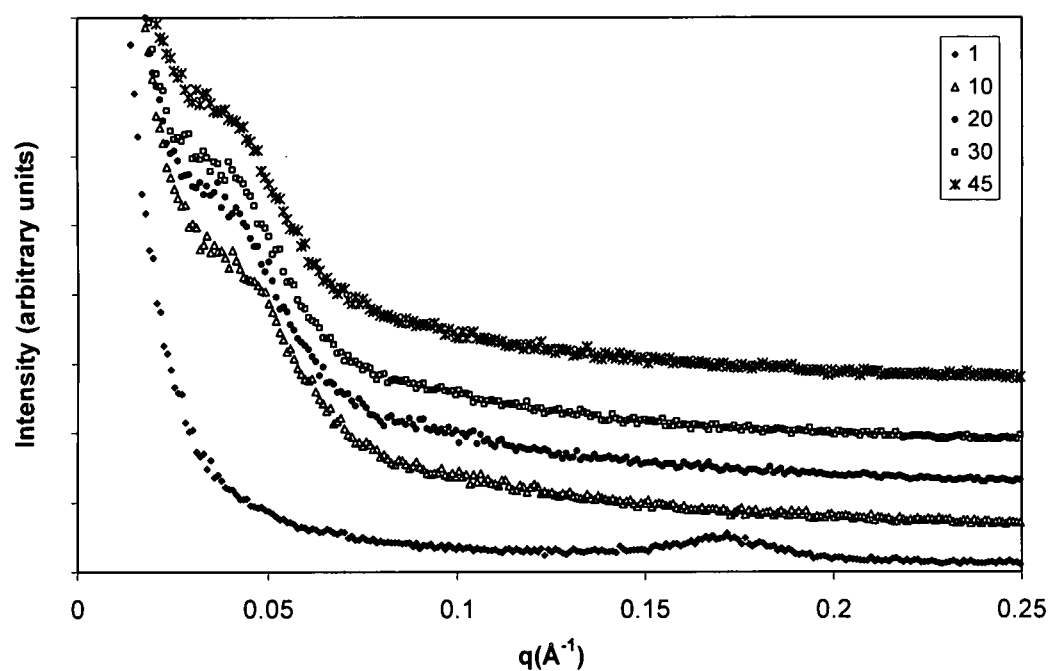


**Figure A-10:** Time-dependent small angle x-ray scattering data for 3 % SC18/Epon 828 with mPDA at isothermal temperature of 100°C (intensity data offset for clarity).

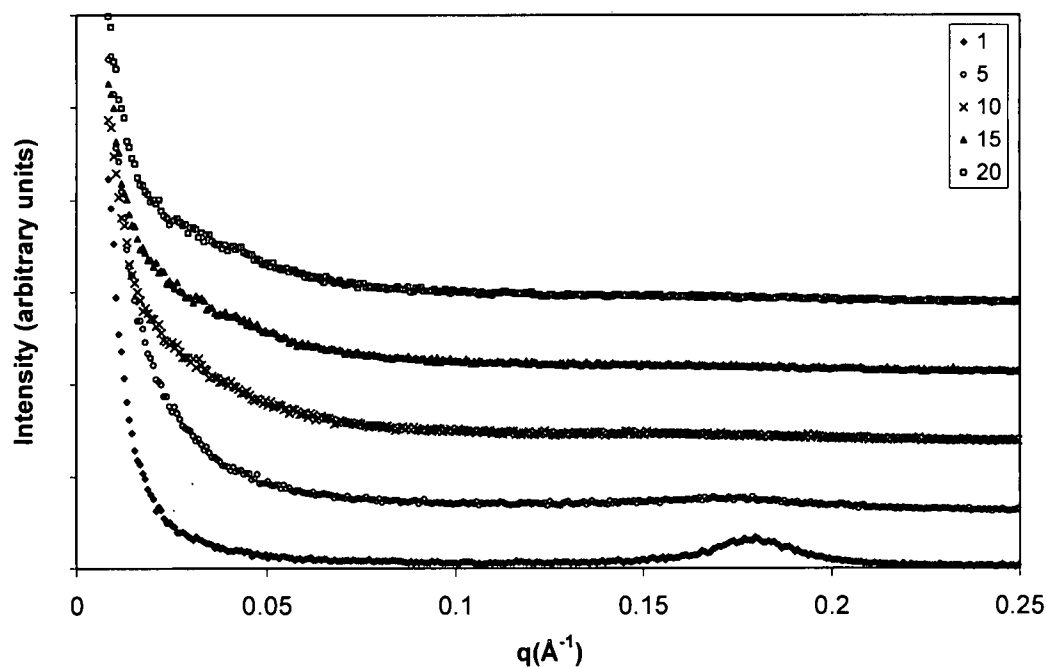


**Figure A-11:** Time-dependent small angle x-ray scattering data for 5 % I.30E/Epon 828 with mPDA at isothermal temperature of 110°C (intensity data offset for clarity).

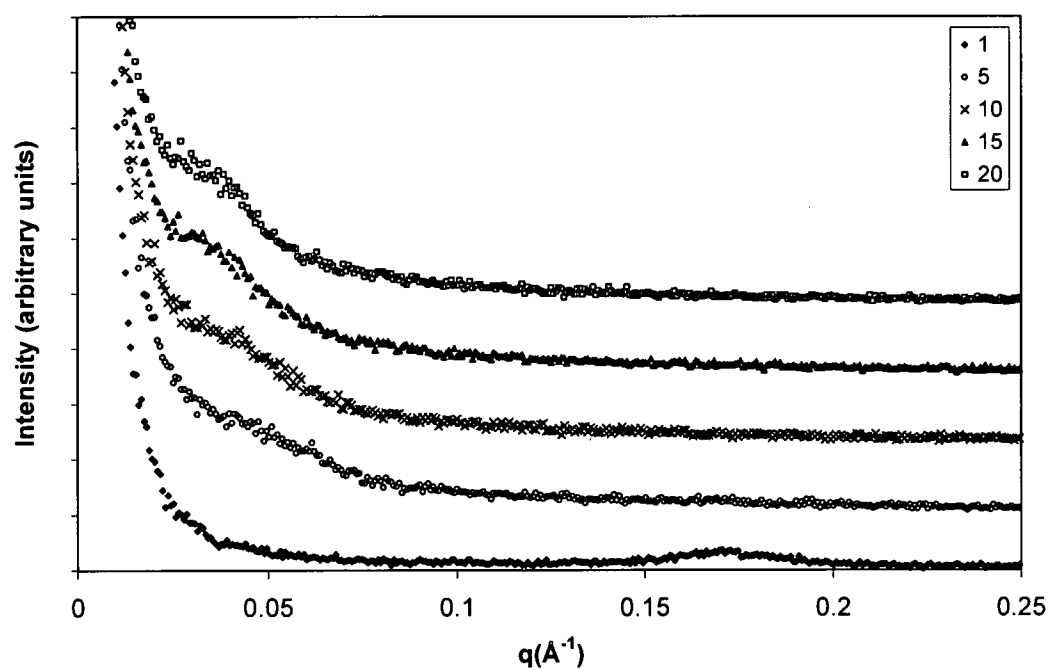


**Figure A-12:** Time-dependent small angle x-ray scattering data for 3 % SC18/Epon 828 with mPDA at isothermal temperature of 110°C (intensity data offset for clarity).

**Table A-1: In-situ SAXS Studies on Isothermal Temperature Processes versus Morphology Development**

Silicate	Isothermal Temperature (C)	Initial d-Spacing (Å)	Loss of Intercalation Peak (Minutes)	Final d-Spacing (Å) <sup>1</sup>	Dominant Final Morphology <sup>1</sup>
I30E	60°	33 Å	168	33 Å	Intercalated, $I_f > I_i$
I30E	70°	38 Å	> 45 <sup>2</sup>	38 Å	Intercalated, $I_f < I_i$
I30E	80°	34 Å	22	42 Å	Mixed
I30E	90°	34 Å	19-20	140 Å	Exfoliated
I30E	100°	35 Å	15	140 Å	Exfoliated
I30E	110°	35 Å	9-10	150 Å	Exfoliated
SC18	60°	36 Å	85	46 Å	Intercalated, $I_f < I_i$
SC18	70°	37 Å	28	140 Å	Exfoliated
SC18	80°	36 Å	10	125 Å <sup>3</sup>	Exfoliated
SC18	90°	36 Å	8	153 Å	Exfoliated
SC18 <sup>4</sup>	100°	37 Å	5	180 Å	Exfoliated
SC18 <sup>4</sup>	110°	37 Å	2.5-3	185 Å	Exfoliated

<sup>1</sup> Final Time: 45 Minutes

<sup>2</sup> Duration of run 45 minutes; exfoliation not initiated within run duration

<sup>3</sup> Final Time: 15 Minutes

<sup>4</sup> Data on 3% weight fraction of silicate

## **APPENDIX B: SCATTERING DATA FOR NON-ISOTHERMAL PROCESSES**

In-situ SAXS data for heating rate processes are shown in Figures B-1 through B-9. Scattering data selected to show significant events and trends is depicted. Experiments were performed on two different organoclays. Plots of significant trends for the two OLSs at a given temperature are grouped for comparison. Offsets are adjusted for clarity and to provide easy comparison of trends. Data exists for every minute of each experiment which in some cases extends over a period of several hours. Data to be shown here were selected to represent the significant trends and events only. Where appropriate, however, all of the data were analyzed for interpretation and discussion. Data are summarized in Table B-1.

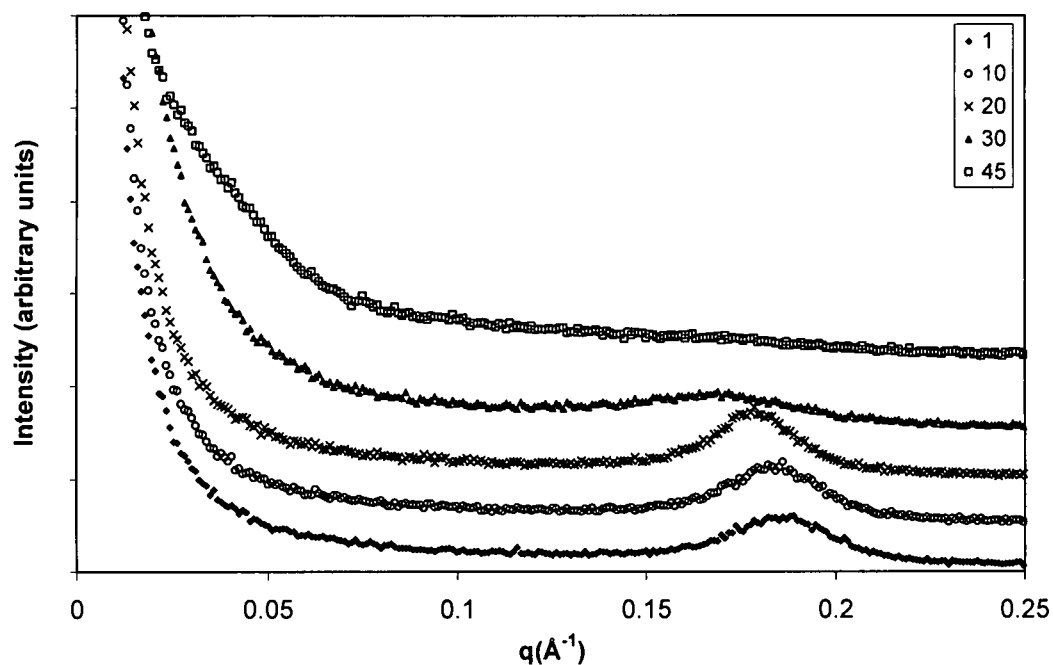


**Figure B-1:** Time-dependent small angle x-ray scattering data for 5 % I.30E/Epon 828 with mPDA at heating rate of 2°C/minute (intensity data offset for clarity).

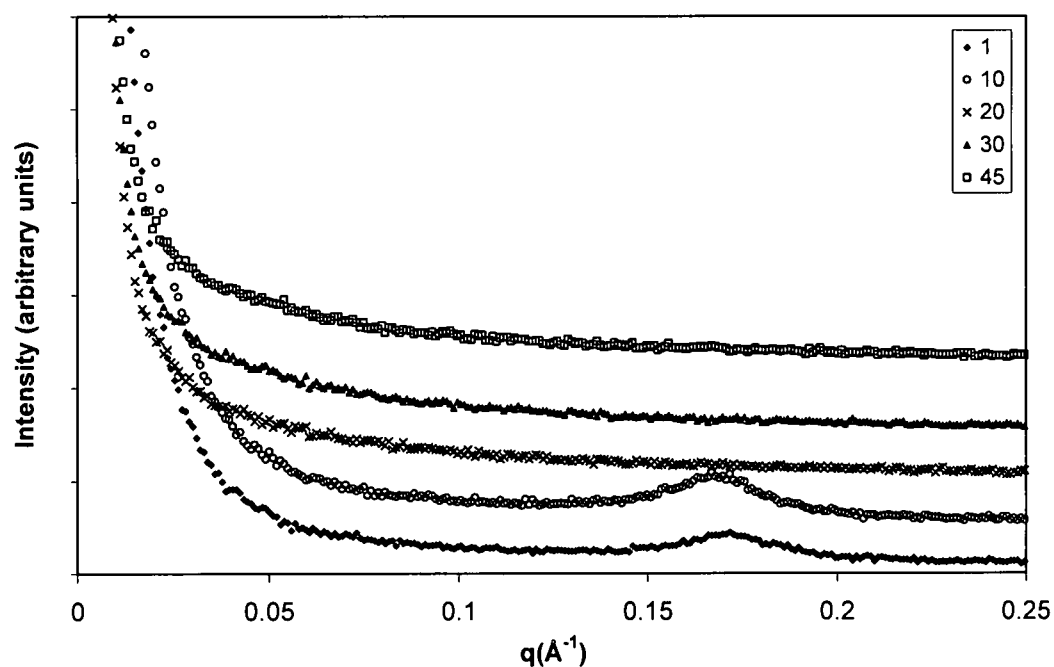


**Figure B-2:** Time-dependent small angle x-ray scattering data for 5 % SC18/Epon 828 with mPDA at heating rate of 2°C/minute (intensity data offset for clarity).

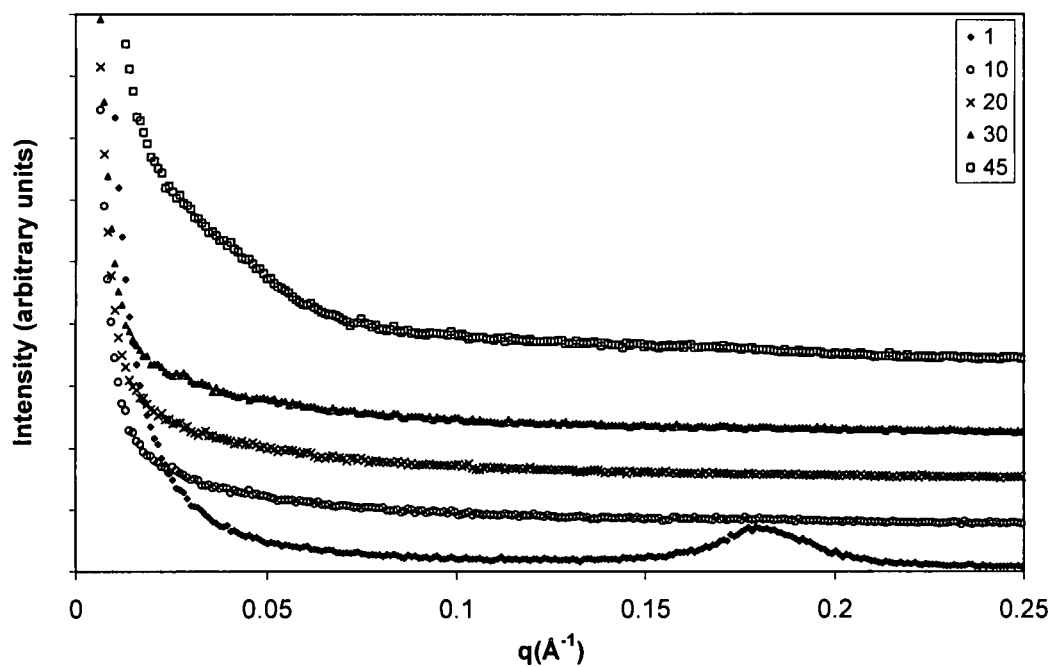


**Figure B-3:** Time-dependent small angle x-ray scattering data for 5 % I.30E/Epon 828 with mPDA at heating rate of 5°C/minute (intensity data offset for clarity).

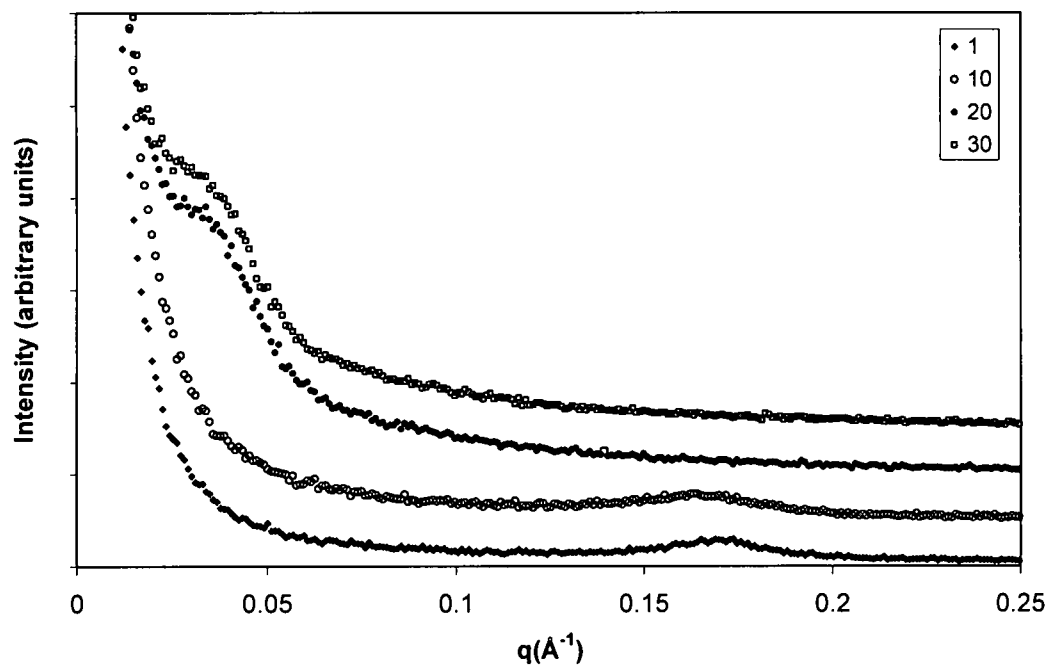


**Figure B-4:** Time-dependent small angle x-ray scattering data for 5 % SC18/Epon 828 with mPDA at heating rate of 5°C/minute (intensity data offset for clarity).

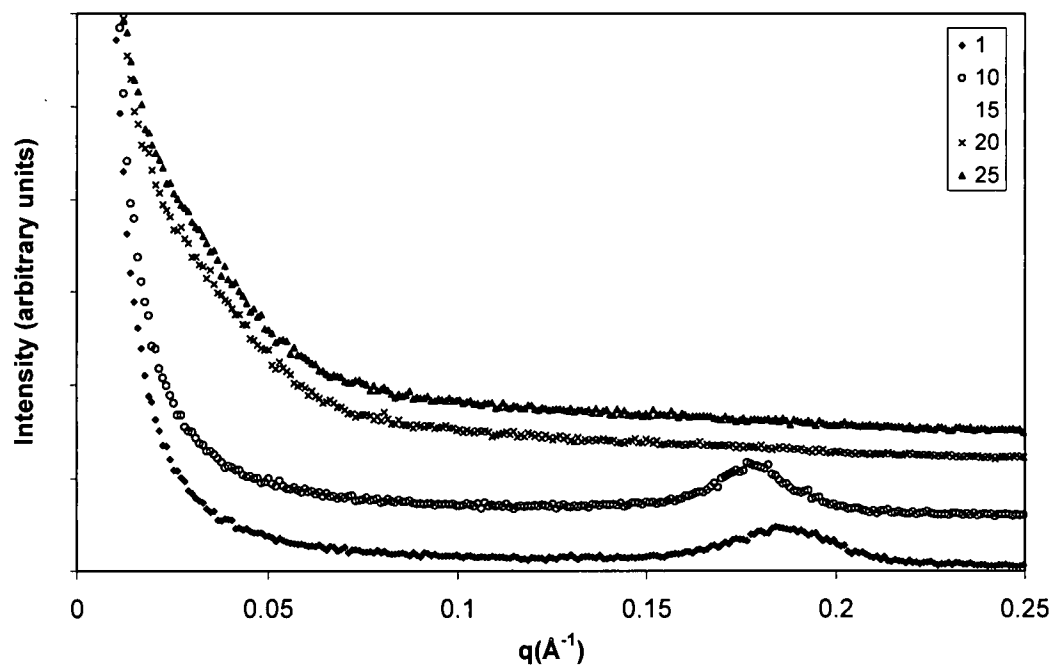


**Figure B-5:** Time-dependent small angle x-ray scattering data for 5 % I.30E/Epon 828 with mPDA at heating rate of 6°C/minute (intensity data offset for clarity). No data available on SC18.

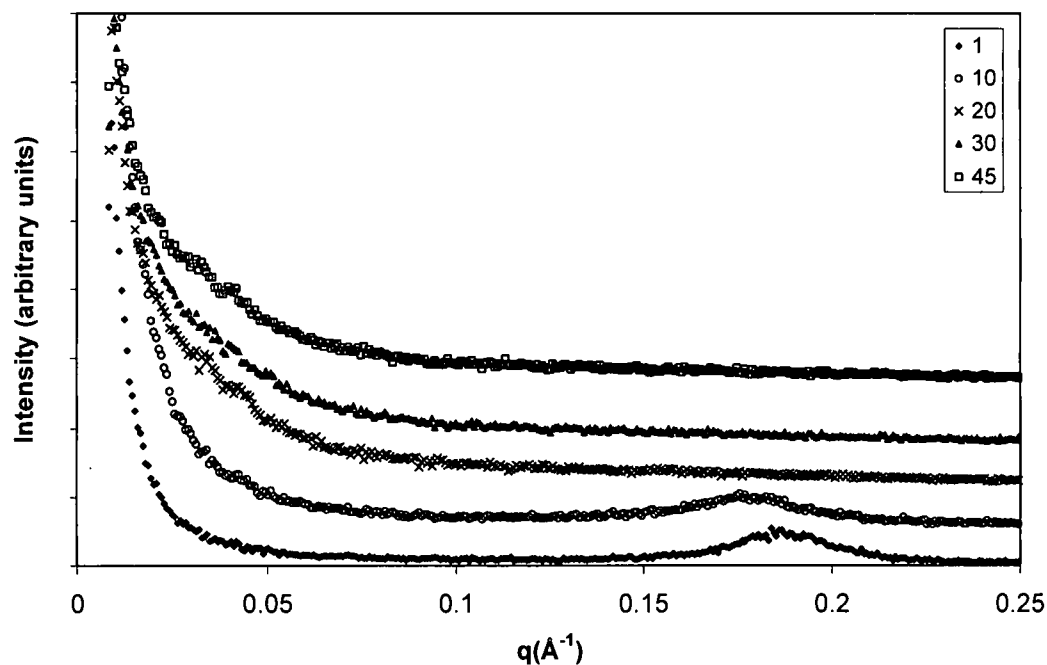


**Figure B-6:** Time-dependent small angle x-ray scattering data for 5 % I.30E/Epon 828 with mPDA at heating rate of 10°C/minute (intensity data offset for clarity).

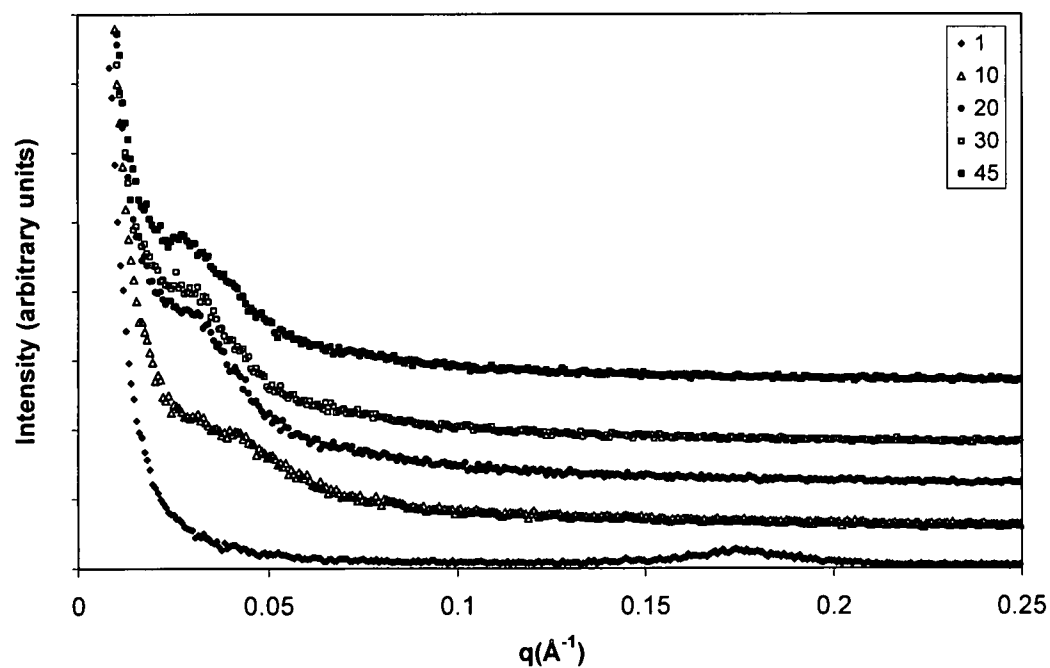


**Figure B-7:** Time-dependent small angle x-ray scattering data for 5 % SC18/Epon 828 with mPDA at heating rate of 10°C/minute (intensity data offset for clarity).

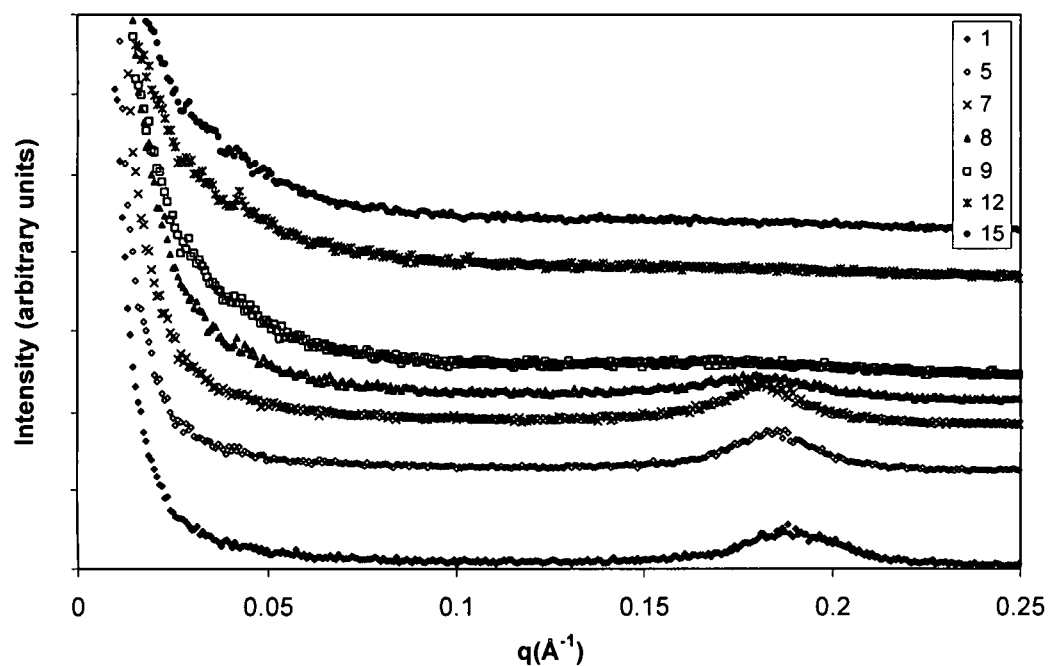


**Figure B-8:** Time-dependent small angle x-ray scattering data for 5 % I.30E/Epon 828 with mPDA at heating rate of 12°C/minute (intensity data offset for clarity).

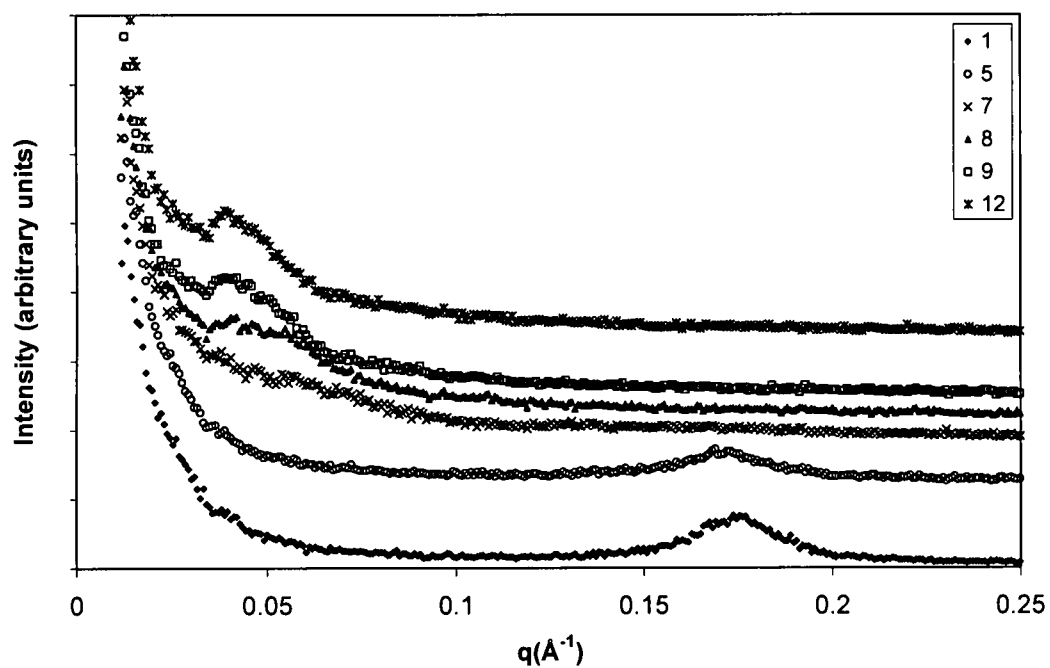


**Figure B-9:** Time-dependent small angle x-ray scattering data for 5 % SC18/Epon 828 with mPDA at heating rate of 12°C/minute (intensity data offset for clarity).

**Table B-2: Temperature Rate Summary**

Silicate	Temperature Profile	Initial d- Spacing (Å)	Loss of Intercalat ion Peak (minutes)	Final d-Spacing <sup>a</sup> (Å)
I30E	2°/Min Ramp	33 Å	36	155 Å
I30E	5°/Min Ramp	33 Å	16	216 Å
I30E	5°/Min Ramp (5.3)	34 Å	15	225 Å <sup>b</sup>
I30E	6°/Min Ramp	35 Å	10	180 Å <sup>c</sup>
I30E	10°/Min Ramp	34 Å	12	216 Å
I30E	12°/Min Ramp	34 Å	10	210 Å <sup>c</sup>
SC18	2°/Min Ramp	36 Å	17	300 Å
SC18	5°/Min Ramp (5/01)	35 Å	9-10	210 Å
SC18	5°/Min Ramp (5.3)	37 Å	12	180 Å
SC18	10°/Min Ramp	36 Å	10	225 Å
SC18 <sup>2</sup>	12°/Min Ramp	36 Å	7	166-170 Å <sup>d</sup>

<sup>a</sup> Final Time: 45 Minutes

<sup>b</sup> Final Time: 30 Minutes

<sup>c</sup> Final Time: 25 Minutes

<sup>d</sup> Final Time: 13 Minutes

## APPENDIX C: SCATTERING DATA AS A FUNCTION OF MATERIAL PRECONDITIONING

In-situ SAXS data for various material preconditioning are shown in Figures C-1 through C-21. Studies were performed at isothermal temperature of 80°C and selected heating rates for comparison with the data on temperature variations. Scattering data selected to show significant events and trends are depicted. Offsets are adjusted for clarity and to provide easy comparison of trends.

### Preconditioning through Advancement via SAXS

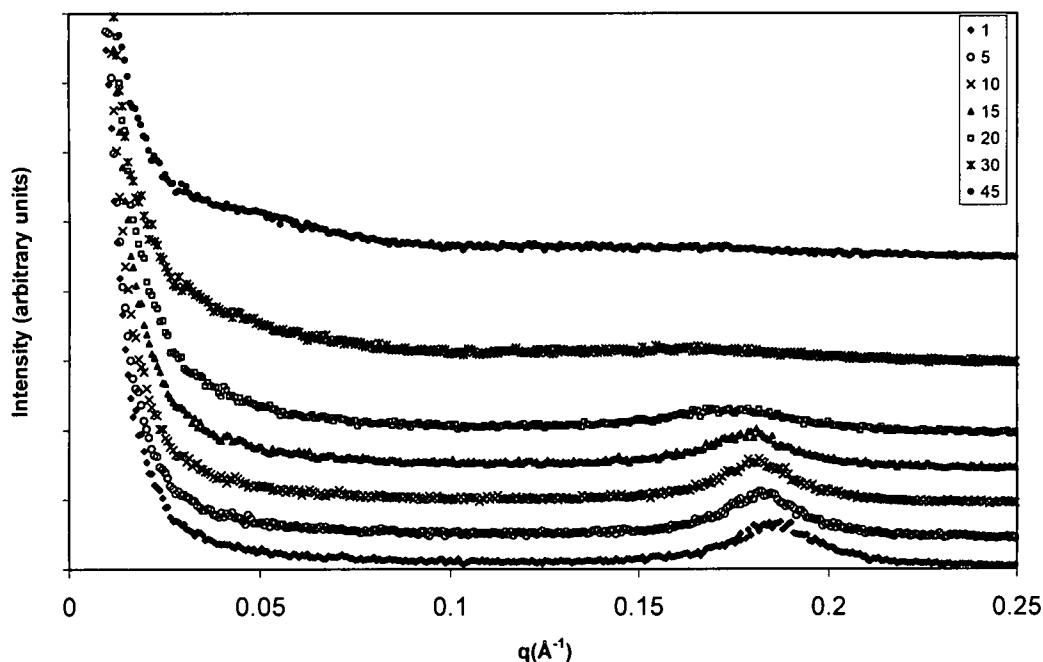


**Figure C-1:** Time-dependent small angle x-ray scattering data for 5% I.30E/Epon 828 with mPDA at isothermal temperature of 80°C with no advancement (repeat of Figure 5).

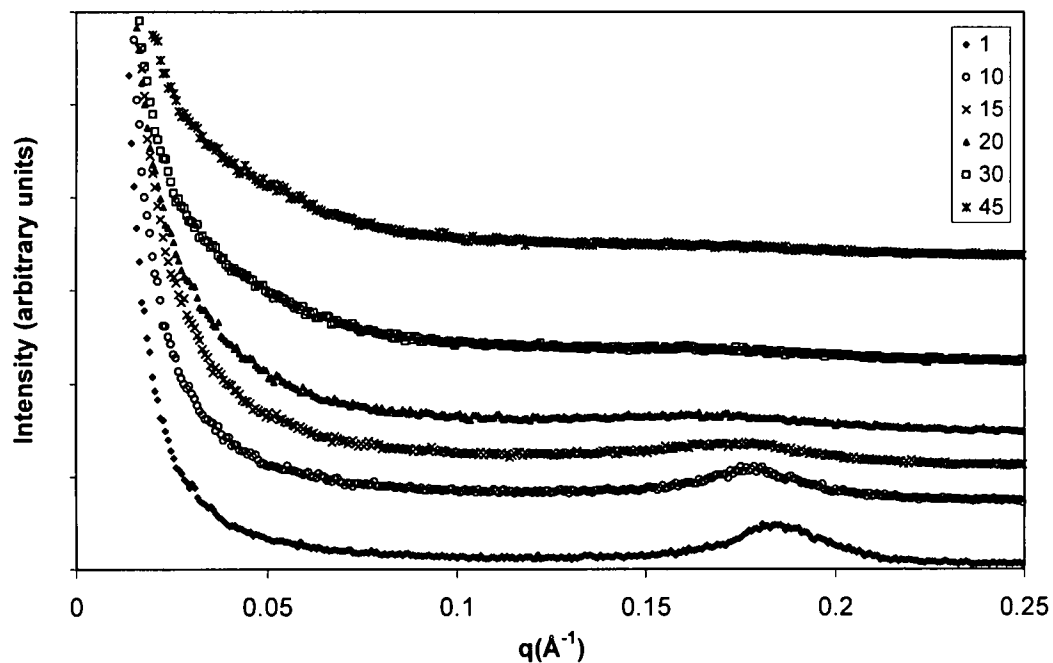


**Figure C-2:** Time-dependent small angle x-ray scattering data for 5% I.30E/Epon 828 with mPDA at isothermal temperature of 80°C after advancement for 1 week (intensity data offset for clarity).

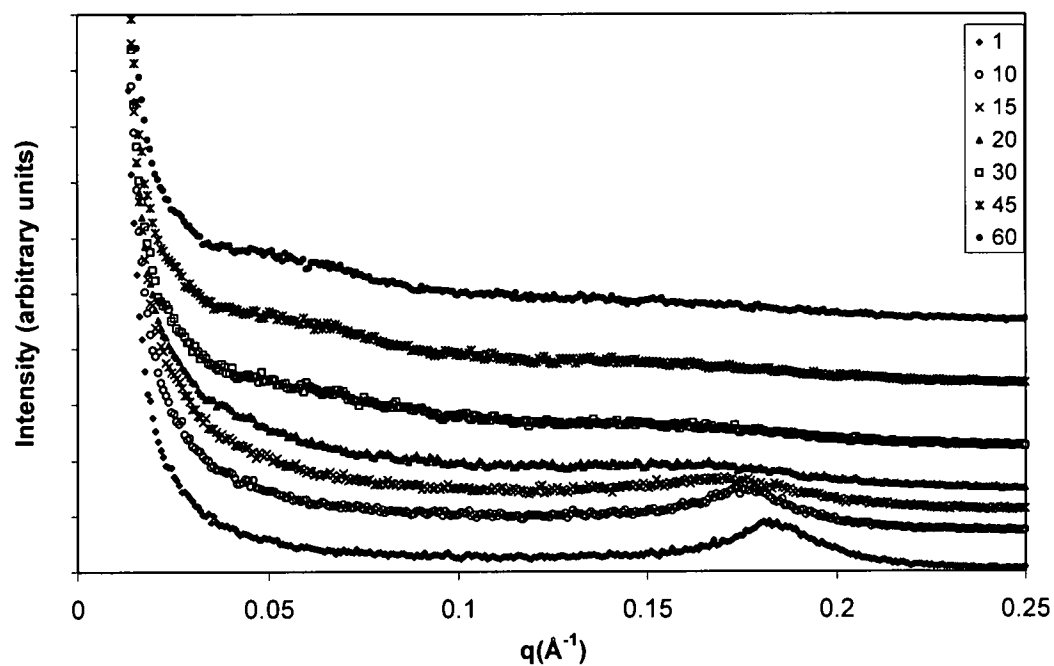


**Figure C-3:** Time-dependent small angle x-ray scattering data for 5 % I30E/Epon 828 with mPDA at isothermal temperature of 80°C after advancement for 4 weeks (intensity data offset for clarity).

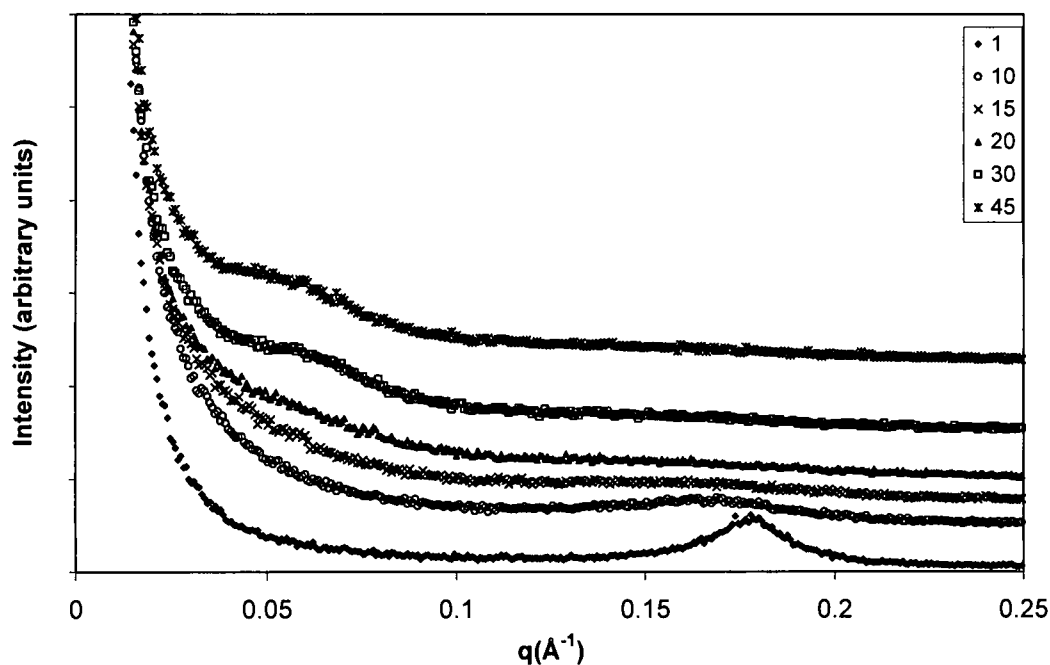


**Figure C-4:** Time-dependent small angle x-ray scattering data for 5% I.30E/Epon 828 with mPDA at isothermal temperature of 80°C after advancement for 8 weeks (intensity data offset for clarity).

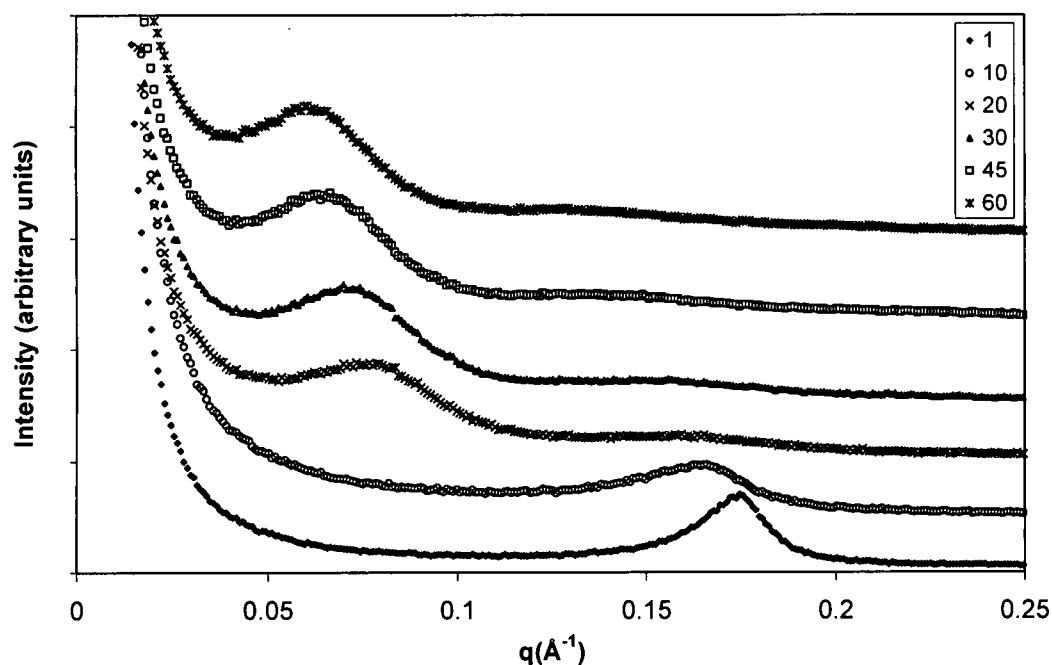


**Figure C-5:** Time-dependent small angle x-ray scattering data for 5 % I30E/Epon 828 with mPDA at isothermal temperature of 80°C after advancement for 18 weeks (intensity data offset for clarity).

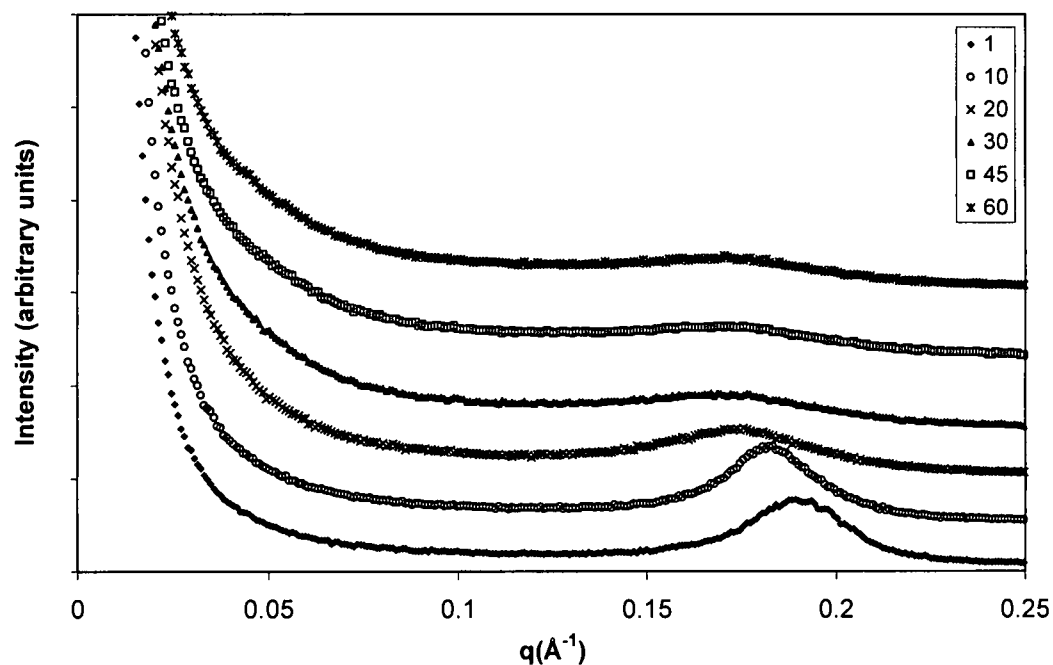


**Figure C-6:** Time-dependent small angle x-ray scattering data for 7 % I30E/Epon 828 with mPDA at isothermal temperature of 80°C with no advancement (intensity data offset for clarity).

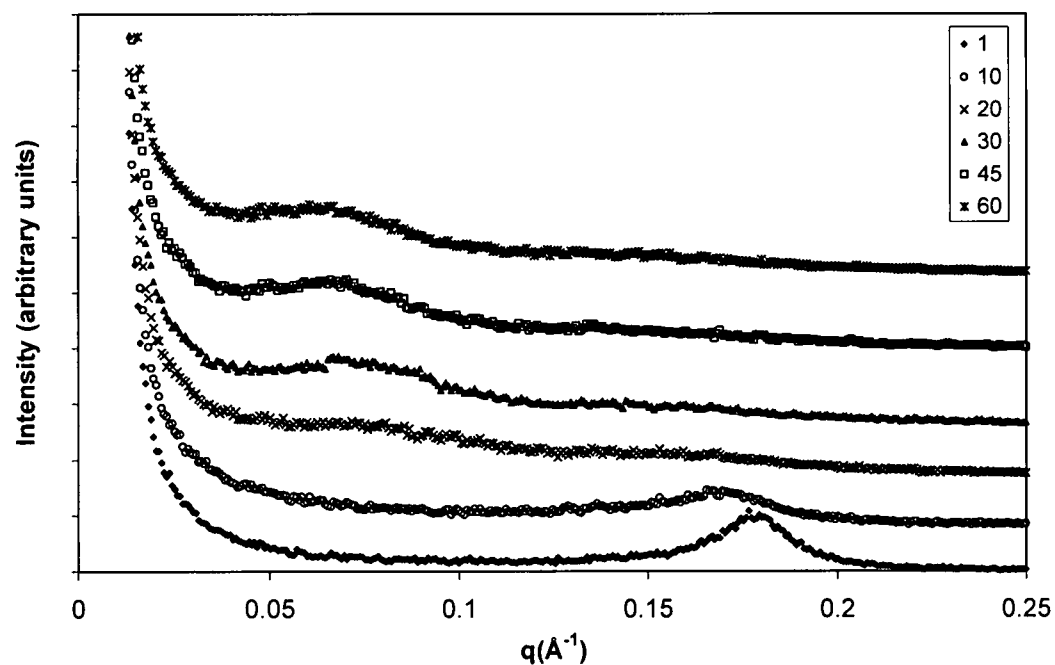


**Figure C-7:** Time-dependent small angle x-ray scattering data for 7 % I30E/Epon 828 with mPDA at isothermal temperature of 80°C after advancement for 18 weeks (intensity data offset for clarity).

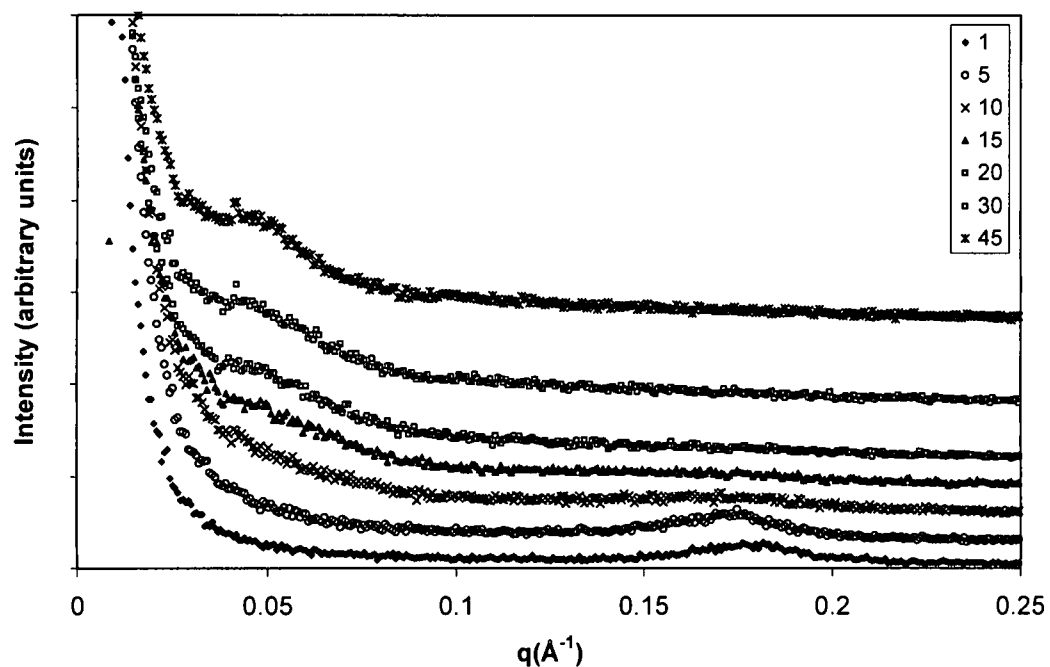


**Figure C-8:** Time-dependent small angle x-ray scattering data for 5% SC18/Epon 828 with mPDA at isothermal temperature of 80°C with no advancement (intensity data offset for clarity).

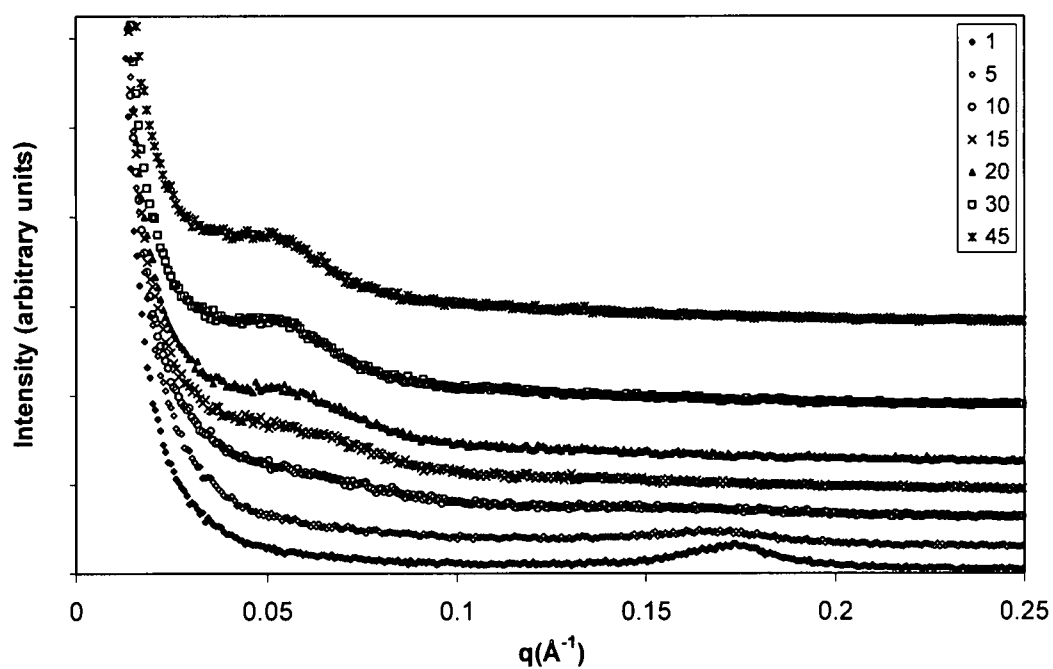


**Figure C-9:** Time-dependent small angle x-ray scattering data for 5% SC18/Epon 828 with mPDA at isothermal temperature of 80°C after advancement for 1 week (intensity data offset for clarity).

**Table C-1: Summary of Advancement Effects at Isothermal Temperature of 80°C.**

<b>Weight Fraction I.30E</b>	<b>Fabrication Process</b>	<b>Initial d-spacing (Å)</b>	<b>d-spacing at 60 minutes (Å)</b>
5%	Baseline	34	42 <sup>a</sup>
5%	Epoxy-silicate mixture aged 1 week	34	45
5%	Epoxy-silicate mixture aged 4+ weeks	36	104
5%	Epoxy-silicate mixture aged 8 weeks	35	105
5%	Epoxy-silicate mixture aged 18 weeks	36	110
7%	Baseline	33	37
7%	Epoxy-silicate mixture aged 18 weeks	35	106

<sup>a</sup> Final Time: 45 Minutes

Error typically within 1 Å

## Volume Fraction Variation via SAXS

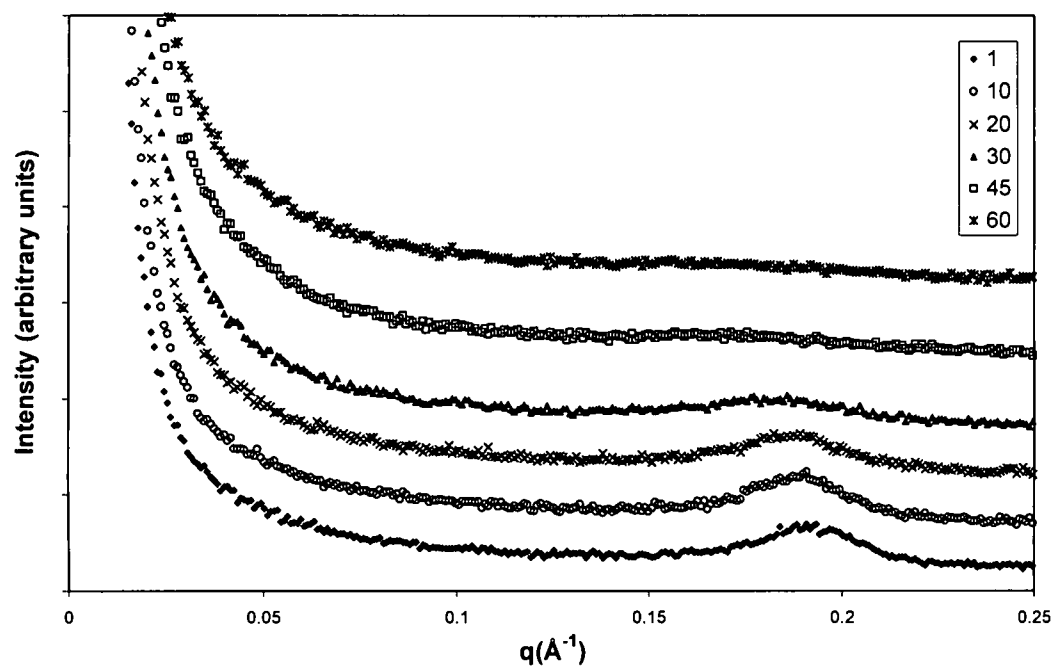


**Figure C-10:** Time-dependent small angle x-ray scattering data for 1 % I.30E/Epon 828 with mPDA at isothermal temperature of 80°C (intensity data offset for clarity).

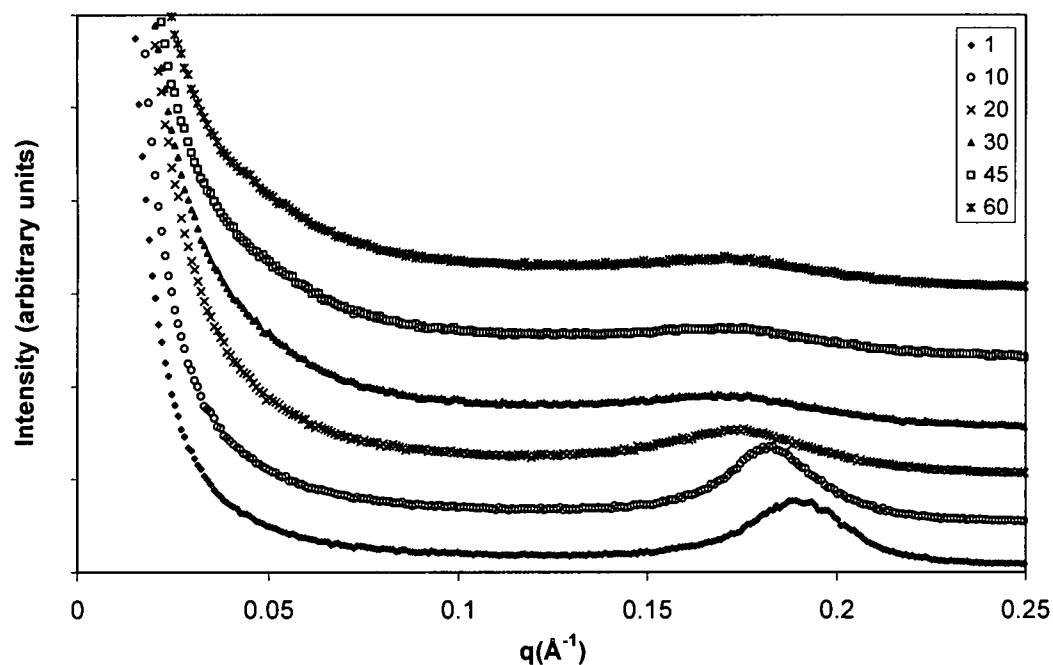


**Figure C-11:** Time-dependent small angle x-ray scattering data for 7 % I.30E/Epon 828 with mPDA at isothermal temperature of 80°C (intensity data offset for clarity).

**Table C-2: Volume Fraction Variation**

System	Weight fraction	Initial d	Final d
828/I30E/mPDA	1%, Iso 80	33	40-41
828/I30E/mPDA	7%, Iso 80	33	37
828/I30E/mPDA	5%, Iso 80	34	42/45

**Preconditioning of Organoclay versus Morphology Development via SAXS**

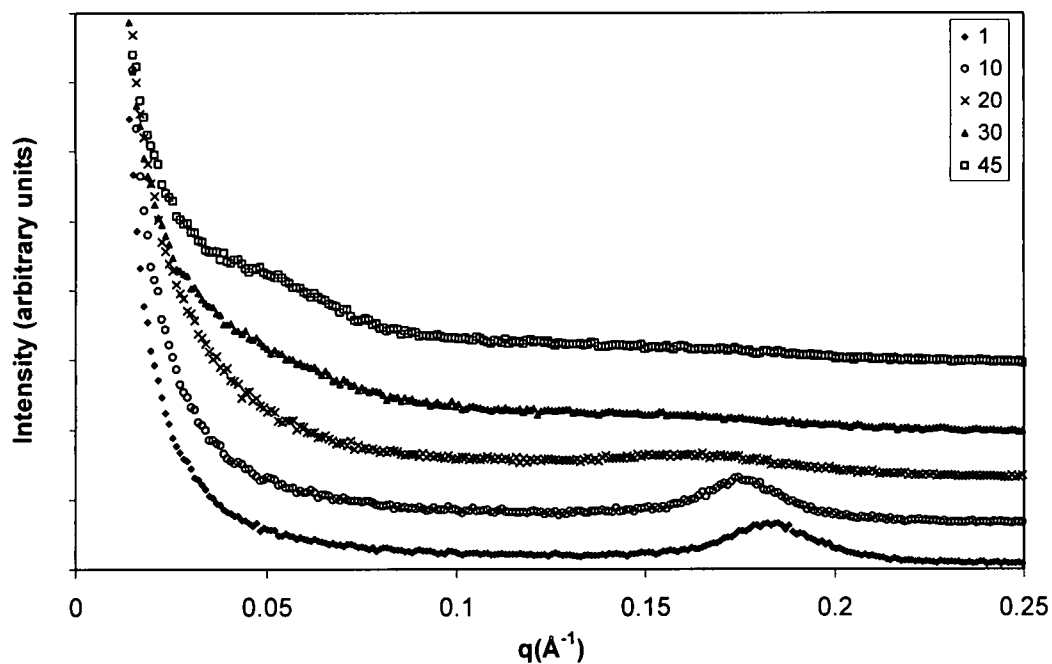


**Figure C-13:** Time-dependent small angle x-ray scattering data for 5 % I.30E/Epon 828 with mPDA without degas step at isothermal temperature of 80° (intensity data offset for clarity).

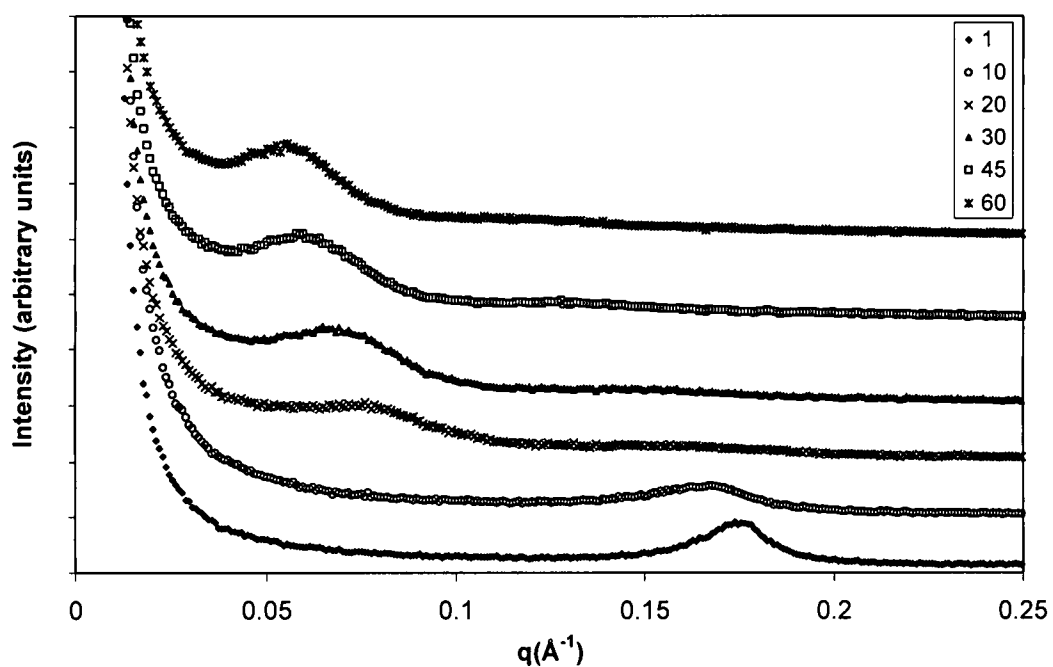


**Figure C-14:** Time-dependent small angle x-ray scattering data for 5 % I30E/Epon 828 with mPDA with no degas at isothermal temperature of 80°C after advancement for 18 weeks (intensity data offset for clarity).

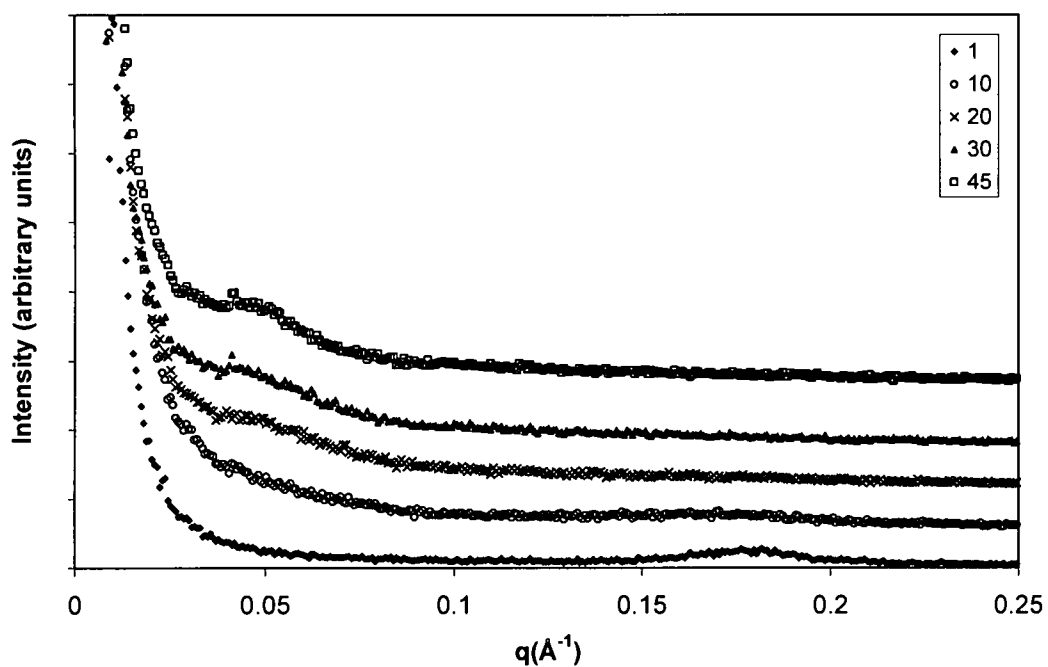


**Figure C-15:** Time-dependent small angle x-ray scattering data for 5 % SC18/Epon 828 with mPDA at isothermal temperature of 80°C (intensity data offset for clarity).

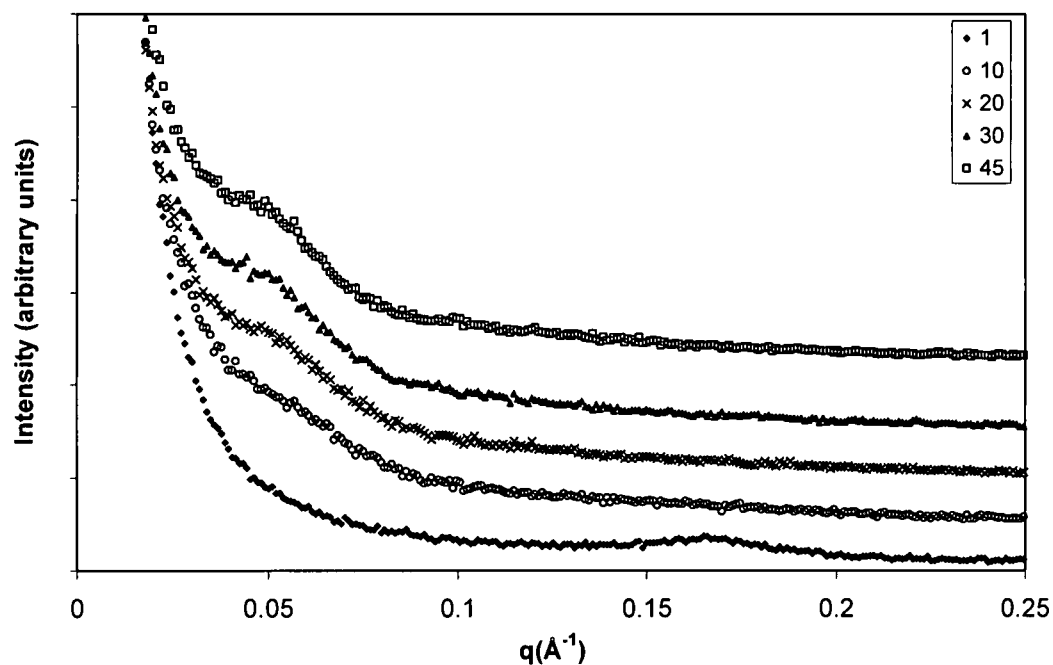


**Figure C-16:** Time-dependent small angle x-ray scattering data for 5 % SC18/Epon 828 with mPDA without degas step at isothermal temperature of 80° (intensity data offset for clarity).

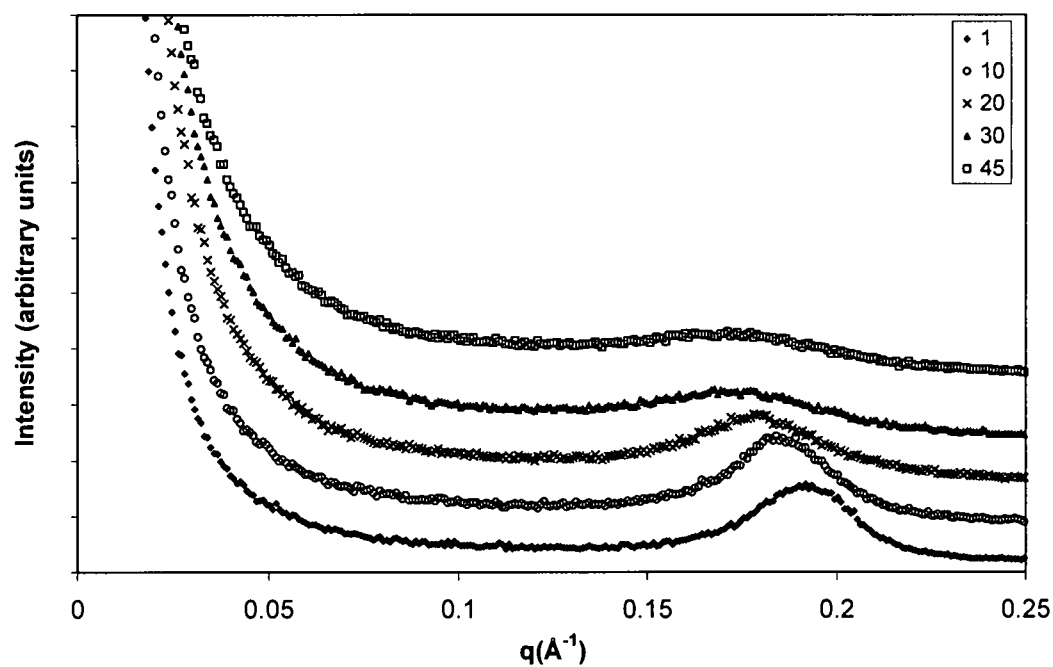


**Figure C-17:** Time-dependent small angle x-ray scattering data for 5 % pre-dried (25°C) I.30E/Epon 828 with mPDA at isothermal temperature of 80°C (intensity data offset for clarity).

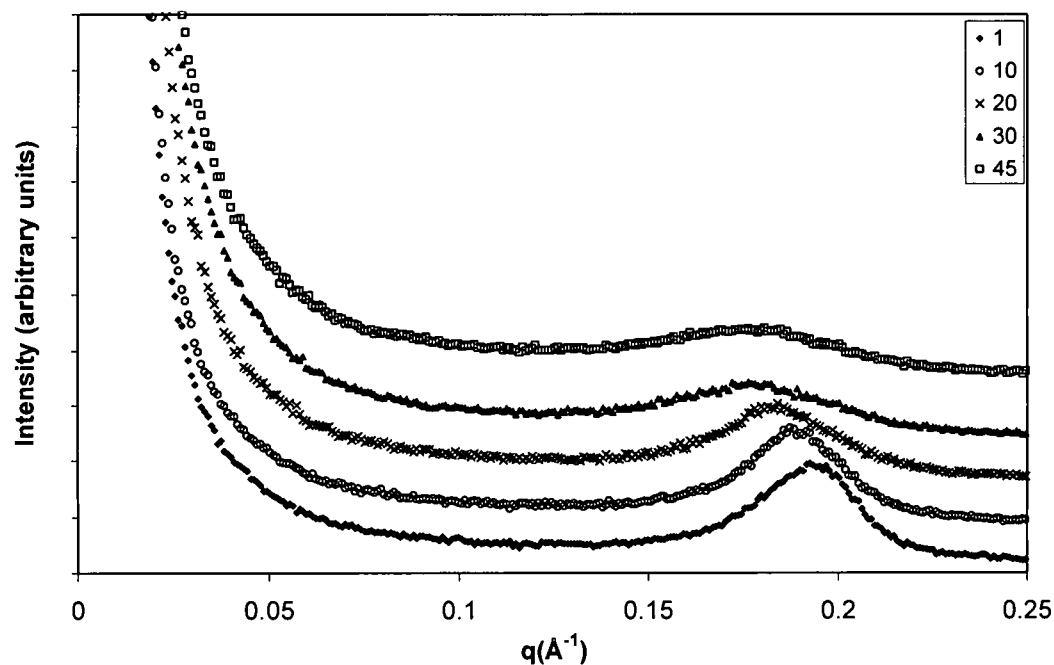


**Figure C-18:** Time-dependent small angle x-ray scattering data for 5 % pre-dried (100°C) I.30E/Epon 828 with mPDA without degas step at isothermal temperature of 80° (intensity data offset for clarity).

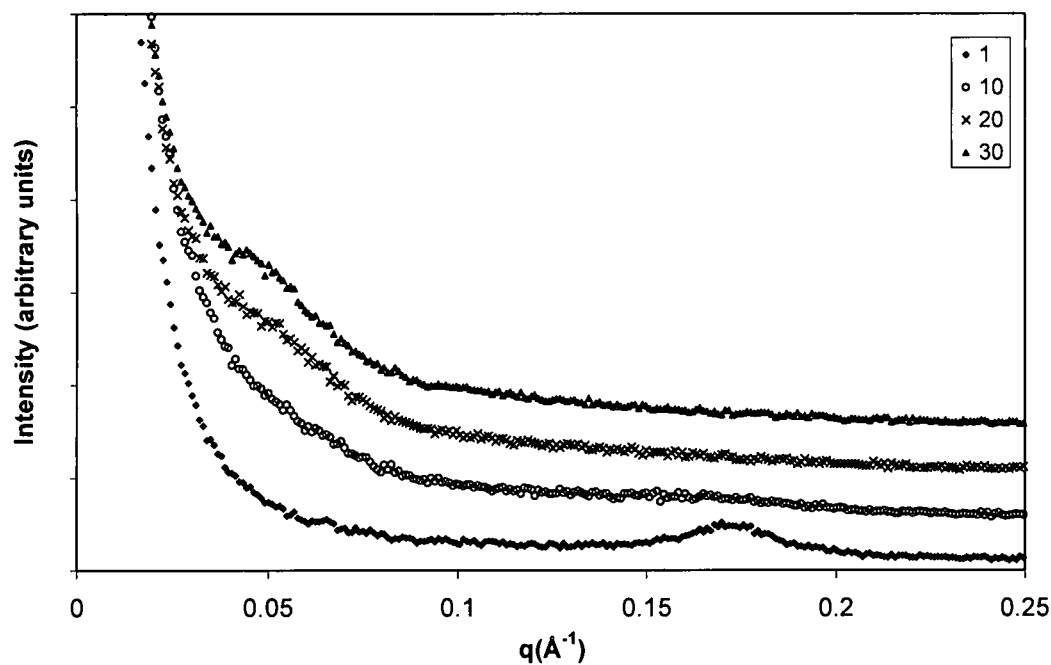


**Figure C-19:** Time-dependent small angle x-ray scattering data for 5 % pre-dried (60°C) SC18/Epon 828 with mPDA at isothermal temperature of 80°C (intensity data offset for clarity).

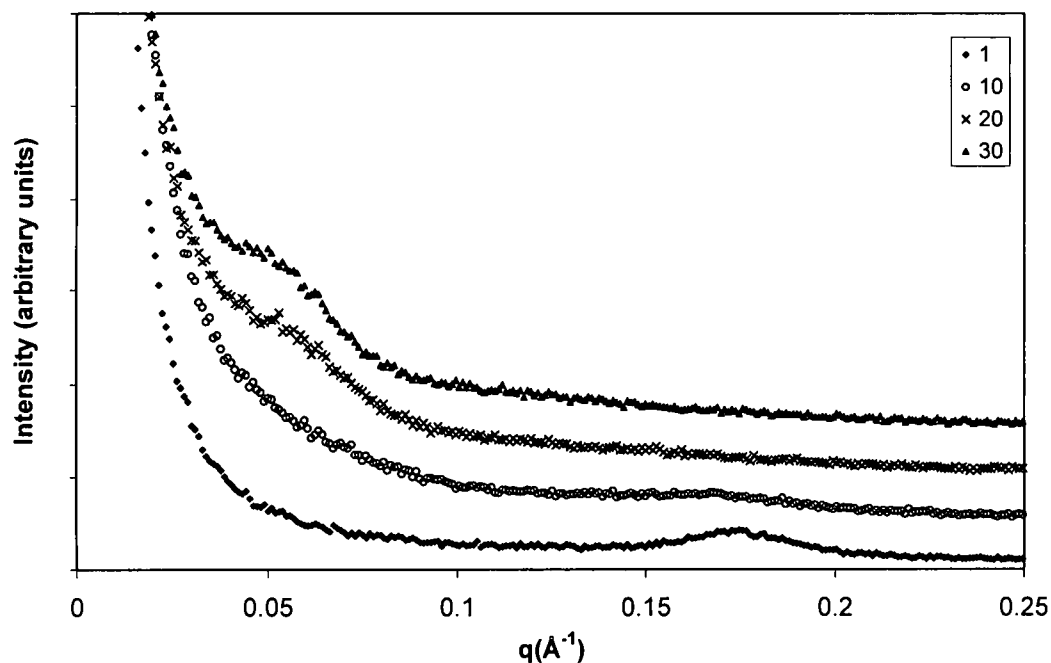


**Figure C-20:** Time-dependent small angle x-ray scattering data for 5 % pre-dried (100°C) SC18/Epon 828 with mPDA at isothermal temperature of 80° (intensity data offset for clarity).

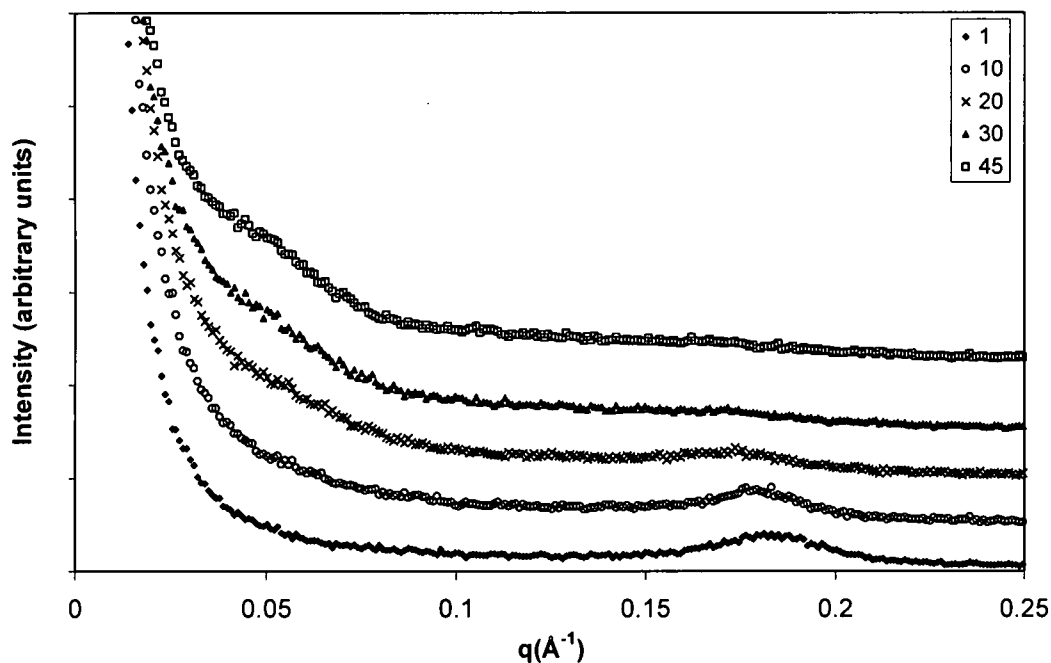


**Figure C-21:** Time-dependent small angle x-ray scattering data for 5 % mixture of SC18+I.30E/Epon 828 with mPDA at isothermal temperature of 80° (intensity data offset for clarity).

**Table C-3: Summary of Processing Variations**

<b>Silicate</b>	<b>Fabrication Process</b>	<b>Initial d-Spacing (Å)</b>	<b>Final d-Spacing (Å)<sup>1</sup></b>	<b>Initiation of Exfoliation (minutes)</b>
50%I30E, 50% SC18	Standard	34	42	~20
I30E	Silicate Dried at 25°C	33	36	25
I30E	Silicate Dried at 100°C	33	35	28
SC18	Silicate Dried at 60°C	36	130	7-)
SC18	Silicate Dried at 100°C	36	131/153	9
I30E	No Degas Step	34	43	17
SC18		38	155	4
I30E	Standard	34	42	16
SC18	Standard	36	125/155	10

<sup>1</sup> Final Time: 45 Minutes

## **APPENDIX D: SCATTERING DATA FOR CURE AGENT STUDIES AND OF CONSISTITUENTS**

In-situ SAXS data for cure agent studies are shown in Figures D-1 through D-15.

Scattering data selected to show significant events and trends are depicted. Experiments were performed on two different organoclays. Plots of significant trends for the two OLSs at a given temperature are grouped for comparison. Offsets are adjusted for clarity and to provide easy comparison of trends. Data exists for every minute of each experiment which in some cases extends over a period of several hours. Data to be shown here was selected to represent the significant trends and events only. Where appropriate, however, all of the data were analyzed for interpretation and discussion. Data are summarized in Table D-1.

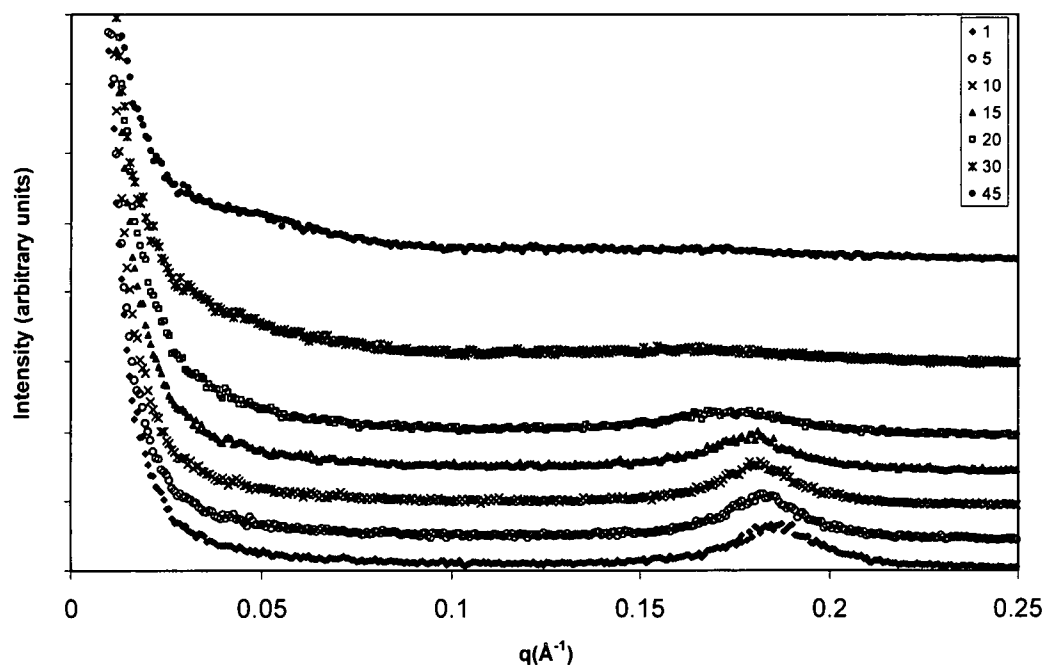


**Figure D-1:** Time-dependent small angle x-ray scattering data for 5 % I30E/Epon 828 with mPDA at isothermal temperature of 80°C aging (intensity data offset for clarity).

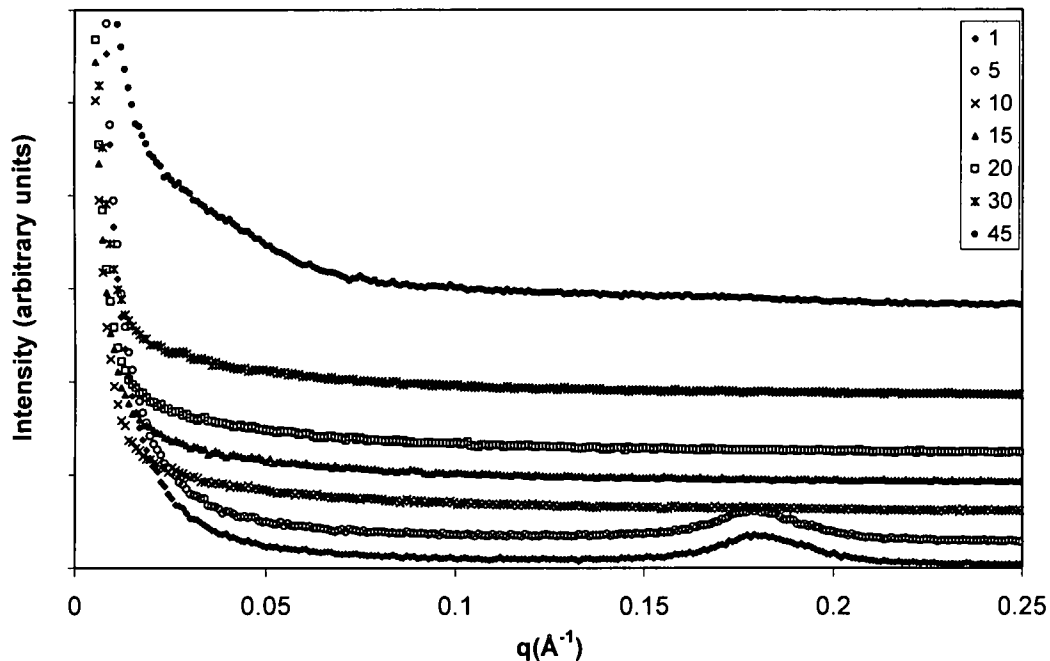


**Figure D-2:** Time-dependent small angle x-ray scattering data for 5 % I30E/Epon 828 with mPDA at heating rate of 5°C/minute (intensity data offset for clarity).

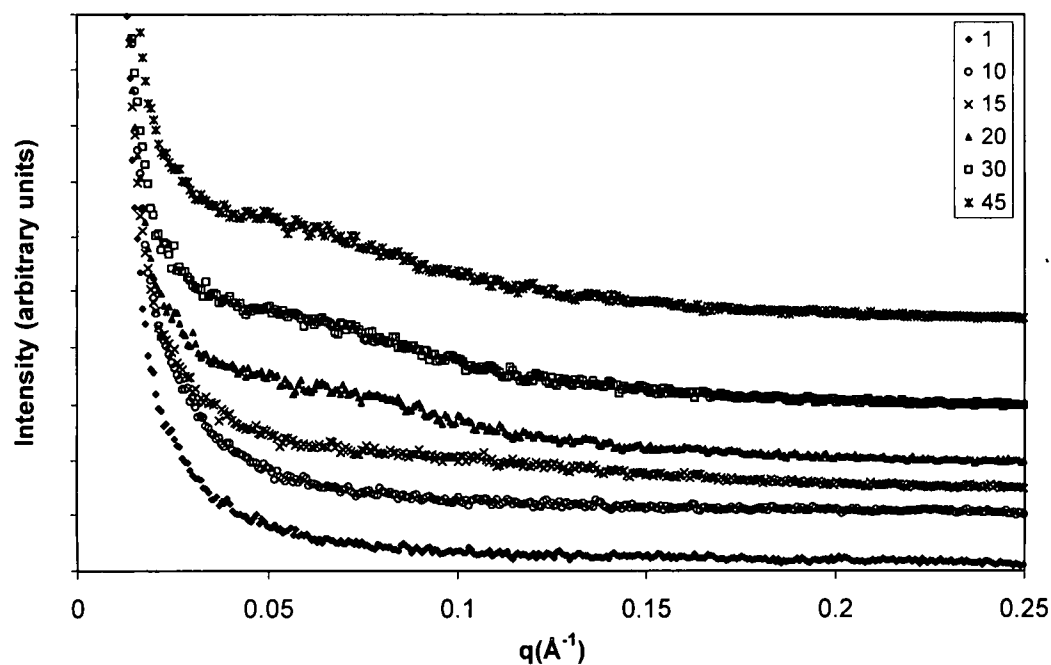


**Figure D-3:** Time-dependent small angle x-ray scattering data for 5 % I30E/Epon 828 with T403 at heating rate of 5°C/minute (intensity data offset for clarity).

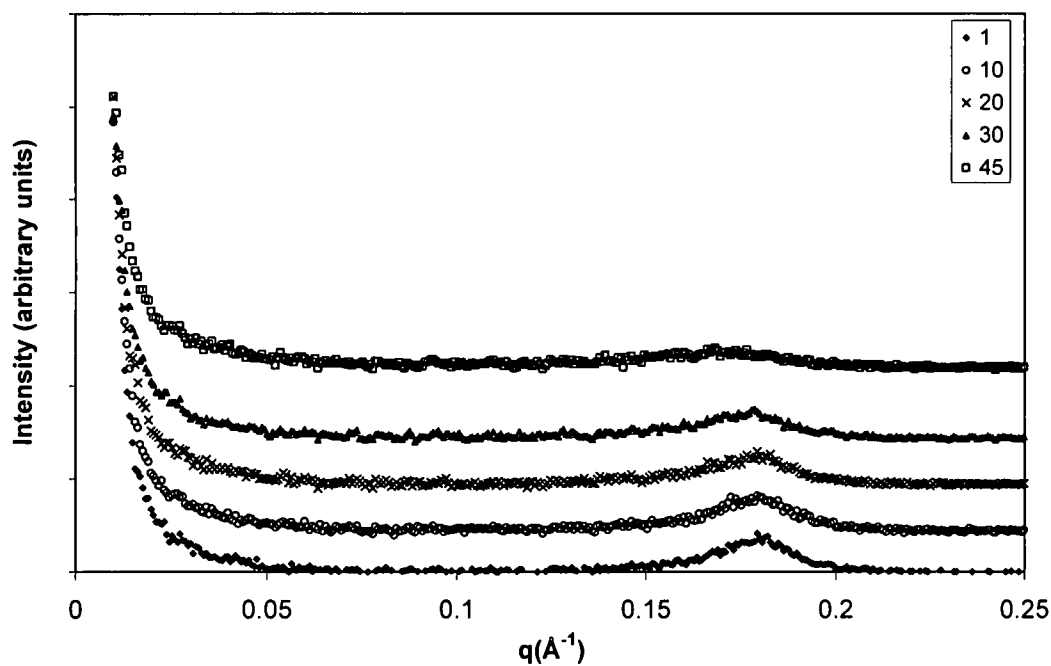


**Figure D-4:** Time-dependent small angle x-ray scattering data for 5 % I30E/Epon 828 with Epi-cure W at isothermal temperature of 80°C (intensity data offset for clarity).

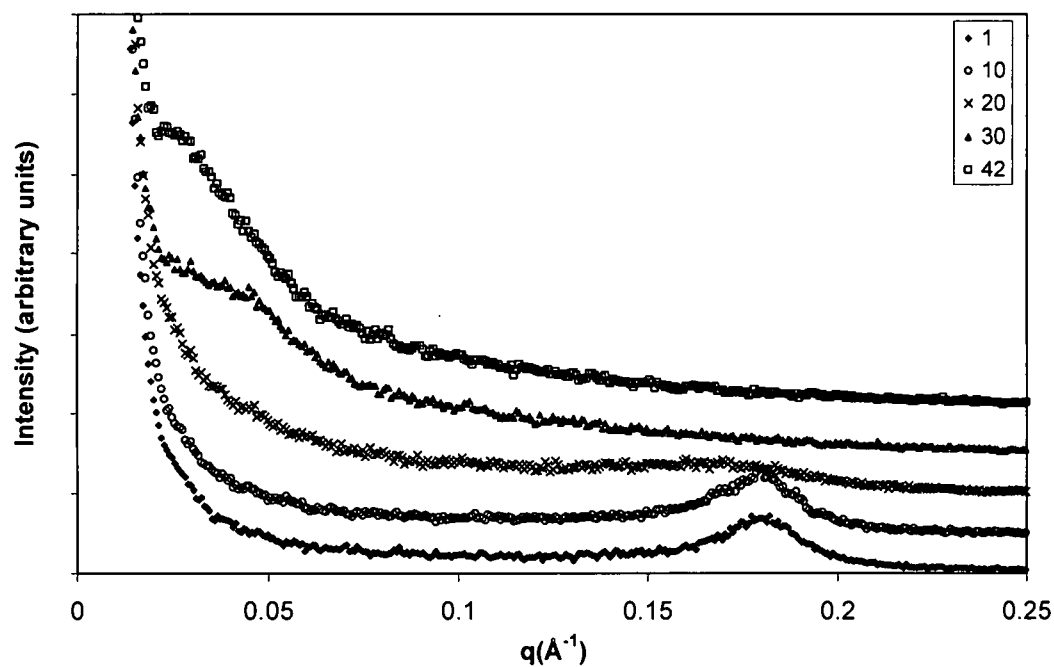


**Figure D-5:** Time-dependent small angle x-ray scattering data for 5 % I30E/Epon 828 with Epi-cure W at heating rate of 5°C/minute (intensity data offset for clarity).

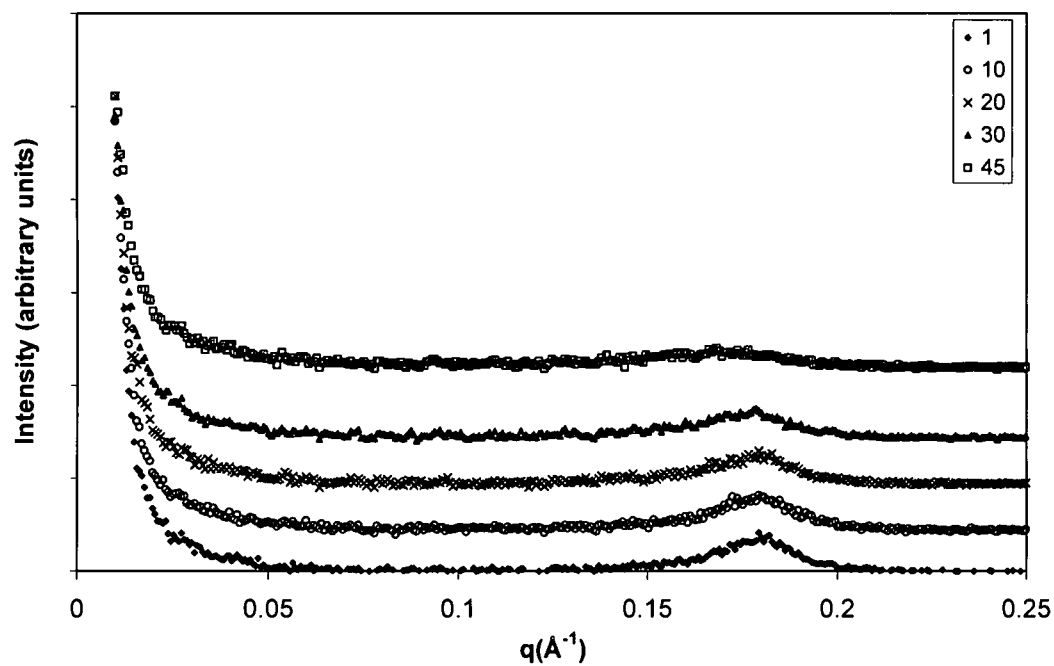


**Figure D-6:** Time-dependent small angle x-ray scattering data for 5 % I30E/Epon 828 with Epi-cure W at isothermal temperature of 80°C (intensity data offset for clarity).

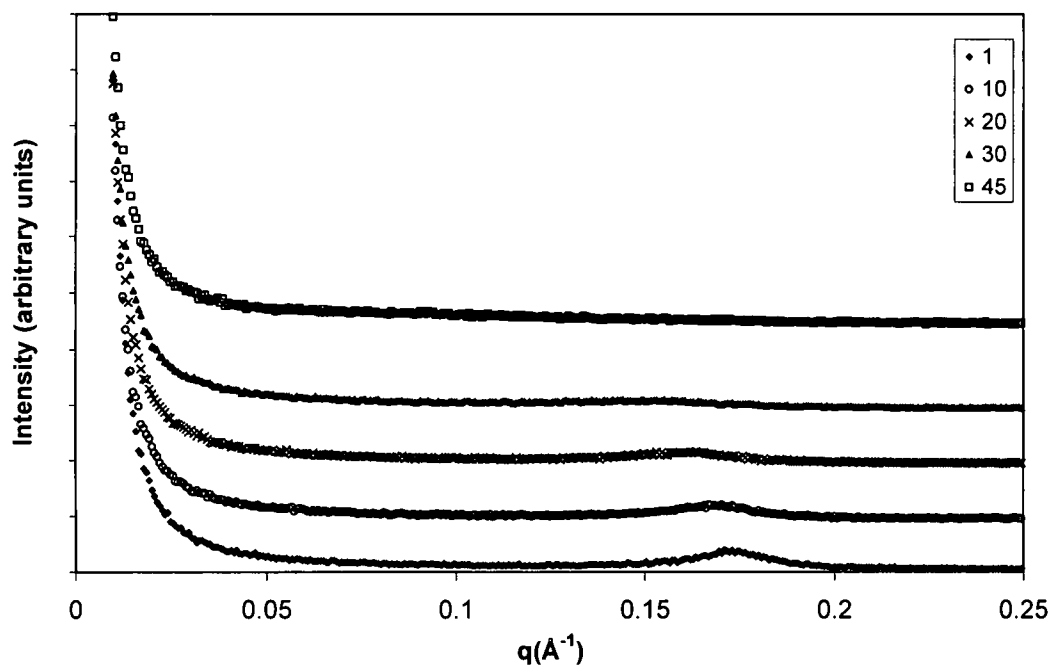


**Figure D-7:** Time-dependent small angle x-ray scattering data for 5 % I30E/Epon 828 with Epi-cure W at isothermal temperature of 80°C after aging for 16 weeks (intensity data offset for clarity).

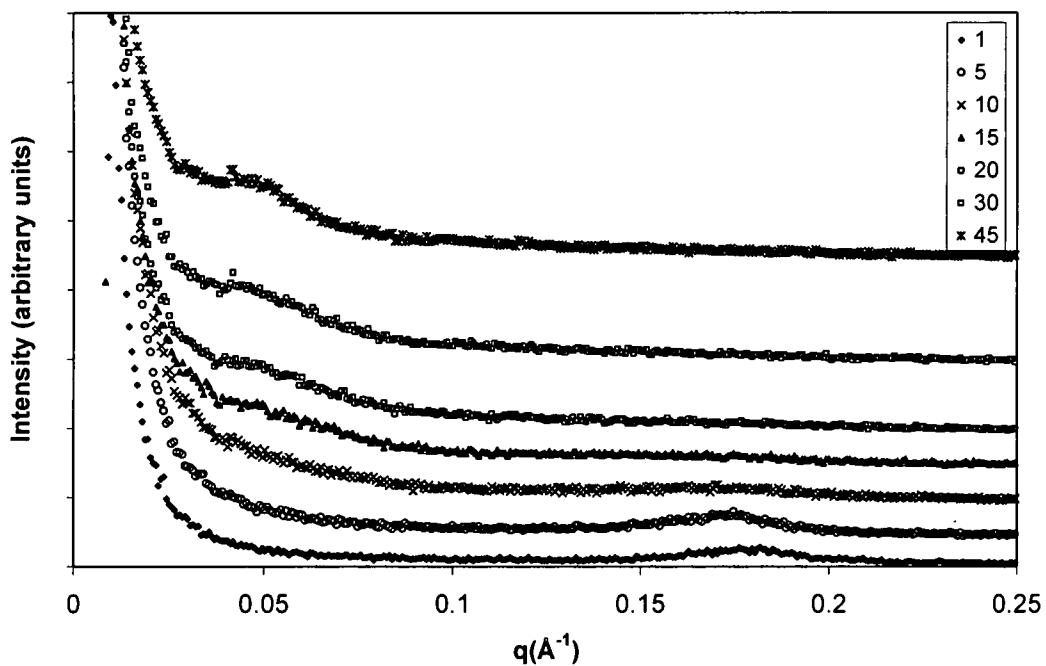


**Figure D-8:** Time-dependent small angle x-ray scattering data for 5 % SC18/Epon 828 with mPDA at isothermal temperature of 80°C (intensity data offset for clarity).

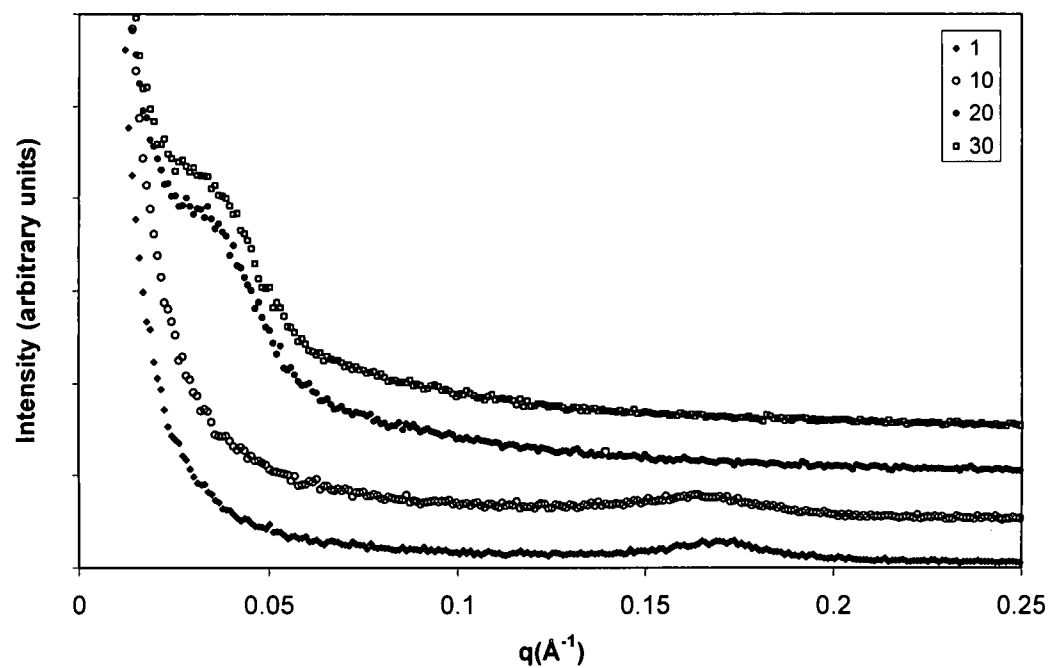


**Figure D-9:** Time-dependent small angle x-ray scattering data for 5 % SC18/Epon 828 with mPDA at heating rate of 5°C/minute (intensity data offset for clarity).

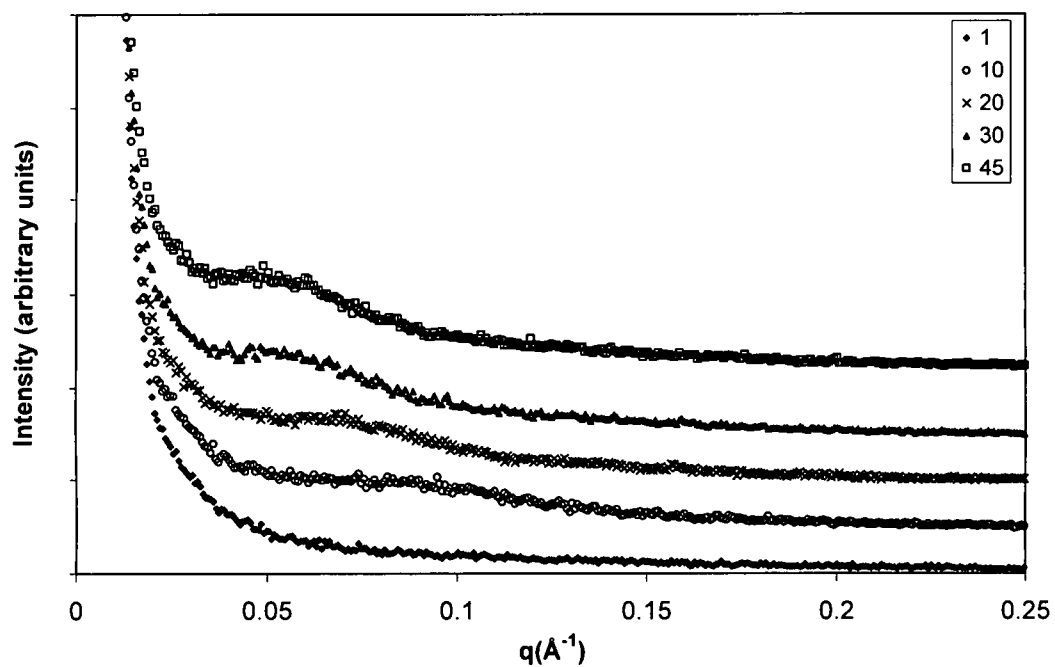


**Figure D-10:** Time-dependent small angle x-ray scattering data for 5 % SC18/Epon 828 with T403 at isothermal temperature of 80°C (intensity data offset for clarity).

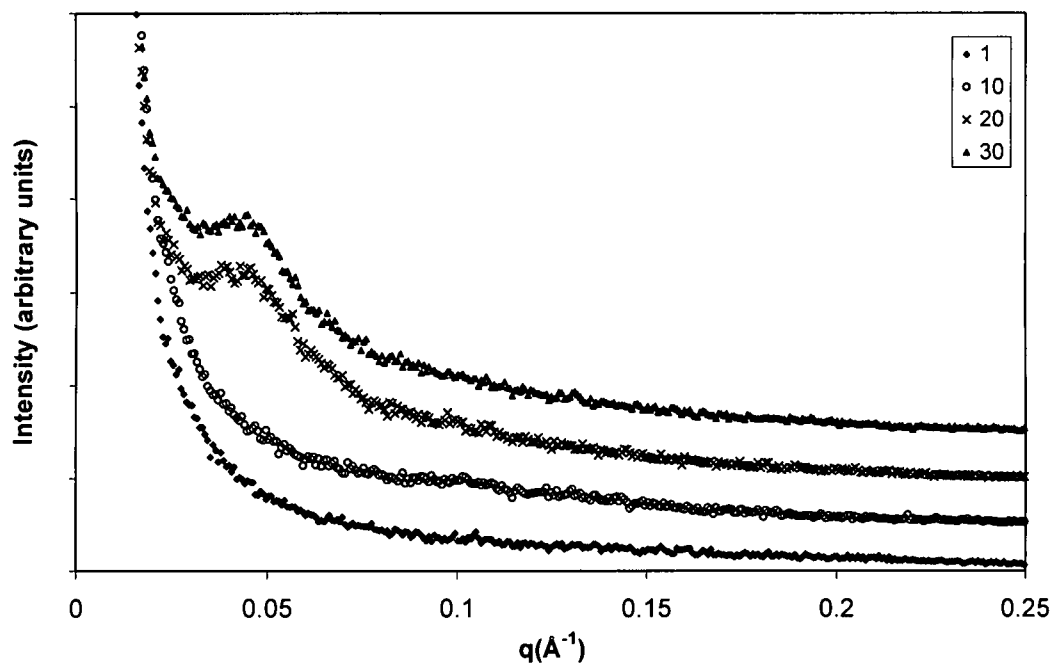


**Figure D-11:** Time-dependent small angle x-ray scattering data for 5 % SC18/Epon 828 with T403 at heating rate of 5°C/minute (intensity data offset for clarity).

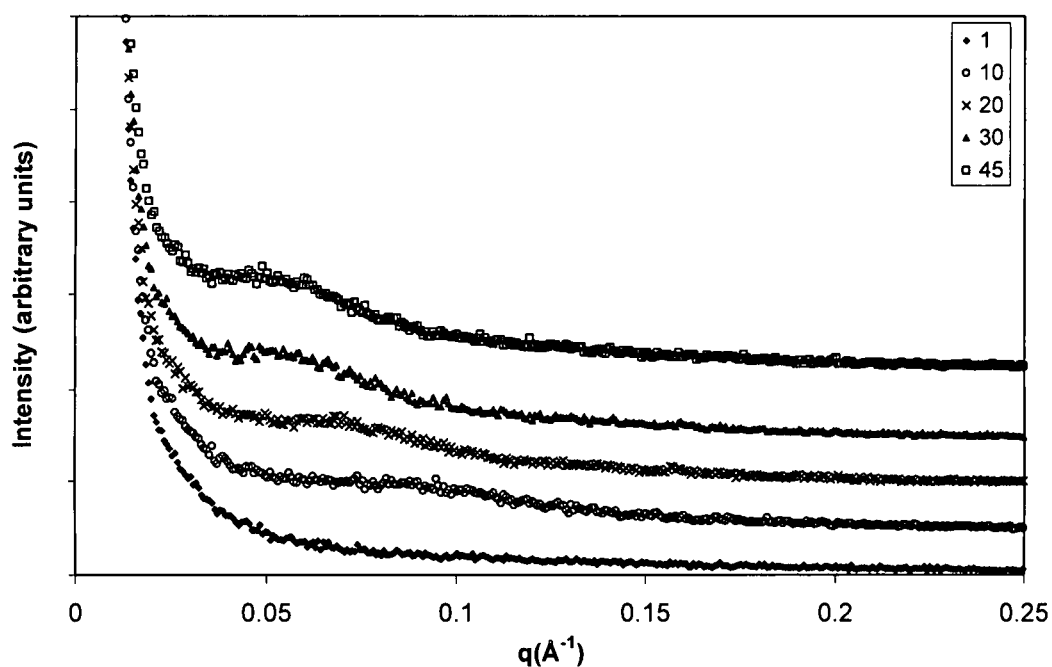


**Figure D-12:** Time-dependent small angle x-ray scattering data for 5 % SC18/Epon 828 with T403 at isothermal temperature of 80°C (intensity data offset for clarity).

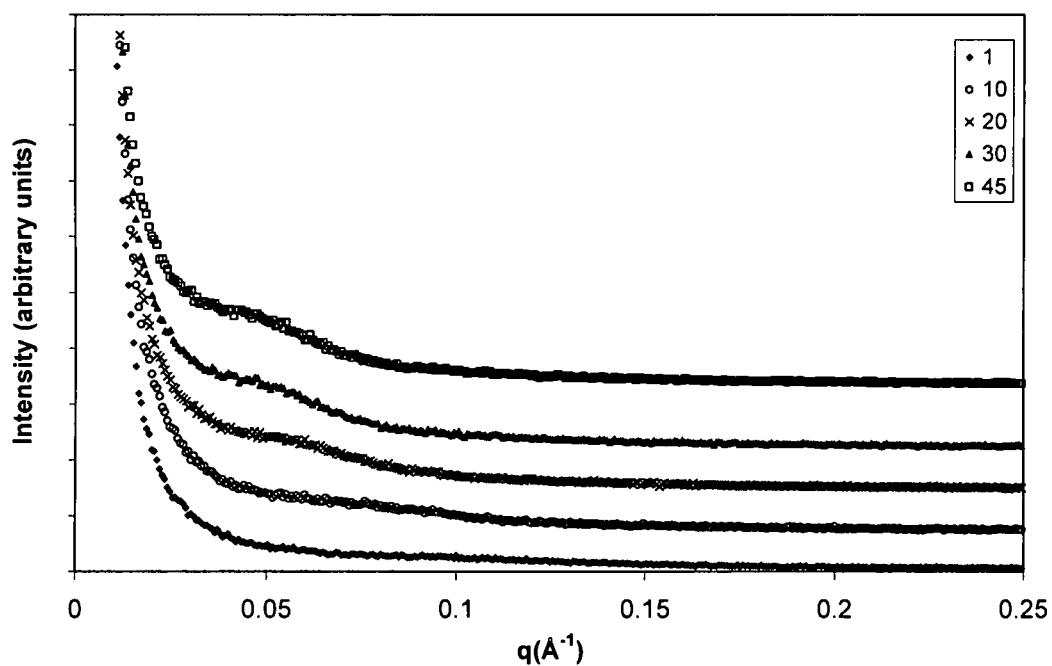


**Figure D-13:** Time-dependent small angle x-ray scattering data for 5 % SC18/Epon 828 with T403 at isothermal temperature of 80°C after aging 16 weeks (intensity data offset for clarity).

**Table D-1: Summary of Cure Agent Variation**

<b>Sample (5% by wt OLS)</b>	<b>Cure Agent</b>	<b>Process</b>	<b>Initial d-Spacing (Å)</b>	<b>Final d-Spacing (Å)<sup>a</sup></b>
I.30E/828	T403	Isothermal 80° C	None	peak at ~25
SC18/828	T403	Isothermal 80° C	None	123
I.30E/828	Epi-Cure W	Isothermal 80° C	35	37
I.30E/828	mPDA	Isothermal 80° C	34	39
SC18/828	mPDA	Isothermal 80° C	36	125 <sup>b</sup>
I.30E/828	T403	5°/minute	None	150
SC18/828	T403	5°/minute	None	157
I.30E/828	Epi-Cure W	5°/minute	35	268
I.30E/828	mPDA	5°/minute	33	150
SC18/828	mPDA	5°/minute	35	217

<sup>a</sup> Final Time: 45 minutes

<sup>b</sup> Final Time: 15 minutes

## Basic SAXS Data Collected for Baselines

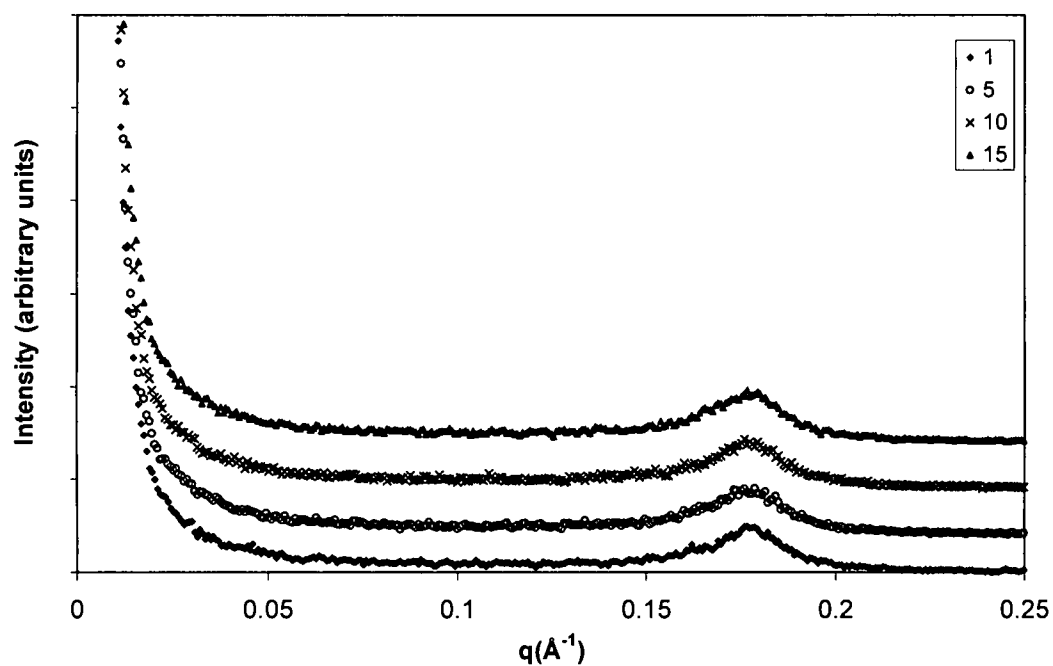


**Figure D-14:** Time-dependent small angle x-ray scattering data for 5 % I.30E/Epon 828 without cure agent at isothermal temperature of 80°C (intensity data offset for clarity).

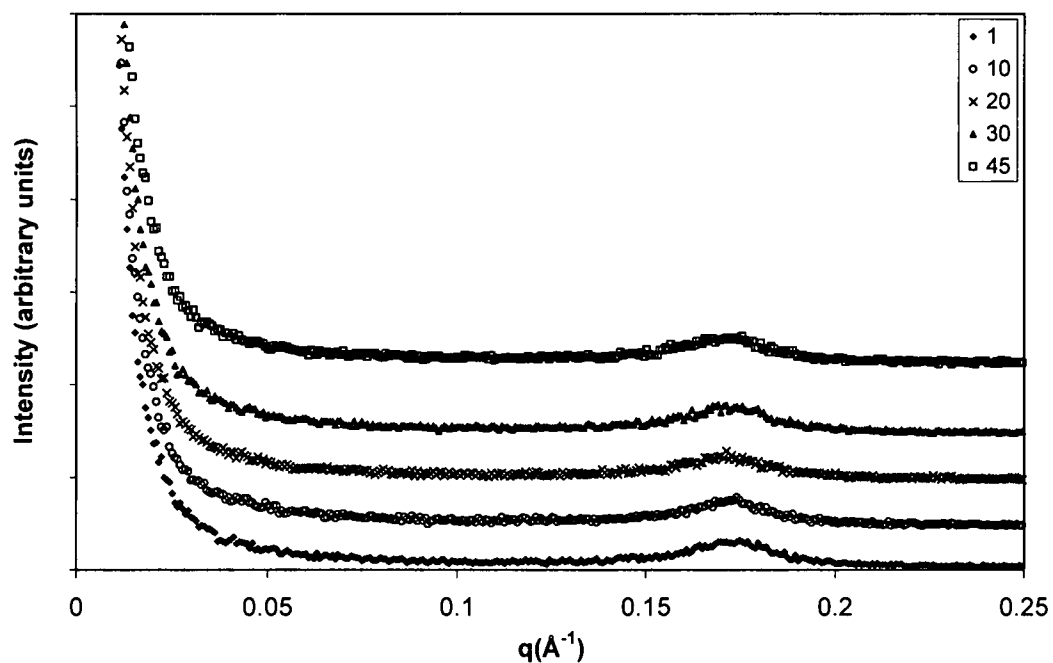


**Figure D-15** cure agent at isothermal temperature of 80°C (intensity data offset for clarity).

## References

1. Alexandre, M., Dubois, P., "Polymer-layered silicate nanocomposites: preparation, properties and uses of a new class of materials", Mtls Sci & Engr, 28, (2000), 1.
2. Pinnavaia, T.J., Beall, G.W., Polymer-Clay Nanocomposites, John Wiley & Sons, Ltd., Chichester, (2000).
3. Deanin, R.D., Schott, N. R., Fillers and Reinforcements for Plastics, American Chemical Society, Washington, DC (1974).
4. Neilsen, L.E., Mechanical Properties of Polymers and Composites, Marcel Dekker, New York, (1994).
5. Moore D., Reynolds R., X-ray Diffraction and the Identification and Analysis of Clay Minerals, Oxford University Press, New York, (1997).
6. Theng, B.K., Formation and Properties of Clay-Polymer Complexes, Elsevier, New York, (1979)
7. Grim, R.E., Clay Mineralogy, McGraw-Hill Book Company, Inc., (1953).
8. Theng, B.K., The Chemistry of Clay-Organic Reactions, John Wiley & Sons, New York, (1974).
9. Holtz, R.D., & Kovacs, W.D., An Introduction to Geotechnical Engineering, Prentice-Hall, Inc., New Jersey, (1981).
10. Vaia, R.A., Giannelis, E.P., "Lattice Model of Polymer Melt Intercalation in Organically-Modified Layered Silicates", Macromolecules, 30, (1997), 7990.
11. Morgan, A.B., Gilman, J.W., Jackson, C.L., "Characterization of the Dispersion of Clay in a Polyetherimide Nanocomposite", Macromolecules, 34, 8, (2001), 2375.
12. Bharadway, R.K., Mehrabi, A.R., Hamilton, C., Trujillo, C., Mmurga, M., Ran, R., Charira, A., Thompson, A.K., "Structure-Property Relationships in Cross-linked Polyester-clay nanocomposites", Polymer, 43, 13, (2002), 3699.

13. Vaia, R.A., Liu, W., J. Polymer Science. Part B: Polymer Physics, 40, (2002), 1590.
14. Okada, A., Kawasumi, M., Kurauchi, T. and Kamigaito, O., "Synthesis and Characterization of a Nylon 6-Clay Hybrid", ACS Polymer Preprints, Vol 28, No 2, (1987), 447.
15. Usuki, A., Kojima, Y., Kawasumi, M., Okada, A., Fukushima, Y., Kurauchi, T. and Kamigaito, O., "Synthesis of Nylon 6-Clay Hybrid", J Mater. Res., Vol 8, No 5, (1993), 1179.
16. Usuki, A., Kawasumi, M., Kojima, Y., Okada, A., Fukushima, Y., Kurauchi, T. and Kamigaito, O., "Swelling behavior of montmorillonite cation exchanged for  $\omega$ -amino acids by  $\epsilon$ -caprolactam", J. Mater. Res., Vol 8, No 5, (1993), 1174.
17. Kojima Y., Usuki A., Kawasumi M., Okada A., Kurauchi T., Kamigaito O., Synthesis of Nylon 6-Clay Hybrid by Montmorillonite Intercalated with  $\epsilon$ -Caprolactam, J of Pol Sci Part A: Pol Chem, 31, (1993), 983.
18. Kojima Y., Usuki A., Kawasumi M., Okada A., Fukushima Y., Kurauchi T., Kamigaito O. Mechanical properties of nylon 6-clay hybrid. J Mater Res., Vol 8, No 5, (1993), 1185.
19. Okada et al, Mater Res, 8, (1993), 1170.
20. Giannelis, E.P., "Polymer Layered Silicate Nanocomposites", Advanced Materials Vol 8, No 1, (1996), 29.
21. Kurokawa Y, Yasuda H, Kashiwagi M, Oyo A. Structure and properties of a montmorillonite/polypropylene nanocomposite. J of Mts Science Letters, 16, 20, (1997), 1670.
22. Moet, A., Akelah, A., Hiltner, A., Baer, E., "Layered silicate/polystyrene nanocomposite", MRS Proceedings, 351, (1994), 91.
23. Vaia, R., Jandt, K., Kramer, E., Giannelis, E., "Microstructural evolution of melt intercalated polymer-organically modified layered silicate nanocomposites", Chem Mater 8, 11, (1996), 2628.
24. Manias, E., Han, W.J., Jandt, K.D., Kramer, E.J., Giannelis, E.P., "Direct Observation of Fracture Mechanisms in Polymer-Layered Silicate Nanocomposites", Mat Res Soc Symp Proc, 457, (1997), 495.
25. Pinnavaia, T., Lan, T., Kaviratna, P., Wang, M., "Clay-polymer nanocomposites: polyether and polyimide systems", MRS Proc, 346, (1994), 81.

26. Lan, T., Padmananda, Kaviratna, D., Pinnavaia, T., "On the nature of polyimide-clay hybrid composites", Chem Mater, 6, (1994), 573.
27. Yano, K., Usuki, A., Okada, A., Kurauchi, T., Kamigaito, O., "Synthesis and Properties of Polyimide-clay Hybrid", J of Pol Sci Part A Pol Chem, Vol 31, (1993), 2493.
28. Vaia, R., Sauer, B., Tse, O., Giannelis, E., "Relaxations of confined chains in polymer nanocomposites: glass transition properties of poly(ethylene oxide) intercalated in montmorillonite", J of Pol Sci: Pol Phys, 35, 1, (1997), 59.
29. Goldman, A., Montes, J., Barajas A., Beall G., Eisenhour D., "Effect of aging on mineral-filled nanocomposites", ANTEC, (1998), 2415.
30. Wang, Z., Pinnavaia, T., "Nanolayer reinforcement of elastomeric polyurethane", Chem Mater, 10, (1998), 3769.
31. Messersmith, P.B., Giannelis, E.P., "Synthesis and Characterization of Layered Silicate-Epoxy Nanocomposites", Chem Mater, Vol 6, No 10, (1994), 1719.
32. Okada A, et al., "Nylon 6-clay hybrid", MRS Proceedings, 171, (1990), 45.
33. Burnside, S., Giannelis, E., "Synthesis and properties of new poly(dimethylsiloxane) nanocomposites", Chem Mater 7, (1995), 1597.
34. Wang, Z., Lan, T., Pinnavaia, T.J., "Hybrid Organic-Inorganic Nanocomposites Formed from an Epoxy Polymer and a Layered Silicic Acid (Magadiite)", Chem Mater 8, (1996), 2200.
35. Laus et al, Italy; "Hybrid Nanocomposites based on polystyrene and a reactive organophilic clay", J of Mtls Sci, 33 No 11, (1998).
36. Park, C. I., Park, O.O., Lim, J.G., Hyun, J.K., "The fabrication of syndiotactic polystyrene/organophilic clay nanocomposites and their properties" et al, Polymer 42, 17, (2001), 7456.
37. May, C.A., Epoxy Resins Chemistry and Technology, Marcel Dekker, Inc., New York, (1988).
38. Lee, H., Neville, K., Handbook of Epoxy Resins, McGraw-Hill Company, New York, (1967).
39. Sperling, L.H., Introduction to Physical Polymer Science, John Wiley & Sons, New York, (1992).

40. Enns, J.B., Gillham, J.K., "Time-Temperature-Transformation Cure Diagram: Modeling the Cure Behavior of Thermosets", Journal of Applied Polymer Science, (1983), 2567.
41. Venditti, R.A., and Gillham, J.K., "A relationship between the glass transition temperature ( $T_g$ ) and fractional conversion for thermosetting systems", J of App Pol Sci, 64, 1, (1997), 3.
42. Kinloch, A.J., Young, R.J., Fracture Behavior of Polymers, Elsevier Applied Science Publishers, London, (1983).
43. Riew, C.K., Kinloch, A.J., Toughened Plastics II: Novel Approaches in Science and Engineering, American Chemical Society, Washington D.D., (1996).
44. Spanoudakis, J., Young, R.J., "Crack propagation in a glass particle-filled epoxy resin, Part 1: Effect of particle volume fraction and size", J of Mat Science, 19, (1984), 473.; Spanoudakis, J., Young, R.J., "Crack propagation in a glass particle-filled epoxy resin, Part 2: Effect of particle-matrix adhesion", J of Mat Science, 19, (1984), 487.
45. Lan, T., Kaviratna, P.D., Pinnavaia, T.J., "Mechanism of clay tactoid exfoliation in epoxy-clay nanocomposites", Chem Mater, 7, (1995), 2144.
46. Kornmann, X., Lindberg, H., Berglund, L.A., "Synthesis of epoxy-clay nanocomposites. Influence of the nature of the curing agent on structure", Polymer, 42, (2001), 4493.
47. Chin, I., Thurn-Albrecht, T., Kim, H., Russell, T., Wang, J., "On exfoliation of montmorillonites in epoxy", Polymer, 42, (2001), 5947.
48. Wang, K.H., Choi, M.H., Koo, C.M., Choi, Y.S., Chung, I.J., "Synthesis and characterization of maleated polyethylene/clay nanocomposites", Polymer, 42, 24, (2001), 9819.
49. Ullett, J., PhD Thesis, University of Dayton, 1992; Brown, J., PhD Thesis, Virginia Polytechnic Institute and State University, 1994.
50. Dennis, H.R., Hunger, D.L., Chang, D., Kim, S., White, J.L., Cho, J.W., Paul, D.R., "Effect of melt processing conditions on the extent of exfoliation in organoclay-based nanocomposites", Polymer, 42, 23, (2001) 9513.
51. Wang, M.S., Pinnavaia, T.J., Chem Mater, 6, (1994), 468.

52. Butzloff, P., D'Souza, N.A., Golden, T.D., Garrett, D., "Epoxy + montmorillonite nanocomposites: effect of composition on reaction kinetics", Polymer Engineering & Science, 41, 10, (2001), 1794.
53. Kornmann, X., Lindberg, H., Berglund, L.A., Polymer, 42, (2001), 1303.
54. Jiankun, L., Yucai, K., Zongneng, Q., Xiao-su, Y., "Study on intercalation and exfoliation behavior of organoclays in epoxy resin", J. Polymer Science. Part B: Polymer Physics, 39, (2001), 115.
55. Brown, J.M., Curliss, D., Vaia, R.A., "Thermoset-layered silicate nanocomposites. Quaternary ammonium montmorillonite with primary diamine cured epoxies", Chem Mater, 12, (2000), 3376.
56. Lan, T., Kaviratna, D., Pinnavaia, T.J., "Epoxy self-polymerization in smectite clays", J. Phys Chem Solid, 57, (1996), 1005.
57. Shi, J. Lan, T., Pinnavaia, T.J., "Interfacial Effects on the Reinforcement Properties of Polymer-Organoclay Nanocomposites", Chem Mater, Vol 8, No 8, (1995), 1584.
58. Lan, T., Pinnavaia, T.J., "Clay-Reinforced Epoxy Nanocomposites", Chem Mater, Vol 6, No 12, (1996), 2216.
59. Lan, T., Pinnavaia, T.J., Chem Mater, Vol 6, No 22, (1994), 16.
60. Becker, O., Cheng, Y., Varley, R.J., Simon, G.P., "Layered Silicate Nanocomposites Based on Various High-Functionality Epoxy Resins: The Influence of Cure Temperature on Morphology, Mechanical Properties, and Free Volume", Macromolecules, 36, (2003), 1616.
61. Barclayk, G.G., Ober, C.K., "Liquid Crystalline and Rigid-Rod Networks", Prog Polym Sci, Vol 18, Pergammon Press Ltd, (1993), 899.
62. Benson Tolle, T.H., Anderson, D.P., "Composite Property Enhancement With Nanoscale Inorganic Fillers," Polymeric Materials: Science and Engineering, American Chemical Society, (2000), xxx.
63. Kressler, J. , Thomann, R., "Nanocomposites based on a synthetic layered silicate and polyamide-12", ANTEC Proceedings, (1998), 2400.
64. Kyu, T., Zhu, G.C., Xhou, Z.L., Tajuddin, Y., Quitubuddin, S., "Novel filled polymer composites prepared from in situ polymerization via a colloidal approach", Journal of Pol Sci Part B: Pol Physics, 34, (1996), 1769.

65. Petrovic, Z., Waddon, A., "Polyurethane Elastomers with Nano-Fillers", ANTEC Proceedings, (1998), 2390.
66. Harcup, Yee, Akkapeddi, "Deformation and Fracture of Polymer Silicate Nanocomposites", Materials Research Society Proceedings, (1998), 204.
67. Zilg, C., Mülhaupt, R., Finter, J., "Morphology and Toughness/stiffness balance of nanocomposites based on anhydride-cured epoxy resins and layered silicates", Macromol Chem Phys, 200, No 3, (1999) 661.
68. Zerda, A.S., Lesser, A.J., "Intercalate Clay Nanocomposites: Morphology, Mechanics, and Fracture Behavior", J of Pol Sci Part B Pol Phys, 39, (2001), 1137.
69. Kornmann, X., Thomann, R., Mülhaupt, R., Finter, J., Berglund, L., "Synthesis of Amine-Cured, Epoxy-Layered Silicate Nanocomposites: The Influence of the Silicate Surface Modification on the Properties", J of App Pol Sci 86, (2002), 2643.
70. Becker, O., Varley, R., Simon, G., "Morphology, Thermal relaxations and mechanical properties of layered silicate nanocomposites based upon high-functionality epoxy resins"; Polymer, 43, (2002), 4365.
71. Turi, E. A., Thermal Characterization of Polymeric Materials, Academic Press, Inc, San Diego, (1981).
72. Xie, W., Gao, Z., Pan, W. Vaia, R., Hunter, D., Singh, A., "Thermal characterization of organically modified montmorillonite", Thermochimica Acta 367-368, (2001), 339.
73. Guinier, A., X-Ray Diffraction in Crystals, Imperfect Crystals, and Amorphous Bodies, Dover Publications, Inc., New York, (1994).
74. Guinier, A., Dexter, D.L., X-Ray Studies of Materials, Interscience Tracts on Physics and Astronomy, Number 20, Interscience Publishers, New York (1963).
75. Guinier, A., Gournet, G., Small-Angle Scattering of X-rays, Structure of Matter Series, John Wiley & Sons, Inc., New York, (1955).
76. Brown, G., The X-ray Identification and Crystal Structures of Clay Minerals, Mineralogical Society of London Jarrold and Sons LTD, Norwhich, (1961).
77. Benson Tolle, T.H., Anderson, D.P., "Morphology development in layered silicate thermoset nanocomposites", Composite Science and Technology, 62, (2002), 1033.

78. Lan, T., Kaviratna, P.D., Pinnavaia, T.J., "Mechanisms of Clay Tactoid Exfoliation in Epoxy-Clay Nanocomposites", J. Chem Mater 7, (1995), 2144.
79. Shi, Lan, Pinnavaia ; "Interfacial Effects on the Reinforcement Properties of Polymer-Organoclay Nanocomposites", Chem Mater, 8, (1996), 1584.
80. Ranad, A., D'Souza, N.A., Gnade, B., "Exfoliated and intercalated polyamide-imide nanocomposites with montmorillonites", Polymer, 43, (2002), 3759.
81. Lan, Kaviratna and Pinnavaia, J Phys Chem Solids, 57, 6, (1996), 1005.
82. Gayer, "Catalytic polymerization of propylene", Ind Eng Chem, 25, 1122.
83. Van Olphen, H., "An Introduction to Clay Colloid Chemistry", John Wiley & Sons, New York (1963).
84. Kornmann, X., Lindberg, H., Berglund, L.A., "Synthesis of epoxy-clay nanocomposites: influence of the nature of the clay on structure", Polymer, 42, (2001), 1303.
85. Wang, Z., Pinnavaia, T.J., "Hybrid organic-inorganic nanocomposites: exfoliation of magaditte nanolayers in an elastomeric epoxy polymer", J. Chem Mater, 20, (1998), 1820
86. Chen, C., Benson Tolle, T., "Aerospace Application for Epoxy Layered-Silicate Nanocomposites", The Dekker Encyclopedia of Nanoscience & Nanotechnology, Edited by James A. Schwarz, Cristian Contescu, and Karol Putyera, Marcel Dekker Inc., New York, (2004), 45.
87. Chen, C., Curliss, D., "Processing, Dynamic Studies and Properties of Exfoliated Aerospace Epoxy-Organoclay Nanocomposites", MRS Symposium Proceedings Series, 703, (2001), 3
88. Personal communications, Nanocor, Inc., September 2002
89. Vaia, R.A., Chem Mater, 6, (1994), 1017.
90. Luo, J., Daniel, I.M., "Characterization and modeling of mechanical behavior of polymer/clay nanocomposites", Composites Science and Technology, 63, (2002), 1607.
91. Ke, Y., Lu, J., Yi, X., Zhao, U., Qi, Z., "The effective of promoter and curing process on exfoliation behavior of epoxy/clay nanocomposites", J of App Pol Sci 78, 4, (2000), 808.

92. Want, Q., Song, C., Lin, W., "Study of the exfoliation process of epoxy-clay nanocomposites by different curing agents", J of App Pol Sci, Vol 90, 2, (2003) 511.
93. Benson Tolle, T. B., Anderson, D.P., "The role of preconditioning on morphology development in layered silicate thermoset nanocomposites", Journal of App Pol Science, 91, (2004), 89.
94. Chen, C., Curliss, D., "Preparation, Characterization, and Nanostructural Evolution of Epoxy Nanocomposites", Journal of App Pol Science, 90, (2003), 2276.
95. Bharadwaj, R.K., Vaia, R.A., Farmer, B.L., "A coarse-grained simulation study of polymer melt intercalation in layered nanostructures", Polymer Nanocomposites, ACS Symposium Series 804, American Chemical Society, Washington, DC, (2002), 209.
96. Brumberger, H., Modern Aspects of Small-Angle Scattering, Kluwar Academic Publishers, Netherlands, (1995).
97. Roe, R.J., Methods of X-Ray and Neutron Scattering in Polymer Science, Oxford University Press, New York (2000).
98. Martin, J.E., Hurd, A.J., J. Appl Cryst, 20, (1987), 61.
99. Chen, J., Poliks, M.D., Ober, C.K., Zhang, U., Wiesner, E.G., "Study of the interlayer expansion mechanism and thermal-mechanical properties of surface-initiated epoxy nanocomposites", Polymer 43, (2002), 4895.
100. Kong, D., Park, C.E., "Real Time Exfoliation Behavior of Clay Layers in Epoxy-Clay Nanocomposites", Chem Mat, 15, (2003), 419.
101. Park, J.H., Jana, S.C., "Mechanisms of Exfoliation of Nanoclay Particles in Epoxy-Clay Nanocomposites", Macromolecules, 36, (2003), 2758.
102. Vassileva, E., Friedrich, K., "Epoxy/Alumina Nanoparticle composites. I. Dynamic Mechanical Behavior", Journal of App Pol Science, 89, (2003), 3774.
103. Triantafillidis, C.S., LeBaron, P.C., Pinnavaia, T.J., "Thermoset epoxy-clay nanocomposites: the dual role of  $\alpha$ ,  $\omega$  -diamines as clay surface modifiers and polymer curing agents", Chem Mat, 14, (2002), 4088.
104. Chang, Thomas and Sperling, J of Pol Sci Part B, Vol 26, (1988), 1627.
105. Giannelis, Krishnamoorrti, and Manias – Advances in Pol Sci, 138, (1999), 125.

106. Wang, Q., Song, C., Lin, W., "Study of the exfoliation process of epoxy-clay nanocomposites by different curing agents", J of App Pol Sci, 90, (2003), 511.
107. Kornmann, X., Berglund, L., Sterte, J., Polymer Engineering & Science, 38, (1998), 1351.
108. Abramoff et al, J Appl Pol Sci, (1992) 46;
109. Landry, C. J.T., Coltrain, B.K., Landry, M.R., Fitzgerald, J.J., Long, V.K., "Poly(vinyl acetate)/Silica Filled Materials: Material Properties of in Situ vs Fumed Silica Particles", Macromol 26, (1993), 3702.
110. Lee, J., Yee, A.F., "Fracture of glass bead/epoxy composites: on micro-mechanical deformations", Polymer, 41, (2000), 8363.
111. Young, Maxell and Kinloch, J of Mat Sci 21, (1986), 380.
112. R.N. Haward, R.J. Young, The Physics of Glassy Polymers, Chapman & Hall, London (1997).
113. Yee, A.F., Pearson, R.A., "Toughening Mechanism in Elastomer-Modified Epoxy Resins Part 2", NASA Contractor Report 3852, National Aeronautics and Space Administration, (1984).
114. Kar, R.J., "Composite Failure Analysis Handbook Vol II, Part 2: Atlas of Fractographs", WL-TR-91-4032, DOT/FAA/CT-91/23; Air Force Systems Command, Dayton, and Federal Aviation Administration Technical Center, New Jersey (1990).
115. Cherry, B.W., Thomson, K.W., "The fracture of highly crosslinked polymers: Part 2: Fractography", J of Mat Science, 16, (1981), 1925.
116. Kim, D.S., Cho, K., Kim, J.K., Park, E.C., "Effects of Particle Size and Rubber Content on Fracture Toughness in Rubber-Modified Epoxies", Polymer Engineering and Science, Vol 36, No 6, (1996), 755.
117. Miyagawa and Drzal, 2003
118. Kemnetz, S.J., Still, A.L, Cody, C.A., Schwindt, R., "Origins of Organoclay Rheological Properties in Coating Systems", Journal of Coatings Technology, Vol 61, No. 776, (1989), 47.
119. Mardis, W.S., "Organoclay Rheological Additives: Past, Present and Future", JAOCS, Vol 61, No. 2, (1984), 382.

R702031626